PHENOMENOLOGICAL EVALUATIONS

Kewaunee-specific phenomenological evaluation summaries are the principal means of addressing the impact of phenomenological uncertainties on plant response. These summaries address a wide range of phenomenological issues and provide an in-depth review of plant-specific features which influence the uncertainty, or act to mitigato, the consequences of such phenomena. The phenomenological evaluation summaries investigate both the likelihood of occurrence and the probable consequences of key severe accident phenomena. The phenomenological evaluation summaries are supported by available experimental information from open literature as well as information which has been developed using the FAI experimental facilities in direct support of the IPE. A combination of these evaluations and MAAP sensitivity analyses is used to assess the importance of the phenomenological issues and the significance of uncertainty. This approach to dealing with phenomena provide a technical basis for maintaining containment systems and functional events in the Kewaunee containment event trees (CETs).

This section of the Kewaunce Level II source term notebook contains the following phenomenological evaluation summaries:

- Direct Containment Heating
- Steam Explosions
- Hydrogen Detonations and Deflagrations
- Molten Core-Concrete Interaction (MCCI)
- Vessel Thrust Forces
- Thermal Loading of Containment Penetrations
- Containment Overpressurization
- Liner Melt-through
- Direct Containment Bypass
- Containment Isolation Failure

FAI/91-123

A PHENOMENOLOGICAL EVALUATION SUMMARY ON DIRECT CONTAINMENT HEATING IN SUPPORT OF THE KEWAUNEE INDIVIDUAL PLANT EVALUATION

Submitted To:

Wisconsin Public Service Corporation
Green Bay, Wisconsin

Prepared By:

Fauske & Associates, Inc.
16W070 West 83rd Street
Burr Ridge, Illinois 60521

Final Issue

April, 1993

TABLE OF CONTENTS

		Page
	LIST OF TABLES	iv
	LIST OF FIGURES	v
	ABSTRACT	vii
1.0	PURPOSE	1-1
2.0	PHENOMENA	2-1
	2.1 Description	2-1
	2.1.1 Controlling Physical Processes	2-1
	2.1.2 Relationship to Containment Failure Mechanisms and Modes	2-4
	2.1.3 Relationship to Source Term	2-4
	2.2 Experimental Results	2-6
	2.2.1 Sandia HIPS Experiments	2-6
	2.2.2 Argonne Wood's Metal Tests	2-9
	2.2.3 Argonne CWTI Experiments	2-9
	2.2.4 SNL-DCH (Surtsey) Experiments	2-19
	2.2.5 BNL Simulant Fluid Test	2-22
	2.2.6 IDCOR/FAI Wood's Metal Tests	2-25
	2.2.7 FAI-DCH Experiments	2-25
	2.2.8 Scaling Effects	2-37
	2.2.8.1 Sweepout and Extent of Entrainment Scaling	2-38
	2.2.8.2 De-Entrainment Scaling (Due to the Change in Flow Direction)	2-39
	2.2.8.3 Time of Flight Scaling	2-42

TABLE OF CONTENTS (Continued)

		Page
2.2.9	External Cooling of the RPV Lower Head	2-42
2.3	Analyses	2-46
2.3.1	Zion Probabilistic Safety Study	2-46
2.3.2	Sandia's Preliminary Calculation	2-47
2.3.3	HARDCORE	2-47
2.3.4	PARSEC	2-48
2.3.5	Kiva-DCH	2-49
2.3.6	CONTAIN	2-50
2.3.7	Simplified Model for Representing Comparable Debris Dispersal Processes	2-50
2.3.8	Jet Breakup Model	2-55
3.0	METHODOLOGY	3-1
3.1	Mass of Debris Distributed into the Containment Atmosphere	3-1
3.1.1	Extent of Entrainment	3-2
3.1.2	De-Entrainment	3-3
3.2	DCH Pressure Rise	3-4
3.3	Likelihood of Hydrogen Combustion	3-4
3.4	Influence of Uncertainties	3-5
3.4.1	RPV Failure	3-6
3.4.2	RPV Failure Mechanism	3-6
3.4.3	Core Melt Progression	3-7
3.4.4	Extent of Debris Particulation	3-8
3.4.5	Influence of Structures	3-8

TABLE OF CONTENTS (Continued)

Page

3.4.6 Potential for Hydrogen Combustion 3-9

4.0 PLANT SPECIFIC APPLICATION 4-1

4.1 Accident Sequence Characteristics 4-1

4.2 DCH Calculations 4-1

5.0 CONCLUSIONS 5-1

6.0 REFERENCES 6-1

APPENDIX A: Proceedings of the ANS/ENS International Topical Meeting on Probability, Reliability and Safety Assessment, Pittsburgh, Pennsylvania, (April, 1989) . . . A-1

APPENDIX B: Calculation of DCH Temperature and Pressure Rise B-1

APPENDIX C: Hydrogen Combustion Limits C-1

APPENDIX D: Scaling of Entrainment and Displacement Rates D-1

APPENDIX E: Calculational Method for Detrainment at a 90° Turn E-1

LIST OF TABLES

Table No.		Page
2-1	Selected HIPS Experiments	2-7
2-2	Summary of Wood's Metal Injection/Dispersal Tests	2-12
2-3	Summary of Characteristic Dispersal Times	2-13
2-4	ANL CWTI DCH-Related Experiments	2-17
2-5	SNL-DCH Experiments	2-23
2-6	Model Comparisons for DCH Test	2-24
2-7	Zion Cavity Building Block	2-31
2-8	CECo/FAI-DCH Experiments	2-36
2-9	DCH-1 Final Debris Distribution	2-53
2-10	DCH-2 Final Debris Distribution	2-54
4-1	DCH Calculations for Kewaunee Nuclear Plant	4-5
B-1	Oxidation of Debris Constituents in Various Environments	B-7
B-2	Properties of Core Debris Constituents	B-8
B-3	Primary System and Core Debris Conditions for DCH Assessment	B-9

LIST OF FIGURES

Figure No.		Page
2-1	Plan view of the experimental apparatus for the ANL Wood's metal tests, taken from [Spencer, 1983]	2-10
2-2	Location of simulated core debris dispersal in the ANL Wood's metal experiment, taken from [Spencer, 1983a]. In the legend, U_g - gas velocity msec, h/D_t - dimensionless height of water in the reactor cavity.	2-14
2-3	ANL thermite apparatus for the CWTI tests, taken from [Spencer, 1987]	2-16
2-4	Schematic of the Surtsey Direct Heating Test Facility, taken from [Marx, 1989]. The apparatus used in both the DCH-2 and the DCH-3 experiments is shown.	2-20
2-5a	1% linear scale building block experiments/reactor cavity	2-26
2-5b	1% linear scale building block experiments/reactor cavity and seal table	2-27
2-5c	1% linear scale building block experiments/2D representation of the lower compartment	2-28
2-5d	1% linear scale building block experiments/ elevation view of 3D lower compartment	2-29
2-5e	1% linear scale building block experiments/ plan view of 3D lower compartment	2-30
2-6	Elevation view of the vessel interconnection to simulate the containment configuration	2-32
2-7	Cross-section of the melt generator, reactor cavity, instrument tunnel and the simulated lower compartment with structures	2-33
2-8	Relationship of the test configuration to the Zion containment buildings	2-34
2-9	De-entrainment modeling of particles making a 90° turn	2-40

LIST OF FIGURES (Continued)

Figure No.		Page
2-10	Thermal transient in a vessel wall with external cooling	2-45
2-11	Characteristic debris length and displacement length for debris movement	2-52
C-1	Normalized peak pressure (P_{max}/P_o) for hydrogen: air:diluent mixtures, comparing CO_2 and steam (AICC = adiabatic isochoric complete combustion, Rh = relative humidity)	C-2
C-2	Experimental data for combustion limits with fans on and off shown with the exponential curve fit	C-3
E-1	Cavity Instrument Tunnel and Opening Into Lower Containment	E-2
E-2	Coordinate System in Instrument Tunnel	E-4
E-3	Sketch of Kewaunee Cavity and Instrument Tunnel	E-5

ABSTRACT

Phenomenological issues on direct containment heating (DCH) have been examined in support of the Kewaunee Individual Plant Examination Program. The approach taken was to (1) synthesize DCH knowledge from analyses of data obtained from Zion-downscaled mockup DCH experiments, and (2) estimate the potential magnitude of DCH for the Kewaunee plant. From the latter evaluation one can assess if the results of such a postulated phenomena would approach conditions sufficient to challenge the containment integrity.

Experiments performed at Sandia (SNL) and Argonne National Laboratories (ANL) include linear scale representations (up to 10%) of part (the reactor cavity and instrument tunnel) or all of the Zion plant. The available experiments were collectively analyzed to identify, for typical high pressure melt ejection (HPME), the effects of the following factors: the potential for dispersal of debris, the effect of water in the reactor cavity and on the lower compartment floor, and most importantly, structural barriers at the instrument tunnel exit. The support structure for the seal table at the tunnel exit has been identified as an effective separator of entrained debris which would greatly suppress the potential for extensive debris dispersal by de-entraining a significant fraction of debris particulate. These experiments clearly show the influence of containment geometry (structures) in limiting the extent of debris dispersal in the containment atmosphere.

During the IDCOR Program, a set of 1% linear scale "building block" experiments were performed to examine the influence of structures such as the seal table and the lower containment compartment. These single purpose tests demonstrated that these structures had a dominant effect in preventing efficient debris dispersal. If used to assess what should be investigated in larger scale experiments, these results point to the reactor cavity and lower compartment geometry as being of primary importance.

With this extensive background of small scale experiments showing the importance of the containment geometry, 5% linear scale experiments were

performed. These included representations of the reactor coolant system, high temperature core debris, the reactor cavity, important structures immediately outside of the reactor cavity (seal table support, steam generators, reactor coolant pumps, etc.), the lower containment compartment and the upper containment compartment. The test series also included one experiment in which the simulated primary system was pressurized with steam. All four experiments produced very similar results and none of the experiments demonstrated any significant direct heating.

Maximum DCH efficiency found in scaled mockups of Zion was from 0% to 2.5%. Based on this result and the modeling of the de-entrainment process, the best estimate calculations for the Zion reactor system result in an estimated pressurization, due to DCH, of less than one atmosphere. An assessment of a combined hydrogen burn shows the containment atmosphere would be inerted for all sequences. Hence, such a combustion process would not occur. However, even if a hydrogen burn is assumed, the resulting pressure does not exceed the containment ultimate capability.

Of principal interest for the DCH issue are the processes of debris entrainment and particulation in the reactor cavity and the de-entrainment of the debris by structures at the instrument tunnel exit. Both of these were modeled and the models were found to be in agreement with available experimental data. Pressure increases were assessed for the debris thermally equilibrating with the containment atmosphere and also for hydrogen burning and equilibration. It was found that the combination of steam released from the RCS as the accident progresses and the rapid steam generation caused when high temperature debris encountered water in containment, would result in conditions that most likely would inert the containment against a hydrogen burn.

As a result of these evaluations, the pressure rises associated with these conservative assessments would not challenge the Kewaunee containment integrity. Therefore, the containment event trees (CETs) do not include this as a phenomenon which could cause containment failure and a direct release of radioactive materials to the environment.

1.0 PURPOSE

Potential failure of a PWR containment due to debris dispersal and direct heating as a consequence of HPME has been the subject of numerous technical exchange meetings between the Nuclear Regulatory Commission (NRC) Staff, NRC contractors, and the nuclear industry. Discussions have been motivated by the concern that a large fraction of molten core debris exiting a failed reactor vessel during a high-pressure blowdown could be finely fragmented and distributed into the containment atmosphere. The timing of the postulated containment failure has an important ramification regarding the radiological releases. That is, if containment failure due to DCH is postulated, natural fission product deposition mechanisms in the containment would not have time to significantly reduce the masses of fission products that could be released initially through the failure location. In addition, the process of high pressure melt ejection has the potential to increase the fission product inventory released to the containment atmosphere.

In Generic Letter 88-20 [NRG, 1988], the NRG states that results from research concerning containment failure induced by direct containment heating have not been conclusive and utilities should consider strategies to deal with this issue while awaiting its generic resolution. The objective of this paper is to evaluate, with due concern for realistic uncertainties in the physical processes, whether there is a significant likelihood for containment failure due to direct containment heating at the Kewaunee Nuclear Power Plant.

The possibility of a localized vessel failure should severe accident conditions result in molten debris draining into the lower plenum was first addressed in the Zion [CECo, 1981] and Indian Point [Con.Ed. and PASNY, 1982] Probabilistic Safety Studies. Along with this, the possibility of dispersing high temperature debris from the reactor cavity due to rapid steam generation in the cavity or due to a high pressure blowdown of the primary system was considered. Sensitivity analyses in these studies considered the consequences, if the debris were to directly exchange heat with

the containment atmosphere. However, these were not considered to be physically possible because of the lack of extensive debris particulation and influential structures in close proximity to the reactor cavity.

In this regard it is necessary to distinguish between high pressure melt ejection (HPME) and direct containment heating (DCH). The former is the process of hydrodynamically forcing melt out of the reactor cavity due to the primary system blowdown. DCH is the process of directly heating the containment atmosphere by the molten core debris should HPME occur. The Zion and Indian Point studies concluded that the first could occur but second could not. Given the geometry of the Kewaunee reactor cavity and instrument tunnel, and given the conditions for a high pressure melt ejection, such a dynamic debris transfer could occur. Therefore, this report will principally focus on those features which influence the potential for debris transport into, and fine scale interaction with the containment gas space.

2.0 PHENOMENA

2.1 Description

Direct containment heating is a postulated event of rapid heat transfer between finely fragmented core debris and the containment atmosphere assuming (1) the occurrence of post core melt reactor pressure vessel failure at a high pressure and (2) that HPME causes extensive debris dispersal. DCH has been hypothesized as a means of early containment failure because the stored energy of the debris, including potential energy releasable through debris oxidation and hydrogen burning, is enough to cause high containment pressure if a large quantity of the core inventory participates. The extent of pressurization thus depends upon:

- the amount of debris which would be discharged at vessel failure,
- the containment geometry which could be conducive to or an impediment to dispersal beyond the reactor cavity, and
- the fraction of the debris which could be finely fragmented and dispersed into the containment atmosphere.

2.1.1 Controlling Physical Processes

The fundamental issue for DCH is whether a massive dispersion of particulated core debris (tens of tonnes) into the containment atmosphere would be possible. Four steps can be identified which would be necessary for such an outcome.

- First, the plant geometry must be such that debris dispersal could occur from the reactor cavity.
- Second, fine fragmentation of debris must occur and be sustained.
- Third, the debris particles must remain dispersed in the flow stream and be distributed throughout the containment gas atmosphere.

- Fourth, the particles must remain airborne long enough to transfer energy and react chemically if in contact with steam or oxygen.

As will be discussed, some bounding analyses have considered that hydrogen combustion would occur and contribute to a pressure increase which would be in addition to that created by the thermal energy transfer. For this to occur, the atmosphere must be such that hydrogen combustion could be sustained (see Fauske & Associates, Inc., 1991 for hydrogen combustion requirements).

Major impediments to these processes are the inherent inability to entrain and finely particulate debris, the number of directional changes which particles must endure, the presence of structure in the flow path, stagnation of the flow at corners or around obstacles, expansion of the flow path into the compartment, and the presence of water both in the cavity and in the lower or annular compartments. Each of these is briefly characterized below.

High velocity gas flow in the reactor cavity would entrain debris but the act of entrainment would also tend to decrease the gas velocity, thereby causing the reactor cavity to pressurize. (This is the subject of Appendix A [Henry, 1989], which provides the basis for the methodology discussed herein.) This would decrease the entrainment potential and increase the potential for displacement of the debris by pushing it along the wall of the cavity and instrument tunnel. Consequently, only a fraction of the melt would be particulated with the remainder exiting the reactor cavity with a large characteristic dimension.

It would also be difficult to maintain an entrained flow of finely particulated, high density debris. Changes in flow direction, stagnation points, and structures all tend to provide for impaction of the particulate on walls, i.e. de-entrainment. Each change in flow direction tends to separate the heavier debris from the gas stream since the debris would move to the outside of the flow curvature as a result of the large density difference. Only the smaller particles, which could respond to the gas flow

more quickly, could avoid separation from the high velocity gas stream. The particulate captured on the structure walls would form a liquid layer or film and would have to be re-entrained to form particulate. Experiments simulating the Zion reactor cavity (which is not necessarily prototypic for the industry) have shown that most of the debris would be ejected from the cavity. For these experiments, the materials dispersed in the flow have a wide range of size from 10 micron to several millimeters. However, the size range can be strongly influenced by the extent of the containment geometry modeled in the experiment. As will be discussed later, virtually all of the dispersed mass is associated with the larger particle sizes when the lower containment compartment structures are modeled. These sizes result in a very inefficient heat transfer process between the hot debris and the containment gases, as demonstrated by the relevant experiments.

Water would have substantial mitigating capacity in direct containment heating scenarios. In many cases, some water would be present in both the reactor cavity and the lower compartment and for others the cavity would be entirely flooded. With the exception of containment bypass sequences with no flow back to the pressurizer relief tank, there would always be water on the containment floor; likely to a depth of at least 15 cm (6 in). Also, for those sequences in which sufficient water would be injected and accumulated in containment to submerge the RPV lower head, CECo sponsored experiments performed at FAI indicate that failure of the vessel wall would not occur [Fauske & Associates, Inc., 1991]. Hence, if the vessel penetrations maintain their integrity, as was clearly the case in the TMI-2 accident, the RPV lower head would not be breached and debris would not be discharged to the containment. Obviously, water would have a major influence on these sequences.

For those sequences with limited water in the reactor cavity which could progress to RPV failure, debris discharged from the vessel breach would undergo dynamic interactions and rapid heat transfer to the water upon impact. Subsequent removal of debris from the cavity would occur simultaneously with removal of the water, and quenching would continue in this multiphase stream. Experiments involving water in the simulated cavities and on the containment floor have consistently verified the efficacy of

water as a mitigator. This will be discussed further in the context of the CECo/FAI 5% linear scale experiments.

Expansion (deceleration) of the flow from the instrument tunnel into the lower or annular compartment and the presence of the extensive structure therein allows for significant de-entrainment and deposition of most particle sizes. As the flow area increases, flow velocities decrease and large particles would no longer remain airborne. Also, impaction on structures would serve to remove particles of all sizes. Only that fraction of the debris which could persist as fine particulate could substantially contribute to direct containment heating.

2.1.2 Relationship to Containment Failure Mechanisms and Modes

Direct containment heating is a postulated mechanism for containment failure immediately after reactor vessel failure. If such a mechanism could occur, the largest potential for the occurrence would be expected during core melt accident scenarios that would maintain a high reactor vessel pressure until the time of vessel failure. The containment failure mechanism would be overpressurization due to a rapid increase in gas temperature as the core debris thermal and chemical energy is transferred to the gas.

2.1.3 Relationship to Source Term

Prior to the core debris transport into the lower plenum which could lead to vessel failure and high pressure melt ejection, fission products such as the noble gases, iodine, cesium and perhaps tellurium would have been released from the fuel matrix and into the primary system. For such conditions, significant quantities would likely be released to the containment through openings in the RPV pressure boundary such as PORV operation, a break in the RCS, failure of the in-core instrument thimbles during the core melt progression process, etc. In addition, the fine particulation of core debris in the reactor cavity, due to high pressure melt ejection, could liberate additional fission products to the containment atmosphere (Appendix A). Therefore, any postulated process which would fail the containment

shortly after RPV failure would also likely occur when the airborne fission product inventory in containment would be at, or near, the maximum. Hence, the potential release would also be at a maximum. After this point in time, the airborne fission products would decay with time due to natural deposition mechanisms such as sedimentation, impaction, condensation, etc.

For sequences with water in the cavity or containment sprays activated, the expected fission product source term would be reduced relative to a dry cavity sequence due to the enhancement of fission product aerosol capture by impaction of the aerosol particles and spray droplets or by increased Stefan flows to steam condensing surfaces. These sequences would also provide an additional heat sink (water) to quench the core debris by steam generation, which also inhibits or prevents hydrogen combustion. The use of sprays also would cool the containment atmosphere, as well as the deposited debris, and to some extent the surface of the RCS, thereby minimizing or eliminating revaporization from the reactor vessel into the containment gas space. Should revaporization and release from the vessel occur, the sprays would scrub the fission products from the atmosphere. Functionally, the injection of water into a reactor vessel with a lower head failure would accomplish the same objectives, i.e., cooling the debris, preventing or minimizing revaporization and establishing long term coolability. Injection into a vessel would essentially prevent any revaporization by cooling the inner RPV surfaces but would be somewhat less effective in scrubbing fission products from the containment atmosphere.

2.2 Experimental Results

Several investigations have been performed and documented which provide a data base for understanding direct containment heating phenomena. These experiments have been carried out at Argonne National Laboratory, Sandia National Laboratory, Brookhaven National Laboratory and Fauske & Associates, Inc. Results of these experiments are briefly described here. Many of the experiments only relate to processes in the reactor cavity and the potential for removal of debris from the cavity. Those experiments which only represent the reactor cavity provide no additional insight to this issue for the Kewaunee IPE and are only briefly summarized below. Therefore, experimental programs related to the influence of structures will be discussed in depth.

2.2.1 Sandia HIPS Experiments

The Sandia HIPS experiments (High Pressure Melt Streaming) [Tarbell, 1984] were conducted following the SPIT series to confirm the dispersal of debris from a simulated cavity geometry and to assess the phenomena of jet geometry, gas solubility, and aerosol generation [Tarbell, 1986a]. In those tests which have been reported [Tarbell, 1986b and Pilch, 1986], a 1:10 linearly scaled model of the Zion cavity was used. This model was either open to the desert or placed within an expansion chamber with one end open to the desert. No attempts were made to maintain the geometric similarity of containment internal structures of Zion for these experiments. Iron-alumina thermite charges with masses of about 176 lb (80 kg) were used. A table of reported tests presented in Reference [Pilch, 1986] is reproduced here as Table 2-1.

In experiments (HIPS-3C, -7C, and -8C) carbon dioxide was used as the cover gas, at pressures between about 3 MPa (435 psia) and 5.6 MPa (812 psia). Pressures as high as 11.7 MPa (1697 psia) were used in two other tests (HIPS-2C and -4W). In two reported experiments (HIPS-4W and -6W), a water-filled cavity was used, and destroyed by overpressure during the blowdown. One experiment (HIPS-8C) featured an annular gap around the thermite generator, simulating the gap around the RPV if the insulation were

Table 2-1

SELECTED HIPS EXPERIMENTS

Test Name	Scale	Thermite Mass (kg)	Thermite Mass (lbm)	Initial Vessel Pressure (MPa)	Initial Vessel Pressure (psia)	Extent Dispersal (%)	Water In Cavity
SPIT-19	1:20	10.3	22.7	12.6	1827	95	No
HIPS-2C	1:10	80.0	176	11.7	1697	99	No
HIPS-4W	1:10	80.0	176	11.7	1697	~95*	Yes
HIPS-5G	1:10	80.0	176	6.7	972	99	No
HIPS-6W	1:10	80.0	176	3.8	551	~95*	Yes
HIPS-7C	1:10	81.5	179	5.5	798	98	No
HIPS-8C	1:10	80.0	176	3.7	537	98	No

*Cavity destroyed during test.

assumed to be removed. The reflective insulation used has substantial strength relative to the expected phenomena, particularly in rapid transient events. Therefore, tests which ignore the insulation do not represent the response of the RGS and containment and are not used in our assessment.

For all the HIPS tests, dense aerosol clouds surrounded the debris jet, and sweepout from the cavities was nearly complete in all cases, above 95%. After tests in which the cavity was placed inside the confinement room, this debris was found either within the room or on the concrete pad just outside its open end. While not an actual representation of the plant configuration, this test series demonstrated the substantial influence of structures to capture the debris outside of the reactor cavity/instrument tunnel.

In the HIPS-7C tests, over 30 percent of the debris was found in the rear of the confinement chamber, much of it against the rear wall. Observations with high speed films show that debris exiting the cavity splashed off the ceiling and rained down in that location. Over 97 percent of the original melt mass was recovered from the chamber and concrete pad, and the rest either landed on the ground beyond the pad or was in the aerosol cloud which billowed out. Thus, the confinement chamber does not model the lower containment structures. On the other hand, it does illustrate that a minimal representation of the structure results in substantial removal of the debris from the gas stream.

In the HIPS-8C tests, aluminum collection pans were placed on the chamber floor to determine the spatial distribution of debris exiting the cavity, and deduce which fraction exited through the keyway outlet, and which fraction exited through the angular gap around the melt generator. About 25% of the debris was concluded to have been released through this gap, deflected off the ceiling, and fallen into pans around the melt generator. This corresponds to the area fraction taken up by the annular opening assuming the insulation had been removed. As mentioned above, this is not representative for the RCS because the reflective insulation around the reactor vessel was not represented in any manner.

2.2.2 Argonne Wood's Metal Tests

The influence of the containment configuration outside the reactor cavity and instrument tunnel was demonstrated by the isothermal Wood's metal experiments [Spencer, 1983a]. In these tests, the Zion reactor cavity-instrument tunnel configuration was mocked-up along with the seal table and biological shield inside the crane wall (missile barrier). Wood's metal, which has a melting temperature of 73°C (163°F) and a density of about 9500 kg/m^3 (593 lbm/ft^3), was used to simulate the debris. The experimental configuration is illustrated in Figure 2-1, and the experimental conditions are summarized in Tables 2-2 and 2-3. As shown in these tables, the parameters investigated included various masses of water initially accumulated within the reactor cavity as well as different gas velocities through the cavity following molten metal discharge from the simulated reactor vessel. The results of these experiments are shown in the bar graphs of Figure 2-2, which is taken from Reference [Spencer, 1983a]. The final debris configuration is reported in terms of (1) the material left within the reactor cavity, (2) that which was dispersed within one equivalent diameter of the instrument tunnel exit, and (3) that fraction of debris dispersed beyond one equivalent diameter of the instrument tunnel. High speed movies showed that a large fraction of the debris is initially transported as a large wave moving along the outer sloping surface of the instrument tunnel which impacts upon the bottom surface of the seal table. The results demonstrate that the structure in the lower compartment is very effective in separating the debris from the high velocity gas stream and depositing the debris on the containment floor in close proximity to the instrument tunnel. More specifically, the structure has a first order effect on the debris distribution in the simulated containment.

2.2.3 Argonne CWTI Experiments

EPRI sponsored a series of reactor material experiments at Argonne National Laboratory known as the CWTI tests (Corium/Water Thermal Interaction) [Spencer, et al., 1983b, Spencer, et al., 1987 and Spencer, et al., 1988]. The experimental configuration represented some major features

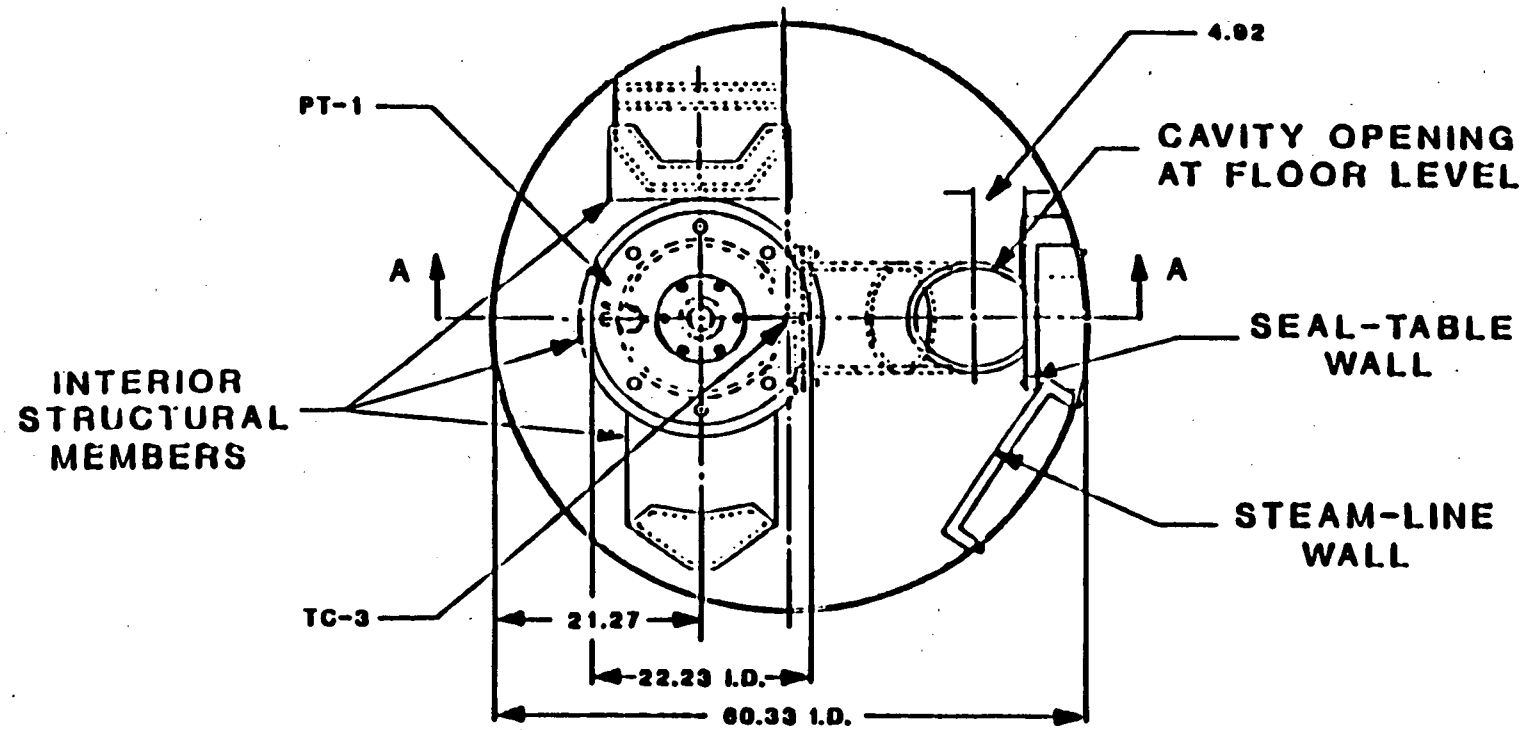

NOTE: ALL DIMENSIONS IN CENTIMETERS

Figure 2-1 Plan view of the experimental apparatus for the ANL Wood's metal tests, taken from [Spencer, 1983].

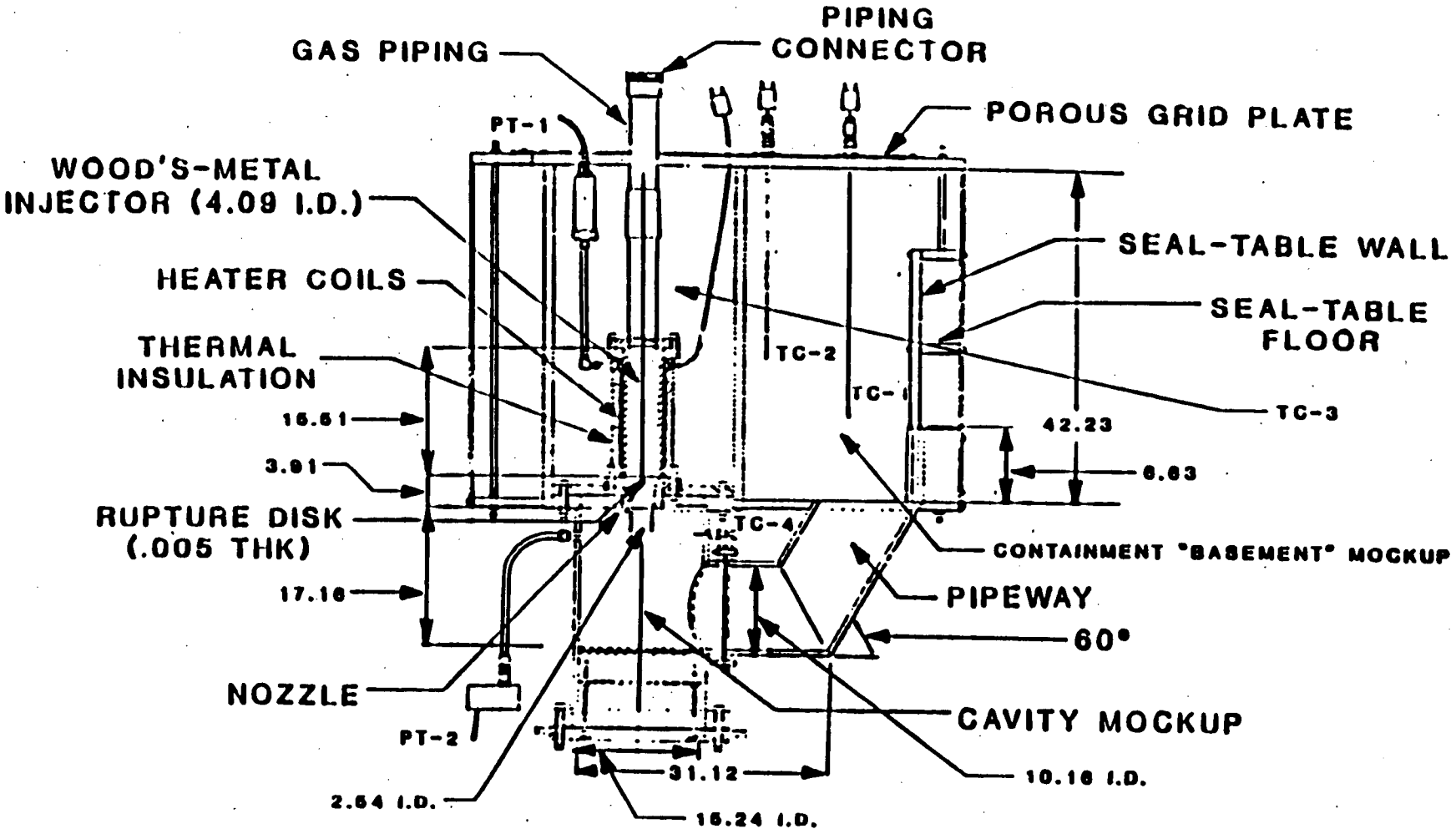

SECTION A-A

NOTE: ALL DIMENSIONS IN CENTIMETERS

Figure 2-1 (cont'd) Plan view of the experimental apparatus for the ANL Wood's metal tests, taken from [Spencer, 1983].

Table 2-2

SUMMARY OF WOOD'S METAL INJECTION/DISPERSAL TESTS

Test Number (Old Ref.)	1 (17)	2 (18)	3 (19)	4 (20)	5 (21)	6 (22)	7 (24)	8 (25)	9 (26)	10 (27)	11 (28)
Injected Material (1)	Gas Only	WM	WM	WM	WM	WM	WM	WM	WM	WM	WM
Cavity Water Level, h/D_t (2)	0.5	Dry	0.1	0.1	0.5	1.0	0.1	0.1	0.5	1.0	Dry
Injector Temperature, °C/°F	---	89/192.2	91/195.8	75/192.2	89/192.2	90/194	89/192.2	88/190.4	87/188.6	88/190.4	89/192.2
Injection Pressure, MPa/psia	0.65/94.25	0.70/101.5	0.68/98.6	(3)	0.55/79.75	0.68/98.6	0.68/98.6	0.30/43.5	0.25/36.25	0.25/36.25	1.40/203
WM Injection Velocity, m/s/ft/s	7.8/25.57	7.8/25.57	7.8/25.57	7.8/25.57	7.8/25.57	7.8/25.57	7.8/25.57	5.4/17.70	5.4/17.70	5.4/17.70	11.7/17.70
Gas Velocity (4° pipe), m/s/ft/s	28/91.80	29/95.08	27/88.52	28/91.80	27/88.52	29/95.08	9.7/31.80	9.3/30.49	9.3/30.49	9.4/30.82	35/114.75
Maximum Cavity Pressurization, kPa	---	10	35	20	80	190	33 (4)	10	60	120	50

NOTES: (1) WM = Wood's Metal (T_{ep} = 73°C).

(2) D_t = pipeway diameter, 10.2 cm.

(3) WM frozen in PT standoff line.

(4) High pressure caused cavity apparatus to rupture at 60° pipe elbow.

Table 2-3

SUMMARY OF CHARACTERISTIC DISPERSAL TIMES

Test Number (Old Reference Number)	1 (17)	2 (18)	3 (19)	4 (20)	5 (21)	6 (22) (4)	7 (24)	8 (25)	9 (26)	10 (27)	11 (28)
Emergence of WM at cavity top, ms	(1)	0	0	0	0	0	0	0	0	0	0
WM contects water/bese ms	---	23	26	25	22	13	26	37	26	18	15
Water crater contects bese, ms	6	---	(2)	(2)	32	32	(2)	48	42	45	---
Creter rim grows redially to R_o, ms	---	---	38	36	36	38	32	---	64	---	---
Gas breaks through at WM treiling edge, ms	---	46	47	39	45	45	43	64	61	58	23
Crater rie/splash grows in amplitude to occlude pipeway, ms	10	---	49	41	47	(3)	46	65	63	(3)	30
Start of water slug dispersal, ms	21	---	76	61	68	66	68	93	88	80	---
End of water slug dispersel, ms	48	---	99	83	108	---	87	110	117	117	---
Horizontal weter jet at seal table recess, ms	36	---	(6)	101	103	95	97	---	122	124	---
Stert of WM dispersel, ms	---	84	(2)	(2)	(2)	~90 est	106	150	(2)	(2)	41
End of water dispersal, ms	290	---	~200	~200	~500	---	~300	~300	~1500	~1500	---
End of WM dispersal, ms	---	650	950	800	~1200	860(5)	~300	~300	---	---	350

NOTES:
(1) Time of gas releaso by rupture disk breach = 0 ee.
(2) Not discernable.
(3) Water occludee pipoway as en initial comdition.
(4) Bend in pipewey failad at 104 ms whila watar alug ejoction was still in progress.
(5) Dispersal took pleca out horizontal piepway stub only.
(6) Upper ceeere did not function.

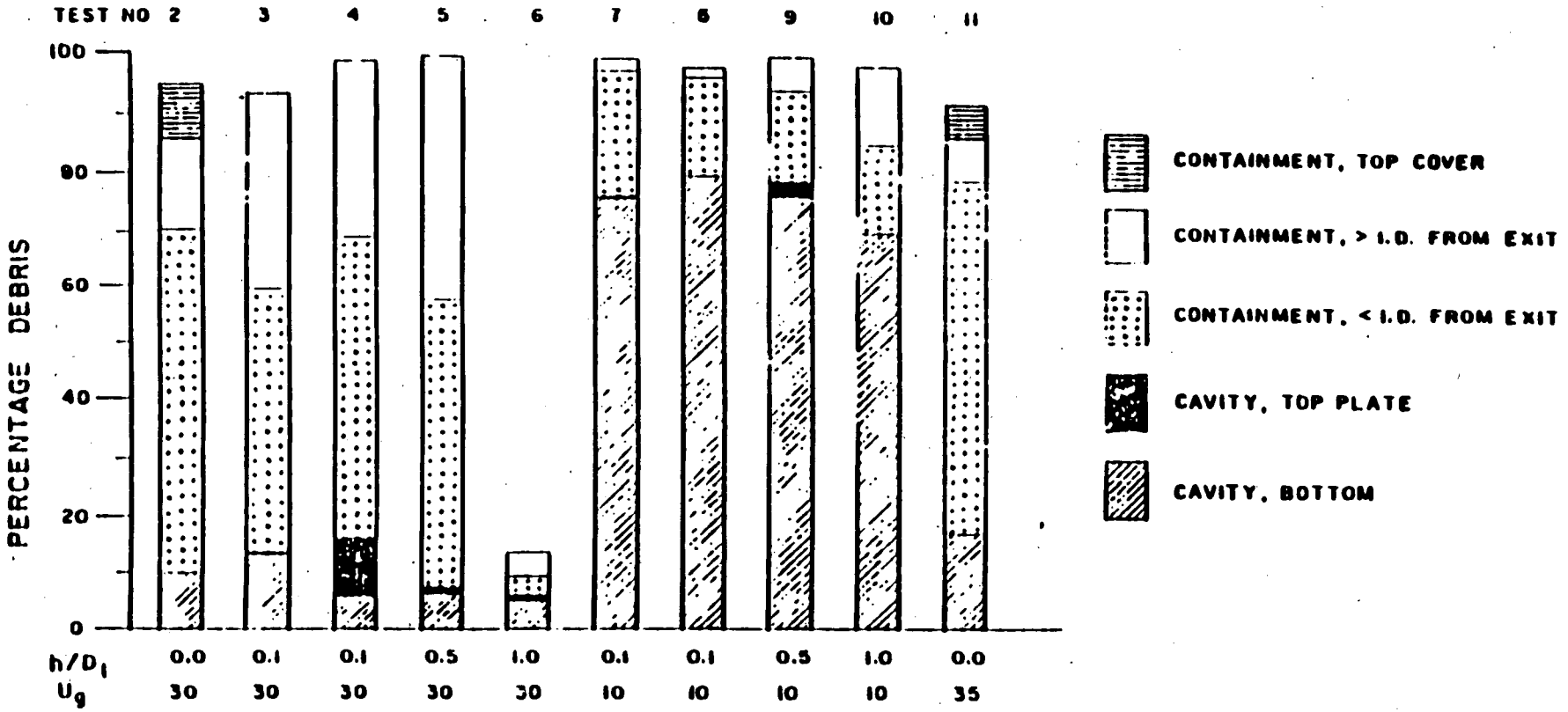

Figure 2-2 Location of simulated core debris dispersal in the ANL Wood's metal experiment, taken from [Spencer, 1983a]. In the legend, U_g - gas velocity m/sec, h/D_t - dimensionless height of water in the reactor cavity.

of a typical PWR large dry lower containment compartment, cavity, and the upper compartment at a 1:30 linear scale. Reactor materials (principally UO_2 and stainless steel) were used and were created by an exothermic thermite reaction. Molten debris was injected downward into a simulated cavity and keyway, see Figure 2-3, which was connected to an expansion volume that was partitioned like the lower and upper compartments of a containment. In some tests, water was present either in the cavity or the expansion volume or both. The objectives of these tests were to examine heat transfer between core debris and water, sweepout of water and core debris from the cavity, steam generation, hydrogen generation, and to characterize the spatial distribution of dispersed debris.

The test apparatus included the thermite reaction vessel (which is the source of the molten core debris), an interaction vessel (which represents the reactor cavity), a pipe simulating the instrument tunnel, an expansion vessel representing the containment, a "trap" above the pipe discharge to simulate a seal table and a baffle plate to separate the expansion vessel into upper and lower compartments. The simulated core debris produced by the thermite reaction was composed of 60% UO_2, 16% ZrO_2, 24% stainless steel (67% Fe, 21% Cr, 12% Ni) and had a temperature of about 3100 K (5120°F).

Tests were performed with low (less than 0.5 MPa or 75 psia) and high (~ 5 MPa or 725 psia) pressure blowdowns as well as with inert and oxidizing atmospheres. Several different initial water level conditions were tested in the interaction vessel ranging from completely empty to essentially full of water before the melt was released from the thermite furnace. Initial conditions and results for DCH-related CWTI tests are listed in Table 2-4 (adapted from [Spencer, 1988]).

The DCH-related tests were conducted by starting a thermite reaction at nominally atmospheric pressure. The melt was subsequently pressurized (by gas from external high pressure gas cylinders) to burst a bottom diaphragm and initiate melt ejection. The duration of the gas blowdown was sufficiently long to assure sweepout of all available melt. Debris that was not swept out remained as a 1 ~ 3 mm thick crust uniformly deposited on the wall of the interaction vessel and the entire pipe surface (for CWTI-5 and -6).

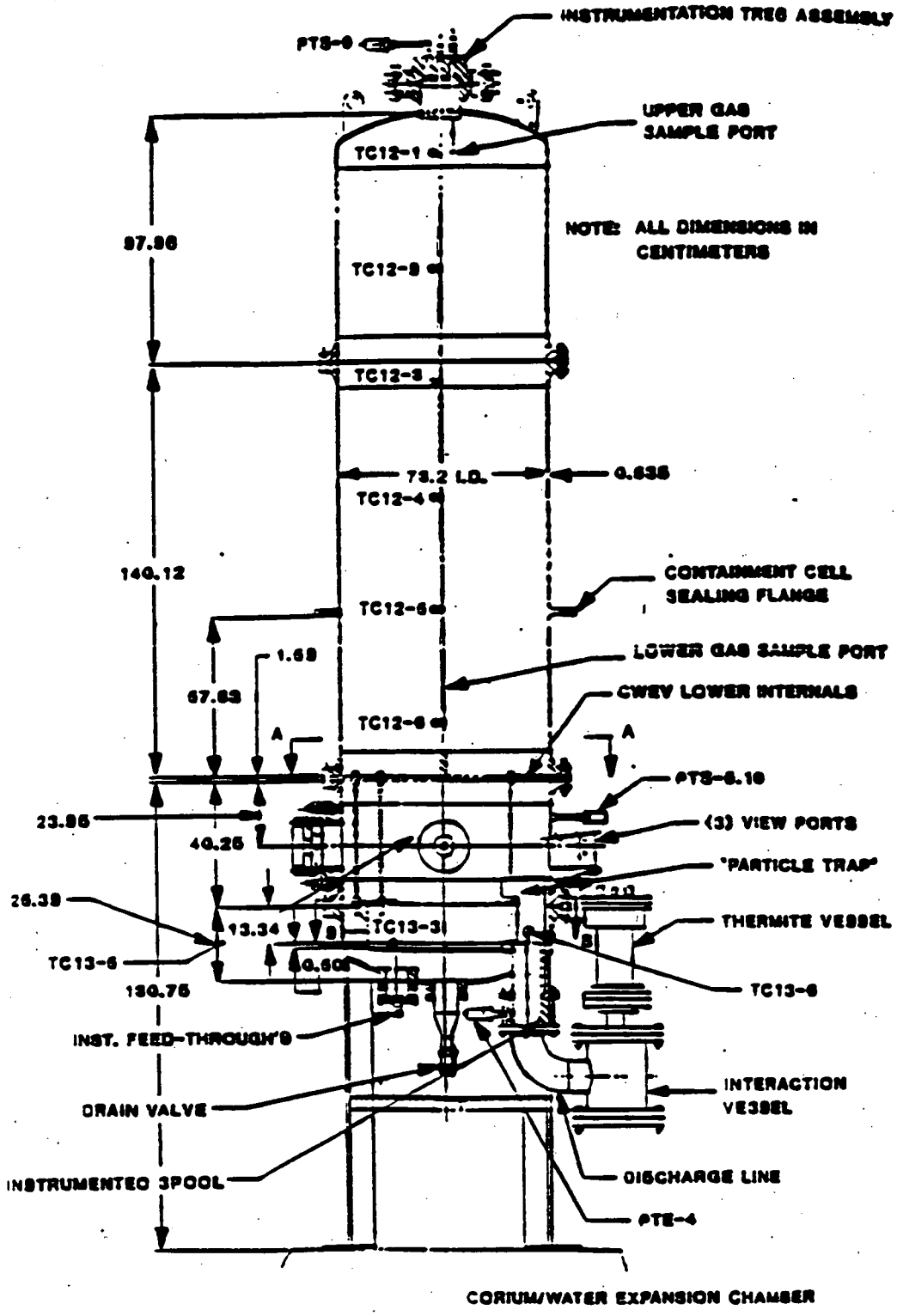

Figure 2-3 ANL thermite apparatus for the CWTI tests, taken from [Spencer, 1987].

Table 2-4

ANL CWTI DCH-RELATED EXPERIMENTS[1]

Test No.	5	6	11	12	13
Driving Pressure, MPa/psia	5.0/725	4.7/681.5	5.1/739.5	2.8/406	4.0/580
Atmosphere	Ar	Ar	air	air	air
Corium Mass Injected, kg/lbm	3.94/8.67	3.75/8.25	2.93/6.45	2.69/5.92	2.27/4.99
Corium Mass Swept Out, kg/lbm	2.44/5.37	1.21/2.66	0.88/1.94	1.31/2.88	0.20/.44
Corium Mass Remained, kg/lbm	1.5/3.3	2.54/5.59	2.05/4.51	1.38/3.04	2.07/4.55
Water in Cavity, kg/lbm	5.6/12.32	dry	dry	4.6/10.12	dry
Disporsal Impediments	s/b[2]	e/b	s/b	none	nomo
Atmosphere Initial Temp, K/°F	419/294.2	408/274.4	411/279.8	422/299.6	298/76.4
Atmosphere Peak Temp, K/°F	417/290.6	461/369.8	435/323	407/272.6	621/657.8
Atmosphere Initial pressure, MPs/psia	0.52/75.4	0.22/31.9	0.22/31.9	0.37/53.65	0.32/46.4
DCH Efficiency[3], %	0	5	1	0	62

[1] 3.33% linear scale model of Zion.

[2] s/b = shroud/baffle.

[3] DCH Efficiency = $\frac{\text{Measured Atm. Heatup}}{\text{Max. Equilibration Atm. Heatup}} \times 100.$

Various mass fractions of debris were observed to be dispersed from the reactor cavity into the simulated containment volume. Debris was collected at various locations in the apparatus including (1) the interaction vessel and pipe, (2) the "particle trap/reflector" at the top of the pipeway as it exited into the bottom of the expansion vessel, (3) on the floor of the simulated containment, and (4) on the top of the simulated lower compartment which represented the operating deck. Characteristic particle sizes for the debris swept out into the air atmosphere ranged from 64 to 700 microns for tests CWTI-11 and -13, which had no water in the cavity. Most particles were in the range 100 ~ 300 microns [Spencer, 1988]. The experiments with water in the interaction vessel or expansion volume prior to melt ejection demonstrated the effectiveness of water for removing heat from dispersed debris, including the energy released due to oxidation. These tests exhibited little or no direct containment heating. Results for test CWTI-12 show no significant contribution to DCH with the codispersal of debris and water into the containment atmosphere. Test CWTI-12 was performed without the presence of the impeding structure and clearly demonstrates the influence of codispersed water. Modest direct containment heating was observed in tests CWTI-6 and -11 which had water only in the pan of the expansion vessel (containment floor). The largest atmospheric heating occurred in test CWTI-13 where no structures and no water were present in either the interaction vessel (cavity) or expansion vessel (containment). This heatup was caused by a sweepout mass of only 0.2 kg. Hydrogen generation and/or oxygen depletion that occurred during these tests were also measured to determine the extent of oxidation and its contribution to the overall energy input to the system.

The most important observation from the ANL experiments concerns the influence of structure on debris dispersal. The "particle reflector" in this experiment was a simulation of the in-core instrument tube seal table configuration in a Zion-like containment. The horizontal baffle plate above the "particle reflector" represented the floor separating the Zion containment into upper and lower compartments. Comparison of results from CWTI Tests 6, 11, and 13 reveals the effect of structure on direct containment heating. All three of these tests were performed with a dry interaction

vessel (reactor cavity), but Tests 6 and 11 included structure in the expansion vessel (containment) while test 13 had no structure. The DCH efficiencies (whose definition is given in Table 2-4 and calculated in [Spencer, 1988]) for Tests 6 and 11 were 5% and 1%, while the DCH efficiency for Test 13 was reported as 62%. Thus, the substantial effect of the seal table structure was to prevent a significant fraction of the debris from entering the containment atmosphere directly. Because of the structure, a major fraction of the entrained debris was deposited on the lower containment floor.

2.2.4 SNL-DCH (Surtsey) Experiments

Sandia has also conducted a series of experiments designated as Surtsey [Tarbell, 1987a; Tarbell, 1987b; Tarbell, 1988a; Tarbell, 1988b]. Experiments DCH-1, 2, 3 and 4 used cavity configurations similar to those of the HIPS 1:10 experiments. These cavities have been completely enclosed in a large expansion vessel, i.e. 3637 cubic feet (103 m^3) capacity and a 145 psia (1.0 MPa) design pressure. No attempts were made to represent the geometry of any containment internal structures such as the seal table, the lower compartment, the operating deck, etc. At the time of this writing, four tests have been performed, and results have been presented in detailed reports for two of these tests [Tarbell, 1987 and Tarbell, 1988a].

DCH-1 involved 44 lb (20 kg) of molten iron-alumina thermite injected into a 1:10 linear scale model of a cavity only, with a nonprototypic exit guide box added to the instrument tunnel exit to direct debris vertically upward along the centerline of the vessel. Figure 2-4 illustrates the Surtsey facility. The thermite was propelled with nitrogen gas initially at 2.55 MPa (370 psia). Peak pressures ranged from 0.09 MPa (13 psia) to 0.13 MPa (18.9 psia) and were achieved less than one second after debris dispersal. High speed film shows that debris shooting upward at 40 m/s (131 ft/s) expanded laterally and filled the entire chamber cross-section within a few meters of the cavity exit.

About 11.6 kg (25.5 lb) were dispersed from the cavity, which includes the correction for estimated oxidation. Melt retained within the cavity and

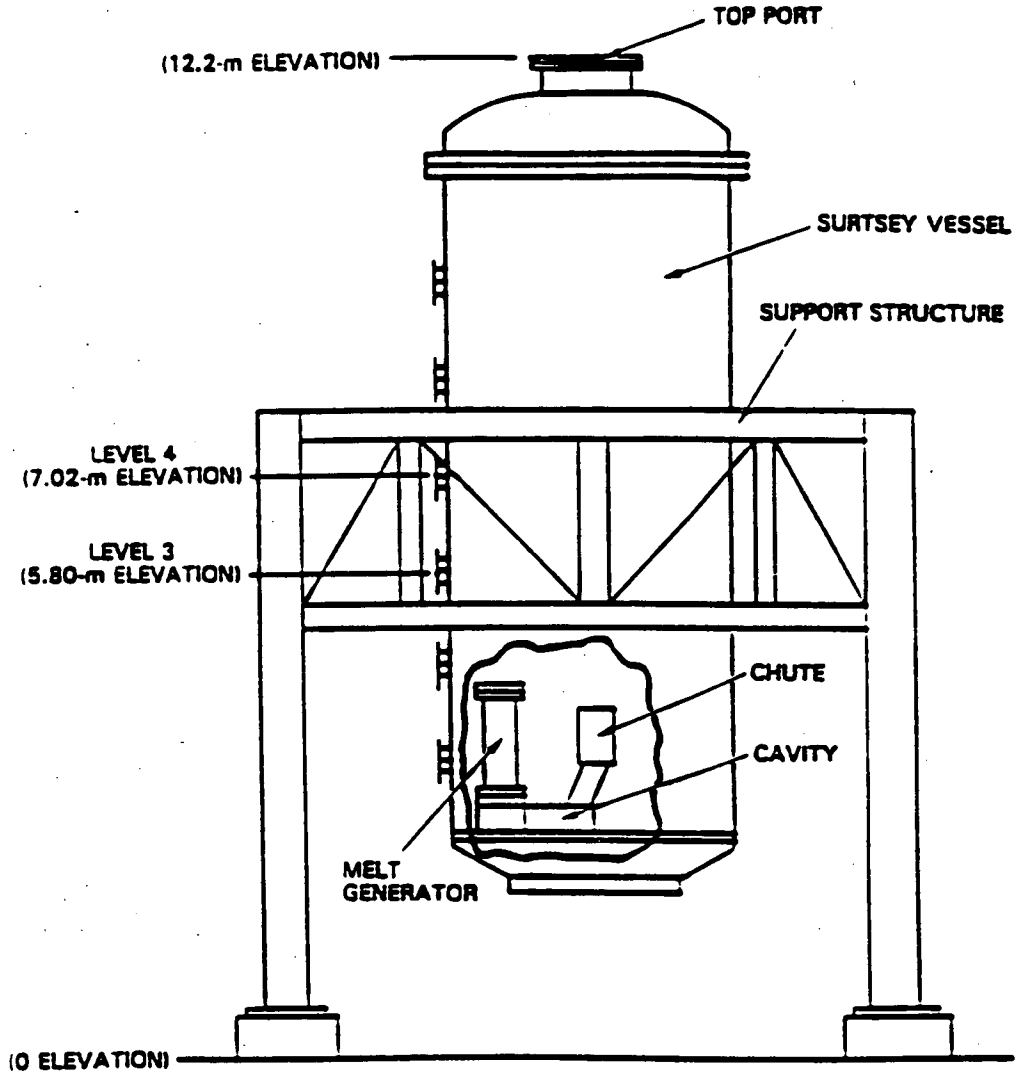

Figure 2-4 Schematic of the Surtsey Direct Heating Test Facility, taken from [Marx, 1989]. The apparatus used in both the DCH-2 and the DCH-3 experiments is shown.

chute was in the form of a thin crust, and a 1.2 kg (2.64 lb) mass was found at the base of the keyway inclination. Aerosol measurements indicated that much material was fragmented to a size under 10 microns, but the measurements may be inaccurate and a large uncertainty is present in the actual amount of such material. The calculated range of aerosolized debris was 5 to 25 percent of the dispersed mass. Mechanical sieving of debris collected in the chamber showed a log-normal size distribution with a mass mean size of 0.55 mm. Thus the bulk of the debris ejected from the cavity was of millimeter size. This test was analyzed using the methodology described in [Henry, 1989] and good agreement was obtained when the specific configuration without structure was considered.

DCH-2 involved 80 kg (176 lb) of molten iron-alumina thermite injected into the same 1:10 linear scale model of a cavity and instrument tunnel with a nonprototypic exit guide box. The thermite was propelled with nitrogen gas initially at 982 psia (6.77 MPa) and peak pressures ranged from 0.22 MPa (32 psia) to 0.31 MPa (45 psia), and were achieved less than one second after debris dispersal. High speed film shows that debris leaving the guide box expanded laterally and filled the entire chamber cross-section within a fraction of a second, likely indicating that the debris-gas two-phase mixture was "choked" at the exit of the guide box.

The total mass recovered from the test chamber, cavity, and melt generator was about 99.5 kg (219 lb), which represents an increase in mass of 24%. This attributed to several potential sources related to the construction of the apparatus and test conduct as well as oxygen uptake by oxidation of the iron in the thermite. The latter source was considered to be the most dominant mechanism. About 91.3 kg (201 lb) were dispersed from the cavity. Five types of debris were identified, with each type being generally associated with a particular area of the apparatus. On the upper third of the vessel in line with the cavity exit, 1-2 mm thick sheets of brittle debris were tightly bonded to the wall. Debris stuck to lower portions of the vessel wall was loosely bonded and formed sheets of 2-4 mm thickness. On horizontal surfaces, debris was found to be approximately 1-mm diameter spheres, and agglomerations of such spheres with irregularly-shaped masses of previously molten debris. Melt retained within the cavity

and chute was in the form of a thin crust, and a 4.4 lb (2 kg) mass was found directly underneath the melt generator. This test was also analyzed using the methodology described in Appendix A and found to be consistent with the proposed methodology considering the simplified geometry used in the experiment.

DCH-3 and DCH-4 were recently reported [Allen, 1991]. The overall results are summarized in Table 2-5 [Tarbell, 1987a]. Test DCH-1 as reported in [Tarbell, 1987b], had the largest efficiency of energy transfer from the debris to the atmosphere with > 90%, while the DCH-4 test was lowest with nominally 35%. The latter was affected strongly by the absence of chemical energy release because of the lack of oxygen in the chamber atmosphere. For consumption of oxygen in the chamber, the degree of oxidation in the DCH-1 test was the greatest, while the DCH-3 debris was the least oxidized. As discussed previously, the methodology presented in Appendix A [Henry, 1989] constitutes part of this assessment. Table 2-6 compares the methodology with the SNL DCH tests. There is good agreement with the measured results when the simplified geometry of the experiments is considered. Therefore, the difference between the SNL experiments and the evaluation of the reactor system is dominated by the absence of structure and not by the experimental scale, the materials used or the driving medium (nitrogen or steam).

2.2.5 BNL Simulant Fluid Test

Brookhaven National Laboratory has performed a series of simulant fluid tests to investigate the extent of entrainment in the reactor cavity and the influence of reactor cavity geometry [Tutu, 1988]. Scaled (1/42) models were constructed of the Zion, Surry and Watts Bar reactor cavity and instrument tunnel configurations. Of particular note for this application is that models of the Zion containment [Ginsberg, 1988] "suggest that the structures exert a strong influence on the flow which issues from the cavity, redirecting the flow and, very likely, changing its droplet size characteristics". These observations clearly point to the inclusion of containment structures in both experimental studies and plant applications such as an IPE.

Table 2-5

SNL-DCH EXPERIMENTS[1,2]

Test	Driving Pressure MPa/psia	Driving Gas	Thermite Mass (kg/lbm)			Atmosphere	
			Initial	Swept-Out	Remained	Peak Temp °C/°F	Peak Press MPa/psia
DCH-1	2.4/348	N_2	20/44	~10/22	~10/22	260/500	0.095/13.78
DCH-2	6.8/986	N_2	80/176	~76/167.2	~4/8.8	880/1616	0.225/32.63
DCH-3	6.0/870	N_2	80/176	~75/165	~5/11.0	860/1580	0.205/29.73
DCH-4[3]	6.9/1000.5	N_2	80/176	~74/162.8	~6/13.2	860/1580	0.19/27.55

[1]10% linear scale model of Zion cavity only, no representation of the containment structures outside of the reactor cavity/instrument tunnel.

[2]Dry cavity and containment.

[3]Inert atmosphere.

Table 2-6

MODEL COMPARISONS FOR DCH TEST

Test Parameters/ Predictiona Measurements	DCH-1	DCH-2	DCH-3	DCH-4
1. Geometrical Parameters end Vessel Presaure				
A_v (m^3/ft^3)	0.002/.021	0.002/.021	0.002/.021	0.002/.021
A_s (m^3/ft^3)	0.5/5.37	0.5/5.37	0.5/5.37	0.5/5.37
L_p (m/ft)	2.8/9.18	2.3/7.54	2.8/9.18	2.8/9.18
L (m/ft)	1.45/4.75	1.45/4.75	1.45/4.75	1.45/4.75
A_c (m^3/ft^3)	0.06/.645	0.06/.645	0.06/.645	0.06/.645
P_v (MPa/psie)	2.5/362.5	6.8/986	6.0/870	6.9/1000.5
2. Debris Sise				
Predicted (μm/ft)	240/.00079	65/.00021	40/.00013	30/.000090
Measured Maas Mean (μm/ft)	550/.0018	Rot Availeble	Not Aveilable	Net Aveilable
3. Mese Diapersed as Fine Particulete				
Predicted (kg/lbm)	20/44	27/59.4	31/68.2	33/72.6
Meaaured (kg/lbm)	11.6/25.52	33/72.6 (Masa Depoeited en tbe Lower Keed)	18.4/40.48 (Mass Deposited on the Lower Heed)	30/66 (Masa Deposited en the Lower Seed)
4. Peak Temperaturo				
Predicted	681/765.8 (Using Measured Msss Dispersed)	1032/1397.6	1104/1527.2	1138/1588.4
Measured (K/°F)	501/441.8	1150/1610	1193/1687.4	1193/1687.4
5. Peak Pressure				
Predicted (MPa/psia)	0.19/27.55 (Using Measured Mass Diapersed)	0.30/43.5	0.32/46.4	0.33/47.85
Measured (MPa/psia)	0.18/26.1	0.33/47.85	0.28/40.6	0.27/39.15

2.2.6 IDCOR/FAI Wood's Metal Tests

During the IDCOR Program, a set of "building block" experiments were performed with the single purpose of demonstrating the extensive influence of structures in the lower compartment. These 1% linear scale models began with the reactor cavity and instrument tunnel, added the seal table, expanded this to a two-dimensional representation of the lower compartment and completed the test series with a three-dimensional representation of the lower compartment. The same driving pressure of nitrogen gas (2 MPa/300 psia) mass of Wood's metal (0.3 kg/10.66 lbm) was used in all tests and the principal measurement was the fraction of the Wood's metal retained in the test section. Figures 2-5a through 2-5e illustrate the various test sections used to sequentially add the influential structure. Table 2-7 lists the Wood's metal retained in the test apparatus and shows that, with only the seal table, virtually no material remains; yet with the 3-D lower compartment, essentially all of the simulated core material remains in the lower compartment, most of it close to the instrument tunnel. (If we assume that the debris which is not retained in the lower compartment could cause direct heating, these results suggest the process would have an efficiency of only about 2.5%.) The observations with respect to structures agree completely with those from the ANL Wood's metal experiments and clearly show the first order influence of structure.

2.2.7 FAI-DCH Experiments

A jointly funded Commonwealth Edison and Fauske & Associates, Inc. experimental program was established and carried out at Fauske & Associates, Inc. [FAI, 1990]. The program addressed the issue of direct containment heating in support of the Zion IPE. In keeping with lessons learned from smaller scaled tests, these experiments were conceived and designed to have a 5% linear scale simulation of the reactor cavity, instrument tunnel, lower compartment (including two steam generators, two reactor coolant pumps and the refueling canal wall) and upper compartment of the Zion containment building. Figures 2-6 and 2-7 show the experimental apparatus and Figure 2-8 describes how the experiment represents the reactor containment. Iron-aluminum thermite was used to simulate the molten core material, with the 20

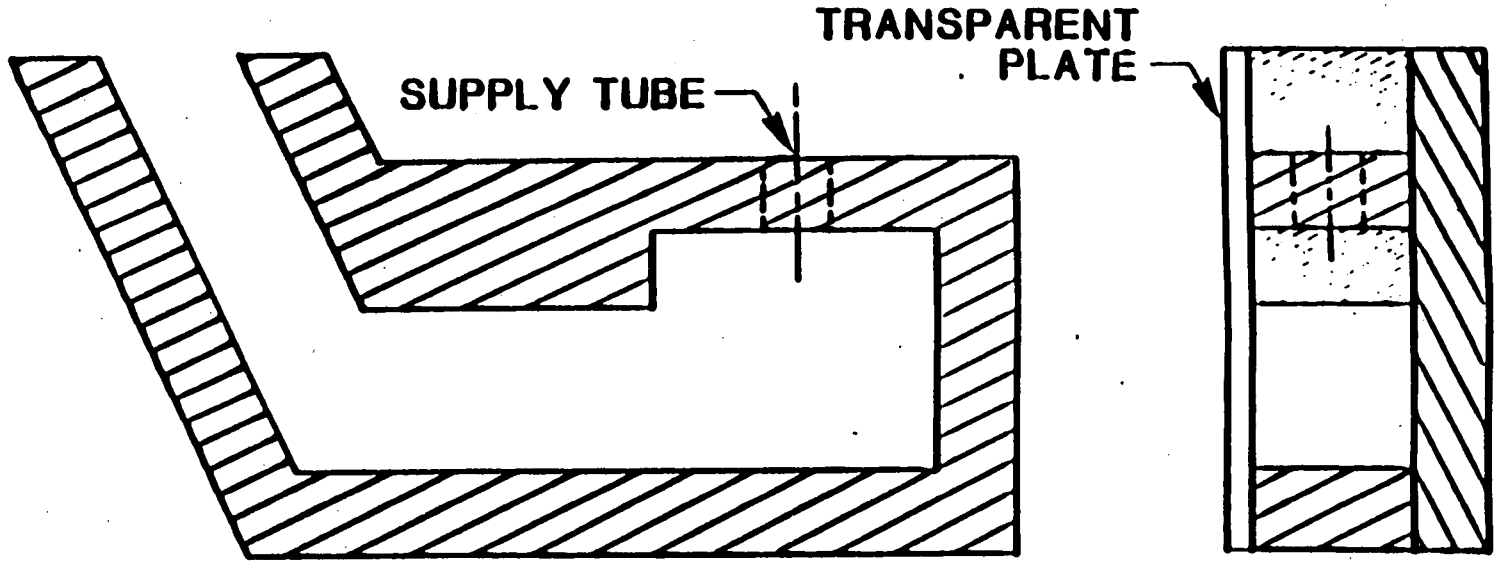

Figure 2-5a 1% linear scale building block experiments/reactor cavity.

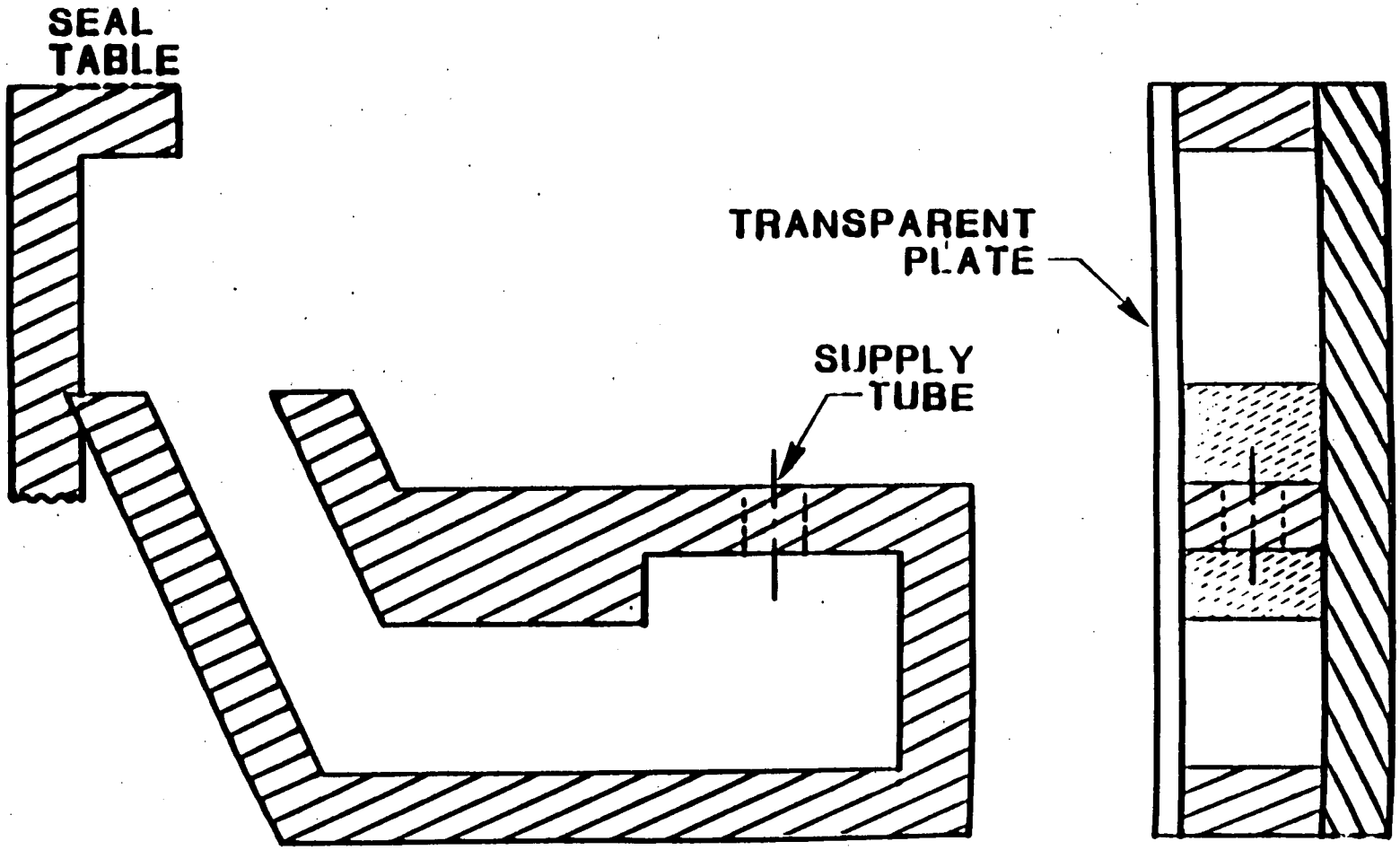

Figure 2-5b 1% linear scale building block experiments/reactor cavity and seal table.

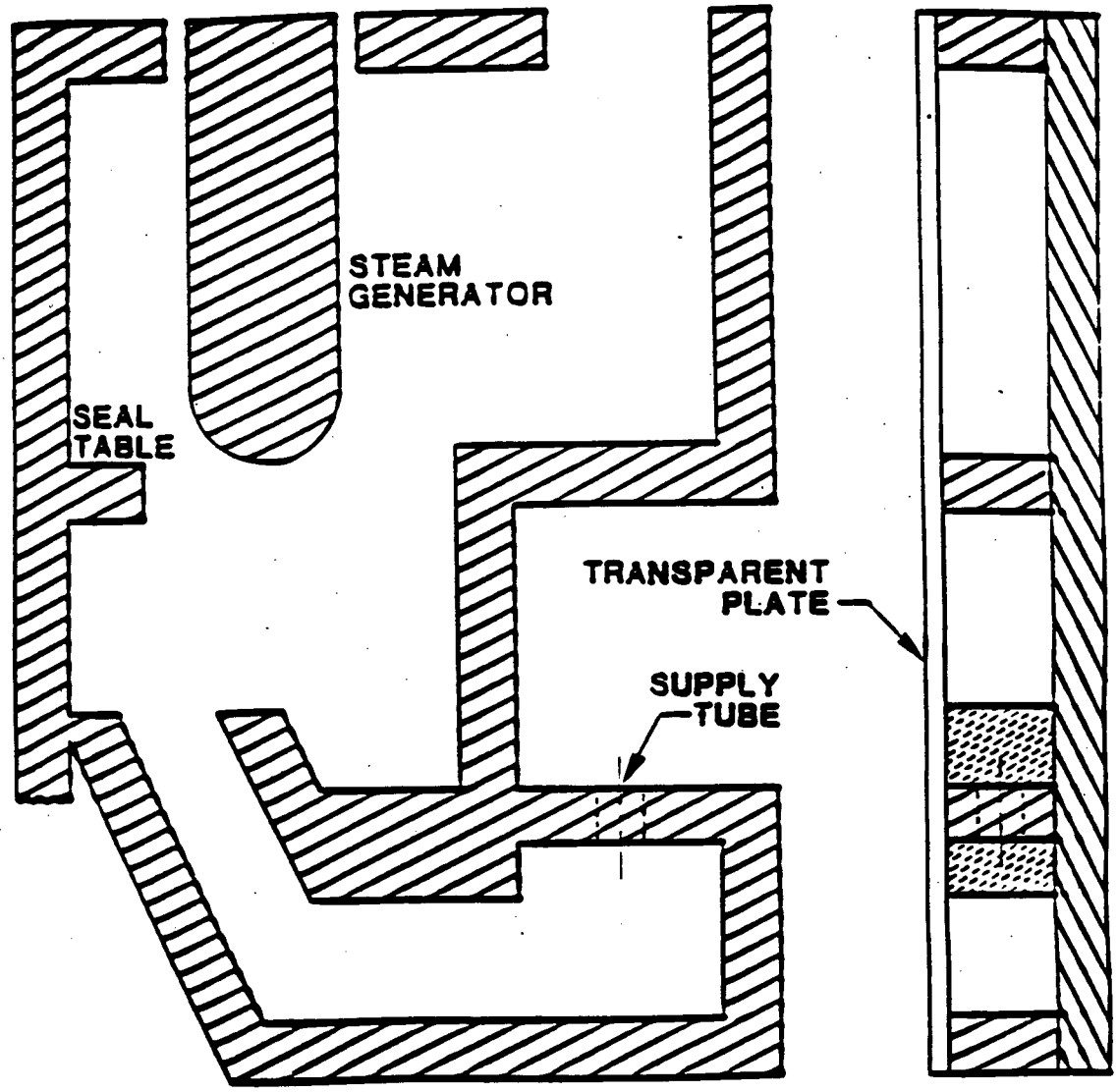

Figure 2-5c 1% linear scale building block experiments/2D representation of the lower compartment.

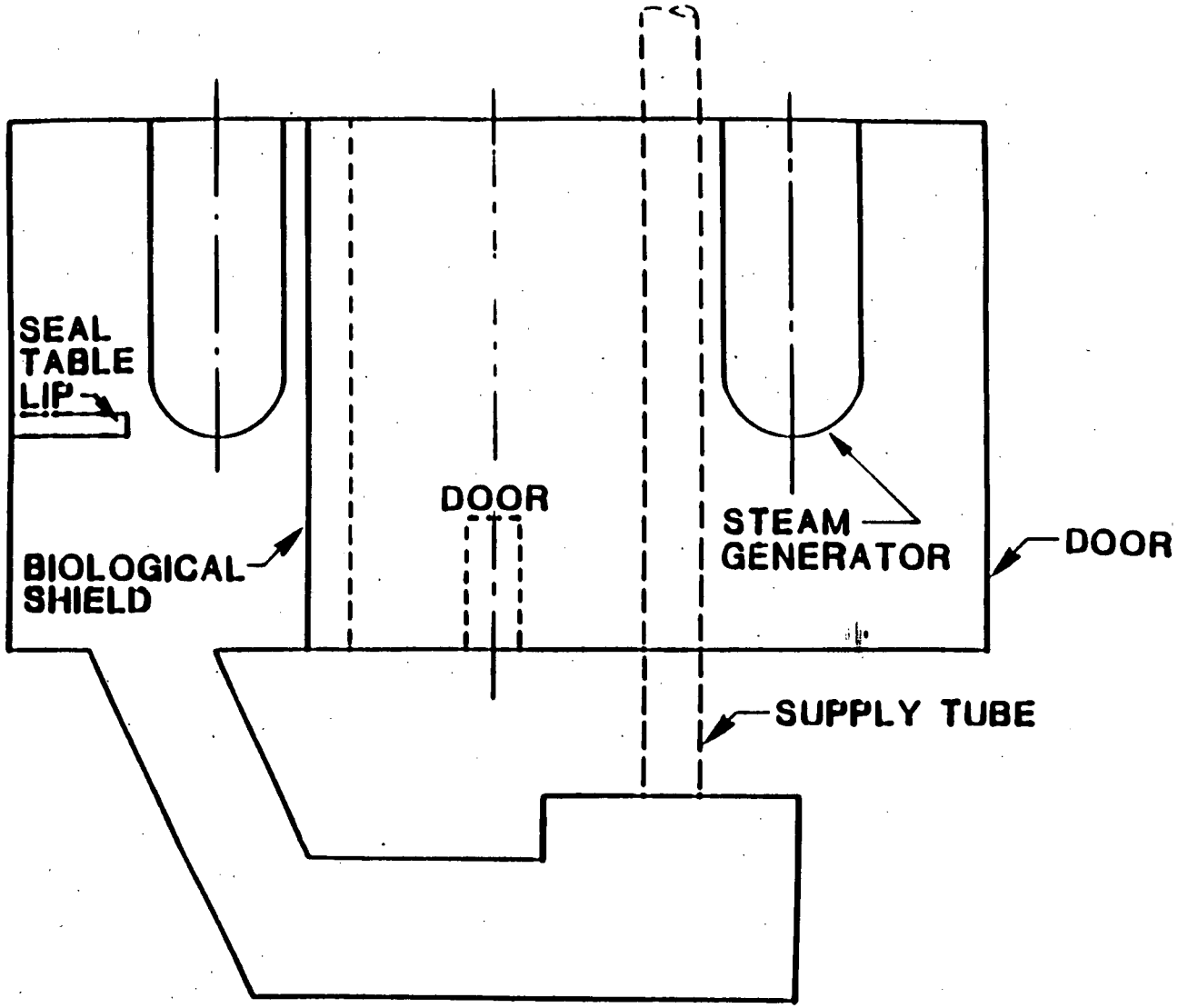

Figure 2-5d 1% linear scale building block experiments/elevation view of 3D lower compartment.

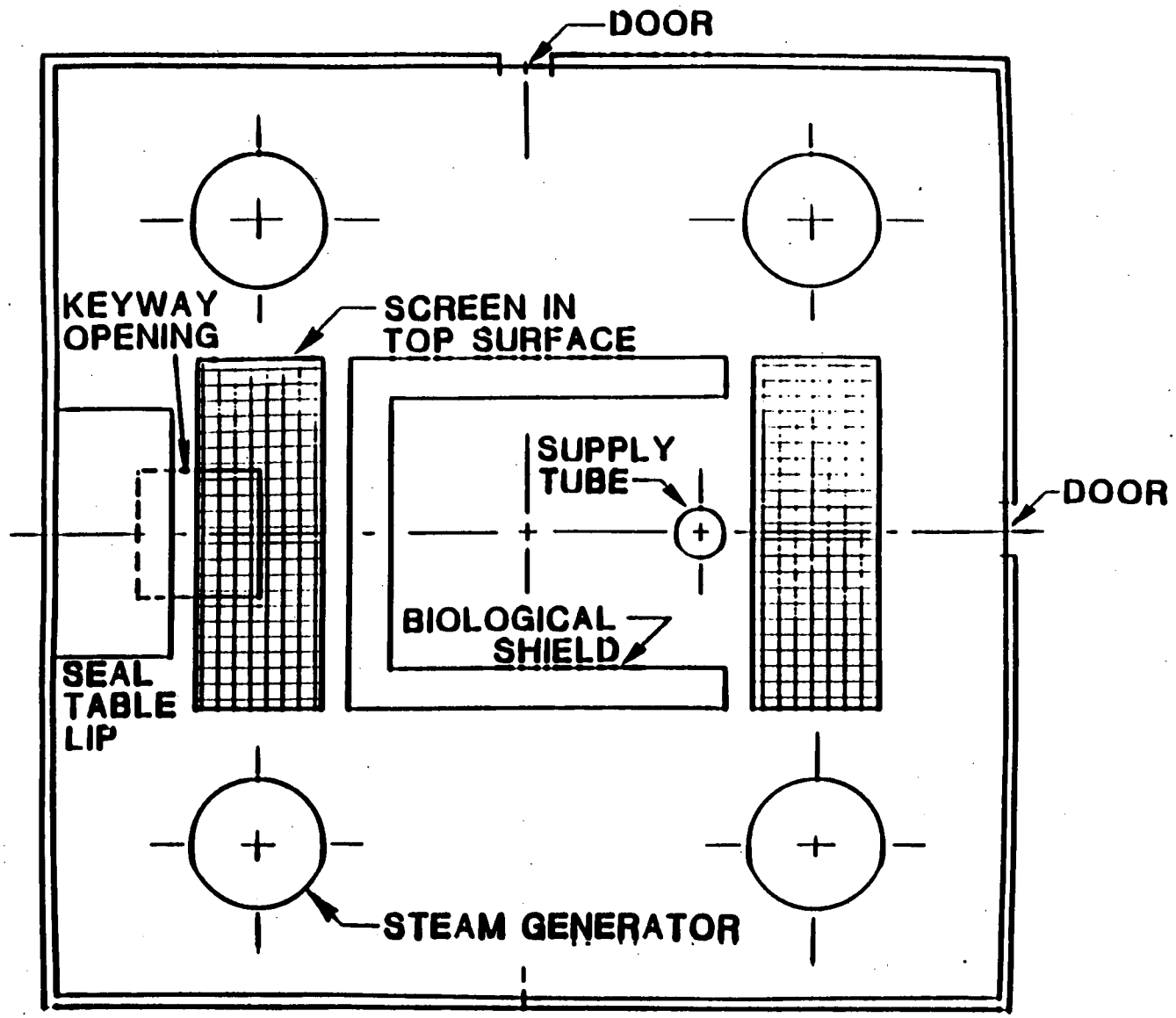

Figure 2-5e 1⅛ linear scale building block experiments/plan view of 3D lower compartment.

Table 2-7

ZION CAVITY BUILDING BLOCK

	Percent of Debris Retained in the Test Section
Reactor Cavity and Seal Table	6.07
2D Lower Compartment	48.0
2D Lower Compartment Within Reduction Flow Area to the Upper Compartment	76.6
3D Lower Compartment	97.4

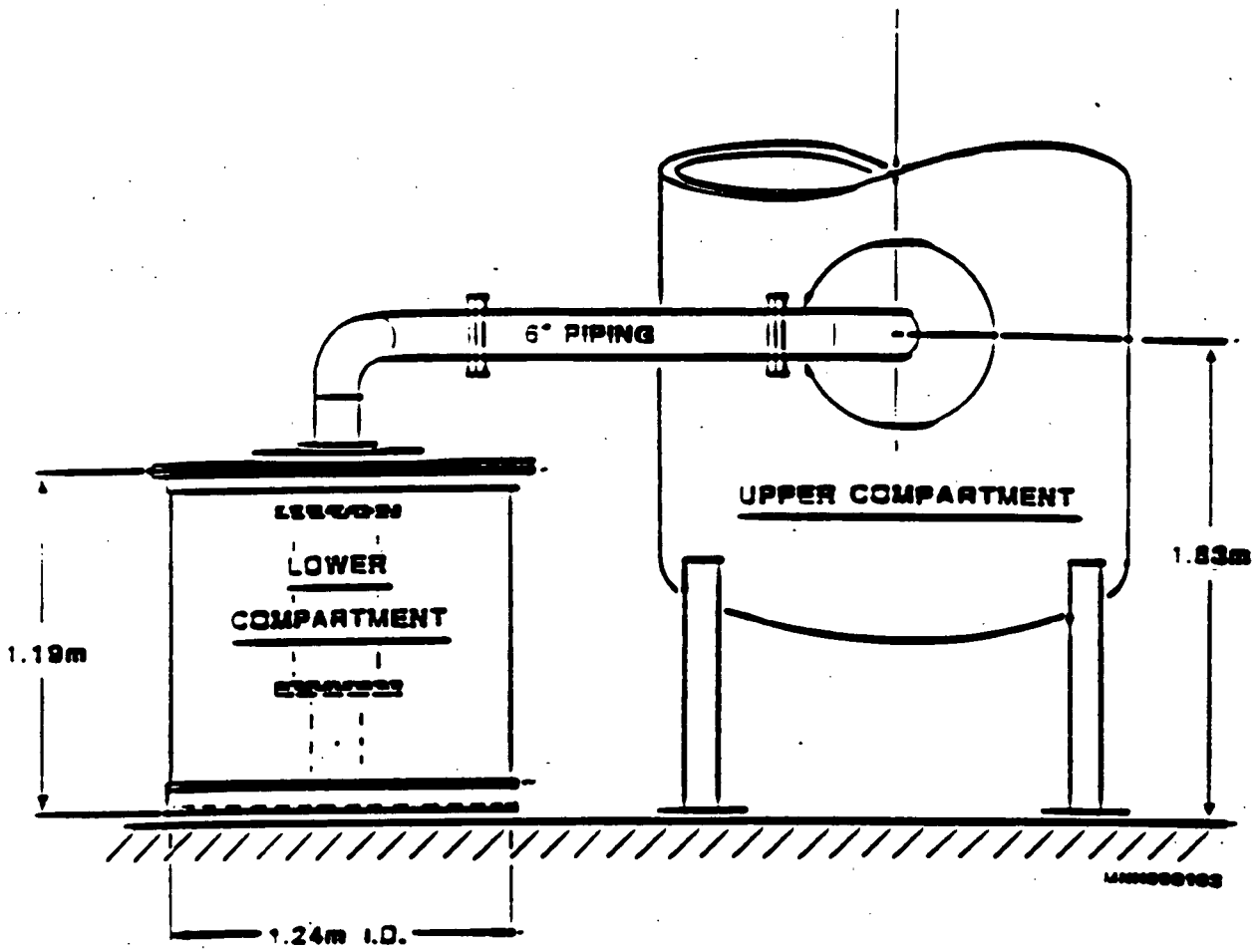

Figure 2-6 Elevation view of the vessel interconnection to simulate the containment configuration.

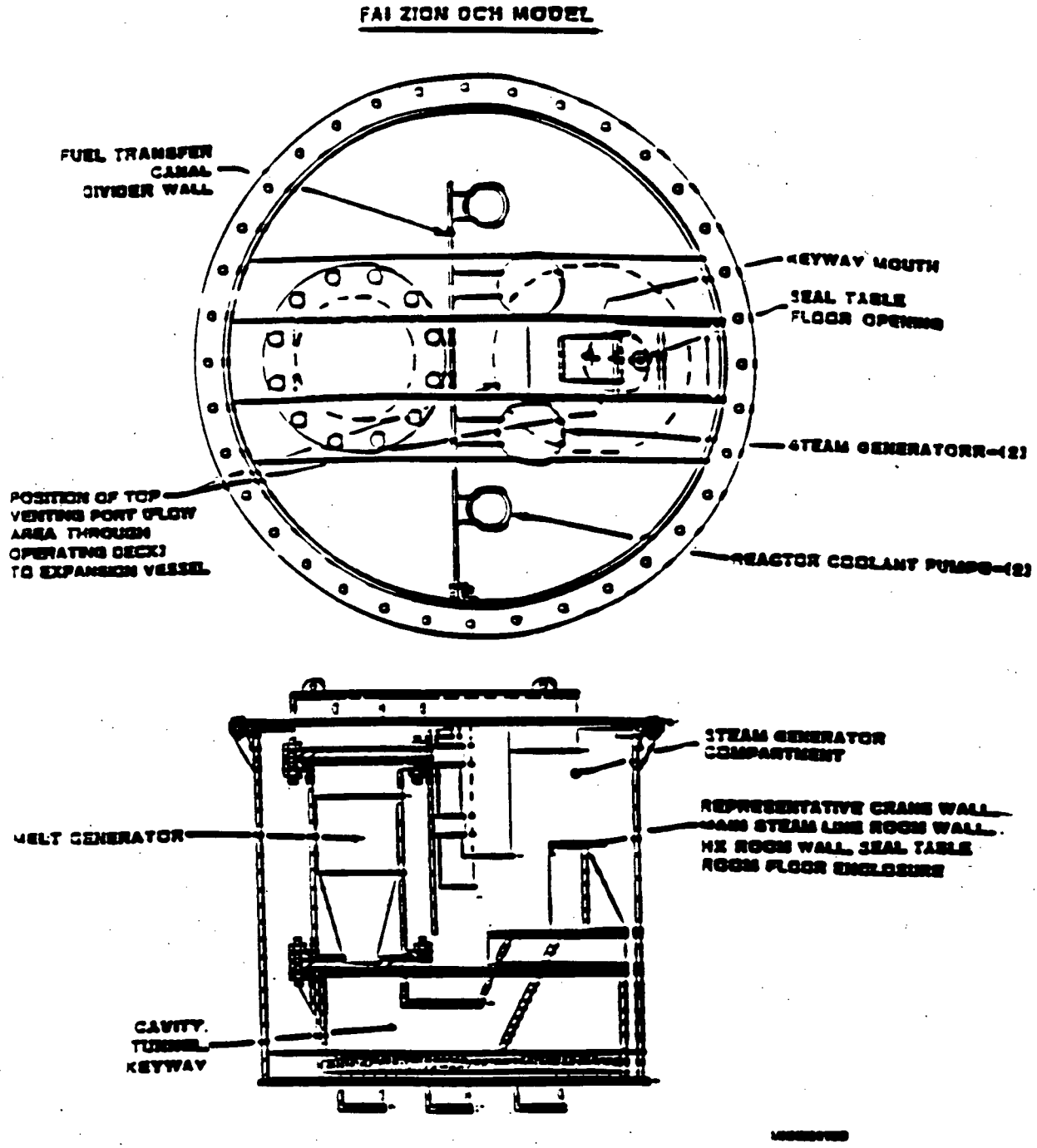

Figure 2-7 Cross-section of the melt generator, reactor cavity, instrument tunnel and the simulated lower compartment with structures.

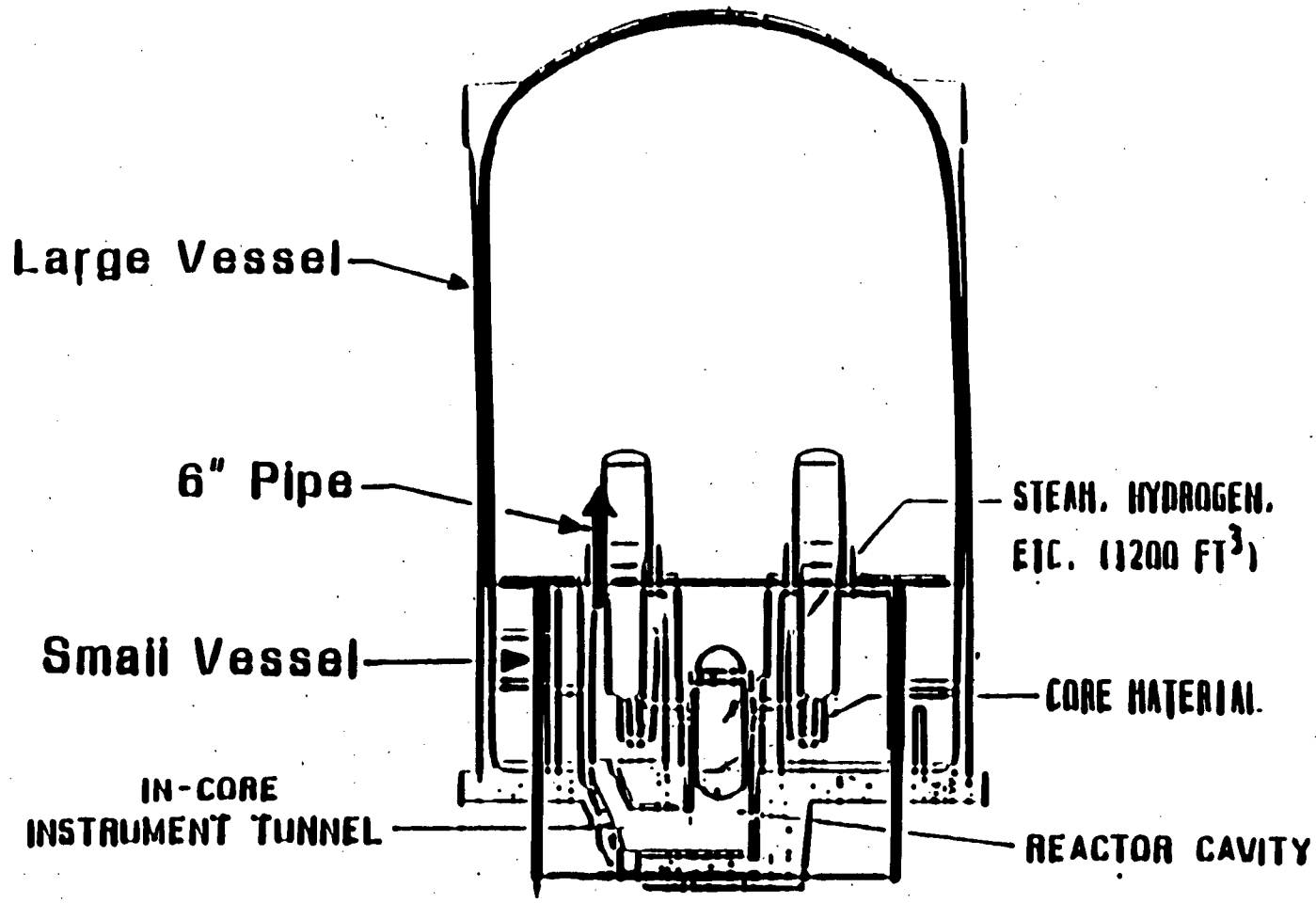

Figure 2-8 Relationship of the test configuration to the Zion containment buildings.

kg (44 lbm) thermite mass representing about twice the scaled debris mass and energy content. This was done to compensate for the greater propensity of freezing on the reactor cavity walls in small scale experiments. The experiments can also be viewed as a study of the effect of lower containment structures on the dispersal of iron-aluminum debris when compared with SNL-DCH tests, which also used iron-aluminum as a core material simulant, but had no containment internal structures. This work represents the most complete geometric similarity of the cavity and containment internal structures for the scaled DCH experiments performed to date.

The experimental matrix included four tests, all with 20 kg of thermite, three driven by nitrogen and one by steam. Water was available on the containment floor in all tests and was also available, to different extents, in the various tests; two having about 1 cm (~ 1/2") of water on the cavity floor, one test had 8 cm (~ 3 in) and the other was performed with a dry reactor cavity. Steam was used to drive the last test and was accomplished by installing a boiler next to the test apparatus to pressure the RCS with steam after the thermite reaction was initiated. Table 2-8 presents the test conditions for the experimental matrix.

Table 2-8 also summarizes the test results and clearly demonstrates that (1) the tests are very similar in their response and (2) caused very little pressurization in the upper containment compartment. Measurements of the containment pressurization showed very little, if any, contribution to direct heating even though 90% of the material was dispersed. Pressurization in the reactor cavity and instrument tunnel, as well as the lower compartment, was essentially due to debris-water thermal interactions in the reactor cavity, the blowdown of the melt generator and steam generated in the debris quenching process on the lower compartment floor. The measured peak temperatures of the lower compartment atmosphere were mostly the results of rapid steam generation due to quenching followed by slow heating of the gas due to debris frozen on structures. This latter energy transfer did not contribute to the pressurization because of the cooling provided by other heat sinks.

Table 2-8

CECo/FAI-DCH EXPERIMENTS

Test	Driving Pressure (MPa/psia)	Driving Gas	Thermite Mass (kg/lbm)		Measured Peak Containment Pressure		Water (kg/lbm)	
			Initial	Swept-Out	Pa	Psia	Cavity	Compartment Floor
DCH-1	3.3/478	N_2	20/44	~18/~39.6	165	23.9	1.1/2.4	90/198
DCH-2	2.9/420	N_2	20/44	~18/~39.6	170	24.7	5.3/11.7	47/103
DCH-3	3.2/464	N_2	20/44	~18/~39.6	155	22.5	Dry	47/103
DCH-4	2.3/333	Steam	20/44	~18/~39.6	172	25.0	1.1/2.4	47/103

Maximum local DCH efficiency of about 2%, based on the peak pressure, was measured in FAI-DCH-1 where only a limited water mass was present in the reactor cavity before the blowdown. This is an upper-bound estimate of DCH efficiency because the steam partial pressure was conservatively estimated (underestimated). The temperature increase in the lower compartment was about 5-6 times as high as in the upper compartment but was dominated by the rapid steam generation since the measured peak temperature was only slightly superheated. The results for all four tests were very consistent with respect to the extent of debris dispersed, the peak temperature in the lower compartment and the pressurization transient in the containment. The only differences are the response caused by dynamic interactions in the reactor cavity (determined by the water mass in the cavity) and the hydrogen generated which is a function of the water in the cavity and the driving medium. Given the similarity of the global response for all four tests, these differences have a second order influence on the containment response.

The results were consistent with CWTI-DCH tests in that significant heatup of the containment atmosphere was not observed in any runs that included the important structural barriers of a seal table and the lower containment compartment. In fact, the capacity of structures to mitigate DCH can be seen by comparing these results to SNL-DCH results which did not represent these structures. It is to be noted that the use of steam to eject the debris simulant yielded a containment temperature and pressure response virtually identical to the nitrogen blowdown tests, even though more hydrogen was generated, i.e., from 7% to 15% of the metal reacted.

2.2.8 Scaling Effects

Experimental observations in scaled experiments must be related to the full scale conditions (reactor system) with similar initial conditions. For complex phenomena like DCH, the scaling effects may distort the time scale of the processes and analyses must be performed to see if such distortion occurs and, if so, whether it is important in the overall conclusion.

As discussed, DCH experiments at FAI and ANL were performed, respectively, using 5% and $3\frac{1}{3}$% linear scale mockups of the containment building.

Contrast these with the SNL-DCH experiments, which included only a 10% linear scale mockup of the Zion cavity without modeling the geometry of the containment compartments. Consequently, only the FAI and ANL tests can be related directly to determine if there is any experimental indication of a scale dependency.

Using the two different scaled experiments available which incorporated all of the major influential features of a reactor system, we find a maximum of 2% contribution to direct heating of the atmosphere and this is reproducible for tests within a given experimental matrix, and between different tests. We also find for experimental scales varying from 1% to 10%, that when the structures are not represented, the dispersion of debris is virtually complete and that significant heating of the gas occurs. Hence, the applicability of the results to the reactor system should focus primarily on the influence of structures. Another feature of the reactor system is the availability of water in the containment which can substantially mitigate the gas temperature rise. This is also discussed below in terms of its influence on scaling.

2.2.8.1 Sweepout and Extent of Entrainment Scaling

The phenomenological discussions in the Zion Study [CECo, 1981] described several mechanisms whereby debris could be swept out of the reactor cavity given the conditions of core melt, failure of the RPV lower head, debris discharge into the reactor cavity and substantial pressure in the RCS. Sweepout mechanisms included (1) roll wave formation and displacement by the follow-on gas flow, (2) wave formation by the impact of high velocity gas with subsequent breakup in the gas stream, and (3) entrainment off the debris surface by the high velocity gas stream. Subsequent experiments at different facilities (ANL, BNL, FAI and SNL) and different scales (1% to 10%) have demonstrated that sweepout would occur given the necessary conditions. Therefore, debris sweepout is not an issue for scaling considerations. However, the extent of debris particulation (entrainment) is an issue to be considered for scaling.

As discussed in Appendix A, the issue for entrainment is not which mechanism applies for debris removal; rather the issue is how much entrainment could occur while other processes are also occurring. Specifically, as debris would be entrained, what would be the feedback on other mechanisms such as displacement of the debris by an imposed pressure difference. Considerations of the simultaneously occurring processes resulted in the model for the extent of debris which could be entrained and accelerated into the gas stream while the remainder was being displaced (driven) from the cavity, as a more contiguous mass, by the imposed pressure difference. Comparisons of this model with the Sandia Surtsey experiments show good agreement with the measured results. Given the co-existence of these processes and the agreement with experiments, what is the influence of experimental scale?

If two processes are occurring simultaneously, the experimental scale should not distort one process with respect to the other. To accomplish this, the ratio of the rates of debris transport should be preserved in scaled tests (see Appendix D).

2.2.8.2 De-Entrainment Scaling (Due to the Change in Flow Direction)

Sandia National Laboratory [Walker, 1987] developed a model for estimating the likelihood of debris particles not deflecting with the flow due to a 90° change in flow direction, thus impacting structural boundaries of the flow path (see Figure 2-9). The model was developed for the Zion-type seal table structure overhanging the instrument chase entrance into the lower containment space, and was benchmarked against HIPS test results mentioned in Section 2.2.2. The model can be applied to any instrumentation tunnel/seal table design that results in a 90° change of flow from the cavity. The model was presented in the following dimensionless form

$$\alpha = \frac{1}{\lambda W} \ln \left[1 + \lambda W \left[\frac{W}{L} - \left[\frac{W}{L} - 1 \right] \alpha \right] \right] \qquad (2\text{-}1)$$

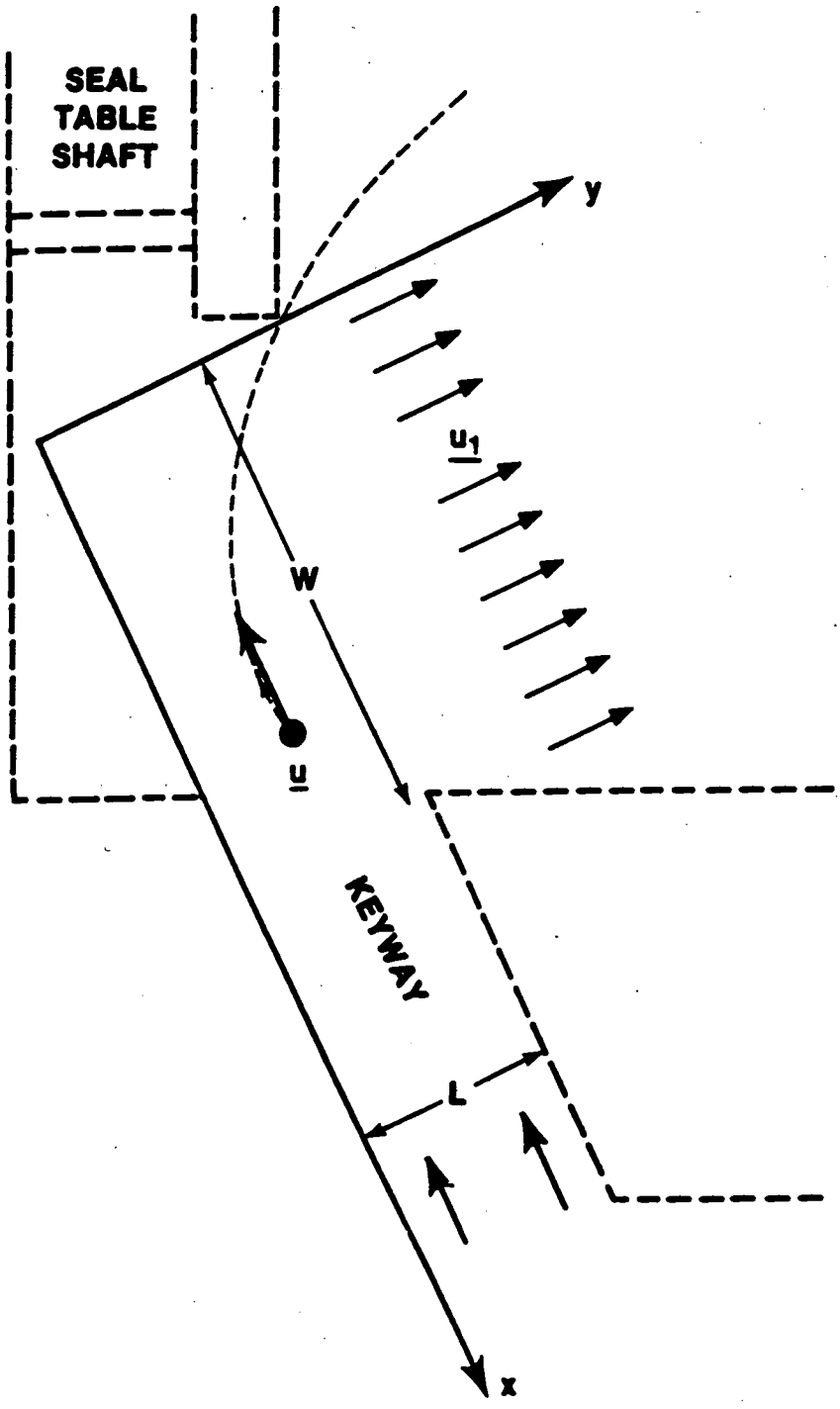

Figure 2-9 De-entrainment modeling of particles making a 90° turn (adapted from [Walker, 1987]).

where

$$\lambda = \frac{3}{4}\left[\frac{1}{d}\right]\frac{\rho_g}{\rho_d} C_d,$$

α = fraction of particles failing to make the turn [dimensionless],

W = aperture through which the particles travel as they turn to leave the reactor cavity [m or ft],

L = instrumentation tunnel width [m or ft],

C_D = drag coefficient [dimensionless],

d = debris particle diameter [m or ft].

The ratio W/L in Equation (2-1) does not change with the linear scale. However, because λ does not necessarily vary with the scale, the term λW will, therefore, change with the scale. How much α is affected by the scale can be examined by the following calculation. Assuming, for Zion conditions, W = 6 m (19.7 ft), L = 3 m (9.8 ft), ρ_g = 1 kg/m^3, ρ_d = 7000 kg/m^3 (0.06 lb m/ft^3), C_D = 0.44 and d = 1.9 mm (0.075 in), the α value is calculated to be 96.4%. On the other hand, a 5% linear scale with W = 0.3 m (1 ft), L = 0.15 m (6 in) and same λ would yield a value of 99.8%. Therefore, the small scale mockup tends to overpredict the de-entrainment compared to the full scale. However, the overprediction is only a few percent. It is noted that the 99.8% α value in the 5% linear scale corresponds to ~ 0.2% entrainment which is close to the low DCH efficiency measured in the FAI-DCH experiments.

Although, a large-fraction sweepout (as mentioned in Section 2.2.6.1) can be expected in full scale, most of the swept-out mass will fail to make the turn at the entrance into the lower compartment, and will most likely be de-entrained onto the floor of the lower compartment. This model is combined with the entrainment fraction model to develop a methodology for relating scaled experiments to the plant. This is discussed in Section 3.

2.2.8.3 Time of Flight Scaling

One of the issues to be addressed for scaled experiments is the influence of the "time of flight" for airborne debris which could be exchanging heat with the local atmosphere or oxidizing. Fractional scaled experiments have shorter lengths, which means that the airborne debris is in flight for a shorter time in the tests than would be the case in the reactor accident sequence. This is an inherent shortcoming of scaled experiments and must be addressed when evaluating the likely plant response.

As discussed previously, the issues of particular note are that all debris cannot be entrained and that all the entrained material cannot remain entrained because of the influence of structure in de-entraining particulate. Therefore, the entrained fraction may only encounter a small fraction of the containment gases as the debris particles traverse the reactor cavity, instrument tunnel and lower compartment. To address this for the reactor system, we will evaluate the energy transfer from the fraction of debris dispersed into the atmosphere by assuming that the debris equilibrates with the containment atmosphere. This eliminates any consideration with respect to the time of flight. The influence of cladding oxidation and hydrogen combustion will be assessed by considering the potential for steam inerting as a consequence of the accident sequence. Also we will perform analyses assuming the hydrogen burns completely. Again this removes any sensitivity to details of the combustion behavior.

In the scaling analysis, the seal table and instrument tunnel are the only structures considered in removing discrete material from the high velocity gas stream. While other structures would certainly be influential, the consideration of the seal table is sufficient to show that the resultant calculated pressurization is much less than that required to challenge the containment integrity.

2.2.9 External Cooling of the RPV Lower Head

Obviously, reactor vessel failure is a necessary condition for direct containment heating. This could be a local failure, such as an in-core

instrument penetration when debris slumps into the lower plenum or a failure of either an instrument penetration or the RPV wall after debris dryout and overheating occur. Therefore, any accident or plant specific conditions which would influence the likelihood of RPV failure must be considered for the IPE evaluation, but more importantly for evaluating possible accident management actions.

The TMI-2 accident provides direct insight on the survivability of in-core penetrations, since none of the limited depth welds anchoring the penetrations to the RPV wall were thermally attacked. This observation can be directly translated to Kewaunee reactor system. Differences between the penetrations are essentially the size of the central passage which is at containment atmosphere and extends upward through the core. Since the weld likely would not fail, the only remaining possibility for localized failure would be debris flow through the central passage. The TMI-2 has a central passage that is less than half the diameter of the Westinghouse PWR penetrations. This difference is addressed in Reference [FAI, 1991] and the evaluation of the penetration thermal response shows that debris would tend to freeze in the central passage like the TMI-2 behavior, due to water cooling in the annulus surrounding the central passage.

In addition, the assessment must consider that, even if the penetration response maintains the integrity of the lower head, the vessel head could fail due to the heatup of the debris and overheating of the vessel wall. Reference [Thinnes and Moore, 1989] suggests that the TMI-2 vessel wall experienced a significant thermal transient as a result of the debris transport to lower plenum at 225 minutes into the accident. Many of the accident scenarios to be addressed in the IPE would have significant water in the reactor cavity and on the containment floor. This could have an important influence on the sequence response if the vessel could be cooled externally. The experiments and the results, which are presented in [Henry, et al., 1991], show that efficient (nucleate boiling) heat transfer is observed on the outside of the vessel surface. Measured heat flux values are several times that anticipated for the reactor system. This is true whether the vessel is insulated or not. Consequently these tests, using a

high temperature thermite melt and at significant scale, indicate the reactor vessel lower plenum could not be failed by debris dryout and overheating if it is cooled externally. Therefore, best estimate evaluations of the accident response for sequences with the lower head submerged on a continual basis conclude that reactor vessel lower head failure would not occur; i.e. high pressure melt ejection would not occur.

The TMI-2 experience suggests that this efficient external cooling should be used in any accident condition in which substantial core damage is detected. (This can be linked, for example, with the measurement of very high radiation levels in containment.) If the analyses reported in [Thinnes, 1989] are modified to consider a nucleate boiling condition on the outer surface of the vessel wall, the thermal transient in the wall would have been substantially reduced. The peak temperature on the inside surface would be determined by the contact of the molten debris and the cold vessel wall. This temperature (T_i) is given by

$$T_i = \frac{T_{cm,o} + T_{s,o}\sqrt{\frac{(k\rho c)_s}{(k\rho c)_{cm}}}}{1 + \sqrt{\frac{(k\rho c)_s}{(k\rho c)_{cm}}}} \qquad (2\text{-}2)$$

where $T_{cm,o}$ and $T_{s,o}$ are the initial temperatures of the molten core material and steel wall respectively and the variables of k, ρ and c represent thermal conductivity, density and specific heat with the subscripts cm and s designating core material and steel. With nucleate boiling on the outer surface and the debris being quenched, the maximum thermal transient is shown in Figure 2-10. As illustrated, the transient is much less than reported in [Thinnes, 1989] and the threat to the vessel integrity is reduced. As a result of the TMI-2 experience and the CECo/FAI experiments, external cooling of the reactor vessel is an appropriate accident management action when substantial core damage is indicated.

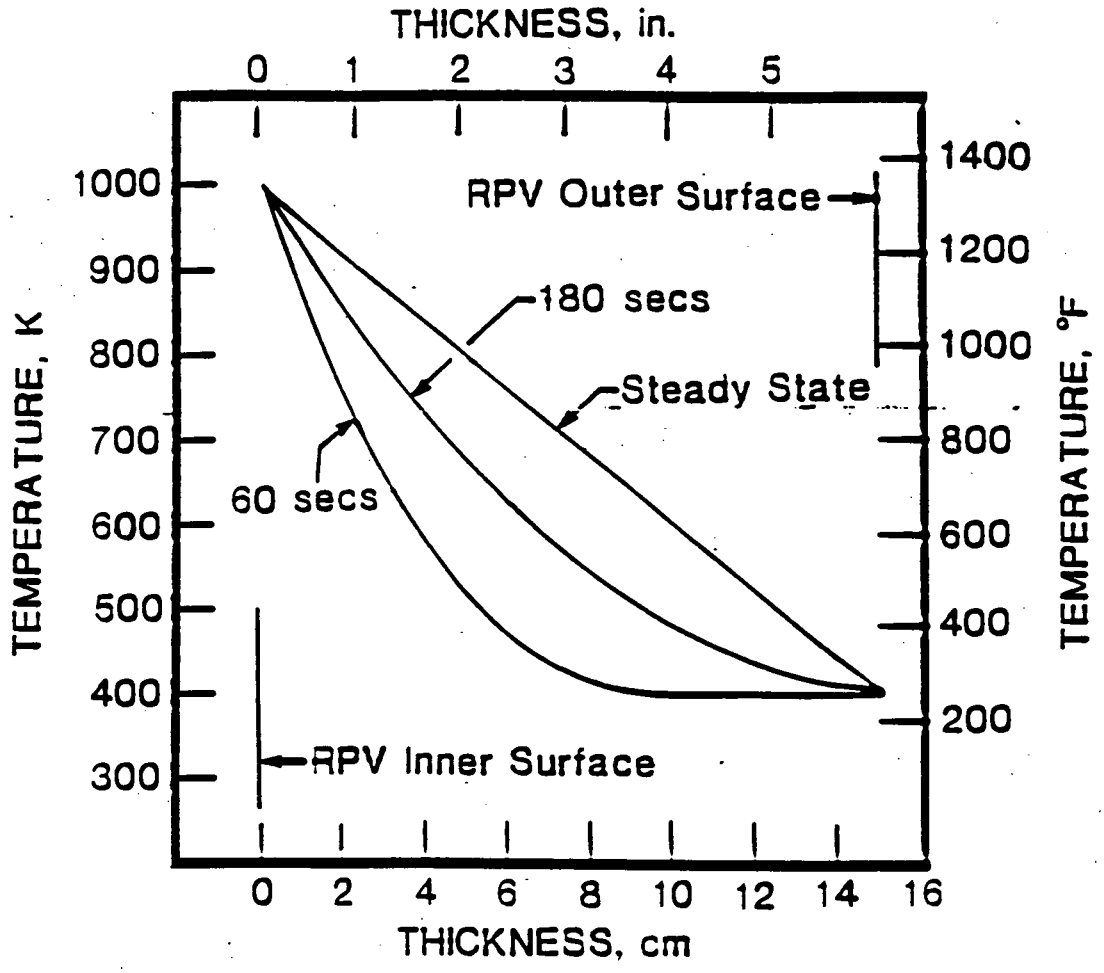

Figure 2-10 Thermal transient in a vessel wall with external cooling.

2.3 Analyses

The direct containment heating issue was first discussed as sensitivity calculations in the Zion Study [CECo, 1981]. Since then a number of efforts, from simple modeling to complex computer codes, have been directed at quantifying the magnitude of direct containment heating. These works include Sandia's DCH preliminary calculations, FAI's DCH model and computer codes such as HARDCORE, PARSEC, Kiva-DCH, and CONTAIN. These will be summarized below along with their applicability to the Kewaunee IPE.

2.3.1 Zion Probabilistic Safety Study

The Zion Study [CECo, 1981] considered a wide variety of ex-vessel interaction scenarios, of which the high pressure melt ejection was notable because of the conclusions regarding debris dispersal. Three phenomena were identified which could eject debris from the cavity should core slump and vessel failure occur. The mechanisms include (1) hydraulic jump at the keyway slope, (2) wave formation during the steam/hydrogen blowdown, and (3) entrainment of the debris by high velocity gases. The first two phenomena provide for a debris configuration which could directly impede the progress of the gas mixture exiting the vessel, resulting in debris sweepout of the cavity. The third phenomenon recognizes the fact that the relatively high gas velocities could entrain, levitate and accelerate large particles to the cavity exit. Since the adjacent lower containment compartment has substantial structure to capture and redirect debris and water to the containment floor, debris ejected from the cavity was anticipated to be deposited and quenched thereafter. Aerosol formation and direct heat transfer to the lower compartment atmosphere were not considered, although sensitivity calculations included in the study did consider the effect of direct heating. The best estimate evaluation attributed the containment pressurization to be dominated by the primary system blowdown and steam formation from debris quenching.

2.3.2 Sandia's Preliminary Calculation

Sandia National Laboratory has performed parametric scoping calculations for the effects of direct containment heating in a sample problem [Pilch, 1986]. These calculations were taken up in two parts, steady-state calculations of pressurization by simple energy balances, and rate-dependent energy release assessments.

The parametric steady-state predictions are energy balance calculations in which an energy inventory is determined for assumed debris constituents at a given temperature, including contributions from oxidation of zirconium, iron, and uranium dioxide (to U_3O_8). The fraction of debris required to participate in direct heating (as aerosol) to cause containment failure by overpressure was presented as a function of mass expelled from the cavity. The calculations show that at least 101,200 lb (46,000 kg) would be required for containment failure assuming 100% DCH efficiency.

The rate-dependent calculations only evaluated the correlations for the Nusselt and Sherwood numbers to predict heat and mass transfer from particles of given diameters. Such calculations presume the processes to generate and maintain a finely divided aerosol and neglect issues related to rate of entrainment and de-entrainment due to structural barriers. Because of the substantial limitations in the parametric calculations, these can only be used to assess the minimum debris quantities required to challenge containment integrity. Hence, these will only be used to compare the minimum mass to that which could be realistically anticipated.

2.3.3 HARDCORE

In parallel to the conduct of the DCH experiments as part of the CWTI program, the HARDCORE and PARSEC codes were developed at Argonne National Laboratory. HARDCORE analyzes debris sweepout, while PARSEC determines the extent of direct containment heating by dispersed debris. HARDCORE is formulated using one-dimensional, Eulerian, three-fluid equations and two-phase flow and heat transfer correlations. The code includes mechanistic modeling of the entrainment rate of liquid droplets from films or layers,

crust formation, correlations for forced convective heat and mass transfer for spherical particles, debris cloud thermal radiation, droplet size, and drag coefficients. Particle-gas interactions assume the debris particulate is a single particle in the gas stream and does not consider the influence of a dense particulate layer separating the gas flow stream and the debris which has not been entrained. The model also does not include the dispersal of debris out of the reactor cavity by any means except entrainment. The code does account for steam oxidation of corium metallic constituents such as zirconium, iron, and chromium and accompanying hydrogen generation. Oxidation rates are set by whichever of the following processes is limiting: transport of steam molecules to the droplet surface or diffusion of ions through the oxide shell assumed to form on each core debris droplet.

Given these assumptions, HARDCORE [Sienicki, 1986] calculates the size of the dispersed corium droplets and the swept-out debris mass. The calculations require the total core debris mass ejected from the reactor vessel, the time-dependent flowrate of blowdown gas, and temperature data as inputs. HARDCORE satisfactorily reproduced the measured values for debris sweepout and debris particle size for Tests CWTI-13 and SNL DCH-1. However, no comparisons with other data have been reported to date. HARDCORE does not treat particle de-entrainment due to structural barriers at the tunnel exit. Given the substantial experimental evidence for other removal processes and de-entrainment, these processes must be incorporated into the calculation before the model can be used to assess the plant response to severe accident conditions.

2.3.4 PARSEC

PARSEC [Sienicki, 1987] is a one-dimensional, coupled Eulerian-Lagrangian code for solving particle-laden fluid flow problems with heat transfer and oxidation reactions. PARSEC calculates the heatup of a gas atmosphere in a closed containment resulting from (1) dispersal of high temperature debris droplets/particles, (2) heat transfer, and (3) oxidation of reactive debris constituents with oxygen or steam to produce hydrogen. PARSEC accounts for the formation of aerosols by the oxidation-enhanced vaporization of metal from the surfaces of the core debris droplets but

neglects the decrease in the mass of an individual droplet. A debris cloud, thermal radiation model accounts for back scattering by debris particles into the cloud and has been shown to be significant. Otherwise, radiation heat loss to the structures could be overpredicted resulting in less atmospheric heatup. Outputs from HARDCORE such as swept-out mass, dispersed debris size distribution, entering debris temperature, entering gas pressure and temperature are used as inputs to PARSEC. Hence, the resulting model is limited due to the limitations to HARDCORE discussed above. PARSEC calculations reportedly sbowed good agreement with CWTI-13 and SNL DCH-1 tests where impeding structures were not present, however, no other comparisons with data have been reported to date. Due to its one-dimensional nature, PARSEC cannot account for internal structural effects mechanistically. Until models representing other modes of debris dispersal and the influence of de-entrainment are included, the model cannot be used to evaluate the response of the plant to severe accident conditions.

2.3.5 Kiva-DCH

Kiva-DCH [Marx, 1989], which is similar to PARSEC, calculates atmospheric heatup due to the release of molten debris into a container. However, in contrast to the one-dimensional PARSEC code, Kiva-DCH simulates the processes in two or three dimensional geometry. Kiva-DCH is a modification of the Kiva computer code which was developed at Los Alamos National Laboratory to simulate spray transport and combustion processes in internal combustion engines. The similarity between the spray and debris droplets allows a straightforward modification for direct containment heating applications. Kiva-DCH utilizes a three-dimensional finite difference scheme for gas flow calculations, coupled with a Lagrangian particle transport algorithm. The debris-wall interaction is treated by assigning a probability for trapping particles on the walls, and for particles dripping off the walls.

Kiva-DCH simulates the transport of the debris through the gas and evaluates radiative and convective heat transfer effects, and chemical reaction of the debris. Theoretically, due to its multidimensional features, Kiva-DCH could be used to simulate internal structure effects on

debris transport of any containment design. However, since Kiva-DCH represents an effort to simulate virtually every individual DCH process, using the most sophisticated turbulent flow model in multi-dimensions, it requires extensive computational resources. Kiva-DCH simulations of SNL DCH-1 and DCH-3 tests showed modest differences between calculations and experimental observations. However, like PARSEC, until the code includes models for processes which compete with entrainment for debris removal from the reactor cavity, and until it includes a representation for de-entrainment, the model cannot be used to evaluate the response of the plant.

2.3.6 CONTAIN

CONTAIN [Bergeron, 1986], developed at Sandia National Laboratory, is a lumped-parameter code for studies of the full scale reactor containment. Many of the models in CONTAIN have been imported directly from other codes. The DCH model implemented in CONTAIN assumed the mass particulated and tbe debris size (user specified) and assesses the transport of finely dispersed debris with the blowdown gas, heat transfer among the gas, debris, walls, removal or trapping of the debris as it is transported, and chemical reactions between unoxidized metals and oxygen or steam. The DCH model implemented in CONTAIN is less mechanistic than the one-dimensional HARDCORE and PARSEC codes and suffers from the same limitation as these codes with respect to assessing the response of the plant to postulated severe accident conditions.

2.3.7 Simplified Model for Representing Comparable Debris Dispersal Processes

A closed form model has been developed [Henry, 1989] for estimating the character of the debris mass dispersed out of the cavity/tunnel by the combination of entrainment and displacement (Appendix A). The thesis for this model is that the entrainment of the debris and its transport into the gas stream (where it would be accelerated), would cause the gas to be decelerated due to conservation of momentum. With a decreased gas velocity and a constant delivery rate (choked flow) from the RPV, the reactor cavity would begin to pressurize which would enhance debris removal due to the

pressure difference. Entrainment rates are represented by the Ricou-Spalding correlation [Ricou-Spalding, 1961] and the entrained debris is assumed to equilibrate with the gas thereby decreasing the gas velocity. Debris displacement is evaluated by imposing the calculated pressure difference on a debris layer with a characteristic length equal to that of the reactor cavity floor. This is shown as dimension L in Figure 2-11. To escape the reactor cavity/instrument tunnel, the debris layer must be displaced over the distance Lp shown in Figure 2-11. The time required for this displacement determines tbe interval for debris entrainment and the ratio of the entrained mass to the total mass represents the fraction of the debris which could be finely particulated. An estimate of the debris size for the particulated fraction is obtained through a Weber number stability criterion based upon the initial (highest) gas velocity through the reactor cavity. For the condition of interest, this results in particle sizes in the range of 100 μm.

The model, which was originally formulated to evaluate fission product releases for HPME and does therefore not include a de-entrainment assessment, was compared to the SNL Surtsey tests which did not represent the containment structures outside of the reactor cavity. Table 2-6 illustrates the comparison of the predicted and measured behavior, and the predictions are in good agreement with the observations for the tests using 80 kg (DCH-2, 3 and 4). Test DCH-1 only used 20 kg and more than half of the debris froze as a thin film on the cavity walls. Freezing was not included in the closed form model, but if we assume that the first 11 kg freezes on the cold walls and insulates the walls for the remaining 9 kg, which could then be entrained, the model predicts that all of the 9 kg would be entrained due to the blowdown. This is consistent with experimental observation.

Application of the model for the mass entrained to the 5% linearly scaled experiments results in a prediction of 5.5. Kg entrained. Tables 2-9 and 2-10 illustrate the debris disposition on CECo/FAI tests DCH-1 and DCH-2. The debris locations are very similar for the test and were virtually identical for the other two tests. If we assume that sum of the masses frozen on the steam generators, refueling canal wall, reactor coolant pumps,

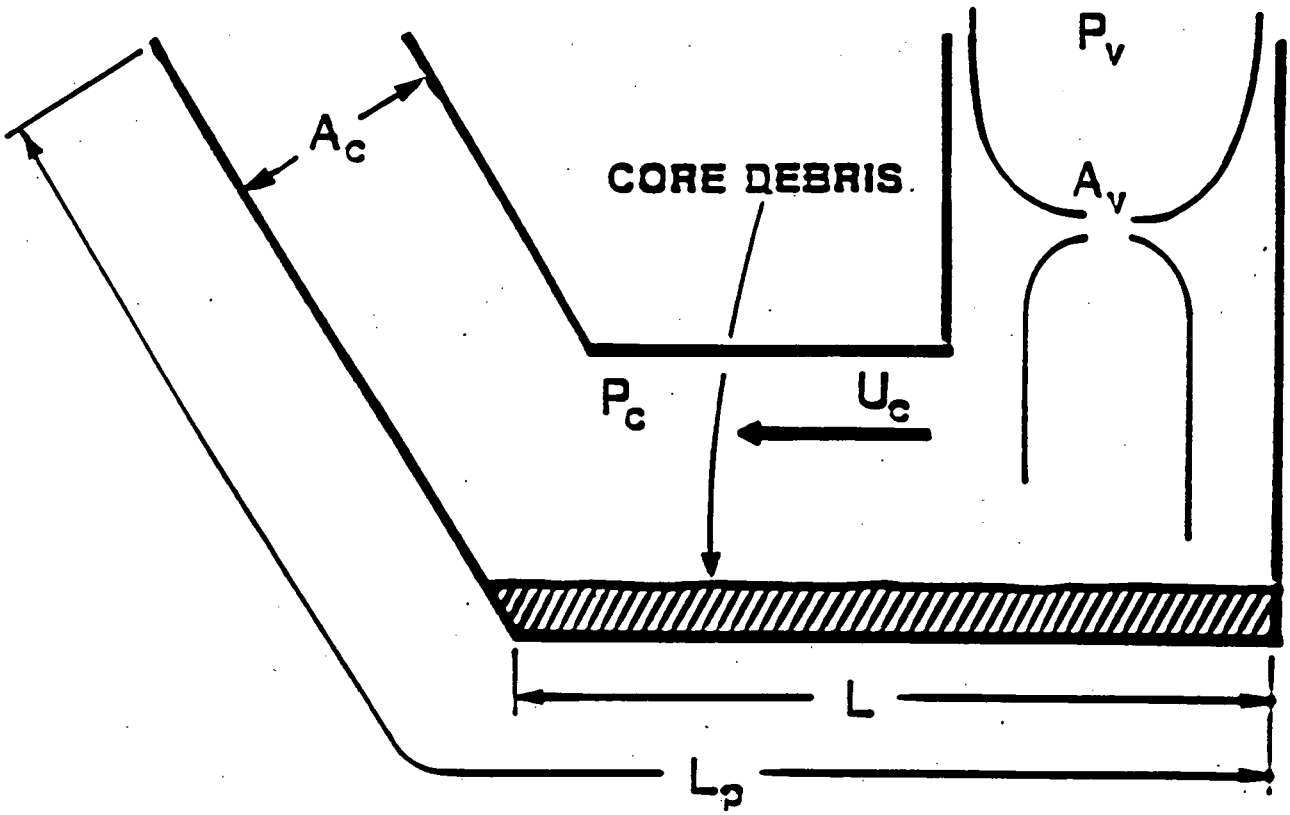

Figure 2-11 Characteristic debris length and displacement length for debris movement.

Table 2-9

DCH-1 FINAL DEBRIS DISTRIBUTION

	Location	Mass (kg/lbm)
1.	Compartment Floor South Half North Half	 6.77/14.89 7.64/16.81
2.	Frozen on Steam Generators, Reactor Coolant Pumps and Refueling Canal Wall	1.26/ 2.77
3.	Frozen on the Reactor Cavity Walls	2.02/ 4.44
4.	Laying on the Top of the Reactor Cavity Box	1.25/ 2.75
5.	Frozen on the Lid of the Lower Compartment	0.58/ 1.28
6.	Inside the G Channel Reinforcement on the Lower Compartment Lid	0.16/ .35
7.	First Elbow in 6" Pipe	0.04/ .008
8.	Second Elbow in 6" Pipe	0.06/ .132
9.	6" Line	---
10.	Melt Generator	0.0 /0
	TOTAL RECOVERED	**19.78/43.52**

Table 2-10

DCH-2 FINAL DEBRIS DISTRIBUTION

	Location	Mass (kg/lbm)
1.	Compartment Floor	
	South Half	5.65/12.43
	North Half	5.51/12.12
2.	Frozen on Steam Generators, Reactor Coolant Pumps and Refueling Canal Wall	2.06/ 4.53
3.	Frozen on the Reactor Cavity Walls	1.96/ 4.31
4.	Laying on the Top of the Reactor Cavity Box	2.11/ 4.64
5.	Frozen on the Lid of the Lower Compartment	0.78/ 1.72
6.	Inside the C Channel Reinforcement on the Lower Compartment Lid	---
7.	First Elbow in 6" Pipe	0.43/ .95
8.	Second Elbow in 6" Pipe	0.24/ .53
9.	6" Line	0.10/ .22
10.	Melt Generator	0.30/ 66
	TOTAL RECOVERED	**19.14/42.11**

and the underside of the operating deck is the debris mass wbich escaped as particulated debris masses of 2.1 Kg (4.6 lbm) and 3.6 Kg (7.9 lbm) were calculated, respectively. This is in agreement with the prediction from the model in that only a limited fraction of the melt could be particulated.

Another facet of the model is that substantial pressurizatioR of the reactor cavity could occur as a result of the debris entrainment. This could lead to a critical (choked) discharge of the debris-gas mixture, which would cause tbe mixture to expand rapidly and fill the cross-section of the Surtsey vessel. While a qualitative argument, it is consistent with the experimental observations. As mentioned above, this model focused on assessing the fraction of melt which could be particulated in the reactor cavity and hence did not include a de-entrainment model. To assess the behavior of the plant, this model for the fraction particulated must be combined with the de-entrainment due to the seal table as proposed by Equation (2-1) [Walker, 1987].

2.3.8 Jet Breakup Model

A model bas been presented for initial jet breakup between the vessel exit and impact with the cavity floor [Frid, 1986]. This model quantifies the effect of effervescence of dissolved gases from the debris through an assumed bubble nucleation density in the jet. Bubble growth at these nucleation sites is tracked, and the jet is assumed to break up when a void fraction of 50% is attained. It is concluded that jet breakup could occur within a few diameters of the reactor vessel, generating particles in the 30-150 micron range. However, when the debris-gas flow encounters the cavity floor and changes direction by 90°, the debris would be expected to be redeposited as a molten layer. Therefore, this aspect was not included in the IPE.

3.0 METHODOLOGY

Much like design basis analyses, if reactor vessel failure were to occur at high pressure, the most important consequence would be the increase in containment pressure. Direct containment heating by core debris expelled at vessel failure has been postulated to be a significant contributor to the containment pressure increase. This section provides a method for estimating the energy released to the containment by the core debris which could be discharged immediately after vessel failure. The resulting pressure increase should then be part of the assessment for the likelihood of containment failure by overpressurization immediately following vessel failure. The methodology described below is somewhat conservative (overestimates the containment pressurization). If the calculated pressure loadings are far less than those which would challenge the containment capability, failure by this means should be assessed as impossible.

First, the extent of debris entrainment which could occur in the reactor cavity/instrument tunnel is determined. Next, we assess the fraction of entrained debris which would escape the directional change at the seal table. Then, we address the effect of hydrogen combustion that possibly accompany DCH. Finally, the potential for containment pressurization is assessed and compared to the containment capability to characterize the likelihood of containment failure due to overpressurization.

3.1 Mass of Debris Distributed Into the Containment Atmosphere

The methodology focuses on (1) the debris mass that could potentially be particulated in the reactor cavity and (2) that fraction of the entrained (particulated) debris which could escape the change in flow direction caused by the instrument tunnel and, to some extent, the seal table. That fraction of the debris which is not particulated would have such a large characteristic dimension that the floor above the seal table would collect all of the debris and prevent it from entering the containment atmosphere.

A limitation exists on the extent of entrainment which could be affected by the RCS blowdown. The entrainment mass is not dependent upon the mass discharged from the RCS, except to the extent that the discharged mass should equal, or exceed, the entrained mass. The assessment of the particle size utilizes the conservative assessment described in Appendix A based on the maximum gas velocity in the reactor cavity and a single droplet Weber number criterion.

3.1.1 Extent of Entrainment

The mass of debris which could be entrained, according to Equation 20 of Appendix A, is proportional to the product of the square root of RCS pressure and tbe size of the breach in the RPV, i.e. the larger this product, the greater the mass which could be entrained. To evaluate the maximum mass which could be particulated, we may consider the pressure to be the pressurizer safety valve lowest set point of approximately 17 MPa (2475 psia). Considering the initial vessel failure to be an instrument tube, the methodology presented in [CECo, 1981 and IDCOR, 1983] would suggest a vessel breach of about 0.3 m (12 in) in diameter at the time of gaseous blowdown. Using the combination of this failure size and the RCS pressure, the calculated entrained mass in tbe reactor cavity can be obtained from Equation (20) of Appendix A. Gas density required in Equation (20) is determined from Equation (24) of Appendix A. Particulation of the melt by the RCS gaseous blowdown would result in a nominal debris size determined by Equation (21) of Appendix A with a critical Weber number equal to 12. For the small LOCA sequences, the RCS pressure would be less, resulting in a small RPV failure size (for the same debris mass). Both of these would reduce the mass of debris which could be entrained. In addition, gas velocity in the cavity would be reduced causing the average debris particulate size to be larger. Therefore, the conditions used for the station blackout like scenario bound the parameters of interest.

This evaluation of the mass of debris particulated is determined by the gas kinetic energy. As such, it is not a function of the debris mass discharged from the RPV, except for the trivial point that the entrained mass is the minimum of the calculated value and the mass discharged from the

vessel. Assessing the particle based on a single particle in the gas free stream underestimates the particle size. Hence, the following section will overestimate the fraction of particulate melt which could escape the directional change at the seal table. Since the melt is assumed to equilibrate with the containment gases, this results in an overestimate of the pressurization due to DCH.

3.1.2 De-Entrainment

Application of Equation (2-1) with a debris size calculated as sbown in Appendix A will result in a prediction that estimates the likelihood of debris particles not deflecting out of the flowpath due to a 90° cbange in flow direction, thus impacting structural boundaries of the flowpath. The model described in Section 2.2.8.2 was developed for the Zion-type cavity and seal table structure. Since Kewaunee's design is somewhat different from Zion, the Zion model would not be applicable to Kewaunee. The equation of motion for a spherical drop of diameter (d) in a gas flow is

$$m\dot{\underline{V}} = mg - C_D\ 4/3\ \pi\ (d/2)^3\ \rho_G|\underline{V} - \underline{U}|(\underline{V} - \underline{U}) \qquad (3\text{-}1)$$

Utilizing the coordinate system in Figure E-2, the sketch of the Kewaunee cavity and instrument tunnel in Figure E-3, and algebraically manipulating Equation (3-1) to incorporate the appropriate variables, the fraction of particles failing to make the turn is given by

$$\alpha = \frac{\ell}{\lambda\Gamma W}\ \ell n\left[\ell + \frac{\lambda\Gamma L}{\gamma}\left[\ell - \alpha\left[\ell - \frac{W}{L}\gamma\right]\right]\right] \qquad (3\text{-}2)$$

where:

$\lambda = 3/4\ (1/d)\ \rho_G/\rho_P\ C_D$,

W = length of instrument tunnel,

ℓ = width of cavity keyway,

L = height of cavity keyway,

ω = width of instrument tunnel,

$\gamma = (L\ell/W\omega)$,

$$\Gamma = \sqrt{1 + \gamma^2}.$$

Figure E-3 depicts how the coordinate system in Figure E-2 was implemented to fit the Kewaunee cavity and instrument tunnel design. For further detail concerning the calculation of α see Appendix E. One notable assumption was that the geometry of the instrument tunnel, which is cylindrical, was assumed rectangular to yield values for W and ω. Another notable assumption made was that the actual seal table plate was blown out. The force required to tear the plate off the table is deemed insignificant to the amount of energy that stored within this flow stream during the RCS blowdown which would occur almost directly after the HPME sequence started. Since some of the entrained material would get deposited on the seal table plate, thus being de-entrained from the flowpath, not all of the calculated entrained mass will be present for de-entrainment. Therefore this adds to the conservatism of this analysis.

3.2 DCH Pressure Rise

Debris of sufficiently small size to be swept past the seal table and remain airborne in the containment atmosphere is assumed to thermally equilibrate with the containment atmosphere. With this assumption, issues with respect to "time of flight" (extent of energy transfer) are included in the methodology in a conservative (overestimated) manner. This is an accepted conservatism in the model.

The method for calculating the containment pressure due to DCH is illustrated in Appendix B.

3.3 Likelihood of Hydrogen Combustion

The particular sequence conditions analyzed are typical of those for a Station Blackout scenario. MAAP calculations for such a sequence may be performed to calculate the pressure in the containment prior to RPV failure. Most of the hydrogen generated by cladding oxidation would still be in the RCS prior to vessel failure and would enter the containment during the

gaseous blowdown; i.e. after the debris discharge has occurred. The blowdown anticipated would be a few tens of seconds long. This is important since the initial debris discharged from the RPV would contact and vaporize the small water mass accumulated due to condensation on the reactor cavity walls and the initial debris discharged from the instrument tunnel could contact water on the containment floor resulting in substantial steam generation. Moreover, the RCS blowdown may involve the flashing of water in the RPV lower plenum. All of these would immediately displace oxygen from the lower compartment and add to the steam inventory in the containment atmosphere at a greater rate than hydrogen would be discharged from the RPV. More importantly, the steam concentration in the region of debris dispersal would be very high. Consequently, it is doubtful that the hydrogen-steam-air environment would be combustible for this sequence. Hydrogen combustion limits are discussed in Appendix C.

3.4 Influence of Uncertainties

For the containment integrity to be threatened by a DCH event, all of the following phenomena must occur.

1. The RPV must fail.

2. RPV failure must occur in a manner that would allow a large mass of core debris to be discharged into the reactor cavity before RPV blowdown would be completed.

3. Core melt progression must occur in a manner where most of the core is molten and slumps to the lower plenum such that it could be discharged immediately following RPV failure.

4. Once the melt is discharged from the RPV to the reactor cavity, the RCS blowdown must be sufficient to particulate and entrain most, or all, of the melt.

5. If sufficient melt is finely particulated, it must remain in this state as it flows out of the reactor cavity-instrument tunnel and into the lower compartment.

6. Burning of the hydrogen in the containment following debris particulation and dispersal must occur before containment integrity can be challenged.

Should any one of these phenomena not occur to a sufficient degree, containment integrity would not be threatened. Each will be discussed below with respect to the "best estimate" behavior and realistic uncertainties. As already discussed, the best estimate assessment is that one of these would occur except for the first two and then only for selected accident scenarios.

3.4.1 RPV Failure

If water accumulation in the reactor cavity can occur, the reactor system would readily experience the consequential external cooling of the RPV well in advance of core damage and drainage of molten debris into the RPV lower plenum. As a result, RPV external cooling would provide a substantial heat removal capability for the debris in the lower plenum and minimize the attack of debris on the vessel wall and the in-core penetrations. Therefore, the only credible RPV failure mechanism would be short term thermal attack on the in-core penetrations. The TMI-2 experience shows no significant damage of the penetration welds. Also, the debris which entered the central chamber of the in-core penetrations froze and prevented any further penetration of the debris. Hence, the available experience argues strongly that the RPV would not be breached as a result of debris attack for those accident conditions with external cooling of the RPV lower head.

The scenarios where long term vessel cooling would not be available would be those where no injection was available into the RCS or containment, i.e. a station blackout scenario. Also, vessel external cooling would not be available in any circumstances if a "curb" exists that prevents water from the lower compartment floor from flowing into the cavity. Herein we have assumed that a penetration would fail shortly after debris drain into the lower plenum. As will be discussed below, this is the configuration which would allow for debris discharge followed by the RCS blowdown; the condition required for debris dispersal. Therefore, uncertainties with respect to the vessel failure are set aside in the analysis by assuming that failure would occur.

3.4.2 RPV Failure Mechanism

Debris drainage into the lower plenum is the specific condition of concern for RPV integrity. This is of interest with respect to vessel failure immediately after debris transport into the lower plenum (i.e., failure of the in-core instrument penetrations) and also with respect to the long term behavior should the penetrations retain their integrity (as was the case in the TMI-2 accident). The former leads to the type of analyses carried out in this assessment where debris could be discharged from the RPV and then dispersed by the RCS blowdown. In the latter case, the likely failure mechanism would be near the top of the debris pool and would be due to creep rupture. Given the strong temperature dependence of the creep rupture phenomenon, the anticipated failure mechanism would be a localized failure (blowout of the vessel wall) followed by RCS depressurization. In this type of failure, most of the debris would not be discharged from the RPV and there would be no potential for a DCH type behavior. In this analysis, uncertainties of this nature have been set aside by assuming that the failure would be localized and at the bottom of the vessel. Deviations from this behavior would decrease the potential for both a high pressure melt ejection and DCH.

3.4.3 Core Melt Progression

As mentioned previously, for the large dry containment virtually a large fraction or all of the core material would need to be available for fine particulation and dispersal before containment integrity could be threatened. The current assessment provided by the MAAP codes allows only fully molten material to slump into the lower plenum and be available for discharge following RPV failure. Should the core melt progression also result in a substantial amount of solid material being discharged to the lower plenum the material discharge rate could be substantially limited as a result of "clogging" by the solid debris. For the analyses presented in this document, this uncertainty has been set aside by assuming that the solid material would not be available for limiting the melt discharge and has used melt fractions well in excess of those that are calculated by the PWR MAAP code. Any deviation from this characterization would decrease the

potential for melt discharge prior to RCS blowdown. Another limitation caused by solidified debris would be a reduction in the melt velocity and therefore a reduction in the rate of ablation for the vessel wall. Hence, the failure size associated with a given melt mass would be decreased thereby reducing the potential for dispersion of the melt from the reactor cavity by the RCS blowdown. Deviations from the core melt progression processes represented in this analysis would decrease the potential for DCH.

3.4.4 Extent of Debris Particulation

Once debris is discharged from the reactor vessel and accumulated in the reactor cavity, the RCS blowdown represents the potential for debris particulation. The action of particulation would also impact the ability of the gas flow to sustain the entrainment process, as discussed in Appendix A. This debris-gas interaction is used in this assessment to determine the response of the reactor cavity under worst case conditions, i.e. full RCS pressure vessel failure at the bottom of the RPV and substantial melt accumulation within the reactor cavity. Application of this methodology to available experiments shows agreement with the extent of debris particulation and, if anything, tends to overestimate the mass of material which could be finely particulated. While this is considered to be one of the controlling processes in the debris particulation and dispersal, other results presented by [Ginsberg and Tutu, 1988] assumed more melt was finely particulated, with no mechanistic assessment of the debris behavior within the reactor cavity. Deviations from the best estimate approach, such as that obtained by using the assumptions of [Ginsberg and Tutu, 1988], would increase the containment loading. However, large deviations from the mechanistic approach would be required before the pressure would approach a value sufficient to threaten the containment integrity. Such large deviations are not considered to be realistic, particularly when considering the influence of structures as discussed below.

3.4.5 Influence of Structures

Numerous experiments have demonstrated the extensive role of structures in limiting the mass of material which could remain airborne during the

debris dispersal. The approach taken uses published results for the structures which require an assessment of the debris particle size. In carrying out this part of the evaluation, the particle size was determined by the Weber number stability criteria based on the maximum gas velocity in the reactor cavity. A comparison of this particle size to the data in the Sandia SURTSEY DCH tests show that such a characterization tends to underestimate the average particle size. As a result, the influence of the seal table structure is underestimated, i.e. the mass of material "trapped" by the structure is understated which therefore overestimates the mass of finely particulated debris which could be distributed into the containment atmosphere. Hence, the major uncertainty associated with this behavior is that of the particle size and these analyses used a size which would overestimate the mass distributed into the containment atmosphere.

In addition, there are other structures in the containment lower compartment which would be effective in removing particulated debris from the containment atmosphere. None of these were credited in the analysis. Neglecting these structures also tends to overestimate the heat transfer to the gas atmosphere and the pressurization that could result by directly heating the containment atmosphere.

3.4.6 Potential for Hydrogen Combustion

The potential for hydrogen combustion is greatly influenced by steam in the containment atmosphere. Calculation results that assume complete hydrogen combustion in addition to direct heating of the atmosphere by the airborne debris mass should be performed to see whether this will result in a pressure sufficient to challenge the containment integrity. This is an additional conservatism with respect to the uncertainties of these physical processes.

In summary, each of the major elements that must be available for a DCH event have been represented in this discussion in a manner which overstates the potential for debris fragmentation, dispersal, and heating of the atmosphere. Realistic uncertainties would decrease each of these such that more

realistic models would result in lower calculated pressures than were calculated by the methodology.

4.0 PLANT SPECIFIC APPLICATION

This section describes the application of the methodology of Section 3 to the Kewaunee Nuclear Plant. However, before the methodology is applied, some sequence specific aspects will be enumerated.

4.1 Accident Sequence Characteristics

As mentioned in Section 1, high pressure melt ejection could occur with significant direct containment heating. Distribution of debris out of the reactor cavity and not the containment floor would have some influence on the long term containment response if containment heat removal were not available. The former would decrease the pressurization rate while the latter would increase this rate. These sequence specific influences will be evaluated for the IPE through Kewaunee specific MAAP analyses.

Large break LOCA accident sequences result in RCS pressures which would be too low for HPME considerations. Coupling this with the above discussion reduces the sequences for consideration to the small break and transient scenarios in which little, or no, injection would have occurred.

4.2 DCH Calculations

The magnitude of DCH can be evaluated in a straightforward manner by the methodology described in Section 3. First, the debris mass entrained from within the cavity is determined from Equation (20) of Appendix A. Cavity dimensions and RPV failure conditions are parameters required in Equation (20). For the sake of clarity, the equation and values of required parameters specific to the Kewaunee Nuclear Plant are shown here.

The entrained mass is calculated as:

$$m_D = 0.19\, A_v \left[P_v\, L_p\, L\, \rho_D \frac{A_s}{A_v} \frac{M_w}{RT} \left(\frac{\rho_D}{\rho_g} \right)^{1/2} \right]^{1/2} \qquad (4\text{-}1)$$

$$= 26144 \text{ kg}$$

where:

A_v = RPV failure area = 0.07 m^2,

P_v = RPV pressure prior to failure = 17 x 10^6 Pa,

L_p = combined length of cavity and instrumentation tunnel = 24.0 m,

L = cavity floor length = 10.06 m,

ρ_D = debris density = 7000 kg/m^3,

ρ_g = cavity gas density = 0.696 (obtained from Equation (24) of Appendix A as shown below),

A_s = cavity/tunnel floor area = 27.1 m^2,

M_w = steam molecular weight = 18,

R = universal gas constant = 8314 J/kmol•K,

T = RPV steam temperature = 625 K (saturation temperature at P_v = 17 MPa).

The cavity gas density is determined from Equation (24) of Appendix A as

$$\rho_g = \frac{P_v M_w}{RT} \left(\frac{A_v}{A_c} \right) \qquad (4\text{-}2)$$

$$= 0.696 \text{ kg/m}^3$$

where

A_c = minimum instrumentation tunnel flow area,

= 5.92 m^2.

The nominal entrained debris size (d) according to a critical Weber number of 12 criterion is given in Equation (21) of Appendix A as

$$d = \frac{We\ \sigma}{\rho_g\ U_c^2} = 369\ \mu m \qquad (4\text{-}3)$$

where

We = Weber number = 12,

U_c = gas velocity over molten material (obtained from Equation (22) of Appendix A as shown below),

σ = debris surface tension = 1 N/m.

The gas velocity over the molten material is calculated using Equation (22) of Appendix A to be

$$U_c = \frac{0.6\ P_v}{P_{co}} \left[\frac{A_v}{A_c}\right] \left[\frac{RT}{M_w}\right]^{0.5} = 216\ m/sec \qquad (4\text{-}4)$$

where P_{co} = initial cavity pressure = 0.3 MPa.

Utilizing Equation (3-2), the fraction (α) of entrained debris that will de-entrain at the 90° turn of the instrumentation tunnel is calculated to be 75.4% using

$$\alpha = \frac{\ell}{\lambda\Gamma W}\ \ell n \left[\ell + \frac{\lambda\Gamma L}{\gamma}\left[\ell - \alpha\left[\ell - \frac{W}{L}\gamma\right]\right]\right] \qquad (4\text{-}5)$$

$$= .754$$

where:

$\lambda = 3/4\ (1/d)\ (\rho_g/\rho_D)\ C_d = 0.089\ m^{-1}$,

$C_d = 0.44$,

W = 1.8 m [Kewaunee MAAP Parameter File calculations, 1991],

ω = 1.8 m [Kewaunee MAAP Parameter File calculations, 1991],

L = 2.4 m [Kewaunee MAAP Parameter File calculations, 1991],

ℓ = 3.3 m [Kewaunee MAAP Parameter File calculations, 1991],

$\gamma = (L\ell/W\omega) = 2.44$,

$\Gamma = 2.64$.

Therefore the debris mass that could be entrained into the atmosphere of the lower compartment is reduced to (1 - 0.754) 26144 = 6432 kg. Heating by this amount of debris, when assumed to participate in a DCH process at 100% efficiency (i.e., to reach thermal equilibration with the containment atmosphere in a very short time frame), will result in containment temperature and pressure rises which are calculated by Equations (B-2) and (B-3) of Appendix B.

Several plant-specific data and initial conditions are required in the calculation of Equation (B-2). These are listed in Table 4-1. Corium temperature is assumed 2500 K at time of reactor failure. Corium compositions as indicated in Table 4-1 are equivalent to a mixture of all Zircaloy cladding, all UO_2 fuel, control rods, and a lower core plate made of stainless steel. Stainless steel is assumed to be composed of 67% Fe, 21% Cr and 12% Ni. Containment conditions such as air mass, steam mass, and temperature are typical values calculated by MAAP for a station blackout sequence. These values are the same as those used in the Kewaunee hydrogen combustion paper. 40% of Zircaloy cladding is assumed oxidized prior to reactor failure which produces 226 kg of hydrogen gas within the core. (This assumption of the extent of zirconium oxidation is consistent with a typical MAAP run for a station blackout sequence.) DCH calculation results are also shown in Table 4-1. When assuming all hydrogen generated both in-core and ex-core burns during the high pressure melt ejection, the final containment temperature and pressure are calculated to be 812 K and 85.8 psia. Without hydrogen burn, tbe final containment temperature and pressure would be only 542 K and 57.3 psia, respectively. These conservative estimates of the containment peak temperature and pressure due to DCH both with and without simultaneous hydrogen burn are well within the containment capabilities.

Furthermore, it is very unlikely that hydrogen in the blowdown stream would burn during the RCS high pressure melt ejection. It is not feasible to form a combustible mixture locally in the cavity or in the annular compartment since the blowdown gas would result in the displacement of air out of the cavity. During the discharge of corium into the reactor cavity, the rapid steam generation within the cavity could increase the

Table 4-1

DCH CALCULATIONS FOR KEWAUNEE NUCLEAR PLANT

Plant-Specific Data and Initial Conditions

Corium compositions (W_j)	76% UO_2 + 16% Zr + 5% Fe + 2% Cr + 1% Ni
Corium temperature	2500 K
Total corium mass	71,710 kg (= 11,105 kg Zircaloy cladding + 54,059 kg UO_2 fuel + 1,136 kg lower core plate + 5,410 kg control rods)
DCH participating debris mass (f_e m_D)	6432 kg
Hydrogen generated in core (m_H)	226 kg (40% Zr oxidation)
Initial mass of air in containment (m_g)	40703 kg
Initial containment temperature (T_g)	410 K
Mass of steam in containment prior to reactor failure (m_s)	33767 kg
Steam mass expelled from RPV (m_{sps})	28717 kg
Primary system volume (V_{ps})	158 m^3
Primary system pressure (P_{ps})/ temperature (T_{ps})	17 MPa/625 K
Containment free volume (V_c + V_{ca})	37382 m^3
Extent of chemical reaction with steam (f_j)	0.5 (see Appendix B)
Extent of chemical reaction with oxygen (f'_j)	0.31 (see Appendix B)

Temperature and Pressure Results

	0% Hydrogen Burning	100% Hydrogen Burning
Final Containment Temperature	516°F (542°K)	1002°F (812°K)
Pressure Increase	14.0 psia (0.096 MPa)	42.5 psia (0.293 MPa)
Final Pressure	57.3 psia (0.395 MPa)	85.8 psia (0.592 MPa)

steam molar fraction in the reactor cavity and lower compartment to much more than 50% beyond which no hydrogen burn is known to occur. This mixture (according to Appendix C) is far from being combustible. Hence, the likelihood of simultaneous occurrence of both DCH and hydrogen burn is not feasible. We, therefore, conclude that:

1. hydrogen combustion is not considered feasible in the best estimate analysis, and

2. even if a burn <u>is</u> postulated, containment integrity would not be challenged.

The fact that the assessment is tolerant of this conservatism adds to the robustness of the conclusion.

5.0 CONCLUSIONS

Of principal interest for the DCH issue are the processes of debris entrainment and particulation in the reactor cavity and de-entrainment of the dense discrete phase by structures. Both of these were modeled and the models were found to be in agreement with available experiments, including the 5% linear scaled tests. These models were used to evaluate the reactor system. Pressure increases were assessed for the debris thermally equilibrating with the containment atmosphere and also for hydrogen burning and equilibration. Neither of these conservative assessments were found to cause pressure increases which would approach containment threatening levels.

The potential for hydrogen combustion was also evaluated. It was found that the combination of steam released from the RCS as the accident progresses and the rapid steam generation caused when high temperature debris encountered water in the containment, would result in conditions sufficient to completely inert the containment against a hydrogen burn.

As a result of these evaluations, DCH related bebavior would not challenge the Kewaunee containment integrity. Therefore, the containment event trees do not include this as a phenomena which could cause containment failure and a direct release of radioactive materials to the environment.

6.0 REFERENCES

Allen, M. D., et al., 1991, "Experimental Results of Direct Containment Heating by High Pressure Melt Ejection Into the Surtsey Vessel: The DCH-3 and DCH-4 Tests", SAND90-2138, Sandia National Laboratory.

Benedick, W. B., et al., 1984, "Combustion of Hydrogen: Air Mixtures in the VGES Cylindrical Tank", NUREG/CR-3273, SAND83-1022.

Bergeron, K., et al., 1986, "Development and Applications of the Interim Direct Containment Heating Model for the CONTAIN Computer Code", Transactions of the Fourteenth Water Reactor Safety Information Meeting, NUREG/CP-0081, Gaithersburg, MD.

Commonwealth Edison Company (CECo), 1981, Zion Probabilistic Safety Study, Chicago, Illinois.

Consolidated Edison (Con.Ed.) and the Power Authority of the State of New York (PASNY), 1982, Indian Point Probabilistic Safety Study, New York, NY.

Fauske & Associates, Inc., 1987, "Approximate Source Term Methodology for Pressurized Water Reactors".

Fauske & Associates, Inc., 1990, "FAI/CECo Direct Containment Heating Experiments for a Zion-like Geometry", FAI/90-60, report submitted to Commonwealth Edison Company.

Fauske & Associates, Inc., 1991, "External Cooling of the RPV - Phenomenological Position Paper", FAI/91-8, Report submitted to Commonwealth Edison Co.

Fauske & Associates, Inc., 1991, "A Position Paper on Detonation/Deflagration of Hydrogen in Support of the Kewaunee Individual Plant Examination", FAI/91-49, report submitted to Wisconsin Public Service Corporation.

Frid, W. E., 1986, "Behavior of a Corium Jet in High Pressure Melt Ejection from a Reactor Pressure Vessel", Proc. of the International ANS/ENS Topical Meeting on Thermal Reactor Safety, San Diego, CA.

Ginsberg, T., and Tutu, N. K., 1988, "Progress in Understanding of Direct Containment Heating Phenomena in pressurized Light Water Reactors", Invited Paper Presented as the Third International Topical Mtg. on Nuclear Power Plant Thermal Hydraulics and Operations, South Korea.

Henry, R. E., 1989, "An Evaluation of Fission Product Release Rates During Debris Dispersal", Proc. of the ANS/ENS Intl. Topical Mtg. on Probability, Reliability and Safety Assessment, Vol. 1, pp. 375-383.

Henry, R. E., et al., 1991, "Cooling of Debris Within the Reactor Vessel Lower Head", Invited paper presented at the ANS Annual Mtg., Orlando, FL.

IDCOR Technical Report 15.2, 1983, "Debris Coolability, Vessel Penetration, and Debris Dispersal".

Marshall, B. W., 1986, "Hydrogen: Air:Steam Flammability Limits and Combustion Characteristics in the FITS Vessel", NUREG/CR-3468, SAND84-0383.

Marx, K. D., 1989, "A Computer Model for the Transport and Chemical Reaction of Debris in Direct Containment Heating Experiments", Nuclear Sci. & Eng., 102, 391-407.

NRC (1988) letter to All Licensees Holding Operating Licenses and Construction Permits for Nuclear Power Facilities, "Individual Plant Examination for Severe Accident Vulnerabilities - 10 CFR 50.54(f)", Generic Latter No. 88-20.

Pilch, M. and Tarbell, W. W., 1986, "Preliminary Calculations on Direct Heating of a Containment Atmosphere by Airborne Core Debris", SAND85-2439, NUREG/CR-4455, Sandia National Laboratories.

Ricou, F. B. and Spalding, D. B., 1961, "Measurements of Entrainment by Axisymmetrical Turbulent Jets", Journal of Fluid Mechanics, 11, pp. 21-32.

Sienicki, J. J. and Spencer, B. W., 1986, "Corium Droplet Size in Direct Containment Heating", ANS Trans., V.53, pp. 557-558.

Sienicki, J. J. and Spencer, B. W., 1987, "The PARSEC Computer Code for Analysis of Direct Containment Heating By Dispersed Debris", AIChE Symp. Series, 257, V. 83, pp 355-362.

Spencer, B. W., et al., 1983a, "Corium/Water Dispersal Phenomena in Ex-Vessel Cavity Interactions", Paper TS-15.5, proc. Int'l. Mtg. on LWR Severe Accident Evaluation, Vol. 2, Cambridge, MA.

Spencer, B. W., et al., 1983b, "Overview and Recent Results of ANL/EPRI Corium/Water Thermal Interaction Investigations", Paper TS-15.2, Proc. Int'l. Mtg. on LWR Severe Accident Evaluation, Vol. 2, Cambridge, MA.

Spencer, B. W., et al., 1987, "Hydrodynamics and Heat Transfer Aspects of Corium-Water Interactions", EPRI NP-5127, Argonne National Laboratory.

Spencer, B. W., et al., 1988, "Results of EPRI/ANL DCH Investigations and Model Development", ANS/ENS Conference on Thermal Reactor Safety, Avignon, France.

Tarbell, W. W., et al., 1984, "High-Pressure Melt Streaming (HIPS) Program Plan", SAND82-2477, NUREG/CR-3025, Sandia National Laboratories.

Tarbell, W. W., et al., 1986a, "Melt Expulsion and Direct Containment Heating in Realistic Plant Geometrics", Proc. of the International ANS/ENS Topical Meeting on Thermal Reactor Safety, San Diego, California.

Tarbell, W. W., et al., 1986b, "Pressurized Melt Ejection into Scaled Reactor Cavities", SAND86-0153, NUREG/CR-4512, Sandia National Laboratories.

Tarbell, W. W., et al., 1987a, "DCH Experiments and Analyses at Sandia National Laboratories", Containment Loads and Molten Core Containment Expert Opinion Meeting, Albuquerque, New Mexico.

Tarbell, W. W., et al., 1987b, "Results from the DCH-1 Experiment", SAND86-2483, NUREG/CR-4817, Sandia National Laboratory.

Tarbell, W. W., et al., 1988a, "DCH-2: Results from the Second Experiment Peformed in the Surtsey Direct Heating Test Facility", SAND87-0976, NUREG/CR-4917, Sandia National Laboratory.

Tarbell, W. W., et al., 1988b, "Direct Containment Heating and Aerosol Generation During High-Pressure-Melt Expulsion Experiments", Trans. Am. Nucl. Soc., 57, 361.

Thinnes, G. L., and Moore, R. L., 1989, "Comparison of Thermal and Mechanical Responses of the Three Mile Island Unit 2 Reactor Vessel", Nuclear Technology, Vol. 87, pp. 1036-1049.

Tutu, N. K., et al., 1988, "Debris Dispersed from Reactor Cavities During High-Pressure Melt Ejection Accident Scenarios", NUREG/CR-5146, BNL-NUREG-52147.

Walker, J. V., 1987, "Reactor Safety Research Semi-Annual Report", NUREG/CR-5039, SAND87-2411.

APPENDIX A

FORMULATIONS OF DEBRIS ENTRAINMENT PROCESSES

Proceedings of the ANS/ENS International Topical Meeting on
Probability, Reliability and Safety Assessment

Pittsburgh, Pennsylvania
(April, 1989)

AN EVALUATION OF FISSION PRODUCT RELEASE RATES DURING DEBRIS DISPERSAL

ROBERT E. HENRY
Fauske & Associates, Inc.
16W070 West 83rd Street
Burr Ridge, Illinois 60521
(312) 323-8750

ABSTRACT

Failure of a reactor pressure vessel under severe accident conditions could result in debris dispersal into the containment if the vessel were at an elevated pressure. This process could influence both containment loading and fission product release from the core debris. Recent modeling approaches have focused on the potential for debris entrainment by high velocity gases resulting from the primary system blowdown. This paper considers both the potential for entrainment, which also results in deceleration of the gas flow as the entrained debris is accelerated, and the simultaneous potential for displacing debris from the reactor cavity without fine scale particulation. If substantial amounts of the debris would be expelled from the cavity region as a relatively continuous mass, limited amounts would be dispersed into the containment atmosphere, and the interfacial area available for heating of the containment atmosphere and for release of fission products from the melt would be minimal. The resulting model is compared with the recent direct containment heating experiments, including those incorporating fission product simulants.

INTRODUCTION

The spectrum of severe accidents involves conditions wherein water is depleted from the reactor core for tens of minutes, thereby causing the core materials to overheat, oxidize, melt, and slump into the lower head of the reactor vessel. At this point, core debris could fail the reactor vessel through either thermal attack of instrument penetrations in the reactor vessel wall, or through attack of the vessel wall itself. If the vessel wall were penetrated, debris would be discharged into the reactor cavity, followed by blowdown of the primary system gaseous inventory. If the blowdown is sufficient to cause entrainment of the accumulated debris within the reactor cavity, this material could be dispersed into the lower containment compartment. Finely particulated debris from the entrainment process, could be distributed into the containment atmosphere, potentially resulting in a rapid heating and pressurization. Debris dispersal was first addressed in the Zion[1] and Indian Point[2] Probabilistic Safety studies and has been further considered in the Industry Degraded Core Rulemaking (IDCOR and NRC programs[3,4] and in recent probabilistic risk assessments such as Millstone-3[5] and Seabrook.[6] It has also been the subject of several experimental studies using both simulant fluids and prototypic materials.[7-11] A major question for application to reactor systems is whether all the debris would be finely particulated, or would it be displaced from the reactor cavity as a comparatively continuous mass with limited particulation?

Particulation would also increase the fission product release rate from the debris. This would be accelerated due to the area amplification and could result in a significant addition of nonvolatile fission products to the containment atmosphere at the time of reactor vessel failure.

MODELING APPROACH

Consider the condition shown in Figure 1, i.e., the RPV at a pressure P_v with a failure site area A_v in the lower vessel head. For elevated primary system pressures the gas flow through the breach would be choked. Gases undergoing rapid depressurization expand isentropically unless sufficient energy is transferred to the gas. Generally, this energy transfer is a comparatively slow process. However, in the situation being modeled the expanding gases would receive heat from both deposited and entrained high temperature core debris. This additional energy transfer could occur within the reactor vessel during the expulsion process as well as in the reactor cavity/instrument tunnel. As an approximation to this process, one can assume that the gas expands isothermally, in which case the gas would receive sufficient energy to remain at a constant temperature. Under this condition, the gas mass flow rate is given by

$$\dot{m}_g = P_c A_v \left(\frac{M_w}{RT}\right)^{0.5} = 0.6\, P_v A_v \left(\frac{M_w}{RT}\right)^{0.5} \qquad (1)$$

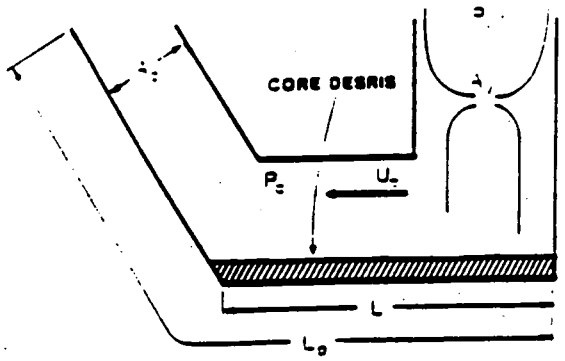

FIGURE 1 SCHEMATIC OF THE MAJOR VARIABLES IN THE MODEL

In a choked isothermal expansion, the ratio of the throat pressure (P_c) and the vessel pressure is approximately 0.6.

Given a sufficient gas velocity, entrainment would occur as long as the molten debris resides in the cavity. This minimum entrainment velocity is given by Kutateladze[12]

$$U_g = \frac{3.7\left[g\sigma\left(\rho_D - \rho_g\right)\right]^{0.25}}{\left(\rho_g\right)^{0.5}} \qquad (2)$$

As an example, let ρ_D = 7000 kg/m³, σ = 1 N/m and ρ_g = 3 kg/m³. For these conditions the entrainment velocity would be about 35 m/sec, which is the minimum gas velocity for entrainment. As illustrated in Figure 2, movement (displacement) of the debris would also be anticipated due to the imposed pressure differential (P_o - P_c) created by stagnation of the gas flow discharged from the primary system. The acceleration of debris along the reactor cavity and instrument tunnel (neglecting friction) wall can be represented by

$$a = \frac{F}{m} = \frac{\left(P_o - P_c\right)b\delta}{\rho_D\, b\delta\, L} = \frac{P_o - P_c}{\rho_D\, L} \qquad (3)$$

Assuming the acceleration to remain constant, the time required for the core material to traverse the length of the flow path (L_p) is

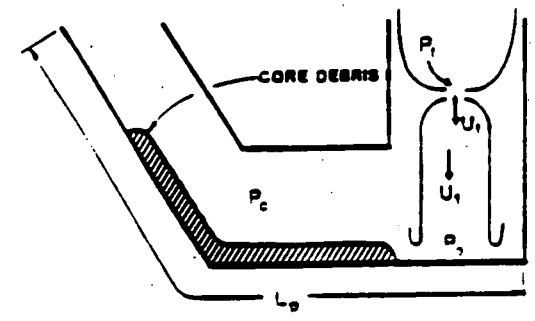

FIGURE 2 SCHEMATIC REPRESENTATION OF DEBRIS DISPLACEMENT

$$t = \left(\frac{2\,L_p}{a}\right)^{0.5} = \left(\frac{2\,L_p\,L\,\rho_D}{P_o - P_c}\right)^{0.5} \qquad (4)$$

While wall friction is neglected, this is compensated by the assumption that the debris has a long characteristic length (L) which is assumed to remain constant. In actuality, the molten debris would deform into "roll-up waves" which would shorten the effective debris length.

The stagnation pressure imposed by the gas stream on the molten debris can be evaluated by considering the unbounded expansion shown in Figure 2. Given a choked flow condition at the RPV failure location, the one-dimensional momentum equation relating the gas flow rate and the pressure difference between the throat and the point where the expansion is complete is given by:

$$\left(P_t - P_c\right)A_V = \dot{m}_g\left(U_1 - U_c\right) \qquad (5)$$

Generally, P_t >> P_c, hence, this can be approximated by

$$U_1 = \frac{P_t\, A_V}{\dot{m}_g} + U_c \qquad (6)$$

Furthermore, assuming an isothermal process as represented in Equation (1), this can be reduced to:

$$U_1 = \left(\frac{RT}{M_w}\right)^{0.5} + U_c = 2U_c \qquad (7)$$

where the first term in Equation (7) is the flow velocity (choked) at the throat for isothermal expansion. Stagnation of this high velocity gas stream would cause a pressure difference to support flow along the lower surface of the reactor cavity/instrument tunnel configuration. Pressurization due to the stagnation can be evaluated by integration of the compressible Bernoulli equation, again assuming the path to be isothermal, i.e.,

$$-\int_{P_c}^{P_o} \frac{dP}{\rho_g} = \int_{U_1}^{0} d\left(\frac{U^2}{2}\right) \qquad (8)$$

This yields a prediction for the pressure ratio (stagnation pressure to the cavity pressure):

$$\frac{P_o}{P_c} = \exp\left[\frac{\rho_1}{P_c}\frac{U_1^2}{2}\right] = \exp\left[\frac{U_1^2\, M_w}{2\,RT}\right] \qquad (9)$$

Since

$$U_1 = 2U_c = 2\left(\frac{RT}{M_w}\right)^{0.5} \qquad (10)$$

the above equation reduces to

$$P_o = 7.4\, P_c \qquad (11)$$

This is the pressure which is imposed on the debris and should be used in Equation (3), hence

$$a = \frac{P_2 - P_c}{\rho_D L} = \frac{6.4\ P_c}{\rho_D L} \qquad (12)$$

As a result, the time for available entrainment, Equation (4) becomes

$$t = \left[\frac{2\ L_p\ L\ \rho_D}{6.4\ P_c}\right]^{0.5} \qquad (13)$$

This development shows that the debris displacement along the channel can be related to the reactor cavity pressure. Therefore, if the cavity pressure is estimated, the time available for entrainment before the debris is displaced out of the reactor cavity and instrument tunnel can be evaluated.

The rate of entrainment between a dense two-phase mixture and the surrounding gas has been addressed by Epstein and Fauske[13] utilizing an entrainment rate relationship developed by Ricou and Spalding.[14] In this approach, the entrainment rate per unit surface area of the debris can be related to the gas velocity by

$$\frac{\dot{m}_D}{A_s} = E_o\left(\frac{\rho_D}{\rho_g}\right)^{0.5} U_c\ \rho_g \qquad (14)$$

Equation (14) can be related to the gas flow rate as

$$\dot{m}_D = 0.1\left(\frac{\rho_D}{\rho_g}\right)^{0.5} \frac{A_s}{A_c}\ \dot{m}_g \qquad (15)$$

By using the minimum cross-sectional flow area, the model evaluates the minimum sizes which could be developed by hydrodynamic fragmentation. Also, since the minimum area usually occurs at the exit of the instrument tunnel, the model accounts for the potential to entrain debris on the reactor cavity floor, deposit the entrained material on the inclined instrument tunnel wall (due to curvature effects), and reentrainment of the molten material by the gas stream. This approach may overstate the potential for debris particulation. As such, this will provide a conservative estimate of the containment load potential. As the debris is entrained, the acceleration of the dense material toward the gas velocity will also cause the gas velocity to decrease. Considering the momentum of the flowing stream to be conserved, the increased momentum of the entrained debris is obtained at the expense of the gas momentum. Assuming that the gas behaves reversibly after the unbounded expansion when it leaves the reactor vessel, conservation of momentum between the gas and debris can be written as

$$\dot{m}_g\ U_1 = \left(\dot{m}_g + \dot{m}_D\right)U \qquad (16)$$

(The speed of the entrained debris is assumed to equilibrate with the gas velocity.) The velocity U_1 is equal to twice the throat velocity as developed in Equations (1), (6), and (7). Further assuming that the entrained debris does not occupy a substantial fraction of the cross-sectional flow area, Equation (16) can be written as

$$\frac{1}{A_c P_c} = \frac{2}{1 + 0.1\ \frac{A_s}{A_c}\left(\frac{\rho_D}{\rho_g}\right)^{0.5}}\left(\frac{1}{0.6\ A_v P_v}\right) \qquad (17)$$

In general $0.1\ A_s/A_c(\rho_D/\rho_g)^{0.5} >> 1$ so Equation (17) this can be further approximated by

$$P_c = 0.03\ \frac{A_s}{A_c^2}\left(\frac{\rho_D}{\rho_g}\right)^{0.5} P_v A_v \qquad (18)$$

Due to the approximations involved, this pressure should be limited to the throat pressure for choked flow, or $0.6\ P_v$. When applied to typical test geometries, this results in substantial overpressurization because entrainment slows the gas velocity dramatically. This pressurization requires on the order of 100 msec and debris dispersal may be finished before the pressure increases to this level. However, this quasi-steady value provides some measure of the cavity pressurization which influences both the gas jet dynamics as it exits the vessel and the potential for moving debris along the cavity floor.

The gas density, which is a function of the cavity pressure, appears on the right-hand side of the above equation. However, since the value on the right-hand side only varies as the square root of the cavity pressure, it will be assumed that this can be adequately represented by an average value of twice the pressure in the reactor cavity immediately prior to ejection of the core debris. With this expression, the value of the reactor cavity pressure can then be substituted into the expression for the material ejection time from the reactor cavity configuration, Equation (13), to yield

$$t = \left[\frac{10.4\ L_p\ L\ A_c^2}{P_v\ A_s\ A_v}\right]^{0.5}\left(\rho_D\ \rho_g\right)^{0.25} \qquad (19)$$

Multiplying the entrainment rate given in Equation (15) by this interval results in an expression for the total mass entrained by the gas stream before the remainder of the debris is "pushed" out of the reactor cavity as a comparatively coherent liquid mass as

$$m_D = 0.19\ A_v\left[P_v\ L_p\ L\ \rho_D\left(\frac{A_s}{A_v}\right)\left(\frac{M_w}{RT}\right)\left(\frac{\rho_D}{\rho_g}\right)^{0.5}\right]^{0.5} \qquad (20)$$

This is the mass which could interact with the gas atmosphere to rapidly exchange heat and pressurize the containment building, i.e., direct containment heating. Such predictions can be compared with the various direct containment heating experiments.

Consider an example with system properties like those used previously with the additional features of a Zion-like reactor cavity as shown in Figure 3, i.e., a debris characteristic length of $L = 12$ m, a path length of $L_p = 21$ m, and a horizontal surface area of 50 m^2. For these conditions the extent of debris which could be entrained by the gas is about 23,400 kg. It should be noted that this analysis only

considers the reactor cavity and instrument tunnel. No consideration is given in these calculations for separation of the debris from the gas stream by structures in the lower containment compartment.

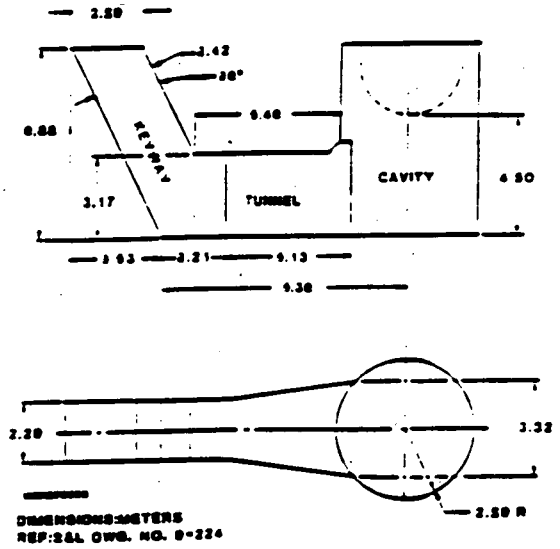

FIGURE 3 ZION-LIKE REACTOR CAVITY AND INSTRUMENT TUNNEL DIMENSIONS

The potential for breaking up molten globules once they are entrained can be related to a critical Weber number (We).

$$We = \frac{\rho U^2 d}{\sigma} \qquad (21)$$

For this order of magnitude assessment, it may be assumed that the entrainment occurs immediately as the gas is released from the reactor vessel such that the initial gas velocity in the cavity is the most appropriate value. Using Equation (1) and assuming the gas in the cavity behaves as an ideal gas, this velocity is given by

$$U_c = \frac{0.6\ P_v}{P_{co}} \left(\frac{A_v}{A_c}\right) \left(\frac{RT}{M_v}\right)^{0.5} \qquad (22)$$

Using the values considered in the previous examples, the initial gas velocity would be about 100 m/sec. An initial cavity pressure of 0.3 MPa is assumed. The particle size, from Equation (21), associated with this velocity is about 110 μm. The maximum velocity which could be developed in the cavity would be the velocity of sound. Hence, U_c should be limited to $(RT/M_v)^{0.5}$. If the sonic velocity at the initial cavity conditions is not sufficient to vent the incoming gas flow, the reactor cavity pressure would increase over its initial pressure to a value sufficient to allow the cavity exit flow to equal the flow from the vessel. For the assumed isothermal expansion, this would occur when

$$P_c = P_v \left(\frac{A_v}{A_c}\right) \qquad (23)$$

At this pressure, the gas density in the reactor cavity and instrument tunnel would be

$$\rho_{ga} = \frac{P_v M_v}{RT} \left(\frac{A_v}{A_c}\right) \qquad (24)$$

Using this density in the Weber number relationship, Equation (21), with the velocity of sound, the stable particulate size can be expressed as

$$d = \frac{U_s^2\ \sigma}{P_v \left(\frac{A_v}{A_c}\right)} \qquad (25)$$

The extent of direct heating represented by the mass of debris calculated to be finely distributed can be evaluated by assuming that this debris achieves thermal equilibrium with the gas in the simulated containment volume. Under such conditions, the final temperature (T_f) achieved by the debris and gas is given by

$$T_f = \frac{m_D c_D T_D + m_g c_v T_i + Q_s}{\left(m_g c_v + m_D c_D\right)} \qquad (26)$$

Assuming perfect gas behavior, the final pressure achieved by the direct heat exchange from the debris to the gas phase can be estimated by

$$P_f = P_i \frac{T_f}{T_i} \qquad (27)$$

This relationship ignores the gas added to the simulated containment as a result of the blowdown process, the oxygen removed from the atmosphere by oxidation, energy transfer from the remainder of the debris, and also energy liberated by further debris oxidation. However, Equation (27) does provide a convenient check on the model with respect to its first order evaluation of peak pressurse as a result of the dispersal process. In particular, the relationship developed for the mass dispersed is substantially less than the total mass injected in many experiments and therefore provides a convenient check on the capability of this model to represent the experiments performed to date.

For actual containment configurations of a more complex nature than that illustrated in Figure 1, the above model overestimates the debris entrainment since the shape of the reactor cavity has not been addressed. One would anticipate that the action of flowing through directional changes would cause entrained debris to re-deposit on the channel walls. This process has however not been included in this model. Hence, the resulting calculation for the reactor core should be expected to somewhat overstate the mass of material which could be finely pulverized. Thus, the fission product release resulting from such entrainment would be overestimated by the model.

Fission product release involves diffusion of the various materials to the melt surface and convective removal of these materials from the surface. In this analysis, it is assumed that

the release is limited by diffusion through the melden material such that the molar flux of species i is given by

$$\frac{\dot{N}_i}{A} = -D_i \left(\frac{dc_i}{dr}\right)_{r=R} \tag{28}$$

For diffusion in a static droplet, the release can be related to an effective boundary layer of 1/3 the radius. Consequently, Equation (28) can be approximated by

$$\frac{\dot{N}_i}{4\pi R^2} = -D_i \frac{9 N_i}{4\pi R^3 \cdot R} \tag{29}$$

which reduces to

$$\dot{N}_i = -\frac{9 D_i N_i}{R^2} \tag{30}$$

or

$$\ln \frac{N}{N_o} = -\frac{9 D_i t}{R^2} \tag{31}$$

The time during which debris may exist in the entrained state can be represented by the time of flight. This period can be estimated as the sum of the debris removal time from the cavity and the transit time through the region above the cavity (such as the lower compartment in a reactor configuration) which will be represented as L_o/U_c. The parameter L_o is the effective height of the compartment. This results in an expression for the dissolved species remaining in the melt as

$$\ln\left(\frac{N}{N_o}\right) = -\frac{9 D_i}{R^2}\left\{\left[\frac{10.4\, L_o\, L\, A_c}{P_v\, A_s}\right]^{0.5} \cdot \left(\rho_D\, \rho_g\right)^{0.25} + \frac{L_o}{U_c}\right\} \tag{32}$$

If the diffusion coefficient is specified, the fractional releases, as dictated by diffusion to the surface, can be evaluated.

COMPARISON WITH EXPERIMENTS

SURTSEY Tests

DCH-1. The DCH-1 test used 20 kg of melten iron thermite in the melt generator with approximately 11.6 kg being dispersed out of the reactor cavity into the large test vessel. The melt was doped with lanthanum oxide, barium molybdate, niobium pentoxide, and nickel to simulate dissolved fission products. Table 1 (from Reference 7) delineates the experimental initial conditions and the masses of fission product simulants. The test configuration, which includes a chute installed on the end of the instrument tunnel, is shown in Figure 4. The important dimensions for model application were taken from Reference 7.

TABLE 1 DCH-1 INITIAL CONDITIONS

Melt Mass	20.0 kg
Thermite Composition	Iron Oxide[a] (Fe_3O_4) 76.2 Mass % Plus Aluminum[b] (Al) 23.8 Mass %
Melt Composition (Fully Reacted)	Iron (Fe) 55.2 Mass % Plus Alumina (Al_2O_3) 44.8 Mass %
Dopants	Lanthanum Oxide (La_2O_3) - 118 g, Barium Molybdate ($BaMoO_4$) - 313 g, Niobium Pentoxide (Nb_2O_5) - 143 g, Nickel (Ni) - 100 g
Ambient Temperature	26°C
Ambient Pressure	0.08 MPa (12.0 psia)
Driving Gas	Dry Bottled Nitrogen (N_2)
Melt Generator Gas Volume	0.109 m^3 (41.1 cm Diameter by 156.7 cm Long)
Initial Gas Pressure	1.86 MPa (270 psig)
Fusible Plug Diameter	4.8 cm

a. Chemalloy MS-30 (100% minus 30 mesh).
b. ALCOA Atomized Powder (flake form).

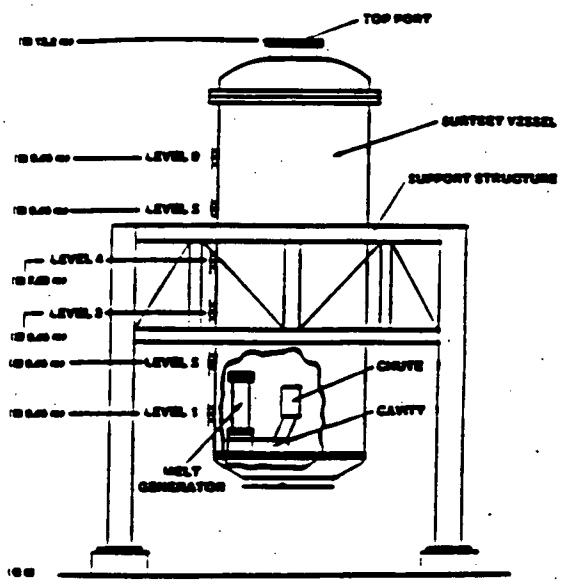

FIGURE 4 SCHEMATIC OF THE DCH-1 APPARATUS IN THE SURTSEY DIRECT HEATING TEST FACILITY

As a result of heating during the thermite reaction, the crucible pressure increased to a maximum of about 2.4 MPa, which would correspond to an average gas temperature of 386K. With the geometrical parameters given in Table 2, the debris particulation can be evaluated through the Weber number criteria. As shown in Table 2, this results in a predicted size which is somewhat smaller than the measured mass mean. This small predicted debris size may be due to the use of the minimum cross-sectional area in the model, which usually occurs at the exit of the instrument tunnel. If a value typical of the horizontal segment of the tunnel (where the entrainment initially occurs) had been used, a larger debris size would have been predicted.

Table 2 also lists the predicted peak pressure and temperature in the SURTSEY vessel along with the measured values. As shown, the model predicts that the total mass used in the melt generation could be dispersed as fine scale debris. Reference 7 lists the locations where debris was deposited and a significant fraction (~ 0.5) was found to be frozen in the melt generator and the reactor cavity. This potential for freezing debris on the reactor cavity and instrument tunnel walls was not included in the thermal-hydraulic model. As a result, the driving potential is sufficient to disperse essentially all of the melt in the generator. Thus, there was sufficient potential to particulate and disperse the available molten materials. This condition of having the potential to entrain and disperse more material than is available in a molten state is only observed for the DCH-1 test, in which only 20 kg of thermite was used. For all subsequent experiments (DCH-2, -3 and -4), 80 kg of thermite was used, and the melt mass exceeds the potential for entrainment and dispersal.

As applied to the DCH-1 test, the model results in a prediction consistent with the observation, i.e., all the available melt would be dispersed. Since the rapidly frozen material was not dispersed, the maximum temperature and pressure calculations are compared to measure conditions by using the measured mass dispersed from the cavity. By using the measured mass, the applicability of the modeling approach to represent the energy transferred to the gas space can be tested. As observed by the comparisons shown in Table 2 for peak pressure and temperature, the model is consistent with the DCH-1 test results.

For the maximum pressure and temperature predictions, the reaction heat was assumed to be negligible. Measurements of oxygen depletion from the atmosphere following the DCH-1 test were not sufficiently accurate to determine the extent of reaction. However, the DCH-4 test, was performed in an inert atmosphere, and the pressure rise and peak pressure were not greatly

TABLE 2 MODEL COMPARISONS FOR DCH TEST

Test Parameters/ Predictions/ Measurements	DCH-1	DCH-2	DCH-3	DCH-4
1. Geometrical Parameters and Vessel Pressure				
A_v (m^2)	0.883	0.882	0.882	0.882
A_v^* (m^2)	0.5	0.5	0.5	0.5
L_p^* (m)	2.8	2.3	2.2	2.8
L_p (m)	1.45	1.45	1.45	1.45
A_c (m^2)	0.86	0.96	0.88	0.88
P_v^* (MPa)	2.5	6.8	8.3	9.9
2. Debris Size				
Predicted (μm)	240	65	46	30
Measured Mass Mean (μm)	559	Not Available	Not Available	Not Available
3. Mass Dispersed as Fine Particulate				
Predicted (kg)	20	27	31	53
Measured (kg)	11.6	33 (Mass Deposited on the Lower Dome)	18.4 (Mass Deposited on the Lower Head)	38 (Mass Deposited on the Lower Dome)
4. Peak Temperature				
Predicted (K)	601 (Using Measured Mass Dispersed)	1032	1184	1135
Measured (K)	581	1156	1183	1193
5. Peak Pressure				
Predicted (MPa)	0.19 (Using Measured Mass Dispersed)	0.30	0.32	0.33
Measured (MPa)	0.18	0.33	0.26	0.27

different from those in the DCH-3 test which had an air atmosphere in the vessel. Consequently, the oxidation must occur over an interval in which the vessel heat sinks are also very important. Therefore, in all of the adiabatic representations of peak pressure and temperature, the reaction heat has been neglected.

DCH-2. This experiment provides a more meaningful test of the model since it used a larger melt inventory (80 kg) and higher nitrogen driving pressure (4.03 MPa). The reactor cavity/instrument tunnel configuration was similar to DCH-1 but did not use a chute at the end of the instrument tunnel.

The driving pressure increased to a maximum of 6.8 MPa during the reaction which corresponds to an increase in the average gas temperature to 491K. Using these values with the geometrical parameters listed in Table 2 results in a predicted mass of finely particulated debris of 27 kg at the diameter of 65 μm - the remainder of the debris being dispersed without fine particulation.

The DCH-2 debris characterization is greatly different from that in DCH-1. Large quantities of debris were found frozen on the vertical walls and the upper head of the SURTSEY vessel. Such observations are consistent with the modeling approach in that 27 kg is predicted to be fine particulated, entrained and dispersed while the remainder of the material would be dispersed as a relatively coherent mass. Molten debris dispersed as a comparatively continuous mass could impact the vessel vertical wall, freeze as a crust, the thickness of which would be dictated by the heat transfer into the steel, and the remainder could continue to flow upward to the head. Finely particulated material would rapidly exchange heat with the vessel atmosphere, freeze and fall to the lower head. Thus, mass recovered from the lower head (33 kg) can be compared to, and is in agreement with, the predicted value of 27 kg.

The predicted peak pressures and temperatures are in agreement with the observed values but somewhat understate the results. This may be due to either limited oxidation during the expulsion process or some heat transfer to the atmosphere from the fraction of debris which was not fine particulated but nonetheless was expelled from the instrument tunnel, impinged on the SURTSEY vessel wall, and froze. Neither of these are currently included in the model. The DCH-4 test with an inert atmosphere, which is discussed later, shows the same general behavior as DCH-2. This indicates oxidation of the fragmented material in these tests is not a first-order process in terms of heating the gas atmosphere. Hence, it is reasonable that the model ignore oxidation.

DCH-1. This test has not been fully reported and the extent of experimental observations is limited.[9] Conditions used for the model benchmark are an initial melt inventory of 80 kg and a configuration like DCH-1 with a chute added to the exit of the instrument tunnel. Table 2 lists the geometrical parameters and the predicted values for debris size, mass dispersed, peak temperature, and peak pressure. As shown, the model predictions are in agreement with the observed peak pressure and temperature. Since the extent of particulated debris is not presently available, the predicted value is compared with that accumulated on the lower head of the SURTSEY vessel as it was with the DCH-2 test. As discussed previously, this represents the finely divided material which frees during transit through the containment atmosphere while also being decelerated quickly after being discharged from the instrument tunnel. Both of these would tend to keep this material in the vessel atmosphere such that it would eventually settle on horizontal surfaces, i.e., the vessel lower head. The comparison shows the model somewhat overpredicts the experimental result.

DCH-4. This test was virtually identical to DCH-3 (including 80 kg of thermite and use of a chute) except the SURTSEY vessel atmosphere was inerted. The model does not use rapid oxidation to assess the peak pressure. Hence, the predictions for this test are very close to those of DCH-3. Table 2 lists the parameters for the DCH-4 comparison. The predicted and measured values of the vessel pressure and temperature are in agreement with the test results. Also, the mass of debris removed from the vessel lower head agrees with the material mass predicted to be finely particulated. Comparison of these results with those of DCH-3 may indicate the level of resolution for the data. In particular, the measured peak temperatures are in agreement, yet the final disposition of debris on the lower head differs by 40%. Hence, this is likely the resolution of the experimental information at this time, subject to more detailed reporting of the experimental results of tests DCH-3 and DCH-4.

In summary, these comparisons with the four DCH tests run in the SURTSEY facility show the proposed model to be consistent with the test observations. These comparisons include the mass which could be finely particulated, the peak vessel pressure, and the peak vessel temperature.

Comparison With Fission Product Release Data

The DCH-1 test used fission product simulants to represent the dissolved low volatile species in the debris. If the time for fission product release is the time of flight, the appropriate time for the DCH-1 test would be the time the material is resident in the cavity (~ 0.04 seconds) plus the time of flight between the cavity mouth and the upper head (~ 0.07 seconds). The results in a flight time of about 0.1 seconds. If the diffusivities are considered to be about 10^{-8} m^2/sec, about 10% of the fission product would be released from the fine particulated material. Since the finely fragmented and dispersed mass was about 50% of the debris in DCH-1, this corresponds to approximately 5% of the inventory. Table 3 lists the measured release fractions for the various

materials in this test. The estimated release value characteristic of the overall inventory of approximately 5% is in general agreement with these data. Such variations are well within the uncertainty bounds of the limited data base for diffusivities in the melt.

TABLE 3 MEASURED ELEMENTAL AEROSOL RELEASE FRACTIONS IN DCH-1

Element	Mass in Relocated Debris[a] (g)	Mass in Aerosol[b] (g)	Release Fraction[c] (%)
Fe	5610	353	6.3
Al	2430	44	1.81
Mo	51.5	9.8	19.0
Ni	51.0	4.8	9.4
Nb	51.0	0.98	1.92
Ba	73.7	1.11	1.51
La	51.3	0.35	0.68

a. Uncertainty in relocated mass = ± 10%.
b. Uncertainty in aerosol mass = ± 53%.
c. Resulting uncertainty in release fraction = ± 54%.

SUMMARY OF RESULTS AND CONCLUSIONS

The issue of fission product release during the primary system blowdown following melthrough of the reactor vessel lower head has been addressed by developing a model for the extent of fine scale debris particulation and the resultant diffusion of low volatility fission products in the melt fragments. This model also relates to the issue of direct containment heating. The model has been benchmarked with the results of the DCH tests performed at SNL. Such comparisons have demonstrated that the model predictions agree with the observed peak pressures and temperatures, especially the tests using a larger melt mass. The current model addresses only the reactor cavity and instrument tunnel configuration and ignores the lower compartment structures. Consequently, the model represents a conservative assessment of the potential influence of direct containment heating on current containment configurations.

The model also predicts the scale of debris particulation and the diffusion of fission products to the surface of this finely divided debris. This model was compared with the results of the SNL DCH-1 test. A comparison of the model predictions to the data show agreement with the test results with the major uncertainty being the diffusivity of the fission products (or their simulants) in the finely particulated debris.

ACKNOWLEDGEMENT

Prepared for EG&G Idaho, Inc. Under Subcontract No. C85-100740 and the U.S. Department of Energy Under Contract No. DE-AC07-76ID01570.

REFERENCES

1. "Zion Probabilistic Safety Study". Commonwealth Edison Company, (September, 1981).

2. "Indian Point Probabilistic Safety Study". Prepared for Power Authority of the State of New York and Consolidated Edison Company of New York, Inc., (March, 1982).

3. "Technical Support for Issue Resolution". IDCOR Technical Report 85.2, Atomic Industrial Forum, (July, 1985).

4. U.S. NUCLEAR REGULATORY COMMISSION (USNRC). "Reactor Risk Reference Document", Draft, NUREG-1150, (February, 1987).

5. NORTHEAST UTILITIES. "Millstone-3 Probabilistic Safety Study". (August, 1983).

6. PICKARD, LOWE AND GARRICK, INC., "Seabrook Station Probabilistic Safety Assessment". Prepared for Public Service Company of New Hampshire and Yankee Atomic Electric Company, PLG-0300, (December, 1983).

7. W.W. TARBELL, ET AL., "Results From the DCH-1 Experiment", Sandia National Laboratory Report, NUREG/CR-4871, (June, 1987).

8. W.W. TARBELL, ET AL., "DCH-2: Results From the Second Experiment Performed in the SURTSEY Direct Heating Test Facility", Sandia National Laboratory Report, NUREG/CR-4917, (January, 1988).

9. W.W. TARBELL, ET AL., "DCH Experiments and Analyses at Sandia National Laboratories", Presentation to the NUREG-1150 Containment Loads and Melton Core Containment Expert Opinion Meeting, (December 15-18, 1987), Albuquerque, New Mexico.

10. S.W. SPENCER, ET AL., "Corium/Water Dispersal Phenomena in Ex-Vessel Cavity Interactions", Proc. Intl. Mtg. on Light Water Reactor Severe Accident Evaluation, Cambridge, Massachusetts, (August 28 - September 1, 1983), American Nuclear Society Publication, Vol. 2, pp. 15.5-1 through 15.5-7.

11. S.W. SPENCER, ET AL., "Hydrodynamics and Heat Transfer Aspects of Corium-Water Interactions, EPRI NP-5127, Electric Power Research Institute, Palo Alto, California, (March, 1987).

12. S.S. KUTATELADZE, "Elements of the Hydrodynamics of Gas-Liquid Systems", Fluid Mechanics/Soviet Research, 4, 1, (1972), p. 29.

13. H.K. FAUSKE and M. EPSTEIN. "Source Term Considerations in Connection With Chemical Accidents and Vapour Cloud Modeling". Journal of Loss Prevention Process Industry. 1. (April. 1988). pp. 75-83.

14. F.B. RICOU and O.B. SPALDING. "Measuremsnts of Entrainment by Axisymmetrical Turbulent Jets". Journal of Fluid Mechanics. 11. (1961), pp. 21-32.

NOMENCLATURE

A	surface area of a droplet of radius R
A_c	minimum cavity flow area
A_s	horizontal surface area of the reactor cavity and instrument tunnel
A_v	RPV failure area
b	width of the cavity
c_i	concentration
c_v	gas specific heat at constant volume
c_D	debris specific heat
D_i	diffusivity (or diffusion coefficient) of fission product i in the melt
E_o	entrainment coefficient
g	acceleration of gravity
L	effective length of the debris
M_w	gas molecular weight
m_g	mass of gas in the volume
$\dot{m}_g$	gas mass flow rate
P_c	pressure in the reactor cavity
P_{co}	pressure in the cavity at the start of the blowdown
P_v	RPV pressure
Q_R	heat of reaction
R	universal gas constant
r	droplet radius
T	absolute temperature
T_i	initial temperature of the gas
T_D	initial temperature of the debris
U	homogeneous mixture velocity of the gas and the entrained debris in the reactor cavity
U_c	gas velocity over the molten material
U_r	relative velocity
U_t	gas velocity after the expansion
ρ	density of the two-phase flowing stream
ρ_D	debris density
ρ_g	gas density
σ	liquid (debris) to gas surface tension
δ	debris depth

APPENDIX B

Calculations of DCH Temperature and Pressure Rise

An important consequence of vessel failure is an increase in containment pressure. Direct containment heating by core debris expelled at vessel failure may be a significant contributor to the total containment pressure increase. This appendix provides a method for estimating the energy released to the containment atmosphere by the core debris released due to high pressure melt ejection following vessel failure.

Although the level of DCH is determined from the amount of energy that is transferred to the containment atmosphere, there are many factors that can affect the actual amount of energy transfer. Overall, the physico-chemical and thermofluid dynamical processes leading to DCH are highly complex. These individual factors and processes can be summarized as follows:

1) The mode of reactor failure which determines

   1.1) reactor vessel pressure at the time of vessel failure,

   1.2) failure size,

   1.3) fraction of core mass that would be ejected into the cavity.

2) The amount, temperature and size of the ejected mass that would be dispersed into the containment atmosphere by the follow-on high velocity steam/gas flow which are affected by

   2.1) quenching of debris by water possibly present in the cavity prior to vessel failure,

2.2) enhanced dispersal of debris by water possibly present in the cavity prior to vessel failure due to vigorous steam generation,

2.3) dispersal process including displacement and entrainment of molten debris.

3) Redirection and subsequent de-entrainment of debris particle due to structural impediment (such as seal table structure).

4) Shortening of particle flight time due to redirection of debris onto floor at the tunnel exit and due to structural barriers in the lower compartment.

5) Deposition of debris on structures.

6) Extent of chemical reactions which include oxidation of metallic constituents with steam and oxygen and hydrogen combustion.

The method to be used to estimate the core debris energy release that could contribute to direct containment heating is based on the assumption that the debris mass successfully entrained into the containment atmosphere equilibrates thermally with the containment atmosphere. The evaluation includes the debris superheat, the debris latent heat, the debris sensible heat, as well as the energy produced by oxidation of corium constituents (Zr, Fe, UO_2) and by combustion of hydrogen.

The final atmospheric temperature (T_e) is the solution of the following energy balance based on thermal equilibration:

debris super heat latent heat of fusion

$$f_e\, m_D \sum C_{cj}\, w_j\, (T_c - T_{cmj}) + f_e\, m_D \sum H_{fj}\, w_j$$

sensible heat — heat of reaction with steam

$$+ f_e\, m_D \sum C_{cj}\, w_j\, (T_{cmj} - T_f) + f_e\, m_D \sum_{H_2O} f_j\, w_j\, \Delta E_j$$

heat of reaction with oxygen — heat of hydrogen combustion

$$+ f_e\, m_D \sum_{O_2} f'_j\, w_j\, \Delta E'_j + \left(m_H + 2\, m_D\, f_e \sum_{H_2O} \frac{f_j\, w_j}{M_j}\, \ell_j \right) \Delta E_H$$

gas and steam sensible heat

$$- (m_s\, C_{vs} + m_g\, C_{vg})(T_f - T_g) - m_{sps}\, C_{vs}\, (T_{PS} - T_f)$$

$$+ \text{HEAT LOSS (assumed zero)} \quad \text{(B-1)}$$

where:

C_{cj} = specific heat of corium species j [kJ/kg • K],

C_{vg} = specific heat at constant volume of air [kJ/kg • K],

C_{vs} = specific heat at constant volume of steam [kJ/kg • K],

ΔE_j = heat of reaction of corium species j with steam [MJ/kg species j],

$\Delta E'_j$ = heat of reaction of corium species j with oxygen [MJ/kg species j],

ΔE_H = heat of combustion of hydrogen [MJ/kg] (set ΔE_H to zero if no H_2 burn is assumed),

f_e = fraction of corium entrained to containment atmosphere,

= 1 - α (α = de-entrainment fraction due to structural impediment obtained from Equation (2-1)),

f_j = fraction of corium species j reacted with steam,

f'_j = fraction of corium species j reacted with oxygen,

H_{fj} = latent heat of fusion of corium species j [MJ/kg],

ℓ_j - molar ratio of hydrogen produced to reactant corium species j consumed during steam oxidation (see Table B-1),

m_D - total debris mass entrained from cavity [kg] (determined by Equation 20 of Appendix A),

m_{cj} - mass of corium species j in the pressure vessel [kg],

m_g - initial mass of air in the containment,

m_H - mass of hydrogen expelled from RPV during high pressure melt ejection,

m_s - total mass of steam in the containment prior to high pressure melt ejection [kg],

m_{sps} - steam mass expelled from RPV at vessel failure [kg],

$= P_{PS}V_{PS}/RT_{PS}$,

M_j - atomic mass of corium species j [kg/kmol],

P_{PS} - primary system pressure at vessel failure [Pa],

T_c - temperature of corium prior to vessel failure [K],

T_{cmj} - melting temperature of corium species j [K],

T_f - final containment air temperature [K],

T_{PS} - primary system temperature at vessel failure [K],

T_g - temperature of air in the containment prior to high pressure melt ejection [K],

R - universal gas constant = 8.314 [kJ/kmol•K],

V_{PS} - primary system volume [m^3],

w_j - mass fraction of corium species j.

Subscript

j - refers to corium species such as ZrO_2, UO_2, Zr and stainless steel (Fe, Ni, Cr).

Summation

$\sum_{H_2O}$ sum over species reacting with steam,

$\sum_{O_2}$ sum over species reacting with oxygen.

Solving Equation (B-1) for T_f yields

$$T_f = \frac{1}{C_{vg} + \gamma C_{vs} + \epsilon \sum C_{cj} w_j} (\epsilon S_1 + \epsilon S_2 + \beta \Delta E_H + C_{vg} T_g + \gamma C_{vs} T_{PS}) \quad \text{(B-2)}$$

where:

$$S_1 = \sum C_{cj} w_j T_c + \sum H_{fj} w_j + \sum_{H_2O} f_j w_j \Delta E_j + \sum_{O_2} f'_j w_j \Delta E'_j$$

$$S_2 = 2 \sum_{H_2O} \frac{f_j w_j}{M_j} \ell_j \Delta E_H$$

ϵ = entrained mass ratio = $f_e m_D / \left(m_g + m_s \frac{c_{vs}}{c_{vg}} \right)$,

β = primary system hydrogen mass ratio = $m_H / \left(m_g + m_s \frac{c_{vs}}{c_{vg}} \right)$,

γ = primary system steam mass ratio = $m_{sps} / \left(m_g + m_s \frac{c_{vs}}{c_{vg}} \right)$.

Information necessary for calculating terms in Equation (B-2) is provided in Tables B-1, B-2, and B-3. Note that S_1 in Equation (B-2) represents a collection of properties of corium such as heat capacity, heat of fusion, heat and extent of reactions, corium composition, and corium superheat. S_2 represents heat of combustion of hydrogen (per unit mass of corium) produced by steam oxidation of metallic contents of debris during high pressure melt ejection. Given large uncertainty in our knowledge of corium properties under postulated severe accident conditions, it is reasonable to view S_1 and S_2 approximately as a constant for plants of similar design under similar accident conditions. On the other hand, parameters like α, β and γ, which represent dimensionless mass of entrainment, of hydrogen and of steam, can vary from plant to plant. However, if

values of α, β and γ are made the same for two plants, a calculation of T_f from Equation (B-2) for one plant will also be for another plant. These parameters will be helpful in scaling results from one plant to another plant without having to repeat similar calculations.

The containment final pressure (P_f), assuming the applicability of the ideal gas laws, is determined from the knowledge of T_f of Equation (B-2) by

$$P_f = \frac{T_f R}{V_c + V_{ca}} \left[\underbrace{\frac{m_g}{M_g}}_{\text{containment air}} + \underbrace{\frac{m_s}{M_s}}_{\text{containment steam}} + \underbrace{\frac{m_{sps}}{M_s}}_{\text{blowdown mass}} \right] \qquad \text{(B-3)}$$

where:

M_g - average molecular weight of dry air,

M_s - molecular weight of steam,

P_f - containment final pressure [Pa],

V_c - containment free volume [m^3],

V_{ca} - cavity/tunnel volume [m^3].

Table B-1
(Adapted from [Pilch, et al., 1986] and [Spencer, et al., 1988]

OXIDATION OF DEBRIS CONSTITUENTS IN AN OXYGEN ENVIRONMENT

Reaction	Heat of Reaction Per Unit Mass of Reactant [MJ/kg]
$Zr + O_2 \rightarrow ZrO_2$	11.8
$Fe + 1/2\ O_2 \rightarrow FeO$	4.78
$3UO_2 + O_2 \rightarrow U_3O_8$	0.483

OXIDATION OF DEBRIS CONSTITUENTS IN AN STEAM ENVIRONMENT

Reaction	Heat of Reaction Per Unit Mass of Reactant [MJ/kg]
$Zr + 2H_2O \rightarrow ZrO_2 + 2H_2$	6.74
$Fe + H_2O \rightarrow FeO + H_2$	0.43
$3Fe + 4H_2O \rightarrow 4H_2 + Fe_3O_4$	0.98
$2Cr + 3H_2O \rightarrow 3H_2 + Cr_2O_3$	4.2
$Ni + H_2O \rightarrow NiO + H_2$	0.04

HYDROGEN COMBUSTION

Reaction	Heat of Reaction Per Unit Mass of Reactant [MJ/kg]
$H_2 + 1/2\ O_2 \rightarrow H_2O$	121

Table B-2

PROPERTIES OF CORE DEBRIS CONSTITUENTS

Material	Density ρ (kg/m^3)	Thermal Conductivity k (W/m K)	Specific Heat Capacity* (J/kg K)	Melting Point (K)	Latent Heat of Fusion (MJ/kg)
Carbon Steel	8,000.	50.0	797[1] 864[2]	1,800.	0.250
Zircaloy	6,500.	18.0	356	2,098.	0.225
Zircaloy Oxide	5,600.	3.0	645	3,000.	1.196
Uranium Oxide	10,100.	3.3	491[1] 698[2]	3,113.	0.274

[1] At temperature of 2501 K.

[2] At temperature of 3001 K.

Table B-3

PRIMARY SYSTEM AND CORE DEBRIS CONDITIONS FOR DCH ASSESSMENT
(In accordance with NUREG-1150, Vol. 3, Appendix J.5)

Reactor Coolant System Pressure (P_{PS})	600-2400 psig
Reactor Coolant System Temperature (T_{PS})	Corresponding Saturation Temperature
Melt Temperature (T_c)	1800-2500 K
Fraction of Core Melted and Ejected	20-80%
Unoxidized Metal Content	20-70%
Hydrogen Cenerated in Core (m_H)	Proportional to Fraction of Oxidized Metal (30-80%)
Completeness of Chemical Reactions*	50-95%

*Large uncertainty remains in estimating the extent of oxidetion reactions with steam and oxygen which depend strongly on the debris temperature. As ballpark figures, the analyses of CWTI-DCH experiments suggest the following

$$f_j = \begin{cases} 0.75 & \text{for fully wet cavity regardless of water in the lower compartment} \\ 0.5 & \text{for dry cavity and wet lower compartment} \end{cases}$$

and

$$f'_j = \begin{cases} 0 & \text{for fully wet cavity with Zion-type impediment at tunnel exit} \\ 0.05 & \text{for fully wet cavity without impediment at tunnel exit} \\ 0.31 & \text{for dry cavity with Zion-type impediment at tunnel exit} \\ 0.67 & \text{for dry cavity without impediment at tunnel exit} \end{cases}$$

These values represent the conditions for the small scale ($3\frac{1}{3}$%) mockup, and should be considered as the lower bound for a reactor scale. The effects of presence of water are made clear in the values of f_j and f'_j.

APPENDIX C

Hydrogen Combustion Limits

Numerous experiments have been performed to establish the combustion limits of hydrogen as a function of hydrogen concentration and inert gases. One such study [Benedick, 1984] provided a demonstration of the inerted capabilities of carbon dioxide. The results for these experiments peformed in the VGES test vessel at Sandia are illustrated in Figure C-1, wbich is taken from Reference [Benedick, 1984]. This also shows the results of other experiments at Lawrence Livermore and Sandia using steam as the inerting material. As shown, the atmosphere becomes inerted at a CO_2 concentration of 52%.

A substantial experimental program was performed in the FITS vessel at Sandia to clearly define the combustion boundaries for a hydrogen-air-steam mixture both in quiescent conditions and in a turbulent environment (fans operational). This set of experiments is particularly meaningful to accident management evaluations because (1) steam is the inerting medium, (2) the boundary is clearly defined and (3) the experimental apparatus took great pains to attempt ignition of the mixture. Figure C-2 taken from Reference [Marshall, 1986] illustrates the test results for both the "fans off" and "fans operational" conditions. Those conditions which are represented as "no burn" represent the mixture state in which neither repeated spark initiators nor a glow plug was capable of initiating a burn.

The experimental information was subsequently formulated into a correlation to represent the combustion limits. This is given by

$$\% \text{ Steam} = 100 - \% H_2 - 37.3e^{-0.007\% H_2} - 518e^{-0.488\% H_2} \qquad \text{(C-1)}$$

and is compared to the experimental results in Figure C-2. This result is particularly meaningful to accident management guidance since it demonstrates that containment buildings could be absolutely inerted against hydrogen combustion with a steam concentration of approximately 53%. This

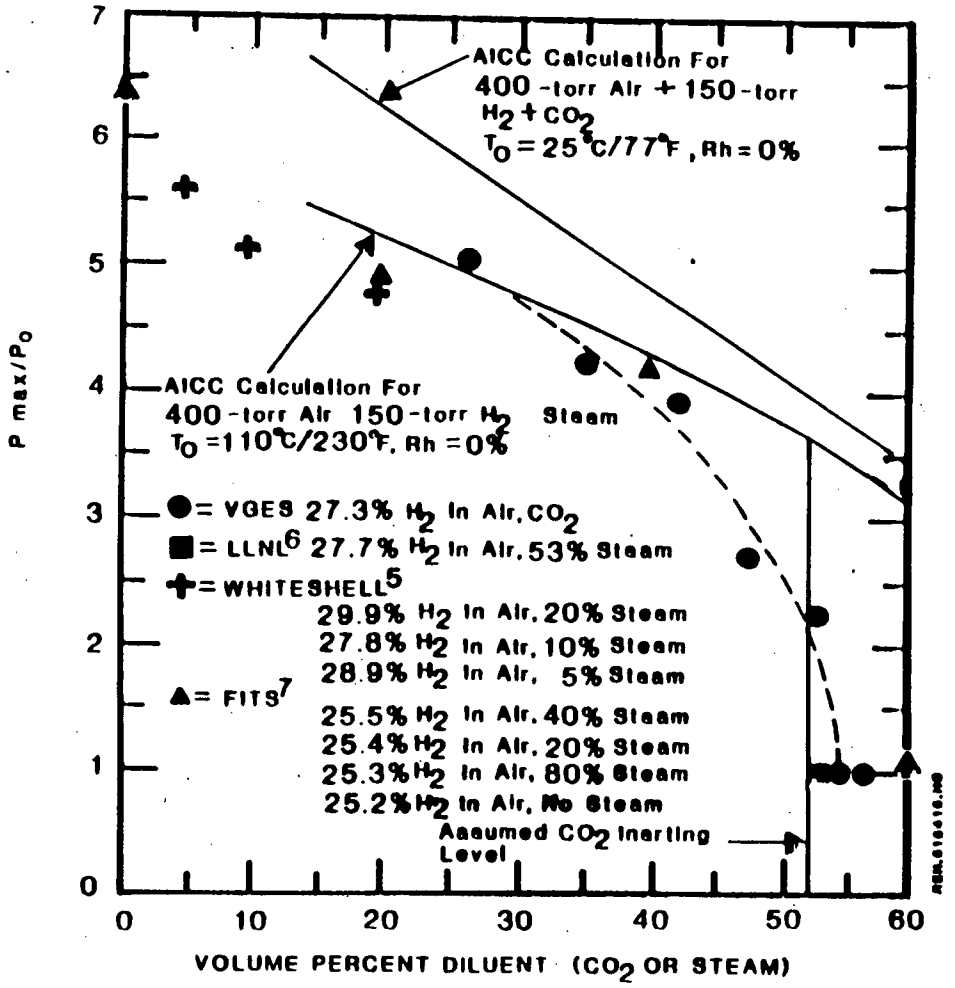

Figure C-1 Normalized peak pressure (P_{max}/P_o) for hydrogen:air:diluent mixtures, comparing CO_2 and steam (AICC = adiabatic isochoric complete combustion, Rb = relative humidity).

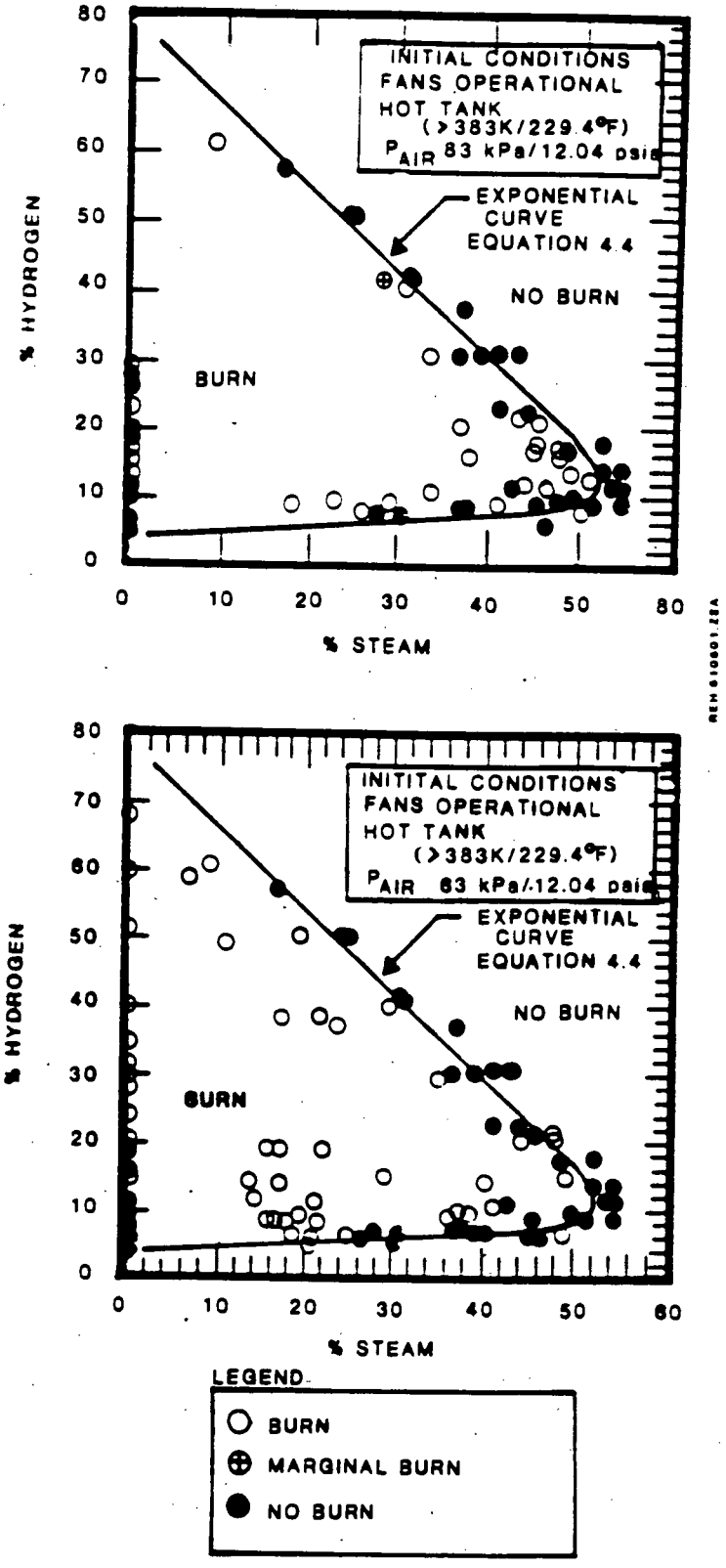

Figure C-2 Experimental data for combustion limits with fans on and off shown with the exponential curve fit.

means that if sufficient steam is released to a non-inerted containment building to produce a steam partial pressure of slightly over one atmosphere, hydrogen combustion would be precluded regardless of how much hydrogen was accumulated in containment. Since steam would be produced as a natural consequence of the accident condition the containment could be completely inerted prior to vessel failure. This should be assessed, where necessary, on a sequence specific basis.

APPENDIX D

Scaling of Entrainment and Displacement Rates

For scaled experiments to provide a meaningful representation of the reactor condition, the experiment should exhibit the same relative rates of debris entrainment and displacement, i.e. the ratio of the rates should be the same. As discussed in Appendix A, we can use the Ricou-Spalding correlation to represent the entrainment rate.

$$\dot{m}_e = C_1 A_s \sqrt{\rho_D \rho_g} U_c \qquad \text{(D-1)}$$

where A_s is the cavity floor area available for entrainment. The displacement rate can be viewed as the mass of core debris over the displacement time.

$$\dot{m}_D \approx m_c / t_D \qquad \text{(D-2)}$$

Assuming a constant acceleration (constant pressure differential), the displacement time is given by,

$$t_D = \sqrt{\frac{2L_p}{a}} = \sqrt{\frac{2\ \rho_D L_p L}{\Delta P}} \qquad \text{(D-3)}$$

where a is the acceleration ($a = \Delta P/(\rho_D L)$) and the terms L and L_p are defined in Figure 2-10.

The pressure differential can be related to the gas dynamic head,

$$\Delta P \approx \frac{\rho_g U_c^2}{2} \qquad \text{(D-4)}$$

such that

$$\dot{m}_D \approx 0.5\ \delta_b \sqrt{\frac{L_p}{L}} \sqrt{\rho_D \rho_g} U_c \qquad \text{(D-5)}$$

Formulating the ratio between the two rate dependent processes yields,

$$\frac{\dot{m}_e}{\dot{m}_D} = \frac{C_1}{0.5}\sqrt{\frac{L_p}{L}}\left(\frac{H}{\delta}\right) \qquad \text{(D-6)}$$

Where H is the height of the horizontal portion of the cavity/tunnel and δ is the height of the debris layer on the cavity floor. This shows that a linearly scaled model preserves the ratio of the relative rates for debris removal from the reactor cavity/instrument tunnel region.

APPENDIX E

Calculational Method for Detrainment at a 90° Turn

A scoping calculation will be developed to establish the amount of dsbris de-entrained at the 90° turn from the cavity instrument tunnel to the lower containment compartment.

As in Figure E-1, the cavity instrument tunnel is assumed to have cross-sectional area $L\ell$ and the opening into the lower containment compartment is assumed to have a cross-sectional area $W\omega$.

The equation of motion for a spherical drop, of diameter d and mass m in a gas flow is:

$$m \dot{\underline{V}} = mg - \frac{1}{2} C_D \pi \left(\frac{d}{2}\right)^2 \rho_G \left|\underline{V} - \underline{u}\right| (\underline{V} - \underline{u}) \qquad \text{(E-1)}$$

where g is the gravitational constant, C_D is the drag coefficient, $\underline{u}$ is the gas velocity and ρ_G is the gas density.

Re-write the equation as

$$\dot{\underline{V}} = \lambda \left|\underline{V} - \underline{u}\right| (\underline{V} - \underline{u}) + g \qquad \text{(E-2)}$$

where ρ_L is the density of the drop and

$$\lambda = \frac{3}{4} \left(\frac{1}{d}\right) \frac{\rho_g}{\rho_L} C_D. \qquad \text{(E-3)}$$

For the regime of gas velocities we are interested in $C_D = 0.44$ and, we can neglect the effects of gravity on the particles. The equation of motion then becomes

$$\dot{\underline{V}} = - \lambda \left|\underline{V} - \underline{u}\right| (\underline{V} - \underline{u}). \qquad \text{(E-4)}$$

Integrating the equation of motion gives

Cavity Instrument Tunnel & Opening Into Lower Containment

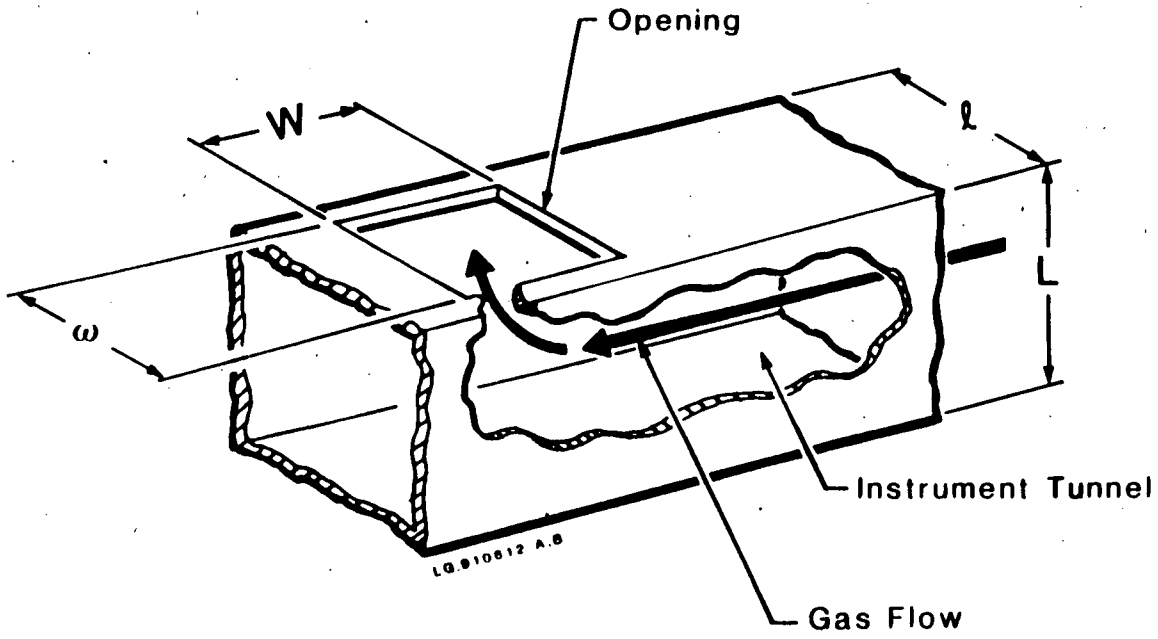

Figure E-1

$$\underline{V}(t) = \underline{u}_1 + \frac{(\underline{V}_o - \underline{u}_1)}{1 + \lambda|\underline{V}_o - \underline{u}_1|t} \tag{E-5}$$

Where $\underline{V}_o$ is the initial velocity of the particle and $\underline{u}_1$ is the velocity of the gas as it leaves the instrument tunnel.

In the coordinate system chosen and displayed in Figure E-2

$$\underline{V}_o = - u \hat{\underline{x}}. \tag{E-6}$$

$\underline{u}_1$ is calculated from $\underline{u}$ using the continuity equation.

$$\underline{u}_1 = \left[\frac{L\ell}{W\omega}\right] u \hat{\underline{y}} \tag{E-7}$$

For convenience define

$$\gamma = \left[\frac{L\ell}{W\omega}\right]. \tag{E-8}$$

In order to separate the equation of motion into its vector components, simplify the denominator of Equation (E-5).

$$\left|\underline{V}_o - \underline{u}_1\right| = \left| -u\hat{\underline{x}} - \gamma u\hat{\underline{y}}\right| = u\sqrt{1 + \gamma^2} \tag{E-9}$$

For convenience define

$$\sqrt{1 + \gamma^2} = \Gamma. \tag{E-10}$$

Now equation (5) becomes

$$\underline{V}(t) = \underline{u}_1 + \frac{(\underline{V}_o - \underline{u}_1)}{1 + \lambda\Gamma ut} \tag{E-11}$$

Separating Equation (E-1) into its vector components gives

$$V_x(t) = \frac{-u}{1 + \lambda\Gamma ut} \tag{E-12}$$

and,

Cooridinate System in Instrument Tunnel

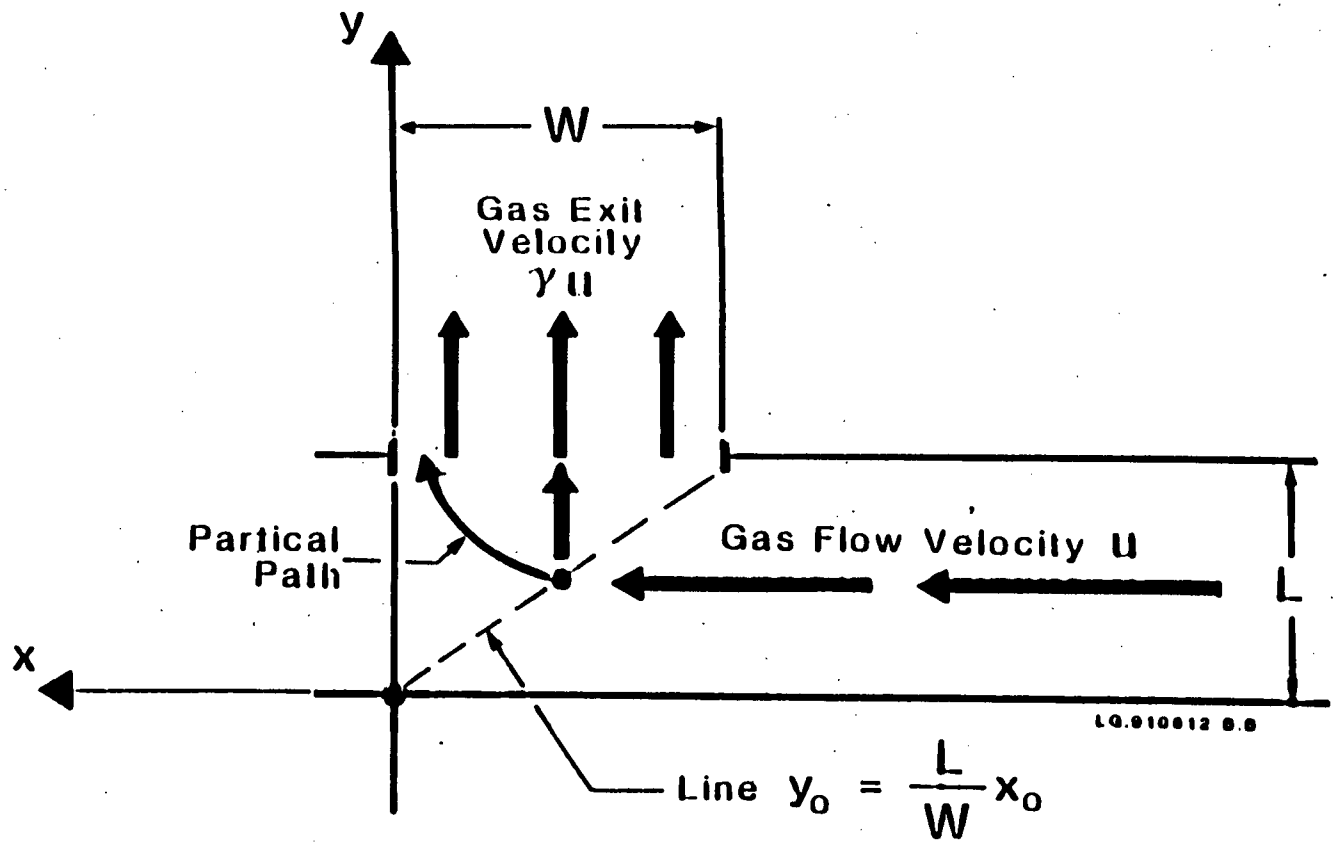

Figure E-2

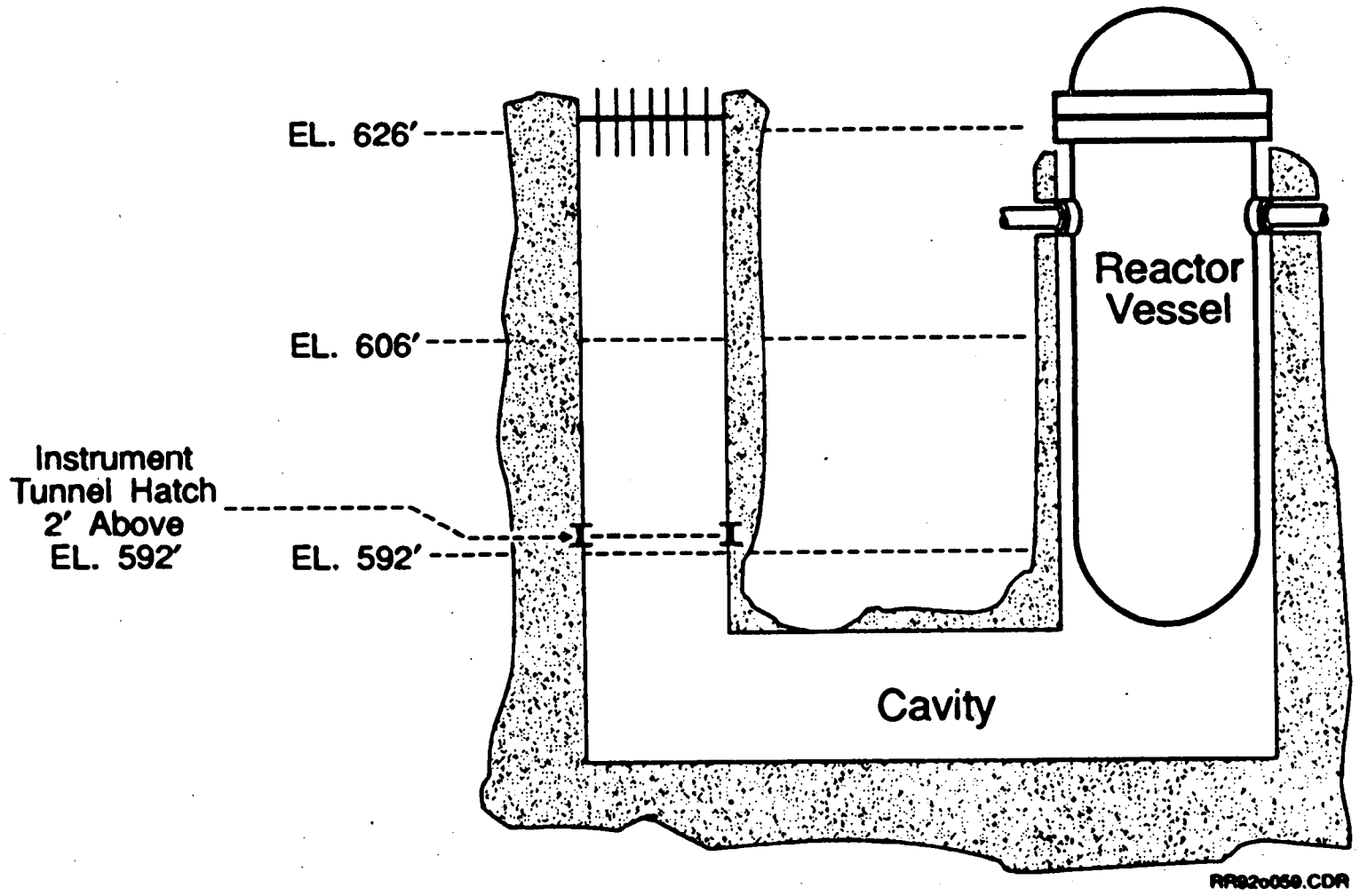

Figure E-2 Sketch of the Kewaunee cavity and Instrument Tunnel

$$V_y(t) = \gamma u - \frac{\gamma u}{1 + \lambda \Gamma u t} \qquad \text{(E-13)}$$

Integrating Equations (E-12) and (E-13) gives

$$x(t) = \frac{-1}{\lambda \Gamma} \ln (1 + \lambda \Gamma u t) + x_o \qquad \text{(E-14)}$$

and

$$y(t) = \gamma u t - \frac{\gamma}{\lambda \Gamma} \ln (1 + \lambda \Gamma u t) + y_o \qquad \text{(E-15)}$$

For simplicity assume that the gas velocity in the tunnel changes from $-u\hat{x}$ to $\gamma u\hat{y}$ along the line $y = \frac{L}{W} X$. The initial conditions, (x_o, y_o), will then be related as $y_o = \frac{L}{W} x_o$.

For some (y_o, x_o) there will be a time t_f at which $x(t_f) = 0$ and $y(t_f) = L$. Let this (y_o, x_o) be (y_i, x_i). All particles at positions $y_o < y_i$ at time t_f will not make the turn. Define $\alpha = \frac{y_i}{L}$ as the fraction of particles not making the turn.

Solve equations 14 and 15 for α. First substitute equation 14 into equation 15 to get

$$y(t) = \gamma u t + \gamma (x(t) - x_o) + y_o \qquad \text{(E-16)}$$

At time, t_f, equation (16) becomes

$$L = \gamma u t_f + y_o (1 - \gamma \frac{W}{L}). \qquad \text{(E-17)}$$

Solving Equation (E-17) for t_f and plugging this expression into equation 16 gives

$$\alpha = \frac{1}{\lambda \Gamma W} \ln \left(1 + \frac{\lambda \Gamma L}{\gamma} (1 - \alpha (1 - \frac{W}{L} \gamma)) \right) \qquad \text{(E-18)}$$

This expression can be solved for α iteratively for different cavity dimensions and particle sizes to find the fraction of core material de-entrained at a 90° turn.

FAI/91-88

A PHENOMENOLOGICAL EVALUATION SUMMARY ON STEAM EXPLOSIONS IN SUPPORT OF THE KEWAUNEE NUCLEAR PLANT INDIVIDUAL PLANT EVALUATION

Submitted To:

Wisconsin Public Service Corporation
Green Bay, Wisconsin

Prepared By:

Fauske & Associates, Inc.
16W070 West 83rd Street
Burr Ridge, Illinois 60521

Final Issue

January, 1993

ABSTRACT

Steam explosion phenomena are evaluated for both in-vessel and ex-vessel events as potential mechanisms for containment failure under severe accident conditions, and therefore as a potential cause for radioactive releases to the environment.

The issue for in-vessel steam explosions is whether an explosion of sufficient magnitude to fail the reactor vessel, with consequential failure of the containment, could occur. This was addressed by evaluating the fundamental physical processes required to create an explosion of such magnitude. The analysis closely follows the IDCOR assessment of this phenomena and concludes that explosions of this magnitude could not be established within the confines of the Kewaunee reactor vessel. This is in overall agreement with the findings of the NRC sponsored Steam Explosion Review Group (SERG) which concluded that the likelihood of an in-vessel steam explosion leading to containment failure (alpha mode failure) was very unlikely.

Ex-vessel steam explosions have been addressed by considering both the potential for rapid steam generation as a result of the explosive interaction and the shock waves that could be formed and propagated to the containment boundary. These analyses clearly indicate that sufficient steam overpressure to challenge the reactor containment integrity would not be achieved under any realistic conditions. In addition, shock waves that could be produced by explosive interactions, when propagated to the containment boundary, result in overpressure values which are well within the steady-state design basis of the containment boundary.

Consequently, the assessment of steam explosions for the Kewaunee plant results in the conclusion that neither in-vessel nor ex-vessel steam explosion events would lead to conditions which challenge the containment boundary. As a result, steam explosions are not included as top events in the Kewaunee containment event trees (CETs).

TABLE OF CONTENTS

		Page
	ABSTRACT	i
	LIST OF FIGURES	iv
	LIST OF TABLES	v
1.0	PURPOSE	1-1
2.0	PHENOMENA	2-1
	2.1 Description	2-1
	2.1.1 Controlling Physical Processes	2-4
	2.1.2 Relationship to Containment Failure Mechanisms and Modes	2-5
	2.1.3 Relationship to Source Term	2-6
	2.2 Industry Experiences With Steam Explosions	2-7
	2.2.1 Nuclear Incidents	2-7
	2.2.2 Non-Nuclear Explosion Boiling Studies	2-8
	2.2.3 Other	2-10
	2.3 Experiments	2-10
	2.3.1 Sandia Thermite and Corium Experiments	2-10
	2.3.2 Aluminum-Water Experiments	2-14
	2.3.3 Liquefied Natural Gas and Water Experiments	2-16
	2.3.4 FAI Thermite Experiments	2-16
	2.3.5 Sandia FITS Tests	2-18
	2.3.6 Summary	2-27
	2.4 Analysis	2-28
	2.4.1 Effect of System Pressure on Steam Explosions	2-29

TABLE OF CONTENTS (Continued)

Page

2.4.2 Shock Waves 2-30

2.4.3 Possible Mechanism for Maximum Steam Generation Rate. 2-34

3.0 METHODOLOGY. 3-1

3.1 In-Vessel Steam Explosions 3-1

3.2 Ex-Vessel Steam Explosions 3-1

3.2.1 Pressure Rise Due to Rapid Steam Generation. 3-2

3.2.2 Shock Waves. 3-3

4.0 PLANT SPECIFIC APPLICATION 4-1

4.1 Issues. 4-1

4.1.1 In-Vessel Steam Explosions 4-1

4.1.2 Ex-Vessel Steam Explosions 4-1

4.1.3 Uncertainty Considerations 4-2

4.2 Conclusions 4-4

5.0 CONCLUSIONS 5-1

6.0 REFERENCES 6-1

LIST OF FIGURES

Figure No.		Page
2-1	Behavior modeled in WASH-1400	2-2
2-2	Comparison of predicted pressure-tima behavior from WASH-1400 (1.575×10^{-2} in. particle size) and available experimental results for steam explosions	2-3
2-3	Measured debris-water energy transfer rates from EPRI sponsored Mark I liner tests	2-17
2-4	FITS containment chamber	2-20
2-5	FITS2B chamber air pressure	2-23
2-6	FITS3B chamber air pressure	2-24
2-7	FITS7B chamber air pressure (no camera data)	2-25
2-8	FITS6B chamber air pressure (saturated water)	2-26
2-9	Comparison of shock wave pressures for TNT and point source explosions	2-31
2-10	Debris dispersion configuration	2-35

LIST OF TABLES

Table No.		Page
2-1	Effective Heat Flux Measurements for Debris-Water Interactions	2-19
2-2	FITSB Initial Conditions and Observations	2-21
2-3	Chamber Air Pressure Data From FITSB (Times From Melt Entry)	2-33

1.0 PURPOSE

A steam or vapor explosion refers to a boiling process in which steam or vapor production occurs at a rate larger than the surrounding media can acoustically relieve the resulting pressure increase, leading to the formation of a shock wave. In previous studies evaluating the public risk associated with severe accident sequences, such as the Reactor Safety Study [NRC, 1975], steam explosions within the primary system have been considered as a potential mechanism for violating both the primary system and the reactor containment building, thereby generating a direct release path for the fission products. The in-vessel steam explosion considered was theorized to result from the following chain of events:

1. loss of cooling water from the core resulting in fuel overheating and melting,
2. the catastrophic collapse of the core debris into the water remaining in the lower plenum,
3. an instantaneous fine scale intermixing of the core debris and water,
4. rapid heat removal from the core material and expansion of the steam against an assumed continuous, overlying liquid slug,
5. impact of this liquid slug on the reactor vessel head with sufficient energy to rupture the head, and
6. ejection of the RPV head as a missile with sufficient velocity to fail the containment wall upon impact.

In NUREG-1116 [NRC, 1985], the NRC sponsored Steam Explosion Review Group (SERG) provided recommendations regarding the likelihood that an in-vessel steam explosion could cause containment failure. The main conclusion of the group report was: "Based upon the probability estimates summarized above, the consensus of the SERG is that the occurrence of a steam explosion of sufficient energetics which could lead to alpha-mode containment failure has a low probability. This conclusion is reached despite the expression of differing opinions on modeling of basic steam explosion sequence phenomenology."

Ex-vessel steam explosions also potentially may occur in the progression of a severe accident should debris be discharged from the reactor vessel into a pool of water. In a containment building, the occurrence of a steam explosion would impose shock waves on submerged surfaces and subcompartment walls. These must be evaluated to determine if the resulting loads could challenge the integrity of interior walls and the containment boundary.

In Generic Letter 88-20 [NRC, 1988], the NRC identified steam explosions as a potential containment failure mechanism that should be assessed as part of an IPE. Both in-vessel and ex-vessel steam explosions have been postulated as a potential mechanism for early containment failure, possibly with an elevated release location. Either of these characteristics could have substantial effects on the consequence evaluation for hypothetical accident sequences. The objective of this report is to evaluate the potential for in-vessel and ex-vessel steam explosions to threaten containment integrity for the Kewaunee IPE.

2.0 PHENOMENA

2.1 Description

Explosive interactions between high and low temperature liquids have been encountered for decades in metal foundries as well as the pulp and paper industries. Experience has shown that these accidents can produce significant damage to typical industrial components (furnaces, casting pits, recovery boilers, etc.) as well as to light industrial buildings. Human casualties have also occurred as a result of these events, but the major hazard to operating personnel from these events has generally been burns resulting from hot molten material dispersed by the explosive interaction. In addition to such non-nuclear experiences, destructive steam explosions have been observed in the BORAX [Deitrich, 1965] and SPERT [Miller, 1964] test reactors as well as in the SL-1 accident [SL-1]. In all of these three test reactor configurations, the destructive explosion followed a rapid (~ 30 ms) reactivity insertion that was sufficient to melt both the uranium-aluminum alloy fuel and the aluminum cladding.

Figure 2-1 illustrates the modeling concept of in-vessel steam explosions used in the Reactor Safety Study [NRC, 1975]. Efficient steam explosions were assumed to occur if molten core material dropped into water. In addition, the expanding mixture was assumed to propel a coherent liquid slug against the vessel upper head. Figure 2-2 shows the calculated mixture pressure, as well as the pressure acting on the upper head, when these global assumptions were made. However, no modeling considerations were given to:

- Could an explosive interaction be initiated?
- How efficient would the interaction be if it could be initiated?
- Could a coherent water "slug" be formed over the interaction zone?
- Could a water "slug" be propagated upward through the vessel upper internals?

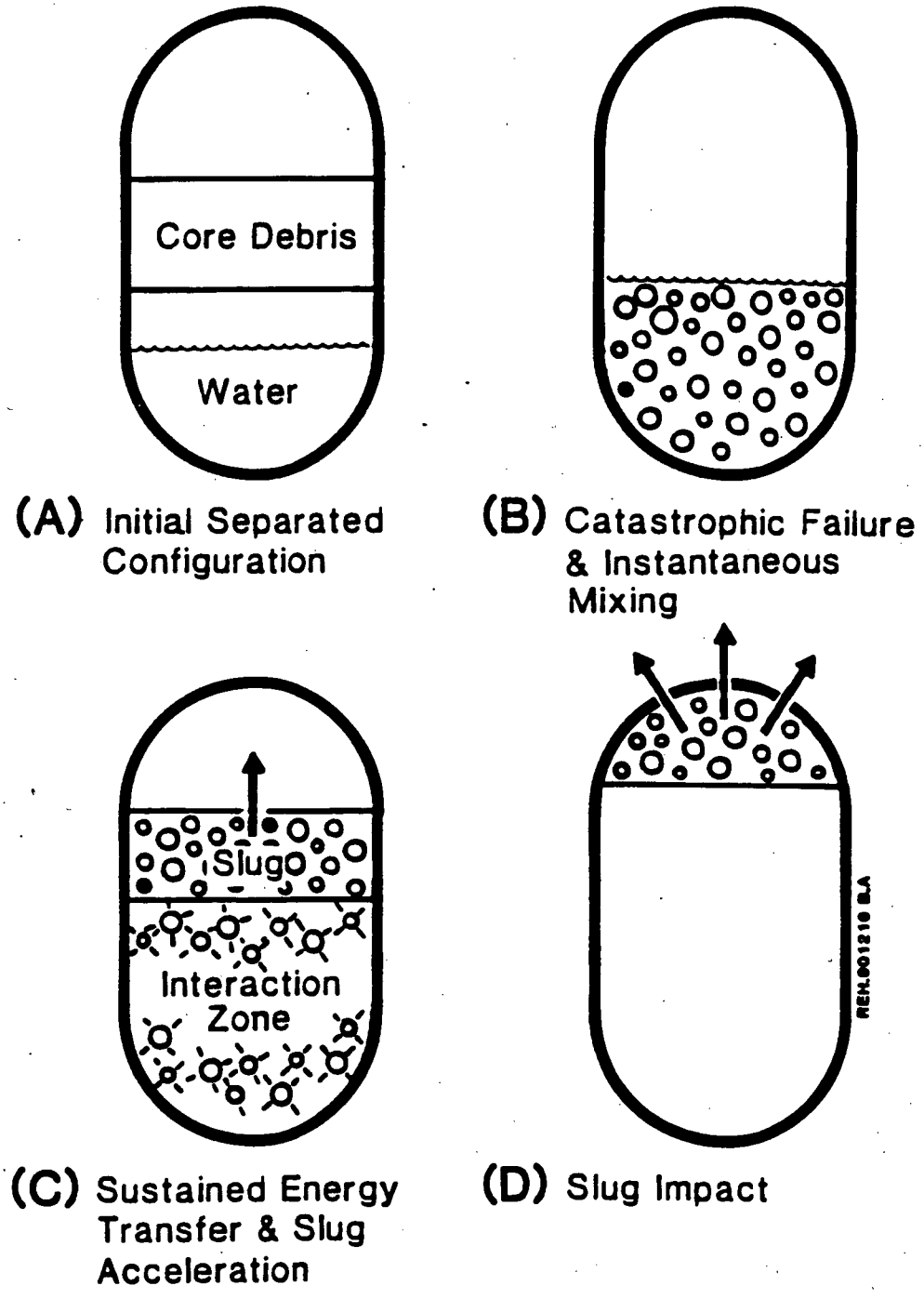

Figure 2-1 Behavior modeled in WASH-1400.

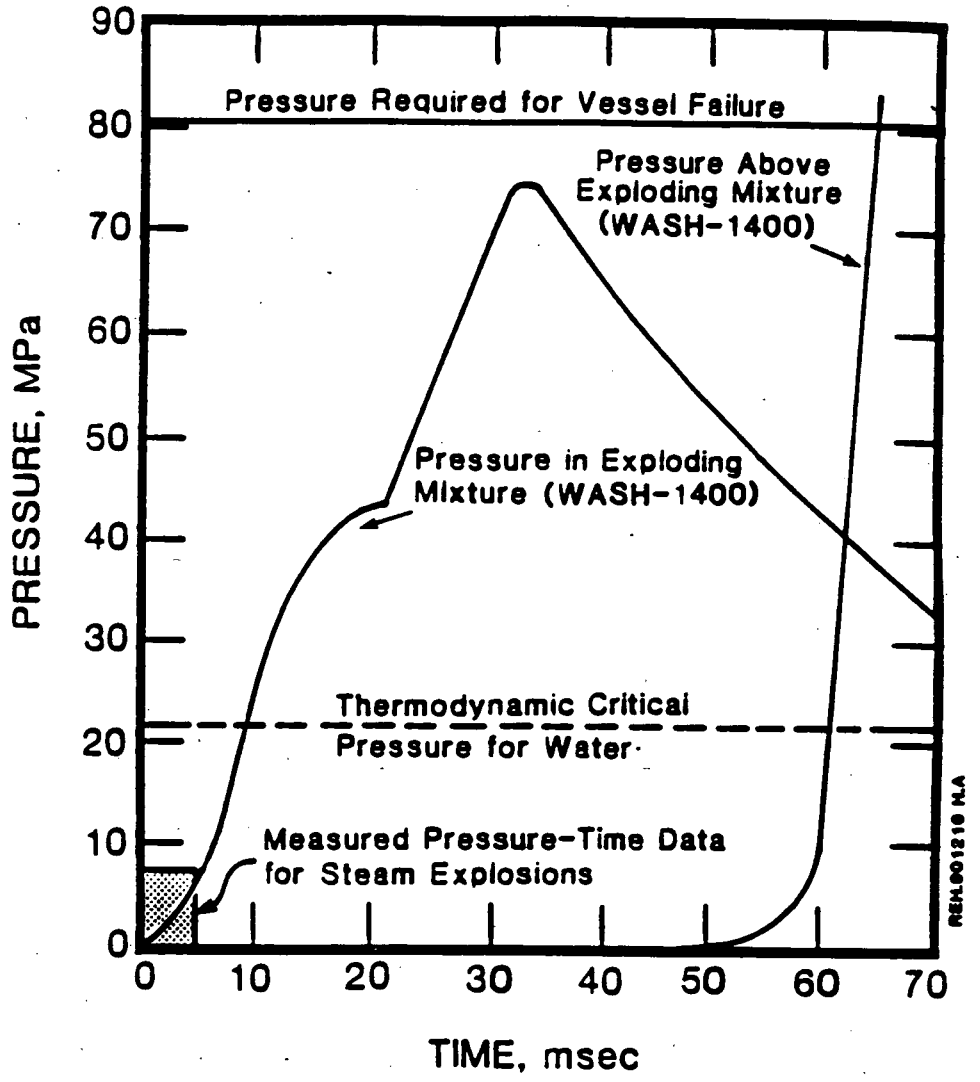

Figure 2-2 Comparison of predicted pressure-time behavior from WASH-1400 (1.575×10^{-3} in particle size) and available experimental results for steam explosions.

Also, the typical pressure-time relationships for large scale explosive experiments, which are summarized in [IDCOR, 1983], are much less than the calculated behavior used in WASH-1400.

2.1.1 Controlling Physical Processes

Large scale steam explosions inside or outside the reactor vessel require that large fractions of hot molten material be very finely fragmented and intermixed with the water on the time scale of the explosion. Such processes were envisioned in [NRC, 1975], but in addition, rapid heat transfer was calculated in the supercritical and superheated steam regions and the resulting energy transfer was delivered to a postulated overlying liquid slug that covered the interaction zone. Without the slug transmission mechanism, the pressure-time curves shown in [NRC, 1975] would have been insufficient to rupture the reactor pressure vessel, which was the mechanism envisioned as causing containment failure (α mode failure).

Consequently, the key physical processes involved in assessing the magnitude of steam explosions within BWRs and PWRs involves an assessment of:

- the energy required to rupture a reactor pressure vessel,
- the amount of core material needed to provide such an energy release,
- a mechanistic description of the fragmentation of the hot material in the water,
- an assessment of the mixing energy requirements when the material is finely fragmented and rapidly intermixed during the explosion,
- the size of an external trigger (if such exists) to initiate the explosion,
- an assessment of the propagation characteristics for the coarsely fragmented system,
- the likelihood of having a water slug over the reactor zone to transmit the energy in a coherent fashion, and

- the ability of this slug to be transmitted through upper core structures within the reactor pressure vessel.

Each of these conditions must be achieved to create an event of sufficient magnitude to rupture a reactor pressure vessel; the failure of a single element is sufficient to preclude an event of such magnitude.

2.1.2 Relationship to Containment Failure Mechanisms and Modes

Both in-vessel and ex-vessel steam explosions have been postulated to be early containment failure mechanisms that would occur immediately following slumping of the core material into the reactor vessel lower head. The largest potential for the occurrence of an in-vessel steam explosion would exist during a core melt sequence with a low primary system pressure. The largest threat to containment integrity as the result of an ex-vessel steam explosion would exist for a core melt sequence with a relatively coherent pour of molten material at vessel failure into a water pool.

Three actual containment failure mechanisms are considered to be encompassed by containment failures induced by steam explosions. For in-vessel steam explosions, a missile (e.g., the reactor vessel upper head) would have to be created with sufficient energy to pierce the containment. For ex-vessel steam explosions two possibilities are considered: the blast could weaken the pedestal walls sufficiently that the vessel moves and tears out one or more containment penetrations; or, the generated steam could over-pressurize the containment. For the in-vessel mechanism, the failure area has been assumed as a large break in the containment wall (i.e., on the order of several square feet). For the first ex-vessel mechanism, where the containment penetrations are torn, the resulting failure would be a function of the number of penetrations torn and the size of the penetration. The failure could be small; more like a "leak before break" condition, or it could be a much larger or "catastrophic" failure. Although it is assumed that this mechanism will result in a small "leak before break" condition. A failure resulting from containment over-pressure would be a large catastrophic failure of the steel shell. The anticipated rate of pressure

increase from a steam explosion is less than that associated with a design basis large break LOCA.

2.1.3 Relationship to Source Term

Containment failure resulting from a steam explosion would influence the expected fission product source term for a sequence by providing a large gas flow path out of the containment shortly after vessel failure. The effect on the source term, however, would strongly depend on the availability of water injection or sprays into the containment during a sequence. For sequences in which containment sprays would be available before the explosive interaction, removal of airborne aerosols would be very effective. So much so, that release to the environment would likely not be much greater than the release of the noble gases. However, such an early containment failure would generally increase the source term for accident sequences without containment injection or sprays, since the airborne fission product concentration would be much greater than for a case with the sprays operating. Also, the relatively large expected failure size would cause a rapid blowdown of the initially available airborne fission products to the auxiliary building or environment thereby reducing the fission product retention effectiveness of the containment. On the other hand, fission products entering the containment atmosphere after the blowdown would experience little driving force from the containment to the auxiliary building or the environment. Thus, fission products evolved by long-term revaporization within the reactor vessel would be subject to the naturally-occurring deposition mechanisms in the containment.

For sequences in which vessel injection was restored after vessel failure or containment sprays initiated, the expected fission product source term would be somewhat reduced. Providing water into the containment via either means would cool the containment atmosphere and contribute to a reduction in the magnitude of long-term fission product revaporization. For those sequences which could experience a lower head failure, use of either containment injection method would assure the debris is covered by water. For an upper head failure, both vessel injection and containment sprays would again act to accomplish this objective.

2.2 Industry Experiences With Steam Explosions

2.2.1 Nuclear Incidents

The explosion model used in the Reactor Safety Study [NRC, 1975] resulted principally from concerns generated by the low pressure BORAX and SPERT destructive experiments and the SL-1 accident. Reactor conditions leading to the SL-1 accident and the destructive transients in BORAX [Deitrich, 1965] and SPERT [Miller, 1964] were produced in a fundamentally different system than that representative of a postulated severe accident in a commercial LWR. It is not only important to realize these differences, but it is essential to understand the resulting implications on the phenomenon as well. These basic differences are delineated below.

1. All three destructive events were produced by power excursions in which the core was driven to molten conditions in 30 msec or less and essentially with water still between the fuel plates. Such strong reactivity transients are not possible in commercial power reactors and water must be removed from the core before overheating could occur.

2. The specific core designs of these reactors could be brought to supercritical conditions by the withdrawal of a single control rod. In these transients, a control rod was rapidly withdrawn which caused a nuclear excursion with sufficient energy deposition to melt the fuel-clad plates, with water still between the fuel plates.

3. Each of these three reactors was fueled with thin uranium-aluminum alloy fuel plates clad in aluminum. Thus, with water between the fuel plates, the fuel and water were uniformly premixed on a fine scale in the as-fabricated geometry. No additionsl melt fragmentation was required to accomplish the explosive energy release.

4. Since the reactors were essentially at room temperature prior to the excursion, the vessels were filled with cold water except for a small freeboard volume at the top, i.e. a long, coherent overlying liquid slug was in place prior to the reactivity insertion.

5. The vessel internal geometry was very simple and open, which provided little attenuation or dispersion of any slug movement.

With these initial conditions, the configuration established was essentially an inertial layer of water above an expanding layer of water, as assumed in the Reactor Safety Study. The essential feature of the strong reactivity transient is that it brought the fuel and clad to melting before this configuration could substantially change. Given these particular characteristics, a slug impact following a steam explosion with the core would indeed be the expected chain of events. However, this is fundamentally different than an initially separated state of high temperature molten core material and saturated water existing at an elevated pressure with substantial internal structure to prevent catastrophic collapse, intimate mixing, and slug formation.

2.2.2 Non-Nuclear Explosion Boiling Studies

In a number of industrial operations, the possibility of contacting two liquids exists -- one hot and relatively nonvolatile and the other cold and volatile. Should such an event occur, boiling occurs in such a sufficiently short time scale that the surrounding medium cannot relieve the expansion acoustically and a shock wave forms, i.e., an explosion. Accidents of this nature have been given various names, e.g., explosive boiling, rapid-phase transitions (RPTs), vapor explosions, thermal explosions, fuel-coolant interactions (FCI), etc. They have been observed in a number of industrial operations, e.g., when water contacts molten aluminum (or other metals), molten salts or paper mill smelt, or when cryogenic liquids such as LNG (liquefied natural gas) are spilled into water. In the first two examples noted above, water is the volatile liquid which explosively boils whereas in the last example, the cryogenic liquid plays the role of the volatile, boiling liquid and water is then the "hot" fluid.

2.2.2.1 Smelt-Water Explosions

Studies of molten salt/water explosions were carried out because industrial accidents involving these reactants have taken place. Emphasis has been placed on events occurring in the paper industry where molten smelt is produced in the recovery boilers. This smelt is a mixture of, primarily,

sodium chloride, sodium carbonate, and sodium sulfide. The smelt temperature is much higher than the critical point of water (~ 1520.6°F (1100K) compared to 750.2°F (647K)). Severe explosions have taken place when water inadvertently contacted molten smelt.

Laboratory investigations [Krause, et al., 1973], [Shick, 1980] into the mechanism of smelt-water explosive boiling events have been primerily useful in delineating the effect of smelt composition on the sensitivity of the salt in producing explosive boiling. For example, pure molten sodium carbonate has never led to explosive boiling. Addition of either (or both) sodium chloride or sodium sulfide leads to smelts which are more prone to explosive boiling. Investigators experimented with many additives both to the smelt and to the water in an attempt to obtain less sensitivity. Most had little or no effect.

2.2.2.2 Melt-Water Interactions

The metals processing industries, particularly those producing aluminum, have also been plagued by explosive boiling incidents. Alcoa has carried out several test programs [Lemmon, 1980], [Hess, et al., 1980] directed primarily at effecting means to prevent such accidents in casting plants. In most tests, molten aluminum was dropped into water and the subsequent events recorded. Many variables were studied such as water temperature, drop height, nozzle diameter, etc. The principal result of these investigations was to show that water containers, suitably coated with an organic-based paint, would not lead to explosions when molten aluminum was spilled into the container. Use of such paints in aluminum plants has indeed reduced the frequency of explosions, but many still occur. In a large number of accidents, the quantity of water was quite small, e.g., when "wet" aluminum ingots were loaded into melting furnaces containing molten aluminum. In contrast to this fact, few, if any, serious events have occurred when small quantities of aluminum were contacted with a large mass of water. Since laboratory tests were often carried out in the latter fashion, most of these have not resulted in explosive interactions.

2.2.2.3 Other

In industries dealing with "reactive" metals, such as titanium, zirconium, etc., only a few serious explosive boiling events have been documented. In most of these, a significant quantity of molten metal has contacted water and, simultaneously, there has been some external shock such as an electrode falling into the metal water mixture. In the few known incidents, damage has been severe, but quite localized. Due to the reactive nature of the metal, however, subsequent hydrogen fires have often compounded the problem and led to extensive damage.

2.3 Experiments

A wide range of laboratory scale and large scale experiments relating to vapor explosions have been performed over the past thirty-five years. The laboratory scale experiments constitute an extensive literature base and are reviewed in detail in [FAI, 1982] and [IDCOR, 1983].

2.3.1 Sandia Thermite and Corium Experiments

Large scale steam explosion experiments have been carried out at the Sandia Laboratories in three different test series, two using an iron-thermite mixture [Buxton, et al., 1979] [Mitchell, et al., 1981] to simulate the degraded core material and the other using both an iron-thermite and a corium-thermite [Buxton, et al., 1980] which had a higher melting temperatures and are more realistic simulants of the anticipated debris character. In both of these experimental series, artificial triggers (explosive detonators) were used to initiate the interaction in some tests.

In the first set of experiments [Buxton, et al., 1979], the iron-thermite melt was discharged directly into a 2.95 ft (0.9 meter) diameter vessel filled with water. For all those experiments carried out with an artificial trigger, the water was at the ambient temperature, assumed to be 70°F (295K). (In these experiments the ambient pressure was always slightly less than 14.5 psig (0.1 MPa).) The melt temperature resulting from the thermite reaction is approximately 4400.6°F (2700K) and results in reaction

products of metallic iron (Fe) and aluminum trioxide (Al_2O_3). The melting temperature for the aluminum trioxide is approximately 3680.6°F (2300K) and that for metallic iron is about 2780°F (1800K). Consequently, solidification of either of these constituents requires a substantial decrease in temperature and the resulting fragmentation process could continue as the melt cools, i.e. lower temperatures reduce the film boiling steam generation rate and allow finer particulation. To externally trigger an explosive interaction, a 1.41×10^{-3} lbm (0.64 g) charge of high explosives was used. Some of the experiments had a considerable delay before the explosion was initiated, i.e. over 3 sec. Many tests in this experimental series observed the presence of spontaneous trigger events as well.

A second test series was performed at Sandia [Buxton, et al., 1980] with a different test vessel (3.94 ft (1.2 m) internal diameter) and molten material generated from both iron-aluminum oxids thermite and a corium-A+R thermite. This latter reaction had products of uranium dioxide, zirconium dioxide, nickel oxide, stainless steel, and molybdenum. The minimum liquidus temperature for this mixture is reported to be 4526.6°F (2770K), which is considerably greater than the 3680.6°F (2300K) temperature for aluminum oxide. Boiling steel would limit the maximum temperature for the corium reaction to 5066.6°F (3070K).

In this second test series, external triggering was also induced by explosive detonators, but two different sizes were used. One was the same as that employed in the first iron-thermite test, i.e. 1.41×10^{-3} lbm (0.64 g) of PETN, and the other was a detonator plus a lead-covered explosive cord 2.49 ft (0.76 m) in length and containing 1.32×10^{-2} lbm (6 g) of PETN. This second method represented a much more energetic trigger than that used in the thermite tests. In fact, the pulse duration for the corium A+R event in Run 59, which used this larger trigger, was not much different than that represented by the trigger alone. Also the measured work (~ 33 Btu (30 kJ)) was less than the work released by the high explosive (~ 39 Btu (35 kJ)). Explosions were observed with the iron thermite as initiated by both spontaneous and artificial triggers. However, with the corium A+R melt only one mild explosion is reported and this was triggered by the 1.32×10^{-2} lbm (6 g) PETN external trigger. The time delay before the trigger is fired (~ 1.3

sec) is longer than the time required to cool the coarsely fragmented particles to the liquidus temperature. The fact that the trigger was needed to mix a considerable fraction of the melt down to an explosive size scale is indicative of the difficulty encountered in making such materials undergo a thermal explosion. A major part of this difficulty is due to the rapid cooling and freezing of the corium particles as described above.

The results of 17 tests were reported [Mitchell, et al., 1981] for both ambient and high pressure initial conditions and also with and without an external trigger. The two experimental series were designated as Melt Delivery and FITS (Fully Instrumented Test Series). The Melt Delivery experiment consisted of 12 tests all run at atmospheric initial pressure without an external trigger. These resulted in eight self-triggered explosions -- two in the water coolant before the melt impacted the reservoir bottom and six when the melt contacted the reservoir base. The initial FITS experimental matrix consisted of five runs -- three at atmospheric and two at an elevated pressure. Two explosions resulted -- one at atmospheric pressure and in the free stream before the melt hit the reservoir bottom, and one at elevated pressure (~ 1 MPa/150 psi) which was initiated by an external trigger when the melt was laying on the reservoir base.

The purpose of the Melt Delivery test series was to develop an efficient means of delivering the melt into the coolant, and that of the FITS experiment was to determine the mechanical work output from such explosions. The melt used in both these experiments was iron thermite ($Fe\text{-}Al_2O_3$) which had an initial temperature of ~ 4400.6°F (2700K). Melt masses of 1.32 - 11.8 lbm (0.6-5.38 kg) were employed which resulted in coolant-melt mass ratios of 366-37 respectively, and the conversion ratio of mechanical work to melt initial thermal energy was reported to be about 1-3%. These tests resulted in eight self-triggered explosions, but explosions were not observed for water-melt mass ratios of 83-113.

The explosivity and initiation site were apparently sensitive to melt mass and shape in the 15 non-externally triggered tests at ambient pressure. There were no self-triggered explosions when the initial melt mass was less than approximately 4.0 lbm (1.8 kg), and there were nine such explosions for

the initial melt mass greater than ~ 6.614 lbm (3 kg). This was interpreted as a threshold for an appropriate melt-water mixture to produce a thermal explosion.

Five different phases were observed in these experiments: (1) melt entry, (2) pre-mixing, (3) triggering, (4) propagation, and (5) expansion of the interaction products. The melt was observed to start coarse fragmentation and pre-mixing virtually upon entry into the water. The triggering and propagation phases of the thermal explosions were observed to start at the leading edge of the melt, both when the melt was still in the free stream and also upon impact with the coolant reservoir base. Propagation of the event was observed to start at the base of the melt and propagate through the mixture at ~ 656-1969 ft/s (200-600 m/s), and this phase was considered to be complete at the start of the expansion of the melt-water mixture.

The FITS-A experiment was conducted in a closed vessel to assess the influence of an external trigger (1.4×10^{-3} lbm (635 mg) PETN, 3.6 Btu (3.8 KJ)) on high pressure cut-off of thermal explosions. In this test series, the Fe-Al_2O_3 melt (4.277-11.86 lbm, 5072°F (1.94-5.38 kg, 3073K)) was poured from ~ 3.94 ft (1.2 m) into tap water (198.4-498 lbm, 50-77°F (90-226 kg, 10-25°C)) producing a 0.98-1.476 ft (0.3-0.45 m) long melt mass at entry and coolant-melt mass ratios of 41-80. Five tests were performed -- three at ambient pressure (12 psig (0.083 MPa)), and two at an elevated pressure (148 and 158.1 psig (1.02 and 1.09 MPa)). Two explosions resulted -- one at ambient pressure which was self-triggered in the free stream, and one at 158.1 psig (1.09 MPa) which was externally triggered.

Tests FITS-4A and 5A are of particular interest because they were designed to investigate the effect of high pressure cut-off on steam explosions. In the FITS-4A test, 9.46 lbm (4.29 kg) of melt was delivered to 498 lbm (226 kg) of water at 77°F (25°C) in an ambient pressure of 148 psig (1.02 MPa) without an external trigger and did not produce an explosion. This benign result was explained on the basis of a dispersed and cooled melt at entry into the coolant. The FITS-5A test was performed at a system pressure of 158.1 psig (1.09 MPa) and was essentially a rerun of FITS-4A but with an external trigger. The FITS-5A run did produce a thermal interaction

after being initiated with the detonator (3.6 Btu (3.8 KJ)), but the mixture had not self-triggered after 0.44 sec at which time all the melt was on the bottom of the coolant reservoir.

2.3.2 Aluminum-Water Experiments

Large scale tests have also been carried out for an aluminum-water system where either external triggers [Long, 1957], [Hess, et al., 1980], [Lemmon, 1980], [Higgins, 1955], [Higgins, 1956] or a shock tube configuration [Wright, et al., 1966] have been employed.

In [Long, 1957], large scale molten aluminum-water experiments were performed to investigate the manner in which steam explosions could be triggered. The reference test, which repeatedly produced explosions, involved the discharge of 22.8 kg (50 lbm) of commercially pure molten aluminum into a clean, mild steel container partially filled with water at temperatures of 59.5-78.1°F (12.8-25.6°C). In contrast to chemical explosions, no flash or fire could be detected either during or after the explosions. The following parameters were varied:

1. discharge rate and mass,
2. drop height,
3. water depth, and
4. aluminum and water temperatures.

Also, different water additives, solid surfaces, and surface coatings were employed in the experiment. It was concluded that three requirements must be met to produce an aluminum-water explosion:

1. Molten metal in considerable quantities must penetrate to the bottom surface of the water container.
2. A triggering action must occur on the container bottom surface when it is covered by the molten metal.
3. The water depth and temperature must lie within certain ranges.

In [Hess, et al., 1980], tests were performed to study the level of external stimulus (a hammer impact) required to initiate explosive interactions in aluminum-water systems. For these experiments, ~ 48.5 lbm (22 kg) of molten aluminum was poured into a square container 0.98 ft (0.3 m) on a side. The molten aluminum temperatures varied between 1346°F (730°C) and 1436°F (780°C) with the water temperature variation being from 37.4°F (3°C) to 89.6°F (32°C). In the experiments, 4 seconds elapsed between the entry of melt into the water and the hammer impact, thereby allowing much of the material to accumulate on the bottom of the container instead of disperse as individual particles in the water. The impact level determined in the experiments of [Hess, et al., 1980] was 0.176 Btu (186 J) and the authors suggest that perhaps only half of this was actually transmitted to the mixture due to inherent losses within the impact on the wall and the transmission of the energy to the coolant.

Other aluminum-water experiments have been carried out by Lemmon [Lemmon, 1980], and Higgins [Higgins, 1955], [Higgins, 1956] where molten material has been poured or injected into water and an explosive interaction was initiated by a strong external trigger. For those experiments reported in [Lemmon, 1980], triggers up to 1.1×10^{-2} lbm (5 g) of primecord were used and a No. 6 blasting cap was employed by Higgins in his experiments. Scoping calculations for the specific experimental configurations used in these references results in an assessment that the external stimulus is orders of magnitude greater than that required to rapidly mix the materials on an explosive time scale.

Another type of aluminum-water experiment of note is the shock tube experiment described in [Wright, et al., 1966]. In these tests, a long column of water was separated from a molten aluminum surface by a diaphragm and a cover gas. To carry out these tests, the recovery gas was evacuated and the diaphragm was ruptured allowing the atmospheric pressure to accelerate a water slug resulting in a strong, direct impact of the cold water column on a molten aluminum surface. Large interaction pressures for these events were measured in the water column.

2.3.3 Liquefied Natural Gas and Water Experiments

Large scale tests [Koopman, et al., 1981] have been performed with Liquefied Natural Gas (LNG) and water using material volumes approaching those of interest for the reactor accident case. In these tests, water is the hot fluid and LNG (mostly methane) is the cold liquid which undergoes the explosive vaporization. This fluid pair is similar to the corium-water system in that the interface contact temperature is far greater than the thermodynamic critical temperature of the LNG, making explosions difficult to initiate. Long delay times were provided in an attempt to accumulate substantial quantities of LNG below the water surface. The magnitudes of the explosions obtained represented the interaction of only a small fraction of the LNG injected.

2.3.4 FAI Thermite Experiments

Two sets of experiments have been performed at FAI in which 44 lbm (20 kg) of molten iron thermite was injected into water. The first [Malinovic, et al., 1989] was performed to study the role of water in protecting the Mark I containment liner under severe accident conditions while the second [FAI, 1990] addressed the influence of water during a high pressure melt ejection. Both of these represent conditions which could cause ex-vessel steam explosions and both facilities were instrumented sufficiently to evaluate the steam generation rates resulting from these interactions.

Interpretation of the rate, in terms of a heat flux based upon the projected floor area where the interaction occurs, provides a means of applying the results to a reactor/containment system. Figure 2-3 illustrates the measured heat flux to the overlying water pool in the Mark I experiments when the test apparatus was instrumented to detect the energy transfer to the test box walls. All tests show a very high energy transfer rate within the first few seconds, the value being between 6.34 and 9.51 M Btu/h-ft^2 (20 and 30 MW/m^2), which subsequently decreases to about 0.285 x 10^6 Btu/h-ft^2 (0.9 MW/m^2) after the debris is frozen. In this set of experiments, 11 tests were performed, 10 of which had water available in the simulated containment prior to the discharge of the molten iron thermite.

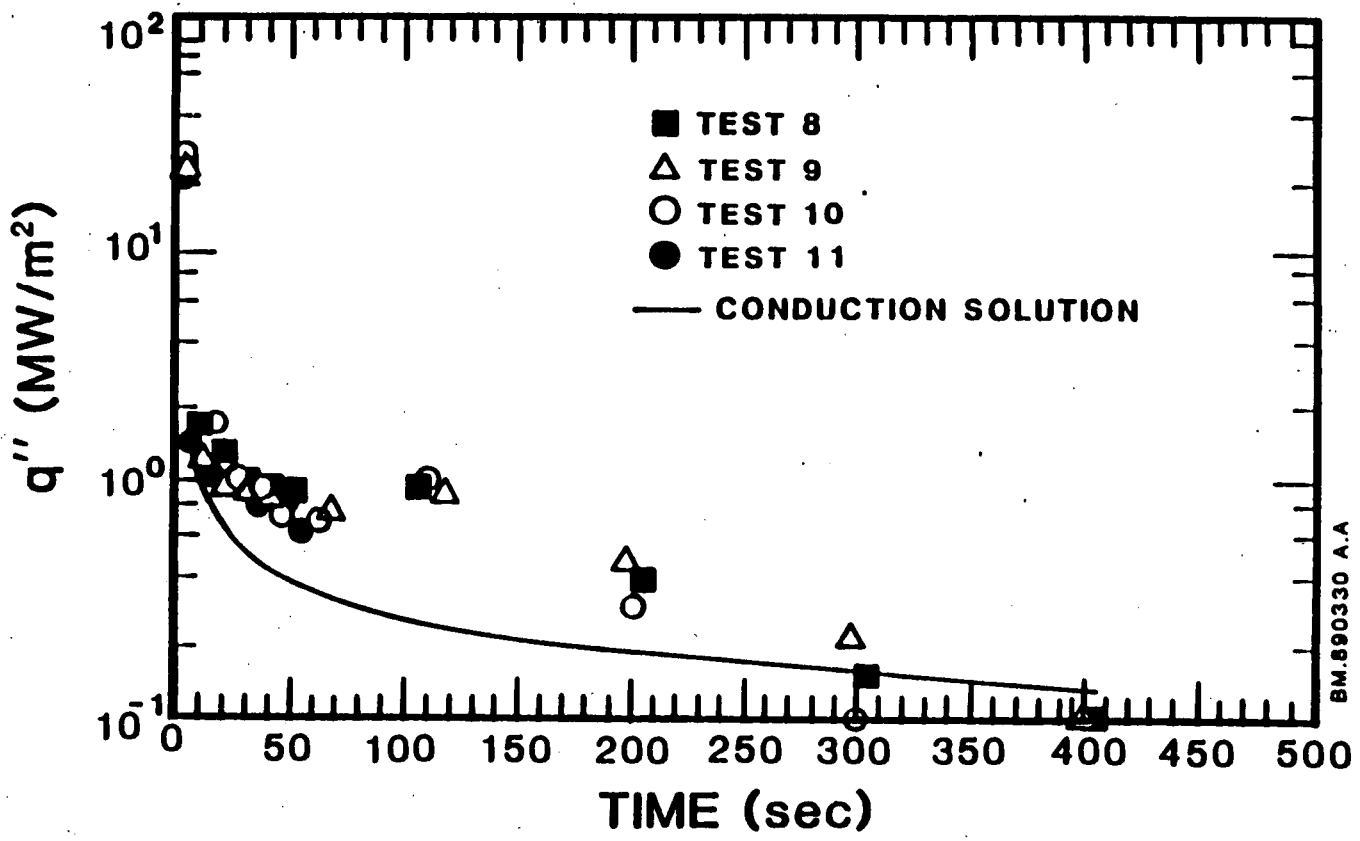

Figure 2-3 Measured debris-water energy transfer rates from EPRI sponsored Mark I liner tests.

In all 10 experiments, rapid energy transfer rates (6.34-9.51 M Btu/h-ft^2 (20-30 MW/m^2)) were observed when the debris was discharged into the water.

FAI direct containment heating experiments [FAI, 1990] also had sufficient instrumentation to estimate the steam generation rates when debris was discharged from the simulated RCS into the reactor cavity and subsequently up onto the containment floor. Table 2-1 summarizes the information for these experiments in terms of the energy transfer rate in the cavity for the three experiments in which water was available (DCH-1, DCH-2, and DCH-4) and also for the energy transfer rates from the debris to the water as the debris was discharged onto the containment floor. Values are also given for estimated additional energy transfer due to the transfer into the steel structural heat sinks in the simulated containment lower compartment. These additional energy transfer rates should be summed with those determined from the containment compartment pressurization rates. As illustrated by this table, the energy transfer rates are large and comparable to those observed in the Mark I tests. It should also be noted that these rates are an order of magnitude greater than those typical of the critical heat flux (CHF) for a horizontal upward facing surface.

2.3.5 Sandia FITS Tests

The Sandia FITS tests provided sufficient pressure transient information to evaluate the average steam generation rate resulting from explosive interactions. Steam generation rates can then be divided by the cross-sectional area of the FITS vessel to determine the effective heat fluxes. Figure 2-4 taken from [Mitchell, et al., 1986] shows a cross-section of the FITS facility. In this test series, about 18.6 kg (41 lbm) of molten thermite was poured into water test containers located in the FITS chamber and the resultant pressure history in the chamber gas space was recorded. Table 2-2, which was also taken from [Mitchell, et al., 1986] summarizes the test conditions and observations made with respect to explosive interactions. Figures 2-5 through 2-8 illustrate the pressurization of the gas space, the first three with initially subcooled water, and the last with saturated water.

Table 2-1

EFFECTIVE HEAT FLUX MEASUREMENTS FOR DEBRIS-WATER INTERACTIONS

Test	Initial Pressurization		Intermediate Period		Long Term Quenching	
	M Btu/h-ft^2	MW/m^2	M Btu/h-ft^2	MW/m^2	M Btu/h-ft^2	MW/m^2
DCH-1	4.75/13.3*	15/42*	3.49/6.02*	11/19*	2.7/5.5*	8.5/17.5*
DCH-2	2.22/10.78*	7/34*	4.12/6.66*	13/21*	2.31/5.17*	7.3/16.3*
DCH-3	N/A	N/A	N/A	N/A	1.27/4.12*	4/13*
DCH-4	1.27/9.83*	4/31*	3.49/6.02*	11/19*	N/A/2.85*	N/A/9*

*Contribution from the heat sinks added to the vaporization calculation.

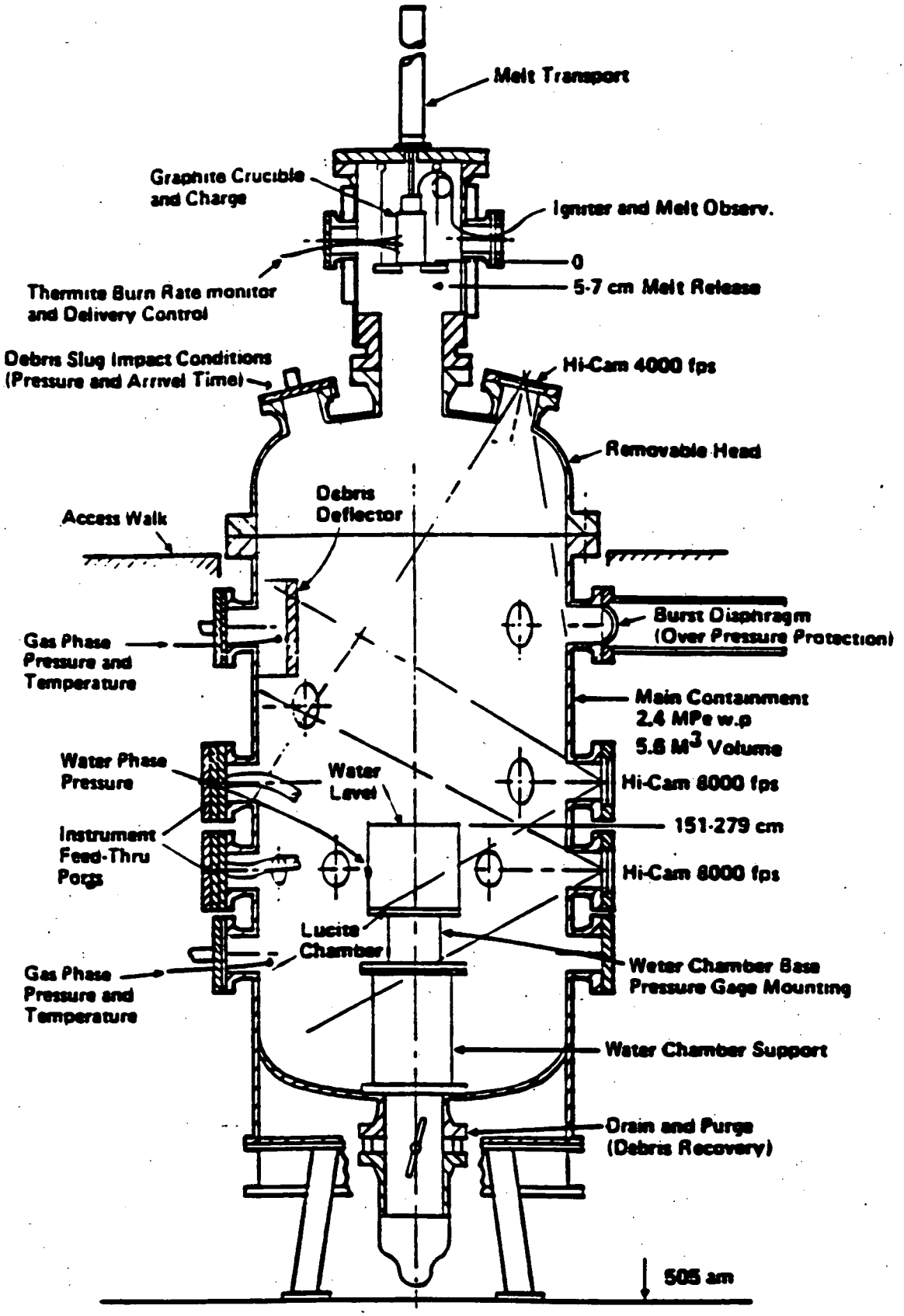

Figure 2-4 FITS containment chamber.

Table 2-2

FITS8 INITIAL CONDITIONS AND OBSERVATIONS

Expt.	Melt			Water			Initial Ratio Water/Melt		Spontaneous Explosion		Other Observations
	Mass (kg)	Entry Vel. (m/s)	Avg. Dia. at Entry[1] (cm)	Geometry (cm) Sq x Deep	Mass (kg)	Temp (K)	Mass	Vol.[2]	Location	Time After Melt Entry (ms)	
1B	18.7	5.4	4.1	61 x 61	226.0	296	12.0	46.0	Surface Unknown	142 275	First explosion. Second explosion.
2B	18.6	6.0	6.0	61 x 30	113.0	298	6.0	23.0	Surface	84	Single explosion.
3B	18.6	6.0	24.0	43 x 30	57.0	295	3.0	11.5	Base	77	Single explosion weak interaction at surface at 70 ms after entry that did not propagate.
4B	18.7	6.8	5.8	61 x 61	226.0	299	12.0	46.0	Surface Base	29 146	First explosion. Second explosion.
6S	18.7	7.2	6.5	46 x 30	63.4	367	3.4	12.9	None	-	Multiple interactions at 40, 57, 82 and 153 ms after melt entry, no propagation or steam explosion.
7D	18.7	7.4	n.o.[3]	43 x 15.2	28.1	291	1.5	5.7	n.o.	80	No camera data, time estimated from water pbase gauges.
8B	18.7	6.5	29.8	61 x 76.5	263.5	260	15.0	57.4	Surface Base	27 146	First explosion. Second explosion.
9B	18.7	7.8	8.6	61 x 48.7	178.0	289	9.0	34.6	Base	98	Single explosion.

[1]Optical measurement.

[2]Melt density 3.8 g/cm^3.

[3]Not observed.

Table 2-2 (Continued)

FITS2 INITIAL CONDITIONS AND OBSERVATIONS
(English Units)

Expt.	Melt			Water			Initial Ratio Water/Melt		Spontaneous Explosion		Other Observations
	Mass (lbm)	Entry Vel. (ft/s)	Avg. Dia. at Entry[1] (in)	Geometry (in) Sq x Deep	Mass (lbm)	Temp (°F)	Mass	Vol.[2]	Location	Time After Melt Entry (ms)	
1R	41.2	17.71	1.61	24 x 24	498.0	77	12.0	46.0	Surface Unknown	142 275	First explosion. Second explosion.
2R	41.0	19.68	2.36	24 x 11.8	249.0	77	6.0	23.0	Surface	84	Single explosion.
3B	41.0	19.68	9.45	17 x 11.8	125.7	71.6	3.0	11.5	Base	77	Single explosion weak interaction at surface at 70 ms after entry that did not propagate.
4B	41.2	22.31	2.26	24 x 24	498.0	70.8	12.0	46.0	Surface Base	29 146	First explosion. Second explosion.
6B	41.2	23.62	2.56	16 x 11.9	139.8	201.2	3.4	12.9	None	-	Multiple interactions at 40, 57, 82 and 183 ms after melt entry, no propagation or steam explosion.
7B	41.2	24.28	n.o.[3]	17 x 6	61.95	64.4	1.5	5.7	n.o.	00	No camera data, time estimated from water phase gauges.
8K	41.2	21.33	11.42	24 x 30	625.0	59.0	15.0	57.4	Surface Base	27 146	First explosion. Second explosion.
9R	41.2	22.97	2.2	24 x 18	374.79	60.8	9.0	34.6	Base	96	Single explosion.

[1]Optical measurement.

[2]Melt density 3.8 g/cm³.

[3]Not observed.

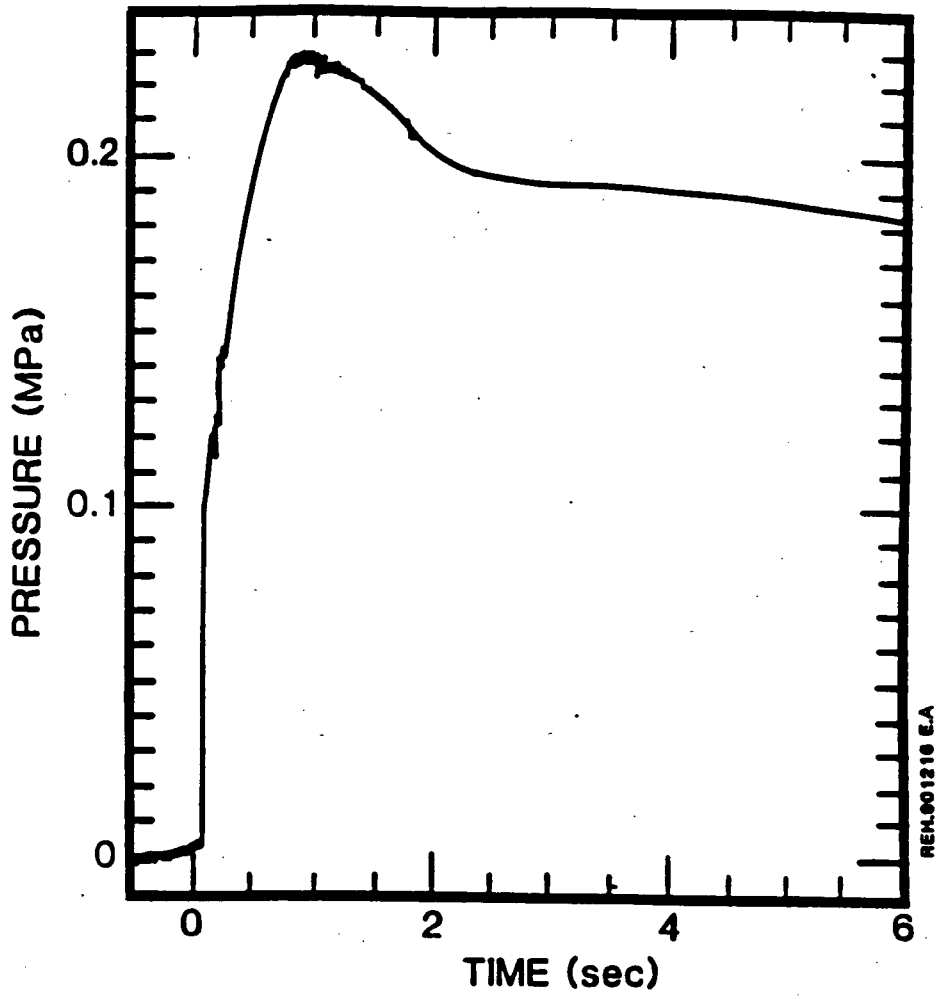

Figure 2-5 FITS2B chamber air pressure.

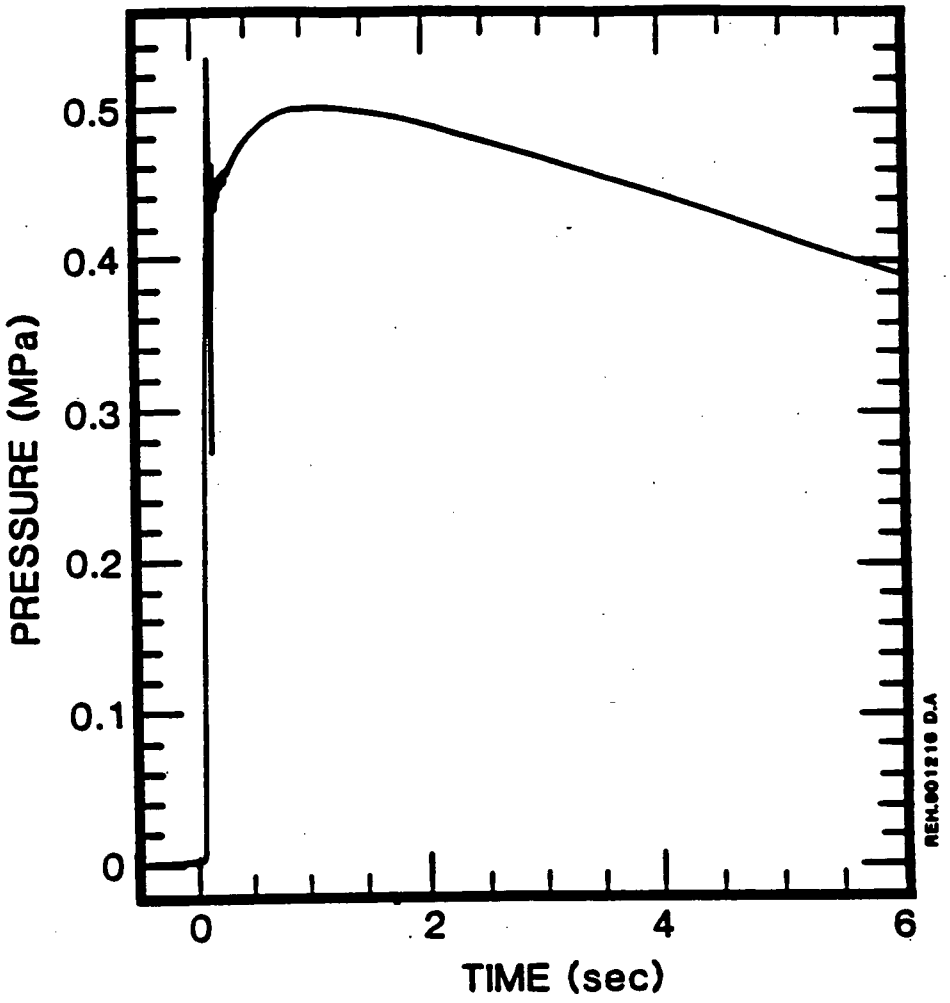

Figure 2-6 FITS3B chamber air pressure.

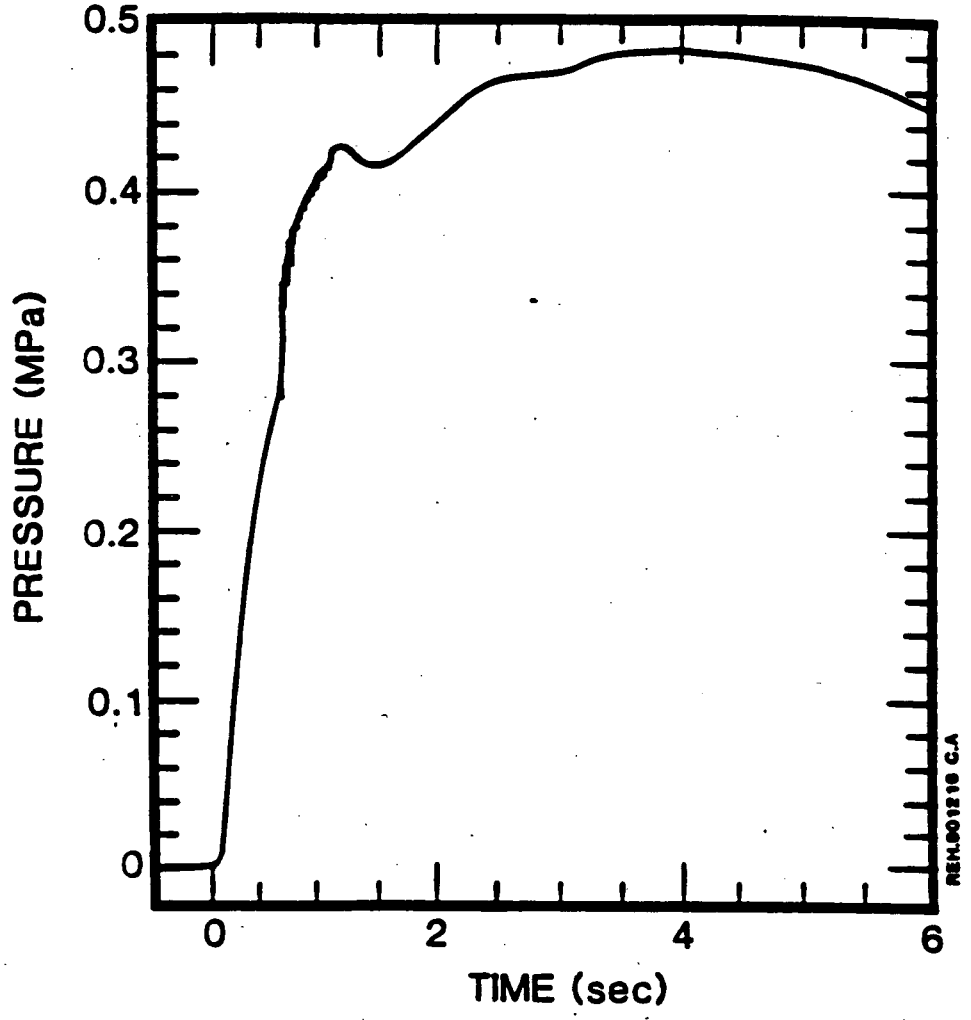

Figure 2-7 FITS7B chamber air pressure.

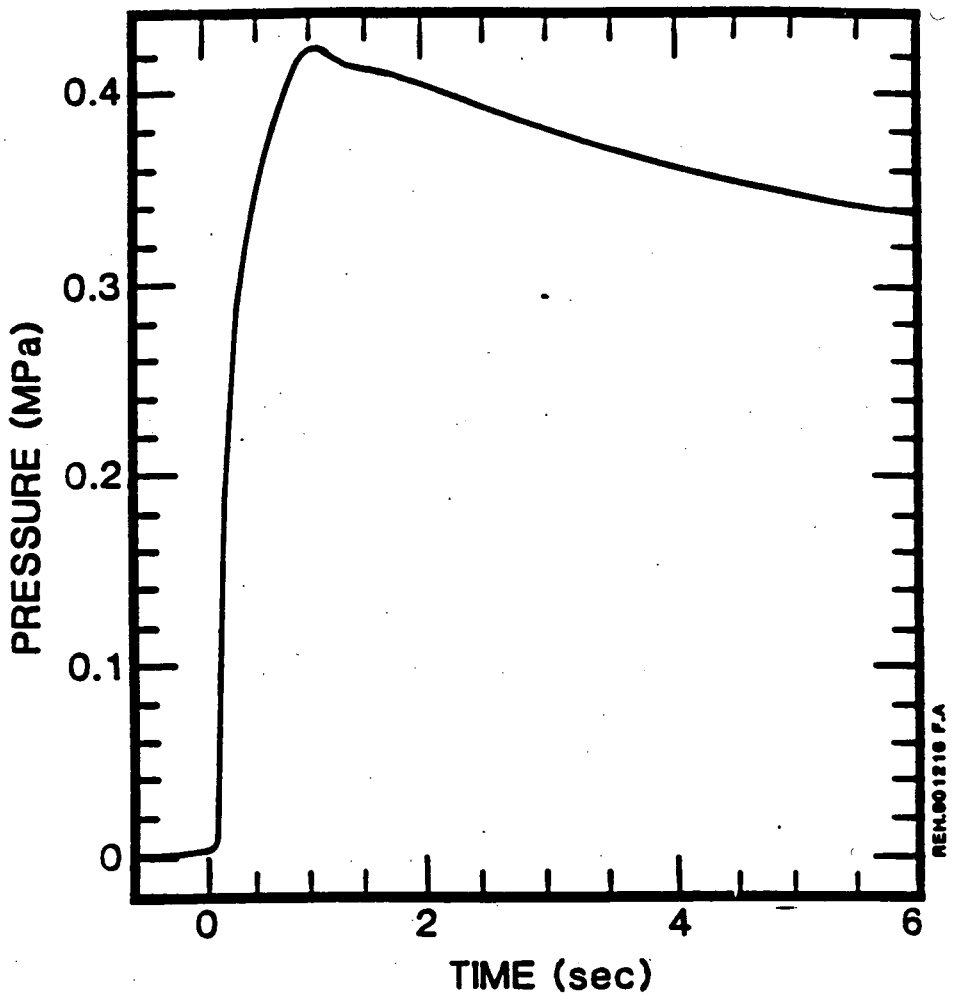

Figure 2-8 FITS6B chamber air pressure (saturated water).

While only some of the experiments had explosive interactions, our principal focus is on the net steam generation rate created by the explosive interaction. The large steel vessel is considered to be pressurized with steam, realizing that this also increases the potential for condensation on the vessel walls. The tests shown in Figures 2-5 through 2-8 are those with the largest vessel pressurization. A comparison of these figures also shows that the time to the peak pressure is approximately 1 sec for these tests, even though the path to this pressure may differ somewhat. (It is noted that Test FITS 7B experienced about 90% of the pressure increase in the first second with the remainder occurring over the next 3 secs.)

We can estimate the average steam generation rate with the ideal gas equation.

$$\frac{dP}{dt} = \frac{RT}{V}\frac{dN}{dt}$$

where each variable has the standard meaning. As an average representation, let us consider that the gas space pressure increases 0.35 MPa (51 psi) in 0.5 sec. The volume of the FITS vessel is 197.7 ft^3 (5.6 m^3) [Marshall, 1986] and if we assume an average gas temperature of 260.6°F (400K), the steam generation rate is 2.65 lb_m-moles/sec (1.2 kg-moles/sec), or a mass addition rate of 47.5 lbm/sec (21.6 kg/sec). As the melt enters the vessel, the dynamic interactions (either explosive or non-explosive) would expel melt and water from the lucite test vessel. To provide an equivalent basis for comparison with the FAI/EPRI Mark I tests, the steaming rate should be represented as a heat flux using the cross-sectional area of the FITS vessel (~ 19.4 ft^2 (1.8 m^2)). Using this area, the average heat flux from the melt to the water is about 8.56 M Btu/h-ft^2 (27 MW/m^2), i.e. a value in close agreement with that observed in the Mark I experiments.

2.3.6 Summary

In summary, the results from significant scale experiments with greatly different geometries can be compiled to develop a basis on which to provide interpretation for the containment response due to rapid steam generation by

dynamic interactions. Specifically, dynamic interactions should be considered with steam generation rates from 3.2 to 9.5 M Btu/h-ft^2 (10 to 30 MW/m^2). The projected area of the compartment floor should be used as the pertinent value for determining the total energy production rate. This can then be used to determine if the uncertainties in this range provide for any substantial change in the overall accident progression or in the accident management decisions that would be exercised in such events.

2.4 Analysis

Numerous models have been proposed to explain the primary steps in the occurrence of a steam explosion. However, no consensus on modeling of steam explosions has emerged to date. The wide variation in views exhibited by the members of the SERG underscores this fact. Since the NRC states that no truly predictive mechanistic model exists (NRC, 1988), this section is limited to a short overview of the two types of models that exist. These basically address the mechanisms for fragmentation of the lower volatility material, and the mechanisms for providing the intimate liquid-liquid contact; the former is required to obtain the characteristic larger heat transfer area, while the latter is required for the characteristic rapid heat transfer rate.

Since fragmentation of the hot material is considered to be a necessary (but not sufficient) condition for a large scale explosive interaction, a rather extensive experimental and theoretical effort has been devoted to the understanding of this process. The fragmentation models may be grouped into the following four general categories:

1. hydrodynamics models: which treat effects between the molten material and coolant independent of thermal conditions;
2. violent boiling models: fragmentation induced in the molten material via the disruptive forces and associated with bubble growth and collapse including spontaneous nucleation;
3. thermal stress theories: molten material breakup as a consequence of surface quenching and solidification; and

4. entrapment/gas release theories: rapid phase change of an entrapped species resulting in sudden expansion and fragmentation of the molten material.

From metal-water experiments it appears that an essential precursor to a vigorous interaction is the establishment of a stable vapor film between the fuel and coolant. The interaction is triggered by the destabilization of the vapor film, allowing extensive liquid-liquid contact. In general, the models developed to explain the mechanism allowing liquid-liquid contact can be roughly classified into two broad types: (1) boiling models, which depend upon the rapid production of vapor after liquid-liquid contact is established and (2) hydrodynamic models, which depend on the breakup of high temperature material due to the large relative velocity between fuel and coolant after collapse of the vapor layers due to arrival of a pressure wave. Some recent models consider that both types msy be present at the same time. There are also purely parametric models which are concerned with the consequences, but not the mixing process physics, once a set of initial conditions is assumed.

2.4.1 Effect of System Pressure on Steam Explosions

Several experimental investigations have focused on the effect of elevated pressures. These include studies using Freon-22 as the working (exploding) fluid [Henry-Fauske, 1979] as well as water [Hohman, et al., 1979] and [Hohman, et al., 1982]. These test series employed fluid pairs which had been demonstrated to explode in a reproducible manner, such that a single parameter (pressure) variation would be meaningful. Increasing the system pressure was observed to prevent explosions in all three studies. Those performed without external triggers found that a reduced pressure (ratio of the pressure and the thermodynamic critical pressure for the working fluid) of 0.05 was sufficient to prevent explosions. This corresponds to a pressure of 1 MPa (150 psia) for water. It was also observed that the explosions became somewhat less efficient as the ambient pressure increased. In fact, in the water experiments, no explosions were observed for system pressures of 0.5 MPa (~ 75 psia).

Experiments performed with external triggers found that explosive interactions could be induced at somewhat higher pressures, but a reduced pressure of 0.10 was found to suppress explosions even with very strong external triggers. For water this is a pressure of 2 MPa (~ 300 psi).

These pressures are well below those for the small LOCA and transient accident scenarios. Therefore, this single experimental observation is sufficient to address the issue of in-vessel steam explosions. Explosive triggers do not exist in a reactor system. Hence, the set of experiments most relevant for the IPE analyses are those without explosive external triggers. These will be used in the application to the reactor system, which would reduce the limiting pressure even further.

For those primary system conditions where explosions could be initiated, the assessment of the threat to the RCS integrity needs to evaluate the magnitude of the explosive interactions and the capability of the interaction to transfer an impact loading to the RPV walls and upper head. This was treated in the IDCOR Program [IDCOR, 1983] in terms of (1) the maximum molten mass and water which could be intimately mixed, (2) the efficiency of the explosion and (3) the capability of transferring an impact load to the RPV upper head. Through these evaluations it was concluded that a sufficient melt-water mixture could not be established to approach the energy yield necessary for challenging the vessel integrity. In addition, no efficient energy transfer mechanism could be found which could transmit the necessary impact load to cause failure of the RPV upper head.

2.4.2 Shock Waves

Modeling of the shock waves induced by steam explosions is only necessary if it is conceived that these would challenge the containment integrity. Figure 2-9 taken from [Glass, 1974] illustrates the decay of substantial shock waves in air as the shock wave expands. A slope corresponding to a pressure amplitude decay proportional to $1/r^2$ is also included for reference and provides a reasonable assessment of the decay characteristic for strong waves. If anything, the higher amplitude portion of the curve decays faster than this simplified representation. If an

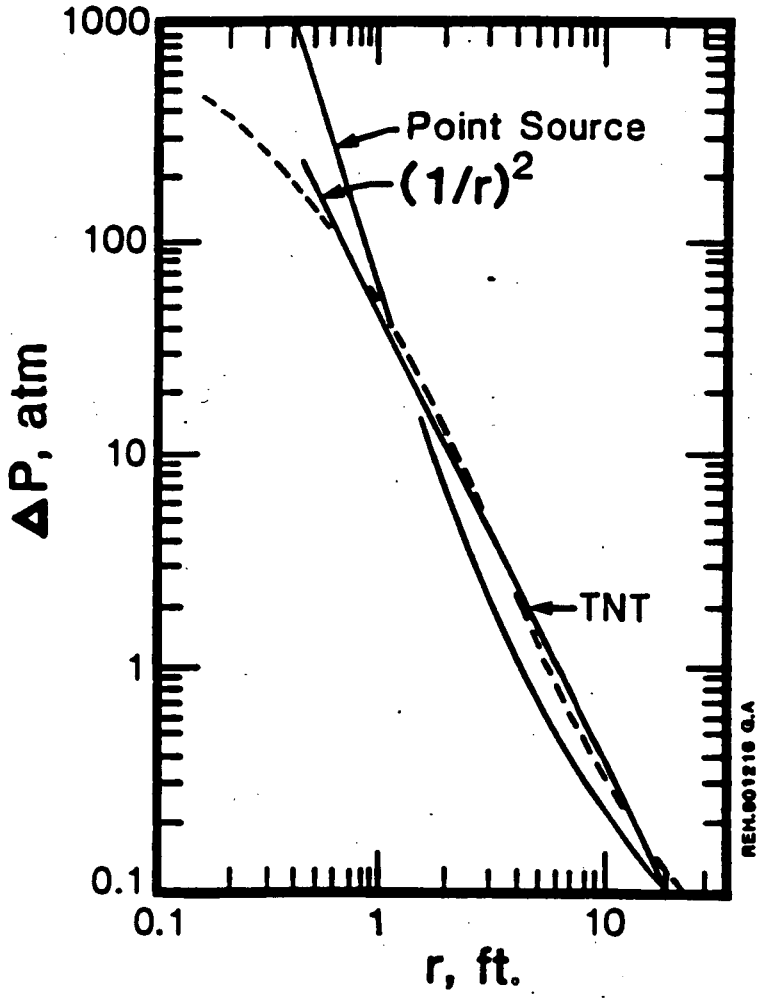

Figure 2-9 Comparison of shock wave pressures for TNT and point source explosions.

interaction zone size is postulated along with a maximum pressure for the interaction, this type of decay can be applied to the Sandia FITS experiments to compare the measured shock wave pressures in these tests with this decay characteristic. Table 2-2 summarizes the experimental conditions for the FITSB series, including the size of the test chamber in which the thermite and water were mixed. As an interaction zone, half of the square dimension is used as the radius for the initial calculation. Also, for the peak pressure achieved in the interaction zone we will use one half the critical pressure (~ 1450 psig (10 MPa)) since this corresponds to a condition in which the critical size bubble embryos equal the size for thermally dominated bubble growth [Henry, et al., 1979]. For pressures greater than this value, the vapor cannot be produced at a pressure higher than the local pressure. Other experiments have shown this value to be an upper bound of the pressure that can be achieved when the system is not tightly constrained.

The expansion from the interaction zone out to the diameter of the FITS vessel, 2.5 ft. (0.76 m) radius, is performed following the approximation shown in Figure 2-9. Since only three different size vessels were used in the eight experiments, only three different shock wave pressures (at the FITS vessel wall) are calculated by this approximate method. These are illustrated in Table 2-3 for the different experiments. As illustrated, this technique substantially overestimates the measured pressure at the FITS vessel boundary. This is not surprising since the curve shown in Figure 2-9 is compared to a chemical explosion which is typically more energetic and has a stronger shock wave than those generated by steam explosions. However, using this upper bound technique with realistic size interaction zones (on the order of 1.64 ft (0.5 m) or less) and extrapolating to the containment boundary (~ 32.81 ft (10 m) or larger) results in shock waves which are less than the design pressure of the containment. Therefore, we conclude that such shock waves would not threaten the containment integrity.

Table 2-3

CHAMBER AIR PRESSURE DATA FROM FITSB
(Times From Melt Entry)

Expt.	Steam Explosion Phase				Calculated Pressure Peak (MPa/psig)
	Explosion (s)		Pressure Peaks (MPa/psig)		
	1st[1]	2nd	1st	2nd	
1B	0.144	0.282	0.095/13.78	0.197/28.6	1.6/218
4B	0.029	0.146	0.020/2.9	0.500/72.5	1.6/218
8B	0.017	0.144	0.01/1.45	0.373/54.1	1.6/218
2B	0.087	n.o.[2]	0.220/31.9	n.o.	1.6/218
3B	0.081	n.o.	0.440/63.8	n.o.	0.7/87
6B	n.o.	n.o.	n.o.	n.o.	0.9/116
7B	±0.20	n.o.	0.01/1.45	n.o.	0.7/87
9B	0.102	n.o.	0.210/30.45	n.o.	1.6/218

[1]Time taken from start to pressure rise. Zero time taken from average of two active melt position sensors 2.5 cm above water surface.

[2]Not observed.

2.4.3 Possible Mechanism for Maximum Steam Generation Rate

The information presented in Section 2.4.2 was taken from a wide variety of experimental information and provides a substantial data base for describing the maximum melt-water steam generation rate in containments. One can provide a theoretical basis for heat fluxes in the range of 9.51 M Btu/h-ft^2 (30 MW/m^2) for a system with co-dispersed debris and water as depicted in Figure 2-10. A steam velocity sufficient to levitate and separate the water droplets from the high temperature dense debris is given by

$$U_g = \frac{3.7 \sqrt[4]{g\sigma(\rho_f - \rho_g)}}{\sqrt{\rho_g}}$$

where g is the acceleration of gravity, σ is the steam-water surface tension and ρ_f and ρ_g represent the saturated water and steam densities respectively. If we consider this to be the maximum steam production rate which could exist without separation of the water droplets from the co-disperse configuration then the heat flux associated with the vapor production rate is given by

$$q/A = 3.7\, h_{fg} \sqrt{\rho_g} \sqrt[4]{g\sigma(\rho_f - \rho_g)}$$

where h_{fg} is the latent heat of vaporization. Substituting the appropriate values for steam and water at 1 atm into this expression results in a value of 9.51 M Btu/h-ft^2 (30 MW/m^2); a value in agreement with those observed in the various experiments. Hence, the major ramification of an explosive interaction could be the co-dispersion of melt and water which then continues to transfer energy and vaporize water into the containment atmosphere at a rate limited by the ability of the water droplets to remain as part of the co-dispersed medium.

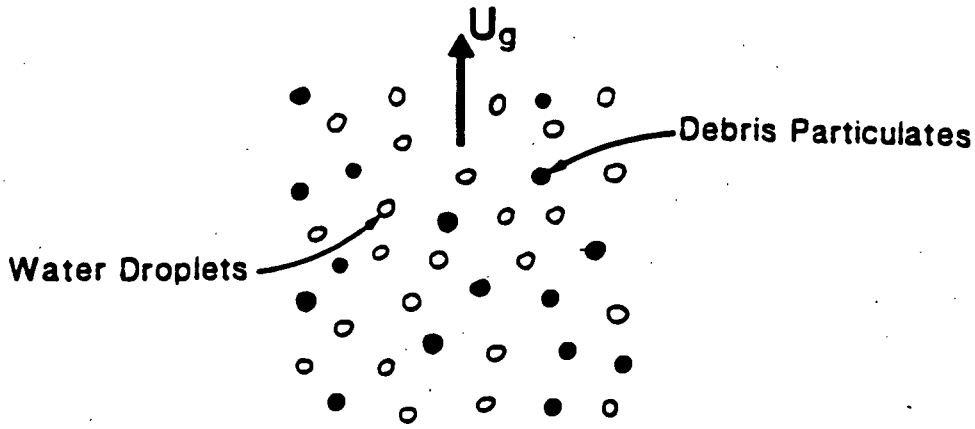

(a) Co-Dispersed Configuration

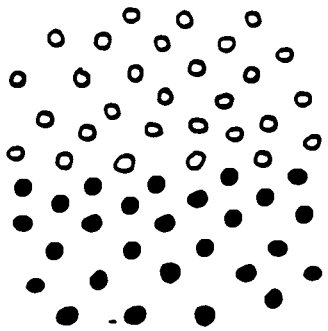

(b) Configuration if the Droplets are Fluidized

Figure 2-10 Debris dispersion configuration.

3.0 METHODOLOGY

The disposition of containment failure due to steam explosions relative to the containment event trees (CETs) involves separate approaches for in-vessel and ex-vessel steam explosions, respectively. The IDCOR work, which is consistent with the recommendation of the SERG in [NRC, 1985], forms the basis for the treatment of in-vessel steam explosions. Results of analyses performed in accordance with significant scale experiments and expansion characteristics of shock waves form the basis for the treatment of ex-vessel steam explosions. This section describes the methodology for addressing steam explosions.

3.1 In-Vessel Steam Explosions

Fundamental experiments (see Section 2.4.1) show that the initiation of steam explosions is very sensitive to pressure levels and is prevented at system pressures beyond 10% of the primary system normal operating pressure. As a result, there is no threat to the RPV integrity by this phenomenon in accident sequences that do not meet this criterion.

For sequences which result in a depressurized (< 1 MPa/150 psia) primary system at the time molten core debris would be expected to flow into the lower plenum, the approach utilizes the IDCOR analysis [IDCOR, 1983]. With the mechanistic evaluations for the melt-water masses which could interact and the assessment of the energy transmission capability, there is no set of credible conditions which could approach conditions sufficient to challenge the vessel head integrity. This is consistent with the conclusions of the NRC sponsored Steam Explosion Review Group.

3.2 Ex-Vessel Steam Explosions

As discussed in Section 2, ex-vessel steam explosions could occur and may be a major mechanism for quenching of core debris should it be discharged from the reactor vessel. There are two aspects to be addressed: (1) the overpressure in the containment due to rapid steam generation and (2) the shock waves which could be created by the interactions.

3.2.1 Pressure Rise Due to Rapid Steam Generation

Based on the possible mechanism for maximum steam generation rate postulated in Section 2.4.3, the steam generation rate due to the explosive interaction of debris and water can be written as

$$\dot{m}_s = \frac{q''_{ex} A_{pool}}{h_{fg}} \qquad (3\text{-}1)$$

where in SI units,

$\dot{m}_s$ - steam generation rate (kg/s)

q''_{ex} - heat flux due to explosive interaction and based on pool area
- 30 MW/m^2

A_{pool} - water pool cross sectional area where explosive interaction occurs (m^2)

h_{fg} - latent heat of vaporization of water
- 2.25 MJ/kg

The pressure increase (ΔP) due to this rapid steam generation, using the ideal gas law, is given by

$$\Delta P = \frac{RT}{M_{H_2O} V} \dot{m}_s \Delta t \qquad (3\text{-}2)$$

where

R - universal gas constant - 8314 J/kg-mol °K

V - total containment free volume (m^3)

M_{H_2O} - molecular weight of water - 18 kg/kg-mol

Δt - explosive interaction time (s)

3.2.2 Shock Waves

The $1/r^2$ decay of shock waves from the interaction zone, through air to the containment boundary was described in Section 2.4.2. The two basic parameters are (1) the 10 MPa maximum attainable pressure (P_{IZ}) in the interaction zone, and (2) the dimensions of the interaction zone. Assuming the interaction zone to be a sphere, we can find the radius of the sphere that contains steam equivalent to the amount generated at the rate $\dot{m}_s$ during the interaction time period Δt (typically on the order of milliseconds) as

$$\frac{4}{3}\pi R_{IZ}^3 = \frac{\dot{m}_s \Delta t}{M_{H_2O}} \frac{RT}{P_{IZ}} \tag{3-3}$$

or

$$R_{IZ} = \left[\frac{3}{4\pi} \frac{\dot{m}_s \Delta t \, RT}{M_{H_2O} P_{IZ}}\right]^{1/3} \tag{3-4}$$

The $1/r^2$ decay law, then, gives the impact pressure at the containment wall as

$$P_{cw} = \left(\frac{R_{IZ}}{X_{cw}}\right)^2 P_{IZ} \tag{3-5}$$

where

P_{cw} = impact pressure at containment wall
X_{cw} = distance from center of interaction zone to containment wall.

4.0 PLANT SPECIFIC APPLICATION

4.1 Issues

4.1.1 In-Vessel Steam Explosions

According to conclusions made in Section 3.1, there are no conditions which could lead to vessel rupture due to an in-vessel steam explosion. Consequently, in-vessel steam explosions leading to containment failure are not included as a top event in the Kewaunee containment event trees.

4.1.2 Ex-Vessel Steam Explosions

4.1.2.1 Pressure Rise Due to Rapid Steam Generation

In order to evaluate the pressure rise from Equation (3-2), the interaction pool area (A_{pool}) and the interaction time (Δt) must be predetermined subject to some uncertainty. However, even when conservative values for A_{pool} and Δt are used, this still results in an insiguificant pressure rise that will not threaten the containment integrity. As mentioned in Section 2.3.5, most interaction times observed in experiments were about 1 second. The plant design of the seal table area inhibits a steam explosion during a high pressure melt ejection (HPME). The seal table is located approximately 34 feet above the floor of the lower compartment where the containment recirculation sumps are located. Event if the RWST was injected into containment, there is no conceivable way for a pool of water to exist in the area surrounding the seal table. Therefore, the only location where a steam explosion could occur is in the cavity. If this interaction is assumed to occur over the entire cavity floor, the steam generation rate would be 361 kg/s and the associated pressure rise within containment would be only 0.002 MPa (0.25 psi). The above calculation uses A_{pool} = 27.1 m^2 (292 ft^2), V = 37382 m^3 (1.32 x 10^6 ft^3), T = 390 K and Δt = 1 second. These values were obtained from the Kewaunee MAAP parameter file [FAI, 1993]. To accommodate the uncertainty in Δt due to a longer vessel blowdown time, Δt may be increased as part of a sensitivity study. Even if Δt = 10 seconds is assumed,

the predicted pressure rise would not be greater than 0.017 MPa (2.5 psi). Therefore, ex-vessel steam explosions would not challenge containment integrity by overpressure.

4.1.2.2 Shock Wave Impact

In order to evaluate the shock wave effects during a steem explosion, the distance from the interaction zone to the containment wall must be determined. As mentioned in the previous calculation, the only possible location in which a steam explosion could occur is in the cavity. The cavity at Kewaunee was designed to keep water out. The only paths for water to enter the cavity is the annulus around the reactor vessel and the hatches on the instrument tunnel. In order for water to get into the cavity via the annulus around the vessel, the containment sprays must be operational. The hatches on the instrument tunnel are water-tight and closed during plant operations, therefore water could only enter through this path if the hatches were left open.

If a steam explosion is assumed to occur, it will more than likely occur in the cavity region of containment. The impact of the steam explosion can be assessed as follows. Using the same steam generation rate as when evaluating the pressure rise due to rapid steam generation ($\dot{m}_s$ = 362 kg/s), with Δt = 0.1 seconds, P_{IZ} = 10 MPa (1470 psi) and T = 580 K (585°F) (corresponding saturation temperature), Equation (3-4) yields R_{IZ} = 0.61 m (2.01 ft). With X_{cw} = 3 m (9.8 ft) [FAI, 1993], approximately the distance from the cavity floor to the containment wall, Equation (3-5) yielde P_{cw} = 4.17 x 10^5 Pa (60 psi). Therefore, when the shock wave arrives at the containment wall, the pressure load would be much less than the containment ultimate capacity. The Kewaunee containment overpressure analysis estimates the mean failure pressure of 151 psig.

4.1.3 Uncertainty Considerations

As discussed in this document, in [NRC, 1985] and in [IDCOR, 1983], a specific chain of events must occur before an in-vessel explosive interaction could challenge the RPV integrity. The failure of any link in this

chain would prevent interactions which could challenge RPV integrity. Evaluations of each link in the chain concludes that the only one which could be achieved is an explosive event, but then only when the RPV pressure is very low, i.e. typically less than 300 psia (2 MPa). Even if an explosion would occur, the mass of material, the efficiency, the slug formation and the slug transmission could not be realized to any significant degree. Given (1) the extent of individual analyses performed on each link in the chain of events, (2) the extent to which each is not satisfied in a realistic analysis and (3) the importance that each be satisfied before the RPV integrity could be challenged, it is concluded that there is no realistic combination of uncertainties which could make such an event credible.

Ex-vessel explosive interactions could occur for sequences which would progress to vessel failure. Here again, the extent of the interaction (and damage potential) is determined by the mass of molten material involved, the efficiency of the interaction and the decay of the shock waves as they propagate from the source. In this evalustion we have assumed.

- an efficient interaction since the shock waves are calculated to decay as for TNT, and
- an unimpeded expansion of the shock waves to the containment boundary.

These global representations are sufficient to determine if ex-vessel explosions could challenge containment integrity. However, best estimate analyses would consider:

- a much smaller interaction zone,
- much weaker shock waves for steam explosions than for chemical explosions, and
- the breakup of shock waves by the structures in the lower containment compartment, in particular the concrete shield walls separating the lower compartment from the annular compartment.

With the conservative assessments used for these individual evaluations, it is concluded there is no realistic combination of uncertainties which could result in a credible threat to containment integrity.

4.2 Conclusions

There is no credible set of circumstances in which ex-vessel steam explosions could challenge the containment integrity. Therefore, ex-vessel steam explosions are not included as a top event in the Kewaunee IPE containment event trees.

5.0 CONCLUSIONS

The influence of in-vessel and ex-vessel steem explosion events on the potential for containment failure have been addressed for the accident conditions of interest. The evaluations for in-vessel events closely parallel those performed as part of the IDCOR program and result in a conclusion that the slumping of molten debris into the RPV lower plenum could not result in sufficient energy release to threaten the vessel integrity. Hence, such interactions could not lead directly to containment failure (alpha mode) and a consequential release of fission products to the environment. This is in agreement with the conclusion of the NRC sponsored Steam Explosion Review Group.

Evaluations of both steam generation rate and shock waves induced by ex-vessel explosive interactions show that these would not be of sufficient strength to threaten the containment integrity. While such explosions could occur, the principal result of these events would be to rapidly cool debris and pressurize the containment to as much as 410 kPa (60 psi). Neither of these would be sufficient to challenge the containment integrity for any realistic accident conditions.

As a result of the evalustions performed for both in-vessel and ex-vessel events, and the conclusion that these would not lead to challenges of the containment integrity, steam explosions are dismissed in the Kewaunee IPE. Examining the analyses with respect to accident management insights does not result in any changes to the existing Emergency Operating Procedures, new accident management strategies, or to the perspectives gained through other phenomenological evaluations. Specifically, the depressurization action in the EOPs is a valid response under the conditions calling for the action, and should not be altered due to any concern with respect to in-vessel steam explosions. Other investigations suggest the presence of water is beneficial in containment and includes the state wherein the RPV lower head would be submerged. The benefits of such accident management actions are not altered by any consideration for ex-vessel steam explosions.

6.0 REFERENCES

Buchanan, D. J. and Dullforce, T. A., 1973), "Mechanism for Vapor Explosions", Nature, Vol. 245, p. 32.

Buxton, L. D. and Benedick, W. B., 1979, "Steam Explosion Efficiency Studies", NUREG/CR-0947, SAND 79-1399.

Buxton, L. D., Benedick, W. B. and Corradini, M. L., 1980, "Steam Explosion Efficiency Studies: Part II Corium Experiments", NUREG/CR-1746, SAND 80-1324.

Commonwealth Edison Company (CECo), 1981, Zion Probabilistic Safety Study.

Deitrich, J. R., 1965, "Experimental Investigation of the Self-Limitation of Power During Reactivity Transients in a Subcooled Water-Moderated Reactor-BORAX-1 Experiments, 1954", AECD-3668.

Fauske & Associates, Inc., 1982, "Assessment of Steam Explosion Potential in Hypothetical LWR Core Meltdown Accidents", Draft Report Submitted to the Nuclear Safety Analysis Center, Electric Power Research Institute.

Fauske & Associates, Inc., 1990, "FAI/CECo Direct Containment Heating Experiments for a Zion-Like Geometry", Fauske & Associates, Inc. Report, FAI/90-60.

Fauske & Associates, Inc., 1991, "A Position Paper on Direct Containment Heating in Support of the Kewaunee Individual Plant Evaluation", FAI/91-123.

Fauske & Associates, Inc., 1993, "Kewaunee Source Term Notebook", FAI/92-88.

Glass, I. I., (1974), Shock Waves and Man, The University of Toronto Press.

Henry, R. E. and Fauske, H. K., (1979), "Nucleation Processes in Large Scale Vapor Explosions", Trans. ASME, Jr. of Heat Transfer, Vol. 101, pp. 280-287.

Hess, P. D., Miller, R. E., Wahnsiedler, W. E. and Cochran, C. N., 1980, "Molten Aluminum/Water Explosions", Light Metals, (E. McMinn, Ed.), p. 387. (Proc. of Technical Sessions Sponsored by TMS Lights Metals Committee at 190th AIME Annual Mtg.).

Higgins, H. M., 1955, "A Study of the Reaction of Metals and Water", AECD-3664.

Higgins, H. M., 1956, "The Reaction of Molten Uranium and Zirconium Alloys with Water", Aerojet Report No. 2914-2, Metallurgy & Ceramics, Aerojet-General Corporation, Azusa, CA.

Hohmann, H., Henry, R. E. and Kottowski, H. M., 1979, "The Effect of Pressure on NaCl-H_2O Explosions", 4th CSNI Specialist Mtg. on Fuel-Coolant Interactions in Nucl. Reactor Safety, Bournemouth, United Kingdom, CSNI Report No. 37, pp. 308-323.

Hohmann, H., Kottowski, H. M., Schins, H. and Henry, R. E., 1982, "Experimental Investigations of Spontaneous and Triggered Vapour Explosions in the Molten Salt/Water System", Intl. Mtg. on Thermal Reactor Safety, Chicago, IL.

IDCOR, 1983, "Key Phenomenological Models for Assessing Explosive Steam Generation Rates", Technical Report 14.1A.

Koopman, R. P., et al., 1981, "Description and Analysis of Burro Series 40 m^3 LNG Spill Experiments", UCRL-53186.

Krause, H. H., et al., 1973, "Smelt-Water Explosions", Finsl Reports to Fourfrinier Kraft Board Institute, Inc., Batelle Columbus Laboratories, Columbus, OH.

Lemmon, A. W., 1980, "Explosions of Molten Aluminum and Water", Light Metals, (E. McMinn, Ed.), p. 817. (Proc. of Technical Sessions Sponsored by TMS Light Metals Committee at 190th AIME Annual Mtg.).

Long, G., 1957, "Explosions of Molten Aluminum and Water", Metal Progress, Vol. 71, p. 107.

Malinovic, B., Henry, R. E. and Sehgal, B. R., 1989, "Experiments Relating to Drywell Shell-Gore Debris Interactions", Natl. Heat Transfer Conf., Philadelphia, PA, AIChE Symposium Series, Vol. 85, No. 269, pp. 217-222.

Marshall, Jr., B. W., 1986, "Hydrogen:Air:Steam Flammability Limits and Combustion Characteristics in the FITS Vessel", NUREG/CR-3468, SAND 84-0383.

Miller, R. W., Sola, A and McCardell, R. K., 1964, "Report of the SPERT-1 Destructive Test Program on an Aluminum, Plate-Type, Water Moderated Reactor", IDO-16883.

Mitchell, D. E., Corradini, M. L. and Tarbell, W. W., 1981, "Intermediate Scale Steam Explosion Phenomena: Experiments and Analysis", Sandia National Laboratory, SAND/81-0124, NUREG/CR-2145.

Mitchell, D. E. and Evans N. A., (1986), "Steam Explosion Experiments at Intermediate Scale: FITSB Series", NUREG/CR-3983, SAND 83-1057.

Moody, F. J., Muralidharan, R. and Dua, S. S., 1989, "Assessment of Ex-Vessel Steam Pressure Spikes in BWR Mark II Containments", Invited Paper to 17th Water Reactor Safety Information Meeting, Rockville, MD.

NRC, 1975, "Reactor Safety Study", WASH-1400, NUREG/75-0114.

NRC, 1985, "A Review of the Current Understanding of the Potential for Containment Failure from In-Vessel Steam Explosions", NUREG-1116.

NRC, 1988, Letter to All Licensees Holding Operating Licenses and Construction Permits for Nuclear Power Facilities, "Individual Plant Examination for Severe Accident Vulnerabilities - 10CFR50.54(f)", Generic Letter No. 88-20, dated November 23, 1988.

Shick, P. E., 1980, "Concentration-Gradient Trigger Mechanism for Smelt-Water Explosions", Paper presented at the American Paper Institute Annual Recovery Boiler Committee Mtg., Chicago, IL, 30-31.

SL-1 Project, "Finsl Report of SL-1 Recovery Operations", IDO-19311.

Wright, R. W., Firstenberg, A. F., Humberstone, G. H., Neal, L. G., Wentz, L. G. and Zivi, S. M., 1966, 'Kinetic Studies of Heterogeneous Water Reactors - Annual Summary Report - 1966", STL-372-50, Space Technology Laboratories, Canoga Park, CA.

FAI/91-49

A PHENOMENOLOGICAL EVALUATION SUMMARY ON THE PROBABILITY AND CONSEQUENCES OF THE DEFLAGRATION AND DETONATION OF HYDROGEN IN THE KEWAUNEE NUCLEAR PLANT INDIVIDUAL PLANT EVALUATION

Submitted To:

Wisconsin Public Service Corporation
Green Bay, Wisconsin

Prepared By:

Fauske & Associates, Inc.
16W070 West 83rd Street
Burr Ridge, Illinois 60521
(708) 323-8750

Final Issue

March 1993

ABSTRACT

This phenomenological evaluation summarizes an assessment of the susceptability to failure of the Kewaunee containment due to hydrogen deflagrations and detonations that may occur during postulated severe accidents. The failure of the containment could provide a pathway for the release of fission products. In particular, the possibility of an early containment failure due to hydrogen deflagration or detonation is of key interest when assessing potential source terms.

This assessment concludes that the postulated containment loadings due to the deflagration of combustible gases in the Kewaunee containment could not cause failure of the Kewaunee containment structure. This conclusion is based on a bounding assessment of the containment pressurization potential assuming complete oxidation of zirconium from the core and of metallic constituents (iron, chromium, and nickel) of the lower core support plate. This assessment conservatively ignores the existence of inerting due to steam produced in the course of degrading the reactor core. The limiting calculation also ignores the possibility of incomplete combustion and the effectiveness of containment heat sinks including active and passive heat removal capability. The likelihood of detonations by direct energy deposition or DDT have been assessed. It is concluded that detonations will not challenge the integrity of the Kewaunee containment. Thus, failure of the containment due to deflagrations and detonations in the Kewaunee containment will not be included as a separate node for either early or long term containment failure in the event tree for the Kewaunee containment.

Recommendations are provided regarding sensitivity studies that might be conducted as part of the Kewaunee IPE to address phenomenological uncertainties and the specifics of sequence dependent timing of interacting phenomena. Sensitivity studies can be used to demonstrate the impact of phenomenological uncertainties and confirm this paper's conclusion regarding the Kewaunee containments capability to withstand potential deflagration and

detonations. Additionally, the plant specific analyses (MAAP calculations) may be reviewed to specifically summarize local effects in the various containment regions of potential hydrogen deflagration. The potential locations of hydrogen deflagrations and detonations should be identified so that they may be used to assess any possible impact on the survivability of equipment and instrumentation, and the performance of containment penetrations during a severe accident.

TABLE OF CONTENTS

	Page
ABSTRACT	i
1.0 PURPOSE	1-1
2.0 PHENOMENA	2-1
2.1 Description	2-1
2.1.1 Physical Processes	2-2
2.1.2 Relationship to Containment Failure Mechanisms and Modes	2-10
2.1.3 Relationship to Source Term	2-11
2.2 Experiments	2-11
2.2.1 Hydrogen Deflagrations	2-11
2.2.2 Hydrogen Detonations	2-14
2.2.2.1 Intrinsic Detonability	2-14
2.2.2.2 Influence of Steam and Temperature	2-19
2.2.2.3 Initiation of Detonations	2-19
2.3 Analyses	2-22
2.3.1 Hydrogen Deflagration	2-22
2.3.2 Hydrogen Detonation	2-24
3.0 METHODOLOGY	3-1
3.1 Flammability	3-1
3.2 Combustion Completeness	3-2
3.3 Combustion Pressure Rise	3-2
3.4 Evaluation of DDT Potential	3-2

TABLE OF CONTENTS
(Continued)

Page

4.0 ASSESSING THE PROBABILITY AND EFFECT OF HYDROGEN DEFLAGRATION OR DETONATION IN THE KEWAUNEE CONTAINMENT 4-1

4.1 Bounding Assessment of Hydrogen Deflagration. 4-1

4.2 Assessment of Hydrogen Detonation Potential 4-13

5.0 UNCERTAINTIES. 5-1

6.0 CONCLUSIONS. 6-1

7.0 REFERENCES 7-1

APPENDIX A: Calculation of H_2-Air-Steam Composition A-1

APPENDIX B: Post-Combustion Pressure Rise Calculation B-1

APPENDIX C: Summary of DDT Potential Evaluation from NUREG/CR-4803. . . . . C-1

LIST OF FIGURES

Figure No.		Page
2-1	Minimum ignition energy for hydrogen deflagrations (reproduced from Camp, 1983)	2-4
2-2	Comparison of ignition source energies (reproduced from Fauske & Associates, 1990a)	2-5
2-3	The flammability floor domain for upward flame propagation for H_2-Air-H_2O (vapor) mixtures. The flammability limit curve is superimposed on the isobaric contours of calculated adiabatic explosion pressures (reproduced from Tieszen, 1987)	2-6
2-4	Theoretical adiabatic, constant-volume combustion temperatures of hydrogen-air-mixtures (reproduced from Sherman, 1981)	2-7
2-5	AICC pressures for various containment initial conditions (reproduced from Shermam, 1984)	2-9
2-6	Degrees of combustion in hydrogen-air-steam mixtures (from Liu, 1981)	2-12
2-7	Combustion completeness for Nevada Test Site premixed combustion tests (reproduced from Ratzel, 1985)	2-13
2-8	The effect of steam addition at intermediate hydrogen concentration (reproduced from Kumar, 1984)	2-15
2-9	Comparative pressure profiles for three 8% (nominal) hydrogen combustion tests having different pre-combustion steam concentrations. Numbers in parenthesis are the steam concentration (reproduced from Ratzel, 1985)	2-16
2-10	Measured values (McGill, Sandia) of the detonation cell width (λ) as a function of hydrogen concentration (reproduced from Tieszen, 1987)	2-18
2-11	Detonation cell width as a function of the equivalence ratio for various steam concentrations (reproduced from Tieszen, 1987)	2-20
2-12	Detonation cell width as a function of temperature (reproduced from Tieszen, 1987)	2-21
2-13	FLAME apparatus DDT results (reproduced from Sherman, Tieszen, Benedick, 1989)	2-23

LIST OF TABLES

Table No.		Page
4-1	Inputs for Assessment of Hydrogen Deflagration in Kewaunee Containment	4-2
4-2	Typical Large - Dry PWR Severe Accident Results	4-4
4-3	Results for Station Blackout in Kewaunee	4-11
4-4	DDT Scaling Assessment for Kewaunee Containment (Vented Regions)	4-18

1.0 PURPOSE

The potential failure of a nuclear power plant containment building due to an energetic hydrogen burn has been the subject of technical exchange between the Nuclear Regulatory Commission (NRC) Staff, NRC contractors, and the nuclear industry. Discussion has been motivated by the concern that hydrogen evolved during a core damage event, could accumulate in the containment building and be ignited. Such an event occurred in containment during the TMI-2 accident. If the combustion was energetic enough to fail the containment, the timing (i.e., before or shortly after vessel failure) and uncertainties in location of the containment shell failure, have two potentially important ramifications regarding the radiological source term. First, natural fission product deposition mechanisms in the containment would not have sufficient time to significantly affect (reduce) the masses of fission products that could be released through the failure location. Second, fission products carried by gas flows from the containment could result in radiological releases to the environment without the benefit of the fission product removal capability of the containment spray system, the water pool in the containment submerging the core debris, or steam driven Stephan flow in the containment.

The objective of this paper is to develop a strategy to account for postulated hydrogen combustion-induced failure of the containment when developing the source term portion of the IPE Level II Analysis for the Kewaunee Nuclear Plant. The occurrence of hydrogen combustion and/or detonation will be assessed to determine the potential for containment failure.

2.0 PHENOMENA

2.1 Description

Hydrogen combustion is the result of a chemical reaction between gaseous hydrogen and gaseous oxygen. The products of such a reaction are steam and energy; the energy is liberated as light and heat. Necessary conditions for hydrogen combustion are the presence of the right amounts of hydrogen and oxygen, and the presence of an ignition source or a trigger.

Given a volume filled with only hydrogen and oxygen gases, minimum concentrations of hydrogen and oxygen are required for hydrogen combustion to occur. A mixture containing too little hydrogen to burn is called "lean", while a mixture containing too little oxygen to burn is called "rich". The presence of another gas that does not particulate in the combustion reaction (such as steam or nitrogen) also acts to inhibit the occurrence of combustion. As the concentration of the inert gas increases, the threshold concentration of lean hydrogen combustion increases, while the threshold concentration of rich hydrogen combustion decreases. Extensive research has been performed for numerous combinations of hydrogen, oxygen, and inert gases to map out the hydrogen and oxygen concentrations that are combustible. These maps are referred to as flammability limits.

Given a flammable hydrogen and oxygen mixture, a trigger is necessary to initiate burning. Typically a spark is sufficient to ignite a flammable mixture. The required trigger energy decreases as the hydrogen gas temperature increases, until a threshold temperature is reached. Above the threshold temperature, the hydrogen is energetic enough to self-trigger (or auto-ignite) combustion of a flammable mixture.

Given a volume containing hydrogen and oxygen concentrations within the flammability limits, and a trigger that initiated combustion, the magnitude of energy release depends on the mass of hydrogen consumed by the chemical reaction. The combustion of one lb-mole of hydrogen releases 1.04×10^5 BTUs of energy. Ignition of gas mixtures with hydrogen concentrations near

the flammability limits have too little hydrogen or oxygen for the flame front to propagate throughout the entire volume and consume all of the available hydrogen; such burns are called "partial" burns. As the hydrogen concentration moves away from the flammability limits, more complete burning of the reactants occurs. Above threshold hydrogen and oxygen concentrations, ignition will cause complete consumption of the reactants or "global" burns. Global burns yield the maximum energy release that can be obtained from hydrogen combustion.

2.1.1 Physical Processes

Two types of hydrogen combustion reactions are pertinent to an IPE: deflagration and detonation. Deflagration is a combustion process in which the combustion front moves at subsonic velocity with respect to the unburned gas, while detonation is defined as sonic or supersonic propagation of the combustion front. This distinction is important because the pressure in the deflagration cannot exceed the adiabatic constant volume process value (adiabatic, isochoric, complete combustion, or AICC). In a detonation, transient overpressures can exceed this value by a factor of two or more, and pressure can vary significantly across the detonation front. Pressure is uniformly distributed during a deflagration because the flame moves slowly with respect to pressure waves. The transient overpressure associated with a detonation lasts only briefly, so structures may be able to withstand detonations when the impulsive load is not excessive.

Factors which determine the type of combustion reaction are concentrations of fuel (hydrogen and carbon monoxide), oxidant (oxygen in air), and inertant (nitrogen, steam, or carbon dioxide in air), initial temperature and pressure, containment geometry, turbulence level, and combustible mixture ignition sources. Composition and the initial thermodynamic state impose limits to both flammability and detonability, while geometry and turbulence can determine the potential for detonation. Turbulence also enhances the burn completeness. In order for combustion to occur, the gas mixture must be flammable and there must be an ignition source. Relatively feeble sources such as static discharge and sparks can cause ignition. Figure 2-1 presents the minimum ignition energy for hydrogen deflagrations.

For the case of 13% by volume of hydrogen in air approximately 0.08 millijoules is sufficient to ignite a hydrogen burn. Figure 2-2 compares various potential ignition sources energies including a match. A match burning for one second can release one joule of energy which is over four orders of magnitude more energy than that required to initiate a hydrogen burn.

High temperatures lead to slow volumetric oxidation, and very high hydrogen temperatures (about 1340.6 F (1000 K)) can cause autoignition. Autoignition is most likely to occur for sequences that release hydrogen rich and very high temperature gases from the reactor vessel into non-inerted compartments. It may also be possible that gas heating induced in the reactor cavity by dried-out core debris could result in very high temperature hydrogen mixtures being delivered to the lower compartment. Again, if the recipient compartment is not inerted, autoignition may occur. The well mixed average containment temperature is not hot enough during severe accident sequences to cause autoignition.

Classical limits for flammability and AICC maximum equilibrium final pressure are presented in Figure 2-3 [Hertzberg, 1981]. The region of concern generally lies below the line of stoichiometric mixtures, in which hydrogen is the limiting reactant. The minimum amount of hydrogen necessary for combustion is slightly over 4% in dry air. The minimum oxygen concentration necessary for combustion is about 5% in dry air, corresponding to about 75% hydrogen. Addition of steam to any mixture of hydrogen and air would reduce the hydrogen volumetric concentration and increase the required threshold concentration for combustion.

Figure 2-4 presents the AICC overpressure ratio resulting from combustion in air, and indicates classical deflagration and detonation limits [Sherman, 1981]. Figure 2-4 shows the lower limit corresponding to upward flame propagation (as indicated in Figure 2-3), and a higher limit corresponding to downward flame propagation (i.e., against the buoyancy forces acting on the flame). Also, the hydrogen concentration required for

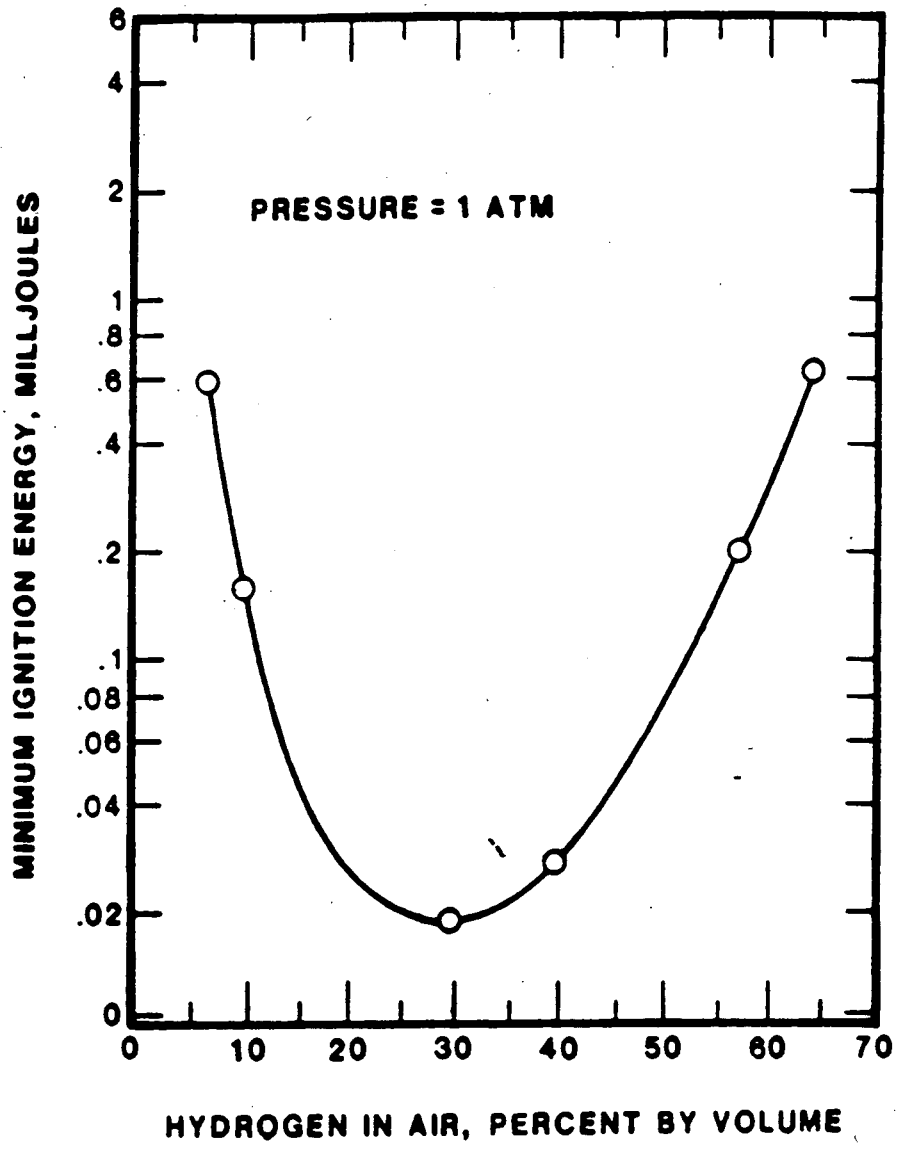

Figure 2-1 Minimum ignition energy for hydrogen deflagrations (reproduced from Camp, 1983).

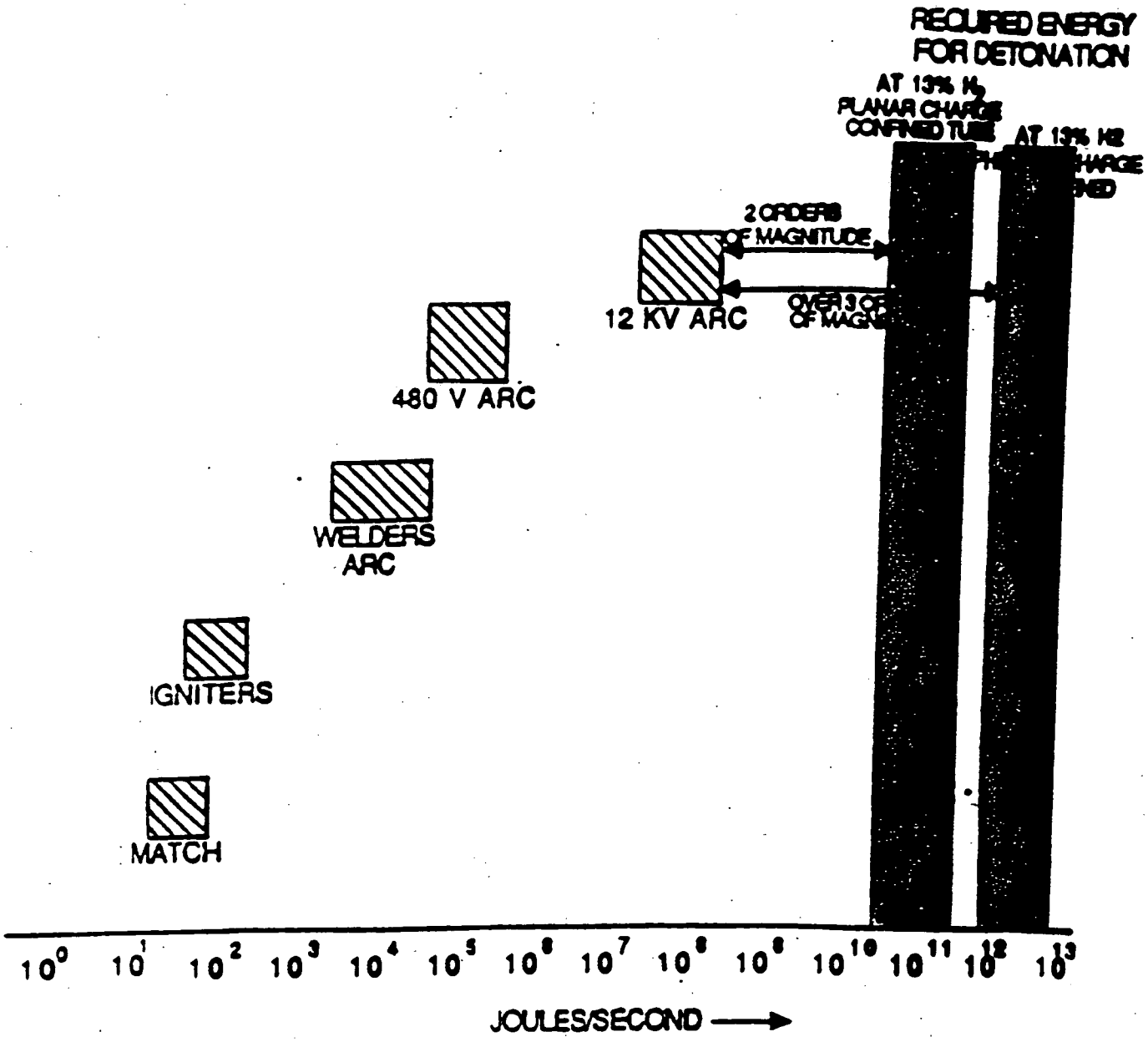

Figure 2-2 Comparison of ignition source energies (reproduced from Fauske & Associates, 1990a)

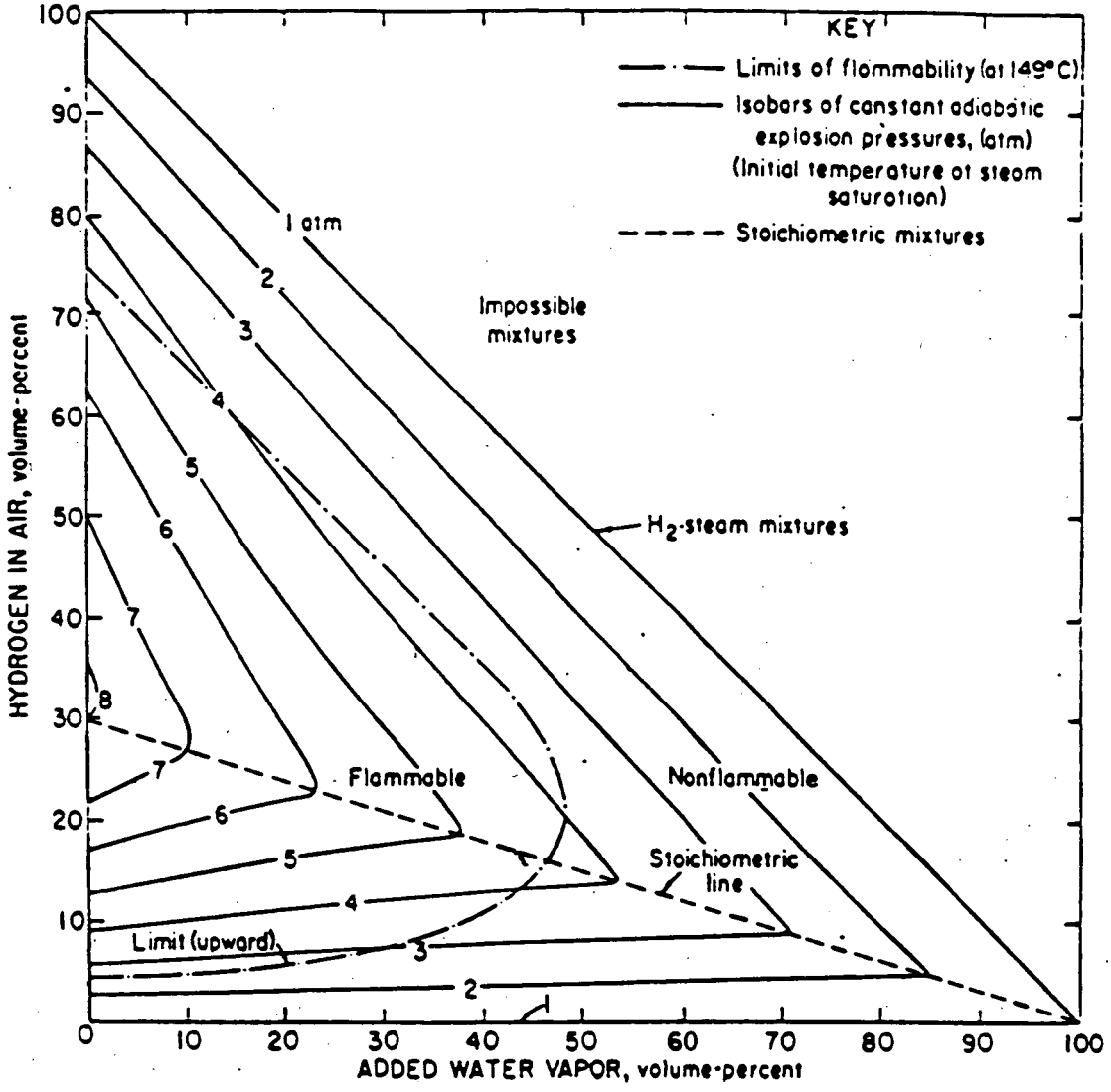

Figure 2-3 The flammability floor domain for upward flame propagation for H_2-Air-H_2O (vapor) mixtures. The flammability limit curve is superimposed on the isobaric contours of calculated adiabatic explosion pressures (reproduced from Hertzberg, 1981).

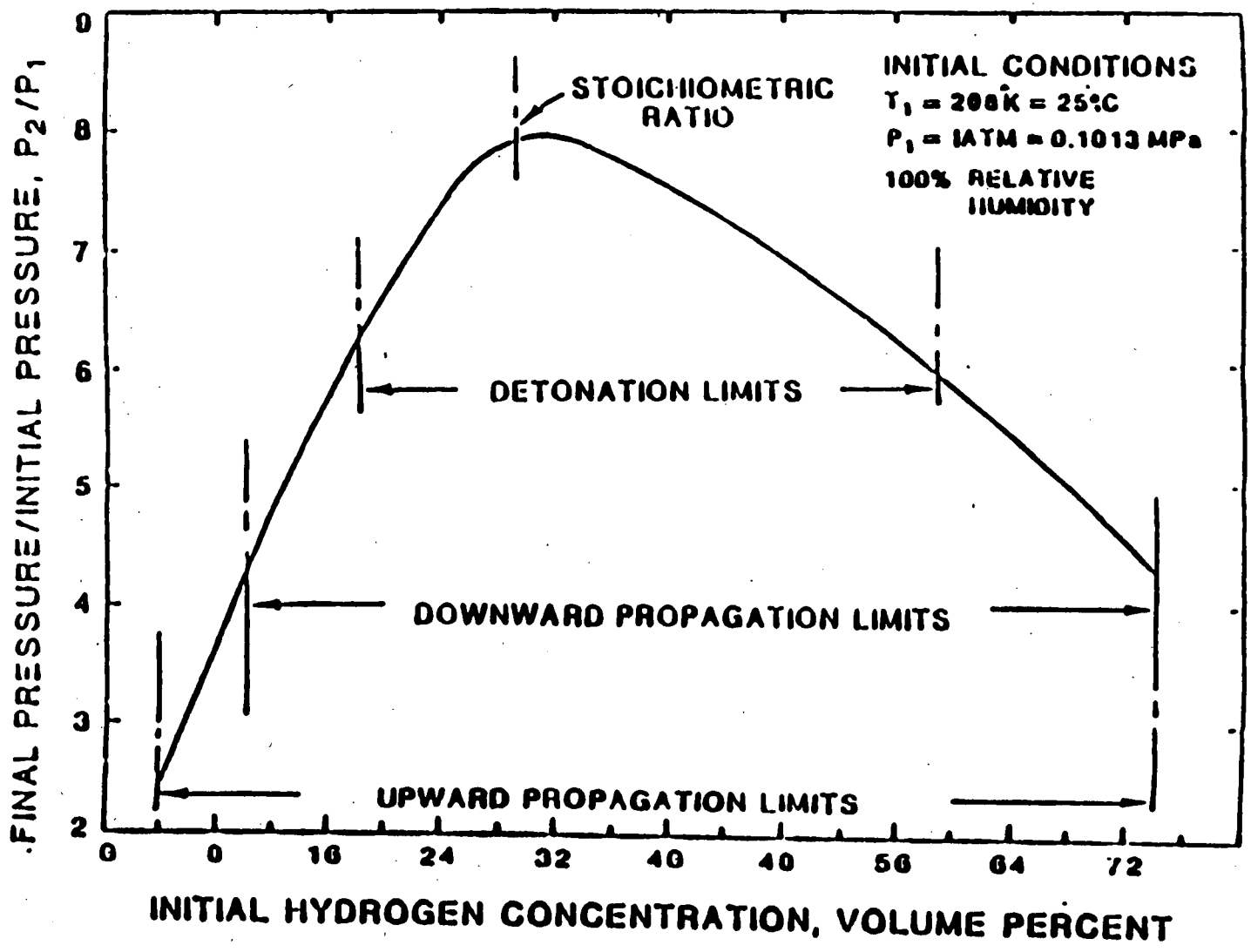

Figure 2-4 Theoretical adiabatic, constant-volume combustion temperatures of hydrogen-air-mixtures (reproduced from Sherman, 1981).

detonation is shown as higher than the threshold for downward flame propagation. However, detonation limits shown in this figure are too simplistic for reactor applications because detonation limits have been shown to be dependent on scale and temperature in a systematic fashion.

The effect of steam on post-combustion pressure is quantified for various initial saturation conditions as a function of hydrogen concentration in Figure 2-5 [Sherman, 1984]. In this figure, the initial pressure is calculated by adding the partial pressure of hydrogen and steam to a humid air mixture originally at 14.7 psi (1.0 atm) total pressure and 80.6 F (300 K). A method for calculation of approximate pre-combustion conditions is shown in Appendix A. The post-combustion conditions for non-saturated conditions, or for mixtures containing carbon dioxide and/or carbon monoxide, can be easily found with iterative solution of the energy equation as shown in Appendix B.

Generally, combustion is incomplete for hydrogen concentrations in dry air less than 8% to 9%, the downward flammability limit. Also, addition of steam reduces the combustion completeness for lean mixtures. Therefore, the pressure calculations indicated in Figures 2-3 to 2-5 are upper bounds. Details are discussed in Section 2.2.

Detonations are more difficult to achieve than deflagrations. An initiation mechanism must exist, and the gas mixture must be intrinsically detonable (i.e., able to sustain a detonation once initiated). Initiation mechanisms are energy deposition and deflagration to detonation transition (DDT) during flame acceleration. Intrinsic detonability is a function of both thermodynamic variables (pressure, temperature, and gas composition) and geometry.

DDT is the most likely mechanism for initiation of detonations in a containment because known energy sources are not large enough for direct initiation to occur. Also, a hydrogen concentration of at least 15% in dry air is probably necessary for DDT in a containment. The required concentration for DDT increases with steam addition. Initiation of detonations is discussed in more detail in Section 2.2.

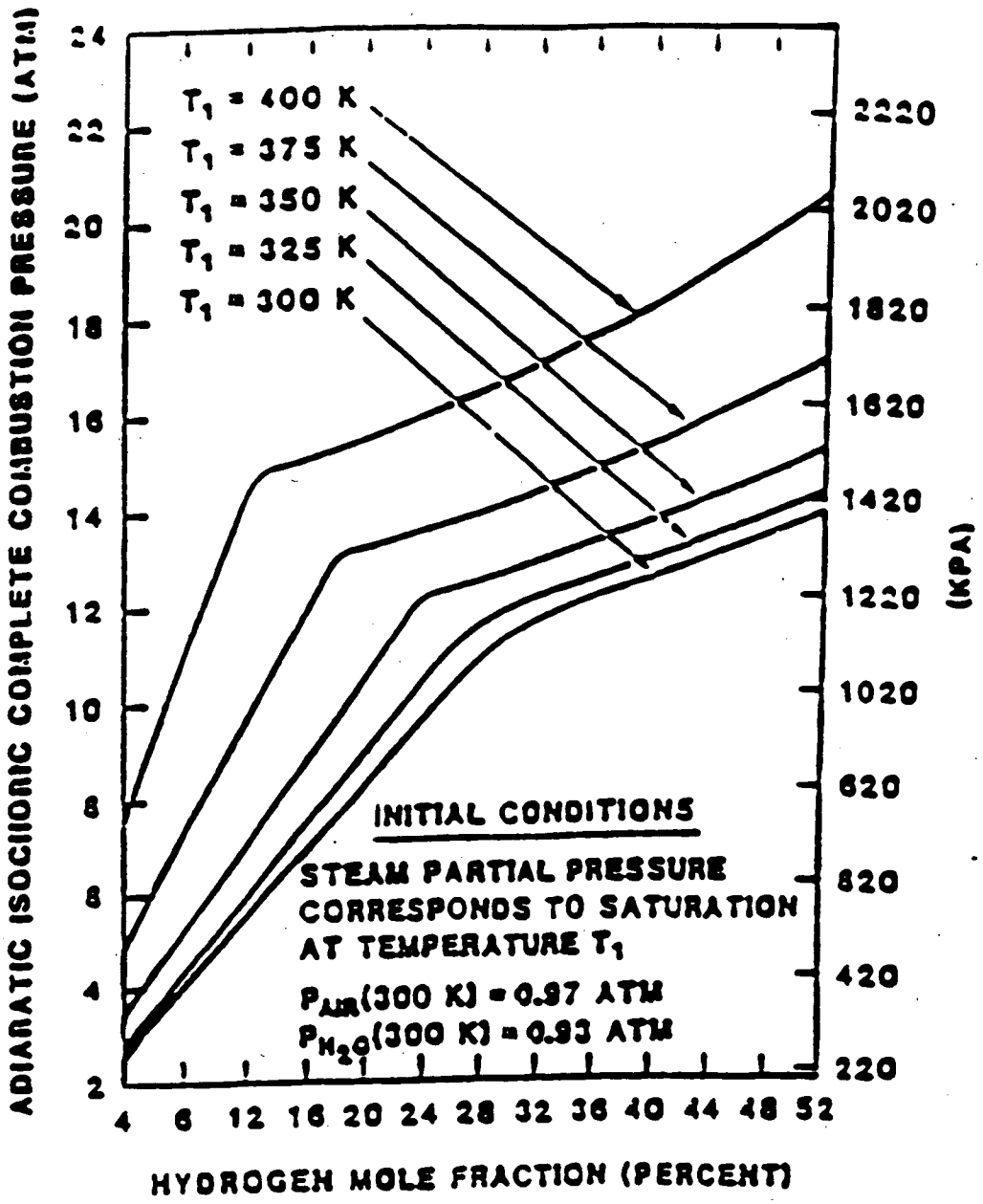

Figure 2-5 AICC pressures for various containment initisl conditions (reproduced from Sherman, 1984).

A mixture of 13% hydrogen in dry air at standard temperature and pressure (STP) is intrinsically detonable. The required concentration decreases quickly with increasing temperature, but increases even more rapidly with steam addition. Mixtures with greater than 30% steam may be immune to detonations. Intrinsic detonability is also discussed in greater detail in Section 2.2.

2.1.2 Relationship to Containment Failure Mechanisms and Modes

Hydrogen combustion is a potential threat to containment integrity because of the increase in pressure and temperature during the event. During severe accidents, there are several potential sources of hydrogen. These sources include in-vessel oxidation of zirconium and stainless steel during core over heating and relocation. Ex-vessel sources include zirconium, chromium, and iron oxidation during core-concrete interactions; zirconium oxidation during high pressure debris dispersal (DCH) and long term relocation of degraded core materials following vessel failure. The quasi-static pressure load on the containment is limited to the AICC pressure, and is generally lower due to both incomplete combustion and heat transfer to structures during the event. The transient load during a detonation lasts only for a period of milliseconds and may be unable to cause containment failure, though equipment damage may still be possible. Because flames may accelerate during a deflagration, equipment damage may occur due to a local impulse loading. The temperature load only lasts from tens of seconds to a few minutes, with the peak being brief and decay being sharp.

From the phenomenological description in Section 2.1.1, it is clear that hydrogen combustion can only occur when sufficient hydrogen and oxygen are present, insufficient steam is present to prevent flammability, and when an ignition source exists. Therefore, hydrogen combustion is not a possible containment failure mechanism for inerted containments. This includes inerting due to steam which is often a direct and natural consequence of the postulated accident sequence and the progression to core overheating and damage. Also, the containment load is highly dependent upon initial conditions which influence combustion completeness and pressure rise. Therefore,

the existence of a combustion event does not automatically imply containment failure. The maximum pressure must be compared against a containment failure criterion (see Section 4).

2.1.3 Relationship to Source Term

Combustion influences the source term primarily through containment failure. That is, if hydrogen combustion can result in containment failure, then the time of combustion becomes significant. In general, combustion can potentially increase the source term because containment failure can occur earlier through this mechanism than through slow pressurization due to loss of decay heat removal. Early containment failure generally increases the source term because the airborne fission product concentration tends to decay with time in an intact containment. In summary, the delay time between fission product release from fuel (either in-vessel or ex-vessel) and release to the environment (due to containment failure) may be decreased due to hydrogen combustion.

Because combustion influences containment gas and structure temperatures, a secondary influence on fission product revaporization occurs. This effect is usually minor in the containment, and is quantifiable with knowledge of the structure's temperature history.

2.2 Experiments

2.2.1 Hydrogen Deflagrations

In the preceeding section, a discussion of ideal adiabatic pressures resulting from hydrogen deflagrations is presented. In practice, at low hydrogen concentrations, this pressure limit is not achieved because combustion is incomplete. As illustrated in Figures 2-6 and 2-7, incomplete burning occurs for hydrogen concentrations below the downward flammability limit, but above that limit combustion is fairly complete. The effect of steam addition is also shown in these figures. There is close agreement between these sets of deflagration data despite a significant disparity in

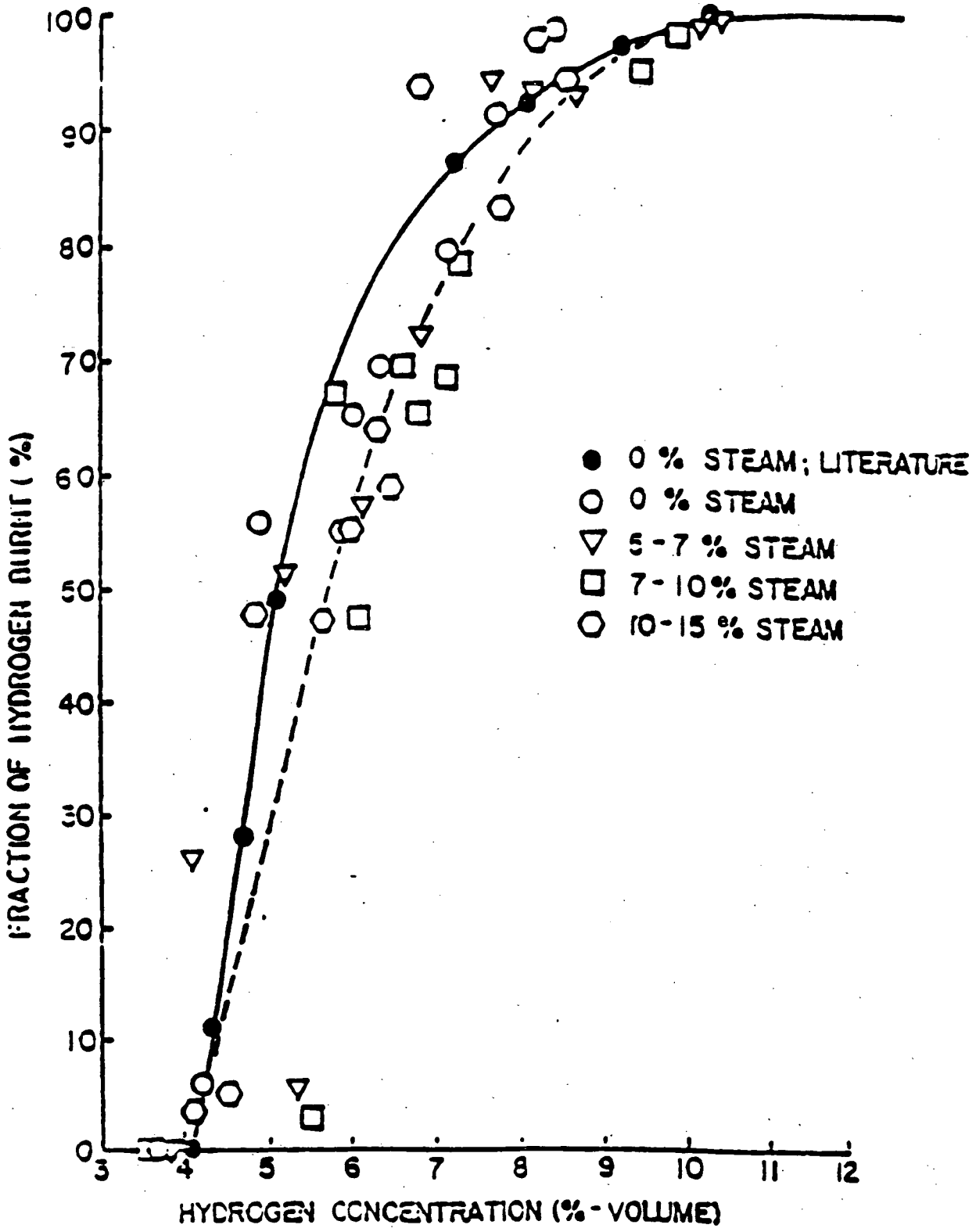

Figure 2-6 Degrees of combustion in hydrogen-air-steam mixtures (from Liu, 1981).

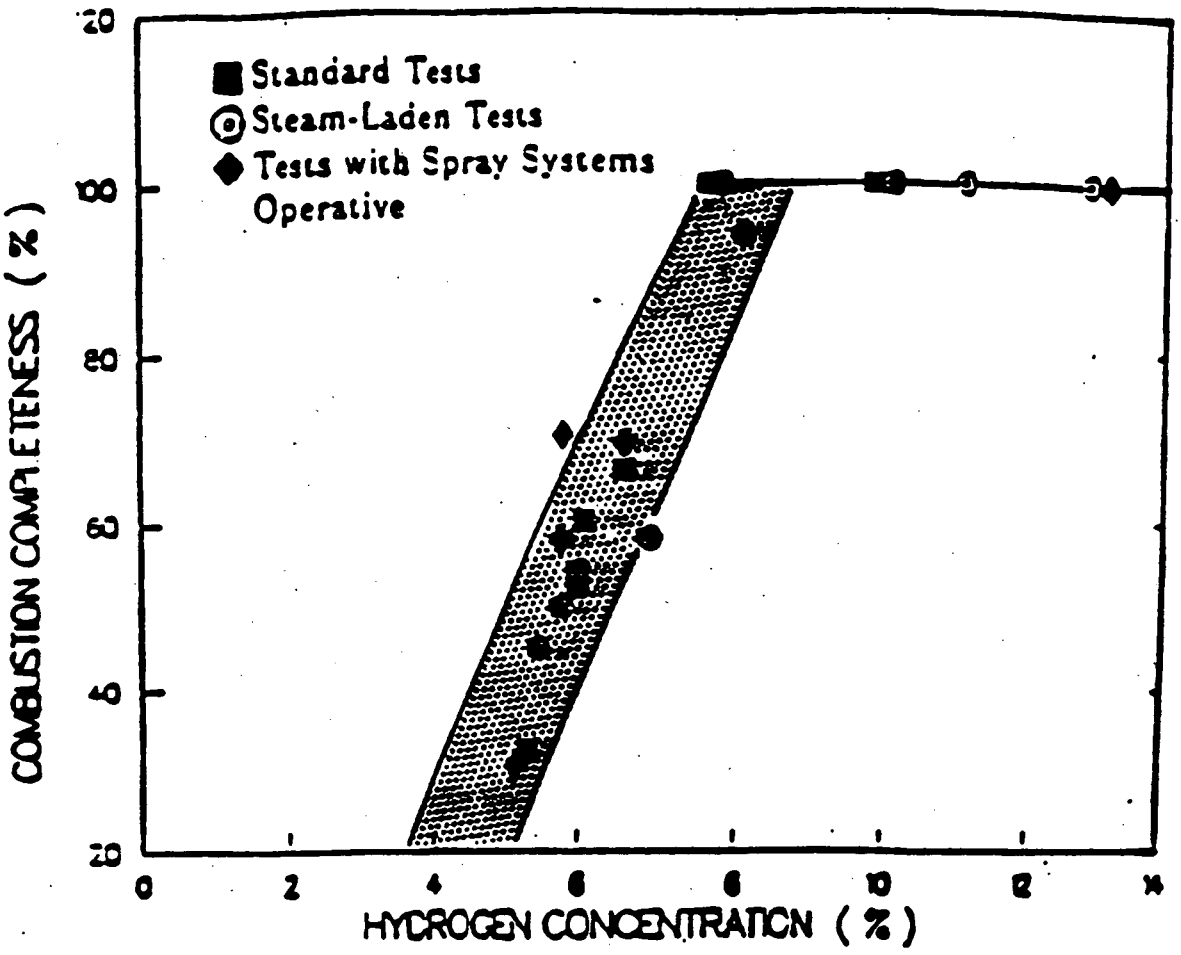

Figure 2-7 Combustion completeness for Nevada Test Site premixed combustion tests (reproduced from Ratzel, 1985).

geometric scale of the vessels used in each experiment (i.e., 0.0763 ft^3 (.002 m^3) and 72324.5 ft^3 (2048 m^3), respectively) [Liu, 1981; Ratzel, 1985]. In both cases, it is evident that addition of steam has an effect on the completeness of combustion, shifting the required hydrogen concentration to a higher value as more steam is added.

Steam affects the combustion completeness, flame velocity, heat capacity, and emissivity of the combustible gas mixture which, in turn, reduces the resultant system pressure rise. Figures 2-8 and 2-9 illustrate this reduction in combustion pressure as a result of increasing the relative concentration of steam for two different size systems 222.48 ft^3 (6.3 m^3) and 72324.5 ft^3 (2048 m^3) spheres [Ratzel, 1985; Kumar, 1984]. Both sets of data were taken with initial hydrogen concentrations of 8%. The pressure rise ratio is reduced by about 50% in the larger apparatus, and by even a greater factor in the smaller apparatus. In each case, combustion was only about 38% complete for the highest steam addition test.

2.2.2 Hydrogen Detonations

2.2.2.1 Intrinsic Detonability

The lowest value of hydrogen concentration for intrinsic detonability is now understood to be dependent upon geometric scale. Increasing scale allows the possibility of detonations at lower hydrogen concentrations. For example, the detonability limits shown in Figure 2-4 were based on observations in a small apparatus. Recently, detonability has been observed for mixtures of 13% hydrogen in dry air at 212°F (100°C) and 9.5% hydrogen in dry air at 212°F (100°C) [Kumar, 1984] in a much larger apparatus (16.93 in (43 cm) diameter tube). In both cases, these detonations were initiated by large explosive charges. The National Research Council reached the conclusion that mixtures of 9 to 11% hydrogen might be detonable based upon these experiments with hot, dry mixtures driven by explosive charges. Of course, explosive charges do not exist in a containment.

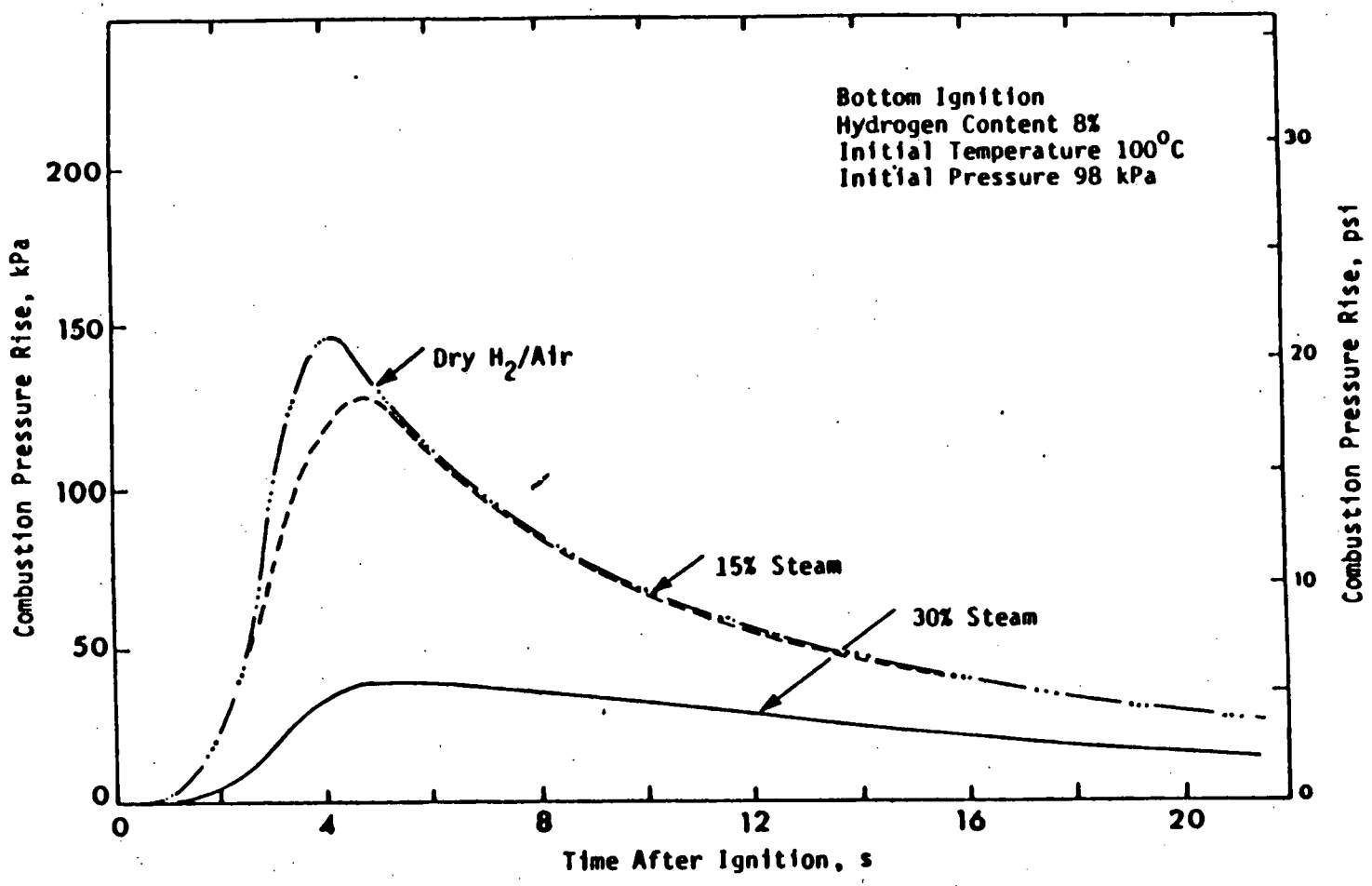

Figure 2-8 The effect of steam addition at intermediate hydrogen concentration (reproduced from Kumar, 1984).

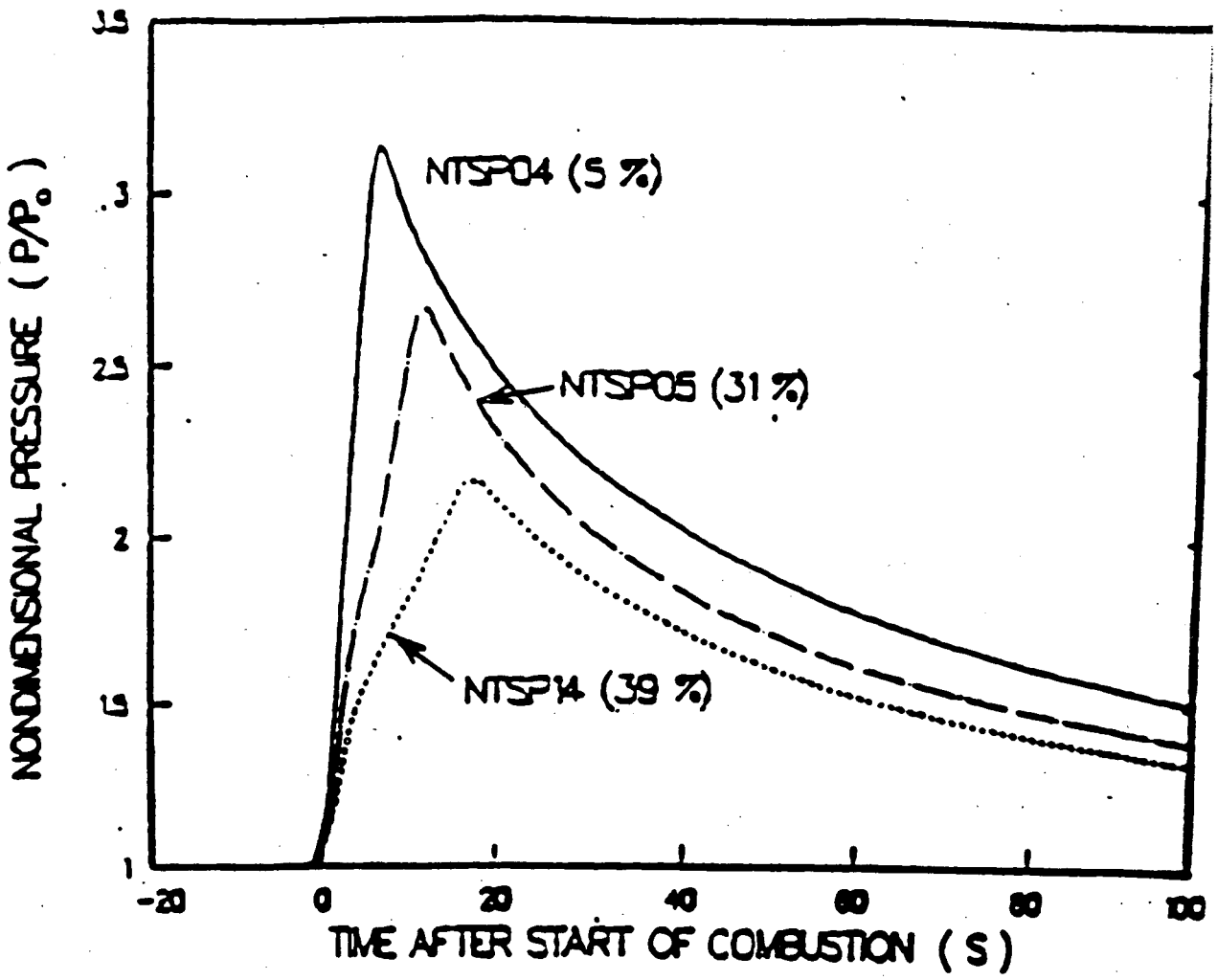

Figure 2-9 Comparative pressure profiles for three 8% (nominal) hydrogen combustion tests having different precombustion steam concentrations. Numbers in parenthesis are the steam concentrations (reproduced from Ratzel, 1985).

The ability for a detonation to be sustained or to propagate has been empirically found to be closely related to an intrinsic property of the mixture known as the detonation cell width, λ [Tieszen, 1987; National Research Council, 1987; Berman, 1986]. The value of λ is lower for mixtures which are more easily detonable (hereafter termed more sensitive mixtures). Detonations have a three-dimensional cellular structure formed by multiple interactions of transverse waves and the main shock front. The structure is observable from the "fish-scale" pattern left on a smoked foil by shock wave intersections. The lowest stable detonation wave mode, called the singlehead spin mode, can be related to a tube diameter D through the relation $\lambda = \pi D$ [Tieszen, 1987]. For less sensitive mixtures, where λ is larger and $\lambda/\pi > D$, detonation is still possible given a sufficiently strong initiator. For an open, unconfined cloud, the detonation criterion is more strict than for tube geometry. The minimum cloud diameter d_s is related to the detonation cell width $\lambda = d_s/6.5$ [National Research Council, 1987].

Measured cell widths for mixtures of hydrogen in dry air at 77°F (25°C) are shown in Figure 2-10. A minimum value of λ occurs near stoichiometry (29.7% hydrogen). For leaner mixtures λ increases rapidly, indicating a decrease in sensitivity. Detonation cell widths are uniformly lower at higher temperatures, indicating greater mixture sensitivity, that is, increased intrinsic detonability. These are plotted in terms of equivalence ratio, denoted by ϕ or ϵ, which is the molar ratio of hydrogen to air divided by the same quotient for dry air at stoichiometry. The equivalence ratio ϕ can be written as

$$\phi = \frac{SX_H}{1 - X_H - X_S} \qquad (2\text{-}1)$$

where

X_H is the hydrogen mole fraction

X_S is the steam mole fraction

$S = 2.387$

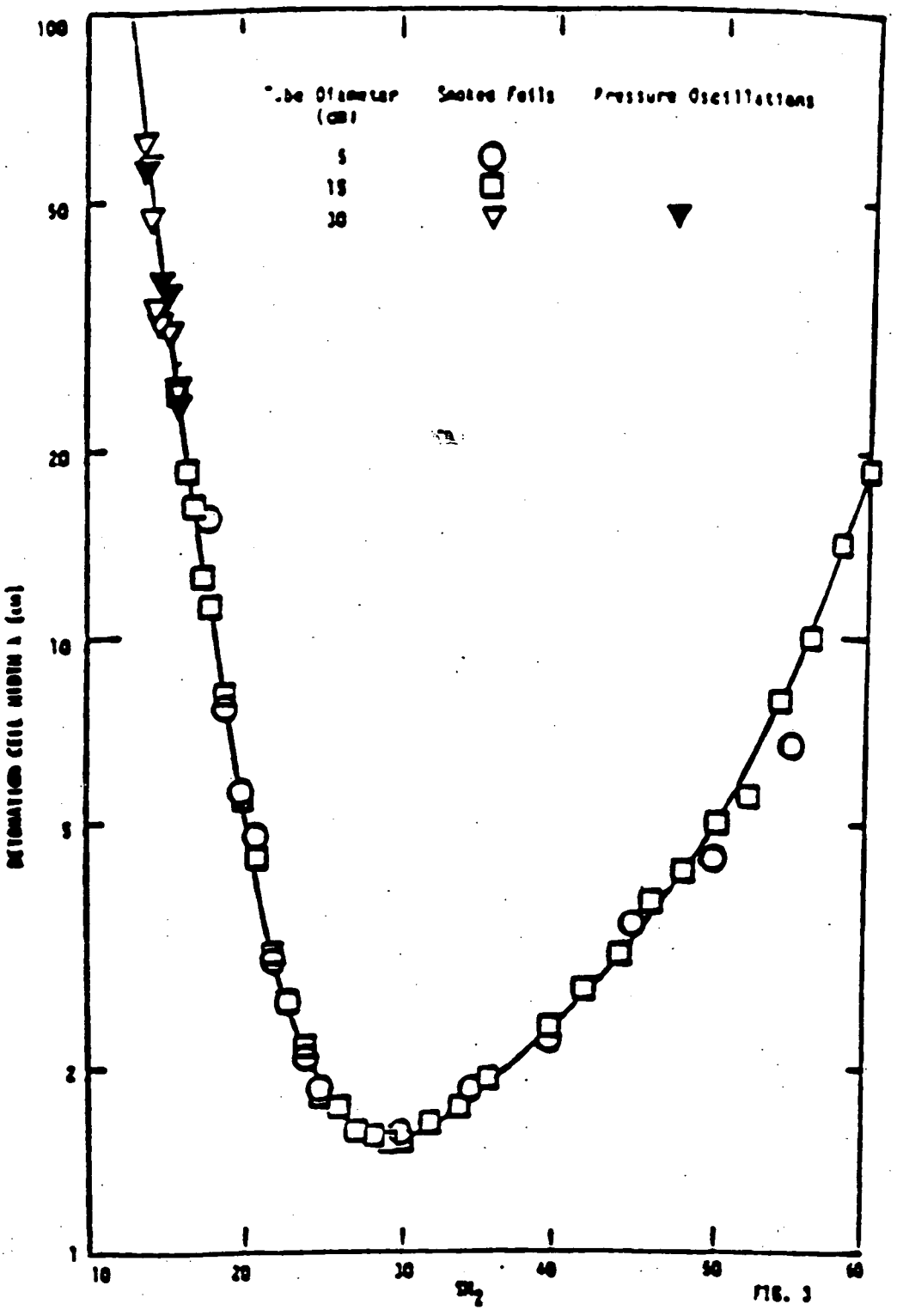

Figure 2-10 Measured values (McGill, Sandia) of the detonation cell width (λ) as a function of hydrogen concentration (reproduced from Tieszen, 1987).

The equivalence ratio for 13% hydrogen in dry air is 0.357. This value is unchanged by addition of steam to the dry mixture because the overall H_2 and O_2 mole fraction decrease in the same proportion.

For the 16.93-in-diameter (43-cm-diameter) heated detonation tube (HDT) apparatus described in [Tieszen, 1987] the critical cell width is 3.14 x 16.93 = 53.16 in., which corresponds to roughly 13% hydrogen from extrapolation of the curves in Figure 2-10. Thus, the observation of a detonation at 9.5% hydrogen [Stamps, 1987] demonstrates that high explosives can induce detonations in less sensitive mixtures. In that experiment 0.2337 lbm (106 grams) of high explosive, or about 474 Btu (0.5 MJ), was the trigger size.

2.2.2.2 Influence of Steam and Temperature

The detonation cell width increases dramatically with the addition of steam as shown in Figure 2-11 [Tieszen, 1987] for mixtures at 212°F (100°C). Thus, steam as a dilutent makes detonation more difficult to achieve. As temperature increases, detonation becomes easier as seen by the decrease in cell width in Figure 2-12 [Tieszen, 1987]. Comparing the two figures, one can clearly see that in this temperature range the steam inerting effect is far more pronounced than the heating effect on detonation cell size.

2.2.2.3 Initiation of Detonations

Detonations are much more likely to be initiated by deflagration to detonation transition (DDT) due to the magnitude of ignition sources present in containment. The energy required for a detonation can be compared with energies of various ignition sources as shown in Figure 2-2 [Fauske & Associates, 1990a]. The largest possible ignition source in a containment, a 12 kv arc, results in a maximum arc energy of 37911 Btu (40 MJ) over four cycles. As shown in Figure 2-2, a 12 kv arc produces a peak rate of energy deposition that is about two orders of magnitude lower than the value for initiation of a planar detonation of 13% hydrogen in a confined tube (0.176 lbm (80 grams) of high explosive per [Shepherd, 1985]). All the ignition

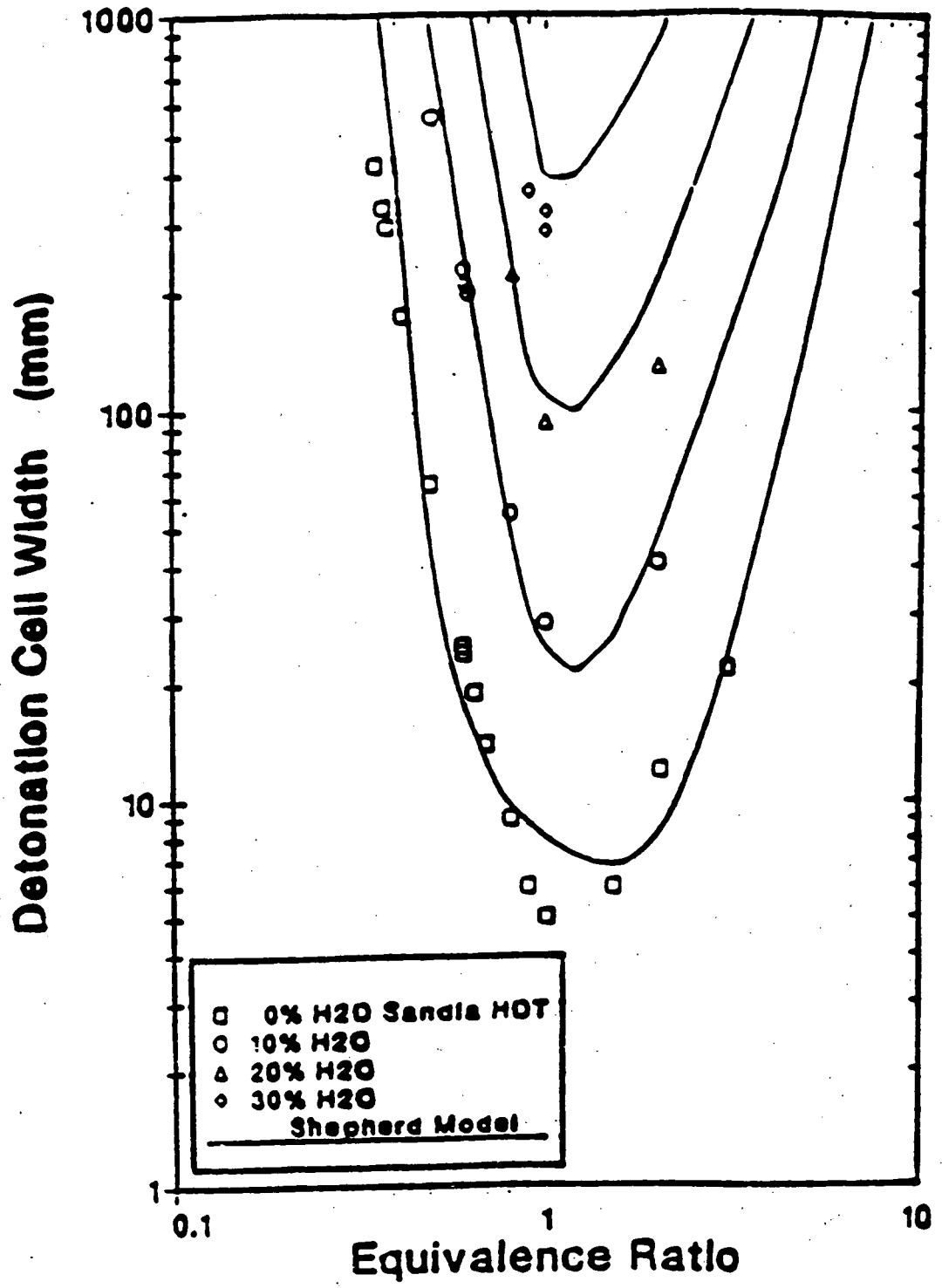

Figure 2-11 Detonation cell width as a function of the equivalence ratio for various steam concentrations (reproduced from Tieszen, 1987).

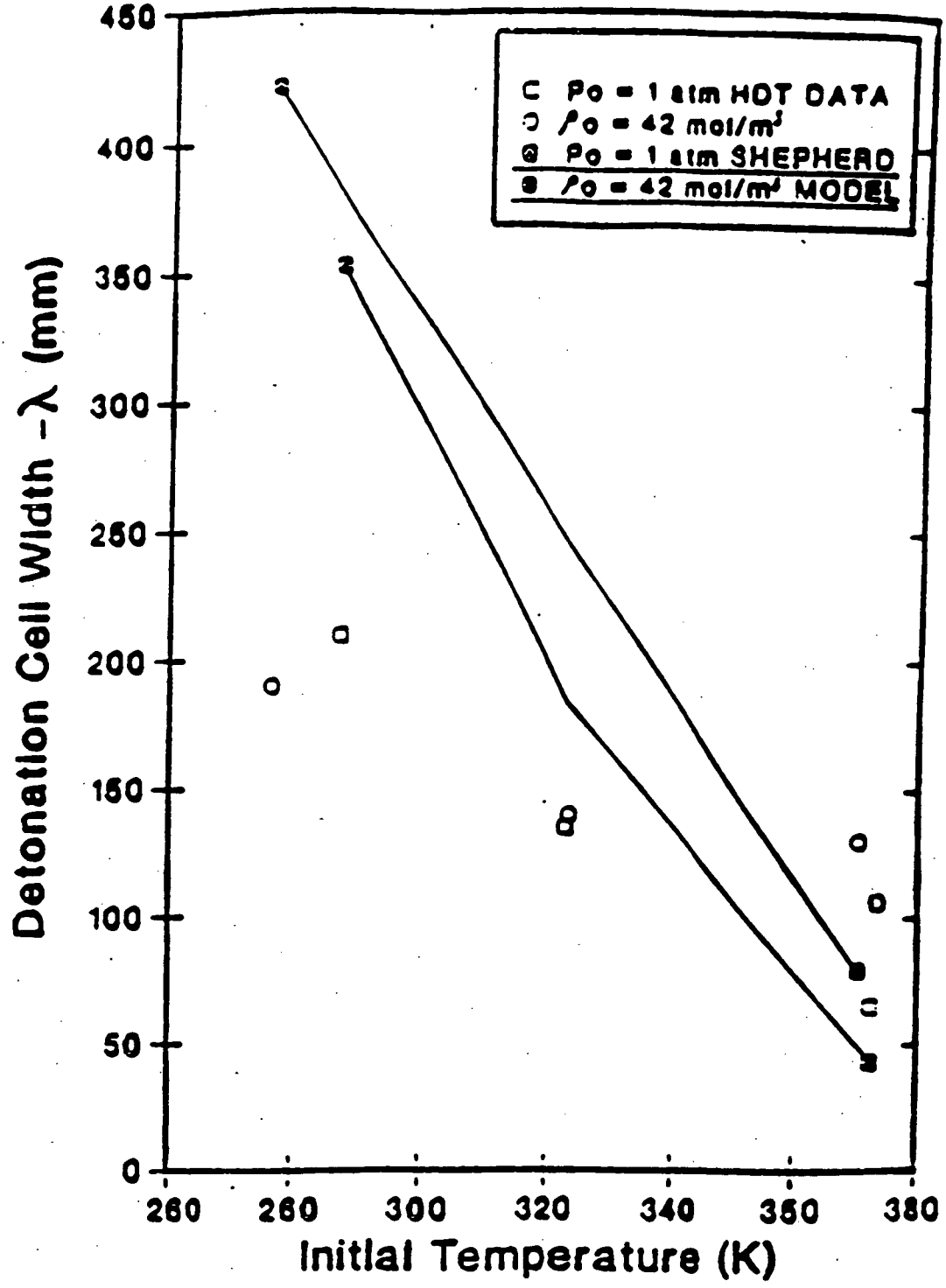

Figure 2-12 Detonation cell width as a function of temperature (reproduced from Tieszen, 1987).

sources indicated in Figure 2-2 are sufficient to cause a deflagration.

The lowest hydrogen concentration for which DDT has been observed is 15% [Sherman, 1989]. The apparatus used was the FLAME facility at Sandia, which is a half-scale model of an ice condenser upper plenum, 8 ft (2.44 m) high, 6 ft (1.83 m) wide, and 100 ft (30.5 m) in length. To promote turbulence, this long rectangular channel can be partially vented on top, and obstacles can be placed along the interior. The 15% low limit corresponds to a case with no venting and periodic obstacles every 6 ft (1.83 m). In a case with no obstacles, 25% hydrogen was required, as shown by Figure 2-13, and for a case with obstacles but 50% top venting, 20% hydrogen was required.

It is very difficult to relate the detonation cell width to a necessary or sufficient criterion for DDT because other characteristic lengths of the geometric configuration are influential. A case of attempted scaling of DDT by λ is reported by [Berman, 1986] who compares two sets of experiments [Stamps, 1987], one in a 3.28 ft by 3.28 ft (1 m by 1 m) channel and another in a 9.84 ft by 9.84 ft (3 m by 3 m) channel. The smaller experiment was performed at stoichiometry, and the larger experiment was performed by lowering concentrations in the belief that scaling with λ could occur. At a concentration of 21% hydrogen (ϕ = 0.63), for which $\lambda(\phi = .63)/\lambda(\phi = 1) = 3$, DDT occurred. This supports the hypothesis that in similar geometries DDT may occur for mixtures with similarly scaled cell widths. In both cases the apparatus included obstacles and was unvented.

2.3 Analyses

2.3.1 Hydrogen Deflagration

Two types of analyses are required for quantification of hydrogen deflagrations: flammability and pressure rise. The current state-of-the-art analytical tool for severe accident analysis is the combustion model developed by the DOE Advanced Reactor Severe Accident Program (ARSAP) [Fauske & Associates, 1990b] which has been incorporated into MAAP 3.0B.

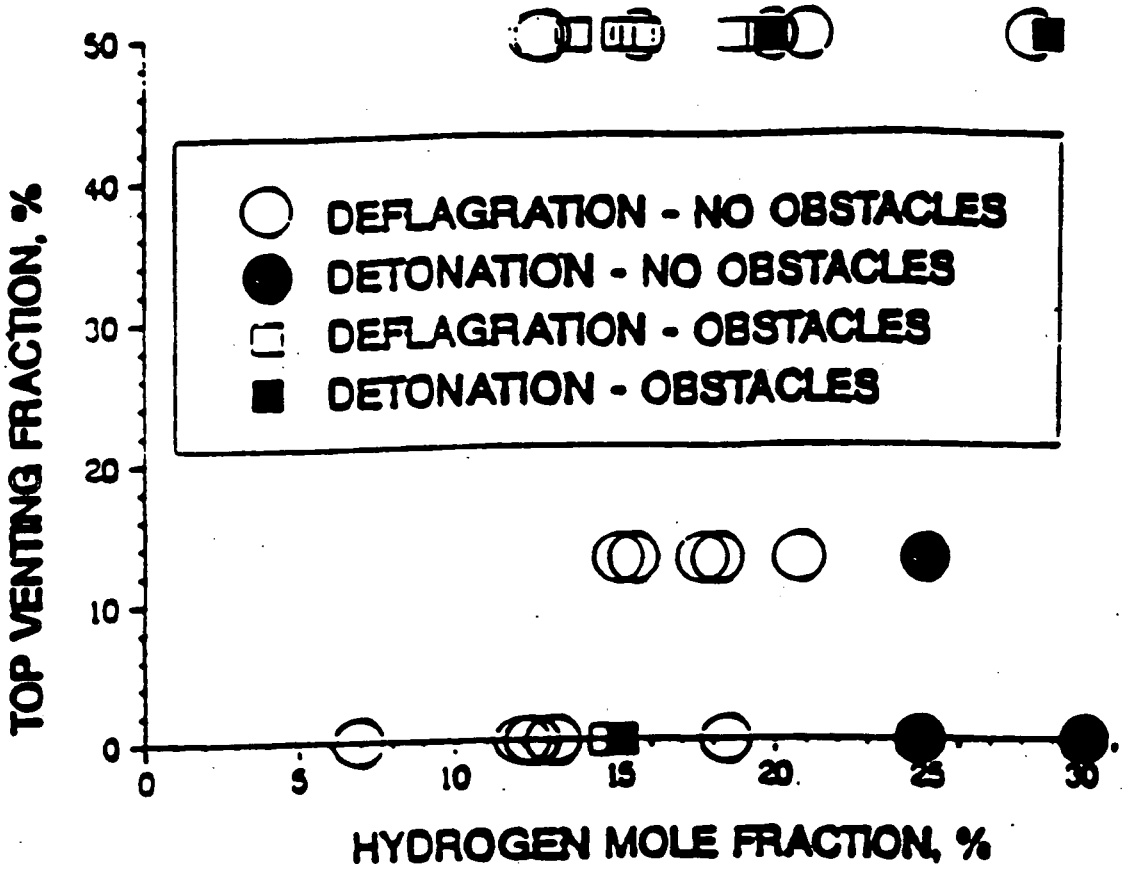

Figure 2-13 FLAME apparatus DDT results (reproduced from Sherman, Tieszen, Benedick, 1989).

In the absence of a more detailed model, the flammability limit diagram (Figure 2-3) can be used to estimate flammability. Mixture mole fractions can be estimated as shown in Appendix A. The combustion completeness can be estimated from Figure 2-7. The combustion pressure rise can be estimated through the methods discussed in Appendix B. Section 3.3 outlines an assessment methodology based on these appendices.

2.3.2 Hydrogen Detonation

No publicly available computer programs exist to predict the detonation cell width, the essential parameter for estimation of mixture detonability. Programs have been developed by NRC for internal use [Shepherd, 1985] and agree fairly well with existing data, as shown in Figures 2-10 and 2-11. An empirical technique for judgement of detonability [Sherman and Borman, 1987] is described in Section 3.4.

3.0 METHODOLOGY

The methodology for determining the potential for hydrogen combustion consists first of identification of sequences in which combustion might occur, and second, estimation of the combustion pressure rise. The potential for detonations is then considered. Finally, the load to containment must be compared with the containment failure criteria. The MAAP code can be used to study hydrogen combustion and the resulting containment load as an integral part of assessing severe accident sequences. Section 3.3 is applied in Section 4.1 in a simplified and conservative manner to assess the potential for containment overpressurization due to hydrogen burn for the Kewaunee containment.

3.1 Flammability

Identification of sequences in which combustion might occur requires calculation of the gas composition (mole fraction of all components), temperature, and pressure histories for all sequences. These states are then compared with a flammability limit diagram such as Figure 2-1. Fortunately, many sequences can be ruled out if one or more of the following conditions are met:

- less than 4% H_2 always,
- greater than 55% H_2O when H_2 present (steam inerting),
- less than 5% O_2 when H_2 present.

If an ignition source exists, then combustion is assured when the flammability condition is met. Otherwise, combustion may never occur. However, random ignition sources could cause ignition at any time. Therefore, when mixtures are flammable and no explicit ignition source exists, a sequence should be evaluated both with and without combustion.

3.2 Combustion Completeness

A model can be used to quantify combustion completeness, or the data of Figure 2-7 will suffice for an estimate. An overestimate of combustion completeness will lead to an overprediction of final pressure, and therefore it may result in a conservative estimate of containment overpressure failure or conservatively early containment failure times.

3.3 Combustion Pressure Rise

Combustion pressure rise is determined through solution of the energy equation as shown in Appendix B. The steps to follow are:

1. Determine the initial gas composition (number of moles of each gas).

2. Determine the combustion completeness.

3. Determine the final gas composition.

4. Determine the heat of combustion.

5. Solve for the final temperature.

6. Solve for the final pressure.

3.4 Evaluation of DDT Potential

The potential for DDT in current commercial and advanced light water reactor containments has been evaluated using a procedure for engineering judgement by Sherman [Sherman and Borman, 1987]. The procedure assumes that the potential for DDT can be evaluated based on the mixture intrinsic flammability (detonation cell width) and type of geometry. Five classes of mixture sensitivity are defined ranging from class 1, most detonable and near stoichiometry, to class 5, least detonable, hydrogen mole fraction less than 13.5% in dry air. Five classes of geometry were defined ranging from

class 1, most conducive to DDT featuring large geometries with obstacles and partial containment, to class 5, unfavorable to DDT featuring large scale and complete unconfinement or small scale spherical geometry with central ignition and no obstacles.

The mole fraction and equivalence ratios in Table C-1 are shown for dry hydrogen-air mixtures. For mixtures that include steam, experimental data and code calculations are used to calculate the corresponding cell widths. Figure 2-11 shows dependence of cell width on hydrogen and steam concentrations. Hence, the mixture class in Table C-1 corresponds to cell widths; the equivalence ratios/mole fractions shown are illustrations for the dry case.

Class 1 mixtures are extremely detonable. They are very likely to undergo DDT in most geometries of interest. Class 2 mixtures are slightly less likely to detonate. Class 3 mixtures have been observed to undergo transition in geometries which favor flame acceleration. Detonations have been propagated through Class 4 mixtures, but to date, DDT has not been observed for a hydrogen concentration less than 15%. Class 5 mixtures are unlikely to undergo DDT, although a detonation has been propagated in a 13.5% H_2 in air mixture at STP.

The procedure for estimating DDT potential is thus as follows:

1. Determine the mixture class from Table C-1 using Figures 2-10 and 2-11.

2. Determine the geometric class as guided by Table C-2.

3. Find the result class in Table C-3.

4. Assign a probability to this result from Table C-4.

4.0 ASSESSING THE PROBABILITY AND EFFECT OF HYDROGEN DEFLAGRATION OR DETONATION IN THE KEWAUNEE CONTAINMENT

Section 3 of this paper describes a method for assessing the effect of hydrogen deflagration or detonation within the Kewaunee containment during the course of a severe accident. This section will describe the application of that methodology to the Kewaunee IPE analysis. A bounding assessment of containment pressurization due to hydrogen burns will be made to assess their potential as a failure mode for the Kewaunee containment.

4.1 Bounding Assessment of Hydrogen Deflagration

The methodology presented in Section 3 for combustion pressure rise is applied in this section. In order to demonstrate the robustness of the Kewaunee large dry containment, very conservative assumptions are made in the following assessment. The initial conditions and inputs used for this assessment are presented in Table 4-1. The values for the net containment volume and zirconium mass were taken from the Kewaunee parameter file [Fauske & Associates, Inc., 1992]. Since steam acts as an inertant, it is conservative to assume a completely dry air is in the containment initially prior to an accident.

Step 1: Containment Hydrogen Composition

Following the method described in Appendix A, the moles of air (n_A) initially in the containment are calculated, using Eq. (A-1) and Table 4-1, to be 3120 lb-moles = (1415 kg-moles). This number represents the amount of air present under normal operating conditions, i.e., prior to a severe accident. The amount of nitrogen doesn't change during the severe accident but the mass of steam does due to the initiating event and condensation on active and passive heat sinks. The mass of hydrogen may be added in time as a result of the severe accident and zirconium oxidation with steam.

Table 4-1

INPUTS FOR ASSESSMENT OF HYDROGEN DEFLAGRATION IN KEWAUNEE CONTAINMENT

CONTAINMENT

Volume (V)	1.32×10^6 ft^3 (3.74×10^4 m^3)
Initial Pressure (P_o)	14.7 psia (1.013×10^5 Pa)
Initial Temperature (T_o)	120°F (332 K)
Relative Humidity	0%
Initial Air Mass (n_A)	3120 lb_m - mol (1415 kg-mol)

CORE

Mass of Zirconium	24,443 lb_m (11,110 Kg)
Mass of Iron, Chromium, and Nickel in Lower Core Plate (73.5% Ni, 16% Cr, 8.6% Fe)	2,200 lb_m (1000.0 kg)

PHYSICAL PROPERTIES

Gas	Constant Volume Heat Capacity (at 900 K)
Nitrogen	0.195 BTU/lb_m-R (0.818 KJ/kg-K)
Oxygen	0.183 BTU/lb_m-R (0.767 KJ/kg-K)
Steam	0.43 BTU/lb_m-R (1.8 KJ/Kg-K)
Hydrogen	2.53 BTU/lb_m-R (10.592 KJ/Kg-K)

REACTIONS	Heat of Reaction [Williams, et al.,1987] (BTU/lb_m-mol or MJ/kg-mol reactant)		
$H_2 + \frac{1}{2}O_2 \rightarrow H_2O$	1.04×10^5	or	242
$Zr + 2H_2O \rightarrow ZrO_2 + 2H_2$	2.57×10^5	or	598
$Cr + \frac{3}{2} H_2O \rightarrow \frac{1}{2} Cr_2O_3 + \frac{3}{2} H_2$	0.86×10^5	or	200
$Fe + H_2O \rightarrow FeO + H_2$	0.12×10^5	or	28
$Ni + H_2O \rightarrow NiO + H_2$	0.01×10^5	or	2.5

Thus, the containment hydrogen composition will vary with accident sequence. In order to perform a bounding assessment, typical conditions for three severe accident sequences predicted by the MAAP code for a Zion-like PWR plant have been selected and are summarized in Tables 4-2. The temperatures, pressures and H_2 mass from in-vessel oxidation are taken to represent the containment conditions right after reactor vessel failure.

Additional mass of H_2 was produced due to molten core-concrete interaction (MCCI) over a long period of time starting from the debris dryout time after the reactor vessel failure. However, as shown in Table 4-2, significantly large amounts of H_2 were produced only during the station blackout sequence. The availability of water from the engineered safety system prevented the debris from attacking the concrete during the small and large LOCA sequences, and thus, minimized the H_2 production.

Among the three typical severe accident sequences in a Zion-like plant, the station blackout would produce the overall largest mass of hydrogen and, therefore, is the most likely sequence to form a flammable mixture if possible at all.

Similar arguments can be applied to Kewaunee as well that the station blackout sequence would produce the largest amount of hydrogen gas. The significant difference from the sample calculation of Table 4-2 is the shorter debris dryout time after it is expelled out of the vessel. This is because of a curb over which water on the lower compartment floor has to flow in order to get to the cavity in Kewaunee and cool the debris residing in the cavity. In the sample calculations of Table 4-2, this curb does not exist. If the debris dryout time is shorter, MCCI will start producing hydrogen at an earlier time.

Table 4-2

TYPICAL LARGE DRY PWR SEVERE ACCIDENT RESULTS[1]

Accident Sequence	Containment at RPV Failure Time		Mass H_2 From Core	Mass H_2 From MCCI[2]	% Zr Oxidation
	Temperature	Pressure			
Small LOCA	242.6 °F 390 K	34.8 psi 2.4×10^5 Pa	617.3 lbm 280 kg	2.20 lbm 0.1 kg	31.6
Large LOCA	241.6 °F 395 K	40.6 psi 2.8×10^5 Pa	485.0 lbm 220 kg	4.85 lbm 2.2 kg	25.1
Station Blackout	278 °F 410 K	34.8 psi 2.4×10^5 Pa	540.1 lbm 245 kg	1287.7 lbm 580 kg	93.1

(1) These results are derived from the PWR sample problems provided in the MAAP User's Manual (Modular Accident Analysis Program (MAAP), MAAP 3.0B User's Manual, March 16, 1990.

(2) Total hydrogen produced during molten core-concrete interaction (MCCI) at time of containment failure.

For conservatism, it is assumed that large uncertainties in the overall mass of H_2 generated and the amount of steam at time of interest for the three sequences exist. However, this can be overcome by assuming in-core hydrogen production due to 100% oxidation of all zirconium and metallic constituents of the lower core plate. This highly conservative amount of H_2 is assumed to enter the containment compartments at the time of reactor vessel failure. With this assumption, the differences among the three sequences also become insignificant. Considering one of these sequences will suffice. Here, the station blackout sequence will be used for sample calculations. The use of MAAP modeling of the Kewaunee plant will be made to determine the containment conditions right after the rector vessel failure for the station blackout.

Figures 4-1 and 4-2 show the containment pressures and temperatures in Kewaunee during a station blackout sequence. Figure 4-3 and 4-4 show the mass of hydrogen generated in-vessel due to zirconium oxidation and the mass of hydrogen in the containment compartments, respectively. Just after vessel failure (3.9 hr), the containment pressure and temperature were 43.7 psi (3×10^6 Pa) and 215 °F (375 K). The total amount of hydrogen generated at time of vessel failure was approximately 562 lb (255 Kg) according to Figure 4-3. This corresponds to approximately 50% of the cladding and lower core support plate being oxidized. Assuming 100% oxidation of all zirconium in the core and metallic constituents of the lower core plate yields 506 Kg of hydrogen available for combustion. Figure 4-4 shows the hydrogen masses in each compartment. These numbers are conservative, due to the fact that no entrainment of corium into the lower compartment was allowed. The reason that no entrainment is so conservative is that the corium remains in the cavity where very little water is present. Due to this lack of water and small floor area, the corium is lumped together and capable of achieving temperatures high enough to initiate MCCI. Due to a larger floor and water present on the lower compartment floor, the corium can spread out and become quenched by the water and the floor area heat sinks. Therefore, very little hydrogen is produced due to MCCI. As you can see from this figure, hydrogen production due to MCCI begins around 40,000 sec. Sensitivity studies can be performed to vary the amount of material that gets dispersed from the cavity, but for this analysis the present case is acceptable. Thus 100% oxidation of cladding and dry containment (no steaming) assumptions are very conservative.

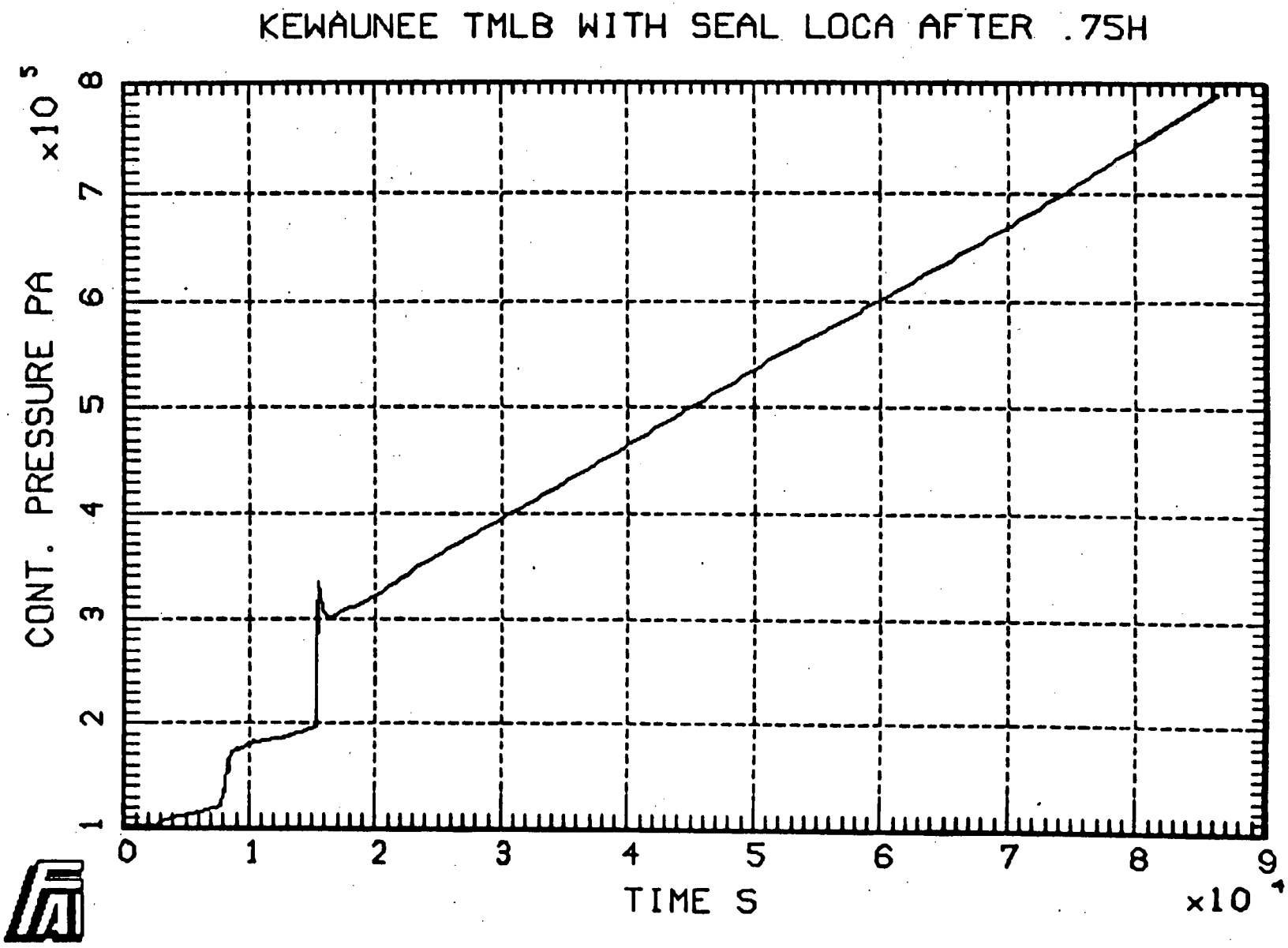

Figure 4-1 Containment pressures in Kewaunee during station blackout.

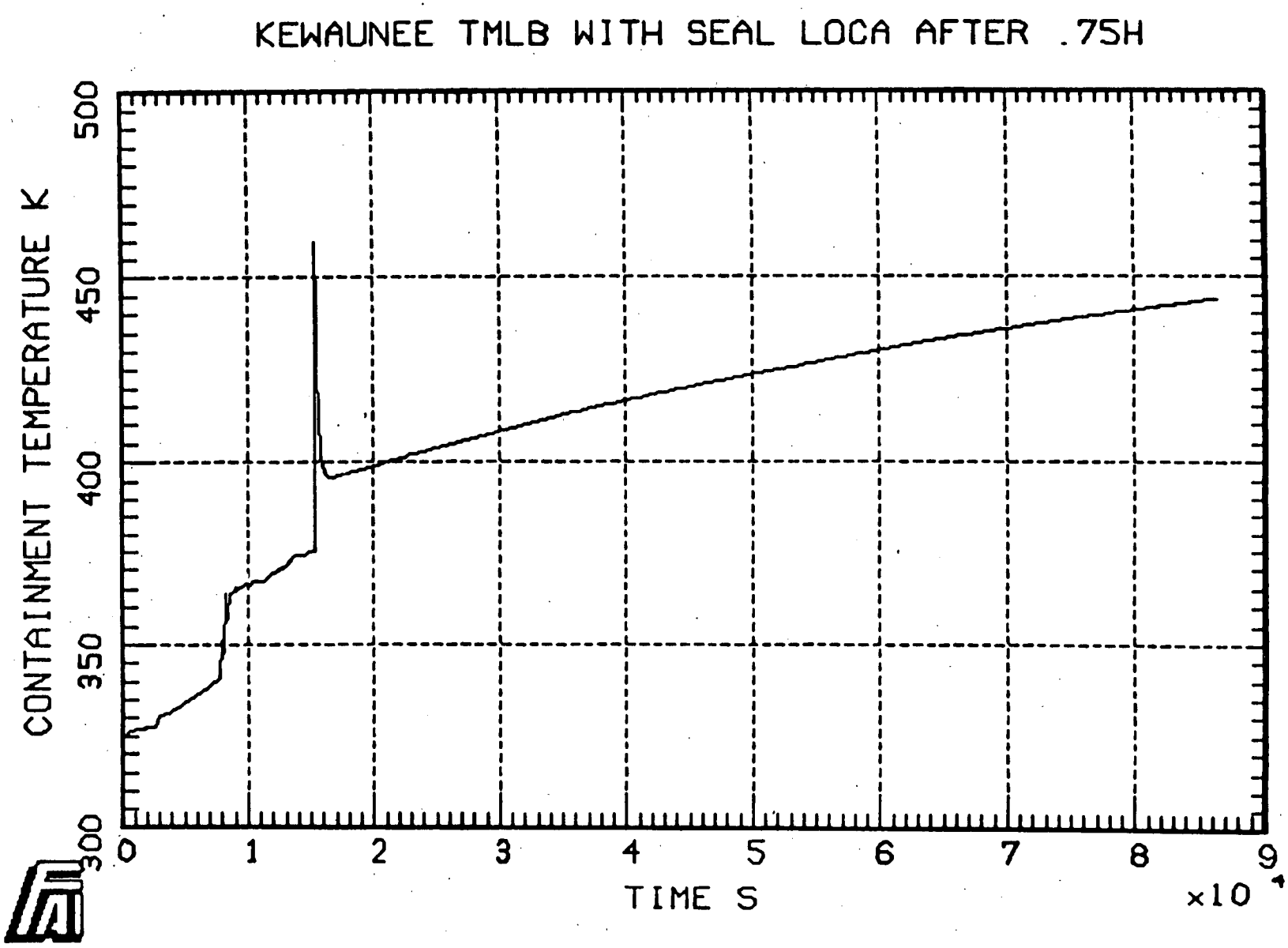

Figure 4-2 Average gas temperature in Kewaunee during a station blackout.

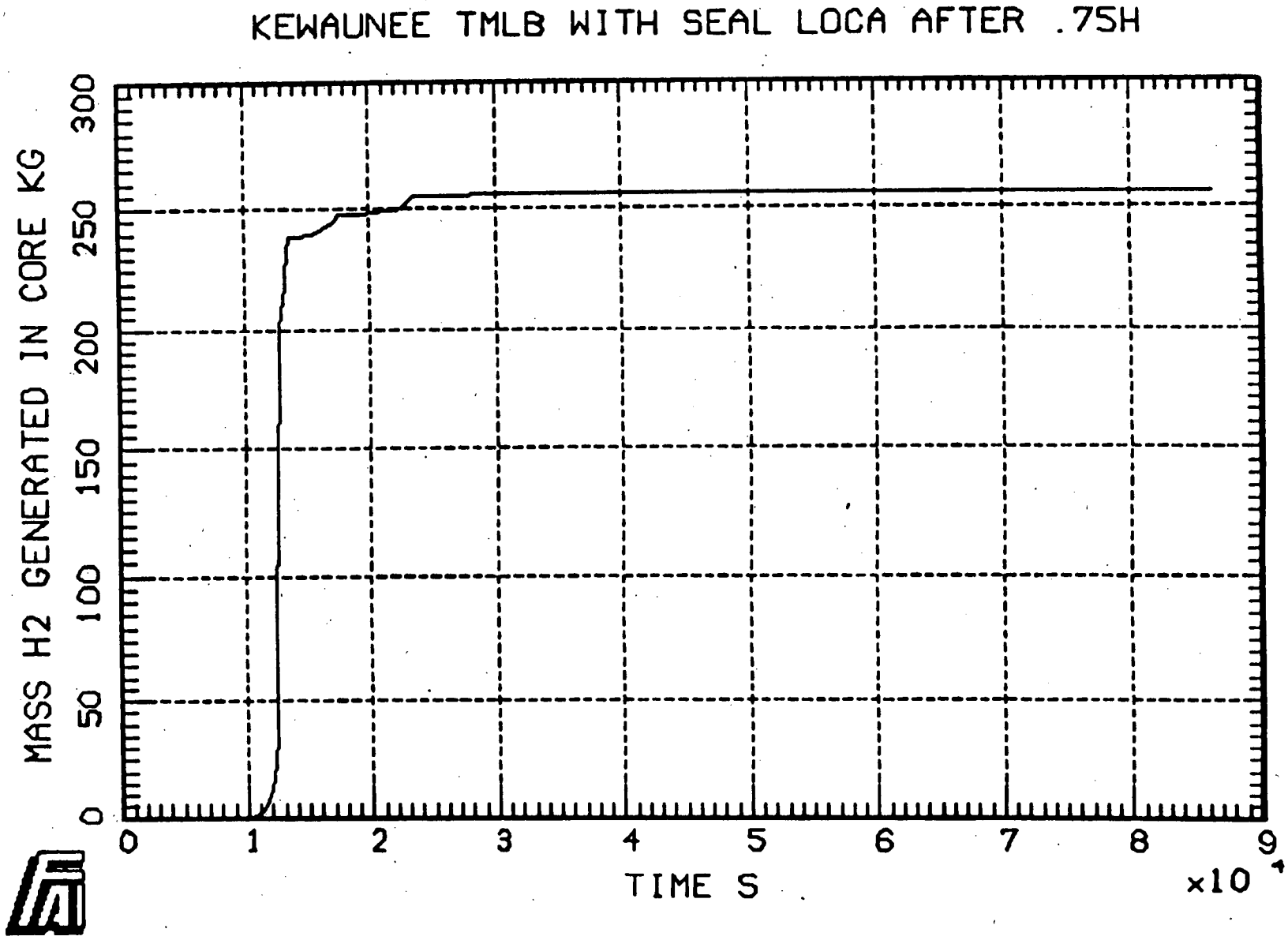

Figure 4-3 Mass of H_2 due to zirconium oxidation in station blackout.

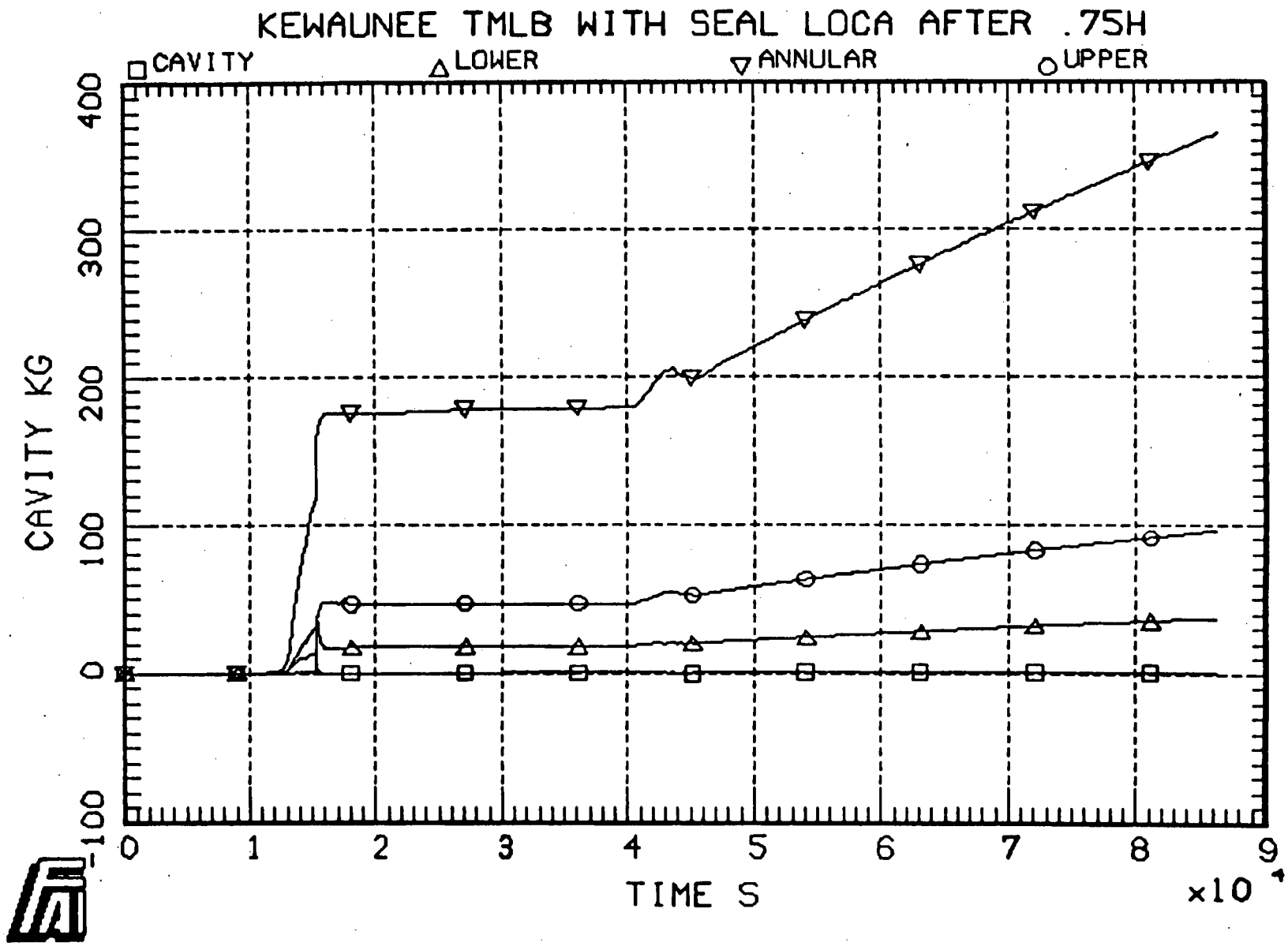

Figure 4-4 Mass of H_2 in containment.

Appendix A can now be used with these data to calculate the mole fractions of steam and hydrogen in the containment prior to hydrogen deflagration. The results are show in Table 4-3. The containment conditions at the time of vessel failure show containment inerting by steam. This can be checked by referring to Figure 2-3 and observing that these conditions fall in the non-flammable region; hydrogen in air = $X_{H,w}$ = 7.97% and added water vapor = X_S = 49.1%.

Step 2: Combustion Completeness

As observed in Step 1, steam inerting is anticipated in a majority of severe accident sequences. The operation of containment heat removal systems is included in the typical LOCA sequences. In the case of a station blackout, no active heat removal systems are available. Furthermore, a limited amount of water may be present in containment to inert it since no injection systems are operable during a station blackout. However, the water inventory in the accumulators alone is sufficient to inert the containment. Given an inerted containment no combustion would occur. Nevertheless, the bounding assessment provided in this section will conservatively assume complete combustion.

Step 3: Final Gas Composition

The gas composition changes following the hydrogen composition. The entire hydrogen mass is assumed to be burned so the final gas composition is free of hydrogen. The containment oxygen inventory is reduced by 289 lb-moles during the burning of the 577.1 lb-moles of hydrogen. At the same time, the steam mass in containment is increased by 577.1 lb-moles. The net result is a small reduction in the number of moles of gas in the containment following the complete combustion of the hydrogen and assuming no condensation of the steam. For the station blackout, the ratio of moles of non-condensible gas after combustion to moles of non-condensible gas before combustion is 0.923.

Table 4-3

Results for Station Blackout in Kewaunee

Initial Conditions	
Air initially in containment (n_A)	3120 lb-mol (1,415 kmol)
N_2 initially in containment	2465 lb-mol (1,118 kmol)
O_2 initially in containment	655 lb-mol (297 kmol)
After RPV Failure	
H_2 from 100% oxidation of Zr	536 lb-mol (243.6 kmol)
H_2 from 100% oxidation of Fe, Cr, Ni of lower core plate	41.1 lb-mol (18.7 kmol)
Containment temperature before combustion (T_p)	279 °F (410 K)
Containment pressure before combustion (P_p)	43.5 psi (3.0×10^5 Pa)
P_{nc}	22.2 psi (1.53×10^5 Pa)
P_s (= P_p - P_{nc})	21.3 psi (1.47×10^5 Pa)
H_2O in containment air	3558 lb-mol (1614 kmol)
H_2O from combustion	577 lb-mol (262.2 kmol)
X_S	0.4904
$X_{H,w}$	0.0797
$X_{H,d}$	0.1563
O_2 after total H_2 combustion	366 lb-mol (166 kmol)
Total gas and steam after combustion	6968.3 lb-mol (3160.8 kmol)
Containment pressure after combustion	113 psia (7.78×10^5 Pa)
Containment temperature after combustion	1542 °F (1112 K)

Step 4: Heat of Combustion

The heat of combustion is simply calculated by multiplying the heat of reaction of one lb-mole of hydrogen combining with oxygen to produce steam by the number of lb-moles of hydrogen. In Table 4-1, the heat of reaction is given as 1.04×10^5 BTU per lb-mole of hydrogen. Oxidation of 100% of the zirconium inventory and the metallic constituents of the lower core plate produced 577.1 lb-moles of hydrogen. Thus, 6.0×10^7 BTUs of energy are released by the complete combustion of this hydrogen.

Step 5: Post-Burn Temperature

The pressure in containment is bounded by calculating the adiabatic isochoric complete combustion (AICC) of the hydrogen. This adiabatic calculation ignores the presence of any passive or active heat sinks in the Kewaunee containment. Thus, all the combustion energy is used to heat the containment atmosphere and produce the largest possible pressure increase. This calculation assumes that all the hydrogen produced during the severe accident accumulates in containment and burns all at one time. This ignores the possibility of hydrogen burning as it is released either by auto-ignition or in localized regions should the flammability limits be satisfied. If the hydrogen is burned as it is released, the passive and active heat removal available in the Kewaunee containment would avoid significant pressurization.

The energy balance for a constant volume burn (see Appendix B) can be used to calculate the post-burn temperature. The result (Table 4-3) for the station blackout is a post-burn temperature of 1542°F (1112 K).

Step 6: Post-Burn Pressure

The post-burn containment pressure for the AICC calculation can be estimate per Equation B-2 in Appendix B. This results in estimated post-burn containment pressure of 113 psia for the station blackout sequence.

This bounding assessment has been based on very conservative assumptions. The assumptions include a large source of hydrogen (oxidation of 100% of the core zirconium and the metallic constituents of lower core plate), no credit for containment heat sinks (passive or active), and no credit for steam inerting. Nevertheless, the resulting post-burn pressure is still calculated to be within the Kewaunee containment's ultimate pressure capacity of 165 psia [Fauske & Associates, Inc., 1991b]. Clearly, the amount of combustible gas, the timing of its release, and its flammability are all sequence dependent. Thus, the MAAP runs performed to quantify the Level II assessments should be reviewed to provide confirmation of the conservatism of these assumptions. Station blackout sequences may be unique in that combustible gases including carbon monoxide may be evolved from molten core-concrete interactions (MCCI) during the ex-vessel portion of a severe accident sequence. During prolonged MCCI the balance of the Zr metal and the iron and chromium from rebar and structural steel may be oxidized and produce hydrogen. MAAP accounts for all these potential sources of combustible gases. The review of the MAAP results including the effectiveness of accident management strategies is recommended to gather plant specific insights. If localized hydrogen burns are predicted, their location and duration should be noted. This information will be of value in assessing their potential impact on the survivability of key equipment and instrumentation as well as the survivability of containment penetrations. Based on this bounding assessment, it is concluded that hydrogen deflagration will not fail the containment boundary for the dominant accident sequences considered in the Kewaunee IPE. Thus, the Kewaunee containment event trees do not need a separate node for hydrogen deflagration.

4.2 Assessment of Hydrogen Detonation Potential

The initiation of a hydrogen detonation by direct deposition of energy in the gas mixture is discussed in Section 2.2.2.3 (Initiation of Detonations) of this paper. A large energy source (explosive charge) is required to initiate a detonation even in the extreme conditions postulated in Section 4.1 (15.6% hydrogen on a dry basis). Figure 2-2 shows that the most energetic ignition sources found in reactor containments are at least several orders of magnitude too small to trigger a hydrogen detonation.

Thus, it is concluded that hydrogen detonation by direct energy deposition is not possible in the Kewaunee containment.

The detonation of hydrogen by a transition from a deflagration (DDT) due to acceleration of the flame front within the containment is also discussed in Section 2.2.2.3. The potential for a DDT induced detonation in the containment will now be assessed. This potential will be assessed in two ways. The first assessment will utilize scaling arguments as discussed in Section 2.2.2. The second assessment will utilize the method presented in Section 3.4 (Evaluation of DDT Potential).

The design of the Kewaunee containment promotes good mixing between the containment regions. Uniform mixing is promoted by both the active containment systems (fan coolers and sprays) and by passive means (natural circulation). These processes and systems help to ensure that the combustible gases are mixed with the significant amounts of steam present in the containment during severe accident sequences. As stated in Section 2.1.1, if the mole fraction of steam exceeds 30% then the containment atmosphere would be immune to detonation. It is of interest to note that calculation results presented in Table 4-3 show that the mole fraction of steam (X_s) can readily exceed 45%.

The open design of the Kewaunee containment provides a geometry that does not support DDT. Significant vent areas exist for the lower and annular compartments. Figure 4-5 and 4-6 sketches Kewaunee containment and annular region. Based on the plant drawings and the observations made during the containment walkdown, it is concluded that the regions in the containment all have significant top venting. This observation is used in the following argument based on scaling the DDT results from the FLAME tests discussed in Section 2.2.

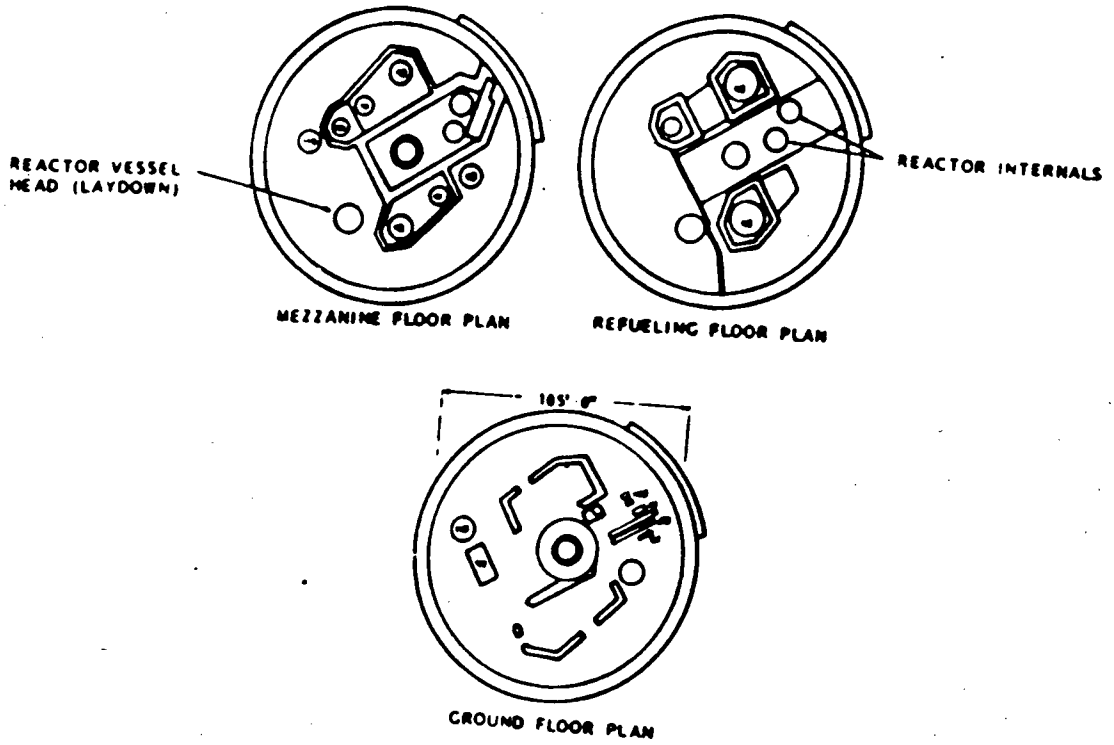

Figure 4-5 Sketch of Kewaunee containment (taken from Kewaunee FSAR).

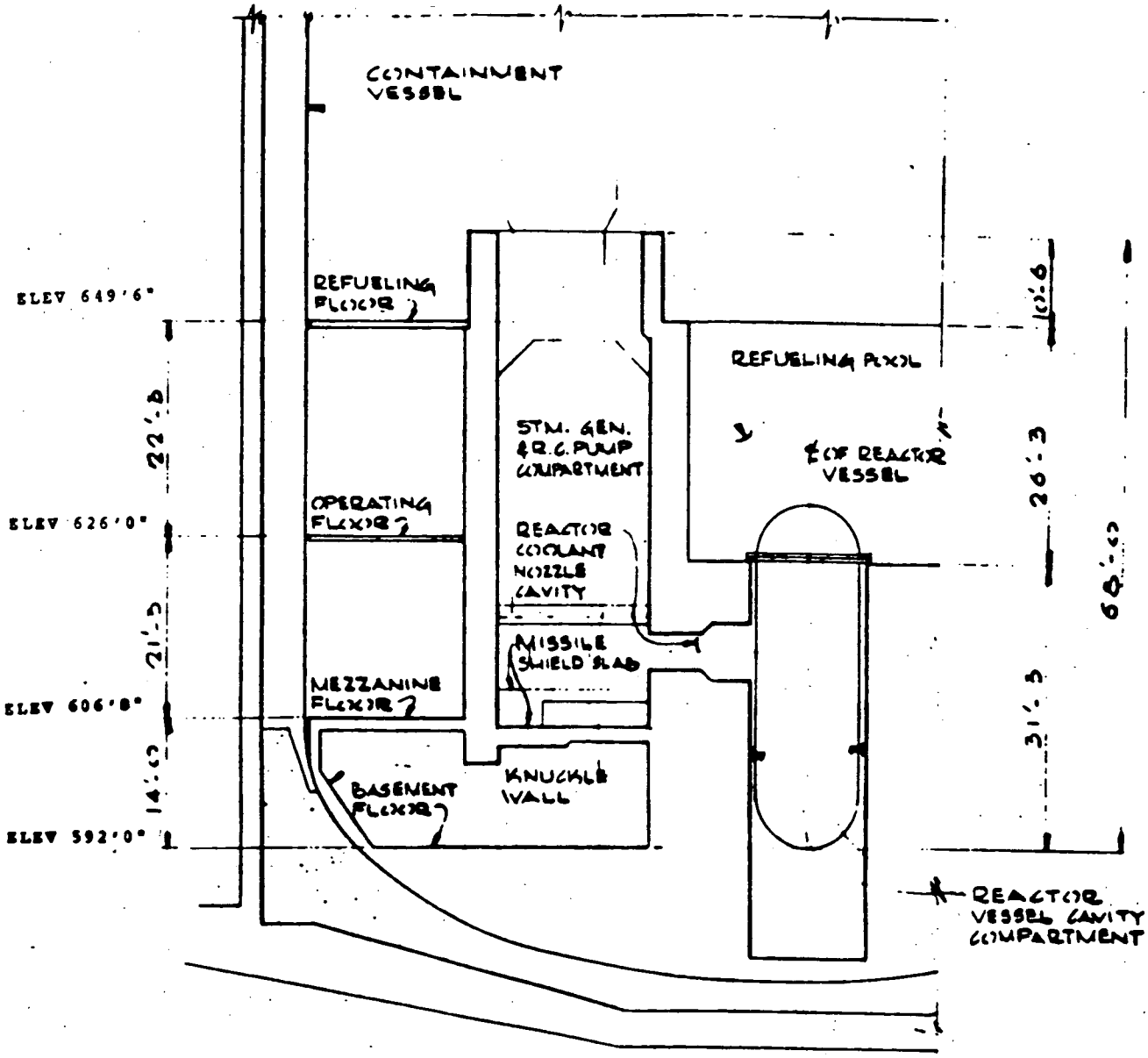

Figure 4-6 Sketch of annular compartment configuration (taken from Kewaunee FSAR).

Equation (2-1) is used to calculate an equivalence ratio (ϕ) to estimate the detonation cell size which would apply in the FLAME facility based on the postulated extreme conditions in the Kewaunee containment. These unrealistic, but extreme, conditions are a dry containment (X_S = 0) and 100% oxidation of the zirconium and the lower core plate (leads to $X_{H,d}$ = 0.1563). These conditions result in ϕ = 0.442 and per Figure 2-11 a detonation cell width of approximately 0.25 m. This detonation cell width could be used to define a scale factor to extrapolate between the FLAME facility (small scale) and the reactor scale. The results from the FLAME facility (see Figure 2-13) show the requisite hydrogen concentrations (15% and 20%) to have DDT for both vented and unvented geometries. The equivalence ratio that applies to these tests results in detonation cell widths of 0.82 ft (0.25 m) (15% H_2) and 0.082 ft (0.025 m) (20% H_2). Scale factors can be calculated by forming the desired ratios of detonation cell widths. For example, the scale factor for 15.63% H_2 for the unvented case would be 0.82 ft/0.82 ft (0.25 m/0.25 m) = 1.0 and for the vented case would be 0.82 ft/0.082 ft (0.25 m/0.025 m) = 10. Such scale factors are then applied to the dimensions of the FLAME facility (6 ft x 19.5 ft duct) to estimate the minimum channel size needed at reactor scale to produce a DDT. This results in very large required dimensions. In fact, the dimensions significantly exceed those that exist within the Kewaunee containment (see Table 4-4). Thus, the geometry in the Kewaunee containment would not produce a DDT given a deflagration occurred in a containment region.

The method for evaluating the DDT potential for the Kewaunee containment presented in Section 3.4 is now applied. The annular compartment is the only compartment analyzed due to its geometry which is the only apparent region which could support a hydrogen detonation, in comparison to the other less likely regions in containment. First the mixture class is determined from Table C-1. The dry basis hydrogen mole fraction conservatively estimated in Section 4.1 to be 15.63% results in mixture class 3 being selected. Second the geometric class is selected from Table C-2. The open containment geometry with significant areas for top venting of the annular

Table 4-4

DDT SCALING ASSESSMENT FOR KEWAUNEE CONTAINMENT (VENTED REGIONS)

Bases: 1) Vented regions
2) Assume 15.63% hydrogen
3) Safety factor of 2
4) Minimum steam inerting, 10% steam

Scale Factor: Ratio of Detonation Cell Widths x $\frac{1}{\text{Safety Factor}}$ x Inerting Factor[1]

$$= \frac{\lambda_{15.63\%}}{\lambda_{20\%}} \times \frac{1}{2} \times 10 = \frac{0.25\ m}{0.025\ m} \times \frac{1}{2} \times 10$$

= 50 (applied to FLAME facility dimensions)

Required Reactor Scale: 50 (6 ft x 19.5 ft) = 300 ft x 975 ft

Kewaunee Key Dimensions:

	Width (ft)	Height (ft)	Top Vent (% Open)
Annular Compartment @ EL. 592'	35	14	33
Annular Compartment @ EL. 606'	35	21	33[2]
Annular Compartment @ EL. 627'	35	22	33[2]
Annular Compartment @ 649'	35	11	100

CONCLUSION: NO POTENTIAL FOR DDT

[1] See Figure 2-11.

[2] This compartment is vented both on top and bottom.

compartment suggest geometric class 4. Table C-3 is now used to combine the mixture class and geometric class results to define the potential results. The potential results is that DDT is unlikely and per Table C-4 the probability of DDT is assigned a value of 0.10. Thus, it is again concluded that containment failure is highly unlikely due to hydrogen detonation in the Kewaunee containment.

5.0 UNCERTAINTIES

The major uncertainties in assessing the potential for deflagration or detonation of combustible gases in the Kewaunee containment relate to the sources of hydrogen and carbon monoxide considered and the flammability of the containment atmosphere. Flammability of the containment atmosphere depends upon the mole fractions of the combustible gases (hydrogen and carbon monoxide), of the oxygen (air), and of the inertants (nitrogen, steam and carbon dioxide). The evolution of hydrogen and possibly carbon monoxide and carbon dioxide, given corium concrete attack is occurring, as well as the evolution of steam, are all time dependent functions. The initiating event and sequence of key events, including potential operator actions or recovery activities, can influence the evolution of both combustible gases and inertant steam in the containment atmosphere. Thus it is prudent to utilize an integrated code (MAAP) to study the interactions between the several rate dependent processes. The MAAP code will be used to conduct sensitivity studies to address phenomenological uncertainties as part of the Kewaunee IPE containment response and source term quantifications. MAAP runs should be reviewed and insights derived regarding the likelihood of deflagrations within the several containment regions. Likewise given the prediction of burns during severe accident sequences, the location and duration of the burns should be noted for use in other assessments regarding the performance of instrumentation within the containment and the performance of containment penetrations.

The key uncertainties associated with the sources of combustible gases during postulated severe accidents in a Kewaunee containment are discussed below.

The in-vessel generation of hydrogen due to the oxidation of zirconium during core overheating, degradation, and relocation represent major sources of uncertainties. Considerable research has been conducted both in the United States and abroad regarding core melt progression and relocation processes. Additional research is in progress and is being planned. A means of addressing the unresolved issues associated with the complex

process of core damage and relocation can be addressed using selected parameters available within the MAAP code. The formation and degree of blockage of the fuel channels during core relocation is a major uncertainty. This can be addressed by considering core melt progression with and without blockage. Likewise the initiation of the relocation of core material impacts the degree of oxidation. This can be addressed by varying the eutectic temperature or core melt relocation temperature considered for such assessments. Lastly, the in-vessel hydrogen generation can be impacted by the duration of vessel failure, given that the time available for steam production and oxidation of zirconium while the debris is captured within the primary system affects the hydrogen production.

The ex-vessel sources of combustible gases also include some uncertainty. In the case of molten core concrete interactions, the amount of concrete attack depends upon the success in cooling the debris on the containment floor. The coolability of core debris is an uncertainty which still remains in the technical community. Different rates of debris coolability can and should be assessed as part of the sensitivity studies performed for the Kewaunee IPE. If debris is rapidly cooled such that core concrete interactions are limited then the ex-vessel sources of hydrogen and carbon monoxide will essentially be precluded. It then becomes important to assure a supply of water for the long term maintenance of the debris coolability. Ex-vessel contributions to hydrogen can also be postulated for high pressure melt ejection and subsequent direct containment heating sequences. The major uncertainty associated with high pressure melt ejection is the likelihood of the high pressure existing in the primary system at vessel failure. Emergency operating procedures direct the operators to depressurize the primary system under certain conditions while for other sequences the initiating event itself may depressurize the primary system. Given that some degree of pressurization is present in the primary system when the reactor pressure vessel is postulated to fail, the next uncertainty that needs to be addressed is the degree of debris dispersal and the amount of material available to be dispersed in a high pressure melt ejection event. These two parameters are suitable for consideration in the sensitivity studies.

Thus it is recommended that in order to insure that these phenomenological uncertainties are completely addressed and documented that they be incorporated as part of the Kewaunee IPE sensitivity studies. However, the assessment performed in this paper based on bounding analyses is sufficient to reach the conclusion that containment failure is not expected in the large majority of accident cases due to deflagrations and detonations for the Kewaunee design. Only sequences that produce large quantities of hydrogen, say 90% of the total possible amount, without sufficient steam generation to inert the containment, can threaten the Kewaunee containment. An example of such a sequence would include recovery from a long duration station blackout. If the containment heat removal functions (containment sprays, fan coolers) are recovered, the operators might deinert the containment by condensing steam when the large quantities of hydrogen are present in the containment. At this point, the containment pressure might be high enough so that the additional pressurization produced by a hydrogen deflagration could fail the containment. This sequence is a severe accident management concern, but it does not invalidate our other conclusions about hydrogen detonation and deflagration. Thus, the sensitivity studies should help confirm this conclusion and provide additional details and insights regarding the containment response to severe accidents for the Kewaunee containment design.

6.0 CONCLUSIONS

The assessment provided in this position paper for the susceptibility of the Kewaunee containment to postulated deflagrations and detonations of combustible gases during severe accidents concludes that the Kewaunee containment would not fail due to this postulated failure mechanism. Potential sources of combustible gases were identified and discussed and a bounding pressurization calculation was provided. Based on adiabatic isochoric complete combustion of the selected bounding sequence, the resulting containment pressure is less than the ultimate capacity of the Kewaunee containment. Clearly this is a grossly conservative assessment, as the actual containment environment during postulated severe accident events that will produce significant amounts of steam and inert the containment against hydrogen burns or detonations. It was concluded based on the evidence presented in this position paper that detonation induced by direct deposition of energy in a detonable mixture of containment gases was not a possible containment failure mechanism. Detonation due to a transition from deflagration to detonation was also considered. Two methods were used to assess the likelihood of the transition to detonation in the Kewaunee containment given the existence of a deflagration. Both of the methods resulted in a very low likelihood of a DDT. Due to the small size of ignition sources required to initiate a deflagration, it is far more likely that combustible gases would be consumed within a containment by deflagration rather than a detonation.

Based upon the assessments provided in this paper and the conclusion that the likelihood of deflagrations or detonations in the Kewaunee containment is very low and improbable, it is concluded that the Kewaunee containment event trees need not incorporate a node for containment failure due to hydrogen deflagration or detonation. It is recommended that to address the range of uncertainties and the uniqueness of specific event timing during postulated severe accidents that sensitivities be performed regarding hydrogen generation and deflagration. The uncertainties and suggested considerations for selecting cases to be included in the sensitivity study are also provided in this paper.

7.0 REFERENCES

Berman, M., "A Critical Review of Recent Large-Scale Experiments on Hydrogen-Air Detonation", Nuclear Science and Engineering, 93, 1986, pp. 321-347.

Camp, A., el al., 1983, Light Water Reactor Hydrogen Manual, NUREG/CR-2726, SAND82-1137, Sandia National Laboratories, Albuquerque, NM.

Farahani A., and Corradini, M. L., 1990, "MAAP Modeling of the Kewaunee Nuclear Power Plant," University of Wisconsin Report to Wisconsin Public Service Corp.

Fauske & Associates, 1992, "Kewaunee Parameter File for MAAP 3.0B Rev. 18," Version 07, August 6, 1992.

Fauske & Associates, 1990a, "Technical Support for the Hydrogen Control Requirement for the EPRI Advanced Light Water Reactor Requirements Document", DOE/ID-10290, U.S. Department of Energy.

Fauske & Associates, 1990b, "Modifications for the Development of the MAAP-DOE Code - Volume III: A Mechanistic Model for Combustion in Integrated Accident Analysis".

Fauske & Associates, 1991a, "Phenomenological Evaluation Summary on Direct Containment Heating in Support of the Kewaunee Individual Plant Examination Program", FAI/91-123.

Fauske & Associates, 1991b, "Phenomenological Evaluation Summary on Containment Overpressurization in Support of the Kewaunee IPE," FAI/91-157.

Hertzberg, Martin, 1981, "Flammability Limits and Pressure Development in Hydrogen-Air Mixtures", Proc. Workshop on the Impact of Hydrogen on Water Reactor Safety, Volume III, NUREG/CR-2017, SAND81-0661, Sandia National Laboratories.

Kumar, R. K., et al., 1984, Intermediate Combustion Studies of Hydrogen-Air-Steam Mixtures, EPRI NP-2955, Electric Power Research Institute, Palo Alto, California.

Liu, D. D., et al., 1981, "Some Results of WRNE Experiments on Hydrogen Combustion", Proc. Workshop on the Impact of Hydrogen on Water Reactor Safety, Volume III, NUREG/CR-2017, SAND81-0661, Sandia National Laboratories.

National Research Council Report, 1987, Technical Aspects of Hydrogen Control and Combustion in Severe Light-Water Reactor Accidents, National Academy Press, Washington, D.C.

NRC, 1982, Safety Evaluation Report Related to Grand Gulf Nuclear Station, Units 1 and 2 (Docket Nos. 50-416 and 50-417), NUREG-0831, Supplement No. 3.

Plys, M. G., Astleford, R. D., and Epstein, M., 1988, "A Mechanistic Hydrogen Combustion Model for Integrated Accident Analysis", ENS/ANS Int. Conference on Thermal Reactor Safety, Avignon, France.

Ratzel, A. C., 1985, Data Analysis for Nevada Test Side (NTS) Premixed Combustion Tests, NUREG/CR-4138, SAND85-0135, Sandia National Laboratories.

Shepherd, J. E., 1985, "Chemical Kinetics and Hydrogen-Air-Diluent Detonations, Tenth International Colloquium on Dynamics of Explosions and Reactive Systems, Berkely, CA.

Sherman, M. P., et al., 1981, "Deliberate Ignition and Water Fogs as H_2 Control Measures for Sequoyah", Proc. Workshop on the Impact of Hydrogen on Water Reactor Safety, Volume IV, NUREG/CR-2017, SAND81-0661, Sandia National Laboratories.

Sherman, M. P., 1984, Hydrogen Combustion in Nuclear Plant Accidents and Associated Containment Loads", Nuclear Engineering and Design, 82, p. 13-24.

Sherman, M. P., and Borman, M., 1987, The Possibility of Local Detonation During Degraded Core Accidents in the Bellefonte Nuclear Plant, NUREG/CR-4803, SAND86-1180, Sandia National Laboratories.

Sherman, M. P., Tieszen, S. R., and Benedick, W. B., 1989, FLAME Facility, NUREG/CR-5275, SAND85-1264, Sandia National Laboratories.

Stamps, D., 1987, Sandia National Laboratories, Handout at the Hydrogen Combustion Peer Review Committee Meeting, Washington, D.C., Called by M. Silberberg, Division of Reactor Accident Analysis, U.S. NRC.

Stamps, D., Benedick, W. B., Tieszen, S. R., 1991, Hydrogen-Air-Diluent Detonation Study for Nuclear Reactor Safety Analyses, NUREG/CR-5525, SAND89-2398, Sandia National Laboratories.

Tieszen, S. R., et al., 1987, Detonability of H_2-Air-Diluent Mixtures, NUREG/CR-4905, SAND85-1263, Sandia National Laboratories.

Williams, D. G., et al., 1987, Containment Loads Due to Direct Containment Heating and Associated Hydrogen Behavior: Analysis and Calculations with the CONTRAIN Code, NUREG/CR-4896, SAND87-0633, Sandia National Laboratories, Albuquerque, New Mexico.

APPENDIX A

Calculation of H_2-Air-Steam Composition

This appendix discusses the approximate method for evaluating the containment air mixture composition that is used to determine its flammability. An initially dry containment atmosphere is assumed. It is assumed that the moles of hydrogen in the dry atmosphere is known and that the pre-burn atmosphere (which includes steam) temperature and pressure are known.

Define

n_A = initial dry air moles
P_o = initial dry air pressure,
T_o = initial dry air temperature,
n_H = moles H_2 added
P_{nc} = partial pressure of non-condensible gases after H_2 added
$X_{H,d}$ = mole fraction H_2 in the dry mixture
T_p = pre-burn temperature
P_s = steam partial pressure at T_p
P_p = total pressure at T_p
n_s = moles of H_2O
$X_{H,w}$ = wet H_2 mole fraction = $n_H/(n_H + n_s + n_A)$
X_s = wet H_2O mole fraction = $n_s/(n_H + n_s + n_A)$
ϕ = relative humidity
V = containment free volume

The initial amount of air is given by

$$n_A = \frac{P_o V}{R T_o} \qquad \text{(A-1)}$$

where

R = 8.314 J/mol-K

Assuming 21% of which is oxygen, we have

moles of oxygen = $0.21\ n_A$, and

moles of nitrogen = $0.79\ n_A$

The mole fraction of H_2 in a dry mixture is defined as

$$X_{H,d} = \frac{n_H}{n_A + n_H} \tag{A-2}$$

Next, the containment temperature and relative humidity, if known, are used to determine the partial pressure of steam

$$P_s = \phi\ P_{sat}(T_p) \tag{A-3}$$

The partial pressure of the noncondensibles at this new temperature is found from the ideal gas law as

$$P_{nc} = P_o \frac{T_p}{T_o} \frac{n_A + n_H}{n_A} = \frac{T_p}{T_o} \frac{1}{1 - X_{H,d}} P_o \tag{A-4}$$

The sum of these two partial pressures yields the total containment pressure:

$$P_p = P_s + P_{nc} \tag{A-5}$$

It is likely that P_p is known instead of ϕ. In this case instead of using Eq. (A-3), Eq. (A-5) is solved for P_s from the known value of P_p and P_{nc} given by Eq. (A-4).

For cases of interest, the ideal gas law may be used for the steam mole fraction without significant error, if the steam inerting has high margin (i.e., the resulting mixture is far from the flammability limit). Therefore the steam mole fraction is

$$X_s = P_s/P_p \tag{A-6}$$

and the hydrogen mole fraction in the wet atmosphere is

$$X_{H,w} = X_{H,d}\left(1 - X_s\right) \tag{A-7}$$

Given the mole fractions, Figure 2-3 can be used to determine if the wet mixture is flammable.

The post-combustion pressure can be found directly from Figure 2-5 if the initial relative humidity is very close to one. Otherwise, the methods of Appendix B can be used.

Example (SI Units)

Suppose the containment volume is 10,000 m^3. It is at 300 K and not inerted initially. Suppose that 100 kg of hydrogen are produced and put into the containment, and steam is generated such that the atmosphere is at 90% humidity at 330 K. Then the initial number of air moles is

$$n_A = \frac{P_o V}{RT_o} = \frac{(1.013 \times 10^5)\ (1 \times 10^4)}{(8314)(300)} = 400.9 \text{ Kg-moles} \tag{A-8}$$

and the dry hydrogen mole fraction is

$$X_{H,d} = \frac{n_H}{n_A + n_H} = \frac{(100/2)}{(401+(100/2))} = 0.111 \tag{A-9}$$

At 330 K (about 57°C) the vapor pressure of water is 0.172×10^5 Pa, so that steam partial pressure is

$$P_s = (0.9)(0.172 \times 10^5) = 1.548 \times 10^5 \text{ Pa} \tag{A-10}$$

At this temperature the noncondensible partial pressure is

$$P_{nc} = (1.0 \times 10^5)\ \frac{330}{300}\ \frac{1}{0.889} = 1.237 \times 10^5 \text{ Pa} \tag{A-11}$$

and the total pre-burn pressure is

$$P_p = 1.392 \times 10^5 \text{ Pa} \qquad \text{(A-12)}$$

The steam and hydrogen mole fractions are therefore

$$X_s = 1.548 \times 10^4 / 1.392 \times 10^5 = 0.111 \qquad \text{(A-13)}$$

$$X_{H,w} = (0.111)(1 - 0.111) = 0.099 \qquad \text{(A-14)}$$

This mixture is flammable according to Figure 2-3. Since the relative humidity is near 1, Figure 2-5 may be used to find the post-combustion pressure.

APPENDIX B

Post-Combustion Pressure Rise Calculation

This appendix describes the calculation of the adiabatic isochoric complete combustion (AICC) temperature and/or flame temperature given initial gas masses, temperature, pressure and energy.

The AICC temperature is found by equating the end state energy to the sum of the pre-burn state energy and the combustion energy release. A constant volume process (isochoric) is thus assumed.

$$\left[\sum_{i=1}^{4} M_i \, c_{vi}\right]_{postburn} T_f = \left[\sum_{i=1}^{4} M_i \, c_{vi}\right]_{preburn} T_p + Q_b \qquad \text{(B-1)}$$

where,

Q_b = heat of combustion,

M_i = mass of i-th comoponent,

C_{vi} = specific heat at constant volume of i-th component,

T_p = prehurn temperature,

T_f = postburn (AICC) temperature,

i = H_2, O_2, N_2, H_2O.

The AICC pressure P_f is estimated by

$$P_f = \frac{n_f \, R \, T_f}{V} \qquad \text{(B-2)}$$

where,

V = containment free volume,

R = universal gas constant = 8.314 J/mol-K

n_f = final gas moles.

APPENDIX C

Summary of DDT Potential Evaluation from NUREG/CR-4803

Table C-1

Classification of Hydrogen-Air Mixtures at 20°C and 1 atm Pressure

Mixture Class	Hydrogen Mole Fraction %	Equiv. Ratio	Cell Width		Hydrogen Mole Fraction %	Equiv. Ratio
			in	mm		
1	24-30	.75-1.0	0.787-0.59	20-15	38-30	1.5-1
2	21-24	.63-.75	1.575-0.787	40-20	48-38	2.2-1.5
3	15-21	.42-.63	9.055-1.575	320-40	63-48	4.2-2.2
4	13.5-15	.37-.42	47.24-9.055	1200-320	70-63	5.6-4.1
5	< 13.5	< .37	no data	no data	no data	> 5.6

Table C-2
Geometric Classes for Flame Acceleration

Geometric Class 1. Large geometries with obstacles in the path of the expanding unburned gases. Partial confinement favors gas expansion past the obstacles. A large tube with numerous obstacles and with ignition going from a closed end to an open end is an example. Class 1 geometries are the most favorable to large flame acceleration.

Geometric Class 2. Geometries similar to class 1 but with some feature which hinders flame acceleration. Examples would be a tube open on both ends or large amounts of transverse venting.

Geometric Class 3. Geometries that yield moderate flame acceleration but are neutral to DDT. Examples are large tubes without obstacles, small tubes (several inch diameter) with obstacles.

Geometric Class 4. Geometries unfavorable to flame acceleration. Examples are large volumes with hardly any obstacles and large amounts of venting transverse to the flame path, or small volumes without obstacles. DDT will not usually occur in a class 4 geometry.

Geometric Class 5. Geometries so unfavorable to flame acceleration that not even large volumes of stoichiometric hydrogen-air mixtures are likely to detonate. The only examples are totally unconfined geometry at large scale, or a small spherical geometry without obstacles and central ignition.

Table C-3

Matrix of DDT Potential Results

Results		Highly Likely	Likely	May Occur	Unlikely	Highly Unlikely
Mixture Class		1	2	3	4	5
Geometric Class						
Very Favorable	1	1	1	2	3	4
Favorable	2	1	2	3	4	5
Neutral	3	2	3	3	4	5
Unfavorable	4	3	4	4	5	5
Very Unfavorable	5	4	5	5	5	5

Table C-4

Classification of the Probability of DDT

Result Class 1.	DDT is highly likely.	P = .99
Result Class 2.	DDT is likely.	P = .90
Result Class 3.	DDT may occur.	P = .50
Result Class 4.	DDT is possible but unlikely.	P = .10
Result Class 5.	DDT is highly unlikely to impossible.	P = .01

FAI/91-54

PHENOMENOLOGICAL EVALUATION SUMMARY ON MOLTEN CORE-CONCRETE INTERACTION IN SUPPORT OF THE KEWAUNEE INDIVIDUAL PLANT EXAMINATION PROGRAM

Submitted To:

Wisconsin Public Service Corporation
Green Bay, Wisconsin

Prepared By:

Fauske & Associates, Inc.
16W070 West 83rd Street
Burr Ridge, Illinois 60521
(708) 323-8750

Final Issue

April 1993

ABSTRACT

Phenomenological issues on molten core-concrete interaction (MCCI) have been examined in support of the Kewaunee Individual Plant Examination (IPE) Program. The approaches taken were (1) to synthesize MCCI knowledge from experimental data, computer codes and analytical tools, and, (2) to develop a failure criterion to determine if such a postulated phenomena could challenge containment integrity at the Kewaunee Nuclear Power Plant.

For Kewaunee, basemat penetration due to molten corium-concrete interaction is a postulated containment failure mechanism. If molten core debris breaches the reactor vessel and contacts concrete surfaces, molten corium-concrete interaction can occur. During postulated severe accidents, water pools may be present in the containment at locations where core debris might collect. The steaming due to boil-off of this water plus contributions due to containment heating by the debris would over-pressurize the containment and induce containment failure prior to basemat penetration by MCCI given no containment heat removal system is available. If containment heat removal is available, the existing water pools can be recirculated (containment sprays) or refluxed (fan coolers) to cool the debris and prevent containment failure or delay it sufficiently that recovery or accident management actions could also be successful in establishing a safe stable state. For some sequences such as station blackout or transients with no injection, no containment sprays and no containment heat removal, the reactor cavity could become dry shortly after reactor failure. If the debris is not dispersed from the cavity at vessel failure in such cases, and no water sources are recovered, the containment basemat could undergo MCCI.

For Kewaunee, MCCI would most likely occur (if at all) in the cavity region of the containment. MCCI will erode concrete in both the sideward and downward directions, but a failure criterion is based on the downward direction because the downward erosion rate is much faster than the sideward erosion rate. The containment is considered failed when the depth of concrete erosion is equal to the combined depth of the cavity floor and the containment basemat.

To estimate the extent of concrete erosion with time, a technique suitable for hand-calculations is presented along with experimental and analytical results relevant to MCCI. This technique expresses conservation of mass and energy for MCCI and proceeds in a piecewise fashion to account for changes in core debris and chemical phenomena as a function of time. The technique is used to find the following: the time interval during which the zirconium in the debris pool is being oxidized, the depth of erosion during the zirconium oxidation phase, and the time to containment failure by MCCI. Inputs to the calculation technique stem from the analytical and experimental results presented herein. Appropriate physical properties required for MCCI calculations (densities, specific heats, etc.) are tabulated herein. Other parameters, most notably the sideward erosion rate to downward erosion rate ratio, are assigned values based upon the BETA and SWISS test series described here. The Kewaunee IPE-plant specific parameter file is used to provide values for the geometry of the cavity and the corium debris itself.

Calculations were performed with this technique for the "dry" case where the debris cannot be covered permanently by an overlying pool. This scenario is best illustrated by the large LOCA case. In the large LOCA, MCCI begins one hour after reactor vessel failure. These assumptions lead to a containment failure time due to MCCI of 97 hours after the initiating event for the dry case.

For the case with the debris covered, calculations were not performed because of the large body of experimental data which has demonstrated the ability of water to rapidly quench molten debris. Once the debris has been quenched, water can ingress into the debris bed to maintain it coolable, assuming the overlying pool is replenished. Also, MAAP runs show minimal concrete ablation in those accident sequences where the debris remains covered. In principle, calculations can be performed for the "wet" case in the same manner as for the dry case to, say, consider sensitivity studies of ingression. These calculations are not performed here since they would simply demonstrate large times to failure, i.e., hundreds of hours, for basemat failure by MCCI.

Based on these calculations, MCCI can be excluded as a containment failure mechanism, relative to other containment failure mechanisms. For the station blackout "dry" case, containment failure would occur due to over-pressurization before failure due to MCCI, as demonstrated by fundamental analyses as well as MAAP results. For the case where the debris is covered, MCCI would be halted by water ingression into the debris bed.

TABLE OF CONTENTS

	Page
ABSTRACT	i
1.0 PURPOSE	1-1
2.0 PHENOMENA	2-1
2.1 Description	2-1
2.1.1 Physical Processes	2-2
2.1.2 Relationship to Containment Failure Mechanisms and Modes	2-4
2.1.3 Relationship to Source Term	2-4
2.2 Experimental Results	2-5
2.2.1 SWISS: Sustained Heated Metallic Melt/ Concrete Interaction With Overlying Pool	2-6
2.2.2 BETA: Large Scale Metal/Oxide Interaction Experiments	2-6
2.2.3 SURC: Sustained-Urania Concrete Interaction Experiments	2-14
2.2.4 Summary of Experimental Results	2-18
2.3 Analytical Approaches	2-18
2.3.1 CORCON	2-18
2.3.2 WECHSL	2-22
2.3.3 DECOMP	2-23
2.3.4 VANESA	2-24
2.3.5 METOXA	2-24
3.0 METHOD	3-1
3.1 Step 1: Define Failure Criteria	3-2

TABLE OF CONTENTS
(Continued)

Page

3.2 Step 2: Determine Overall Time Interval to Exceed Most Limiting Failure Criterion. 3-3

4.0 APPLICATION OF THE METHOD TO THE KEWAUNEE NUCLEAR POWER PLANT 4-1

4.1 MCCI Failure Criterion (Step 1) 4-1

4.2 Time Interval to Exceed the Failure Criterion (Step 2). 4-4

4.3 Uncertainty Considerations. 4-8

5.0 CONCLUSIONS. 5-1

6.0 REFERENCES 6-1

APPENDIX A: Derivation of Concrete Erosion Calculations. A-1

APPENDIX B: Code Input and Calculations. B-1

APPENDIX C: MCCI Calculation Source Code C-1

LIST OF FIGURES

Figure No.		Page
2-1	The SWISS experimental apparatus	2-7
2-2	BETA experimental apparatus	2-8
2-3	Results of the BETA V1.8 experiment	2-12
2-4	Results from the BETA V2 experiments series	2-13
2-5	SURC-4 experimental apparatus	2-16
2-6	SURC-3 experimental apparatus	2-17
4-1	Reactor vessel supports in Kewaunee plant	4-2
4-2	Kewaunee reactor cavity compartment	4-3

LIST OF TABLES

Table No.		Page
2-1	BETA Experimental Matrix	2-10
2-2	SURC Test Matrix	2-15
2-3	Summary of Selected Core-Concrete Interaction Experiment Initial Conditions	2-19
2-4	Observed Eroded Concrete Depth and Mass	2-20
3-1	Molten Core-Concrete Interaction Calculation Data	3-4

1.0 PURPOSE

The potential failure of a containment building due to molten core debris attack on its concrete floor has been a subject of concern for the Nuclear Regulatory Commission (NRC) Staff since the Reactor Safety Study [NRC, 1975] identified it as the mechanism for two possible containment failure modes. One concern is that molten core debris ejected from a failed reactor vessel would come into contact with the containment floor and eventually erode a large enough volume of concrete, such that either the reactor cavity walls would lose their load-carrying capability or the basemat would be penetrated and core debris would exit the containment. Also, debris attack would generate steam and noncondensable gases that would contribute to the potential for containment failure by over-pressurization.

In [NRC, 1988], the NRC recommends that the extent of molten core-concrete interactions (MCCI) be assessed to determine its potential to cause containment failure. The objective of this paper is to develop a strategy for accounting for containment failure due to MCCI in the source term portion of the Kewaunee Nuclear Power Plant IPE. In this paper, only containment failure due to concrete ablation during MCCI is considered. Over-pressurization caused by noncondensable gases generated during MCCI is not considered here.

2.0 PHENOMENA

2.1 Description

Thermal attack of structural concrete in a containment building can occur during a core melt sequence if the molten core debris breaches the reactor vessel and contacts the concrete surfaces in the containment building. In a PWR plant, the concrete surface that experiences the most severe thermal attack typically is the cavity floor. The interfacial heat transfer between the core debris and concrete drives the thermal decomposition and erosion of the concrete. The thermal attack on the concrete can be broken up into three different phases: a short-term, localized attack as debris leaves the reactor pressure vessel; an aggressive attack by high-temperature debris immediately after the core material is released from the primary system; and a long-term attack in which the debris temperature would remain essentially constant and the rate of attack is determined by the internal heat generation.

Immediately after vessel failure, debris is discharged from the vessel into the reactor cavity. This material, which may be molten, induces an aggressive localized jet attack upon the concrete surface, given the absence of water in the cavity. A pool in the cavity could greatly mitigate this attack, depending upon its depth. The thermal attack is localized to the area below the failure. Estimates of this attack based on analyses in [IDCOR, 1985] show the depth to be 3.94 to 7.84 inches (10 to 20 centimeters), depending upon the primary system conditions at vessel failure.

After the jet attack, the reactor cavity floor region may be covered by high-temperature debris which aggressively attacks the concrete substrate. Free water, bound water, and gases generated by concrete decomposition are then released. The gases stir the melted material and promote convective heat transfer between this material and the concrete. The combination of the sensible heat added to the concrete, the endothermic chemical reactions involved in releasing water vapor and decomposing the concrete, and the

latent heat of fusion for melting the substrate extracts a considerable amount of energy from the high-temperature melted material. In fact, the aggressive attack generally requires more energy than is generated by the decay power. Such additional internal heat generation can result from the oxidation of metallic constituents within the melted material by the steam and possibly by carbon dioxide released from the concrete substrate. Typically, the high-temperature, aggressive attack is driven by internal heat generation and secondly, to a lesser extent, by the initial stored energy.

During the long-term attack, the debris remains at an essentially constant temperature, and the rate of attack is determined by the difference between the internal heat generation and the heat losses to the containment environment. Without water, these heat losses are principally due to convection and radiation, and are somewhat influenced by the natural convection of high-temperature gases throughout the containment. The resulting concrete attack rate is much reduced from that typical of the high-temperature attack phase and occurs over a much longer interval. The noncondensable gases generated during this period contribute to long-term overpressurization of the containment.

2.1.1 Controlling Physical Processes

The major physical phenomena affecting the extent of concrete erosion by core debris are closely interrelated and therefore difficult to separate. For the purpose of this discussion, these phenomena are identified as follows: rate and amount of core debris expulsion from the reactor vessel; melt-water dynamic interaction and melt spreading; configuration of the debris mass on the concrete; depth of the melt bed; and the quenching effect of water. The following are brief discussions of how the controlling phenomena influence this issue.

The core debris flow rate from a failure in the bottom of the reactor vessel determines the initial velocity with which the melt spreads. As the initial spreading rate decreases, there is an increase in the time for heat transfer from the melt to the concrete floor and, if present, an overlying

water pool. Thus, the initial spreading rate and and the energy losses from the melt influence the extent of initial melt spreading.

The initial extent of melt spreading is also very dependent on the effects of the water/debris dynamic interaction on the heat transfer from the molten debris. If the interactions between the melt and water cause the debris to disperse, or cause violent oscillations at the melt-water interface, these interactions might lead to heat transfer rates far in excess of heat transfer rates associated with critical heat flux boiling. If not, the melt-water interface would undergo film boiling rather than nucleate boiling.

After the molten debris has initially spread out, two types of debris configurations are possible: a discontinuous porous debris bed composed of discrete particles; or a continuous slab of partially molten pool. The debris bed configuration has been shown to occur when sufficient water is available to quench the debris as it leaves the reactor vessel. Otherwise, a continuous slab configuration typically occurs because there is less water available than would be necessary to ensure debris fragmentation. It is possible that a debris bed can evolve into a continuous debris slab. If the porosity in the bed limits the bed dryout heat flux below decay power heat removal requirements, the debris bed would heat up and eventually melt into a continuous debris configuration. The debris configuration strongly affects the quenching capability of overlying water.

The depth of the debris also affects how effectively energy is removed from the debris. If it is postulated that the initial debris layer is so thick that the rate of heat removal from the debris is exceeded by the internal heat generation rate, then the debris would reheat and ultimately remelt. Further spreading of molten or partially molten debris would then occur, aided by gas agitation from concrete erosion if the concrete were sufficiently heated. The debris would spread until the heat removal rate was sufficient to freeze it, or was constrained by the cavity. In [NRC, 1988], the NRC has stated that a debris layer less than 9.84 in (25 cm) in depth may be considered to be coolable.

The last phenomena to discuss is the quenching effect of water. For a debris bed, the physical mechanism of cooling is water ingression into the bed with outflow of steam from the bed. The coolability limit for debris beds is a hydrodynamic limitation within the bed itself that strongly depends on the porosity, and is fairly independent of the debris bed depth. For a thin debris slab or shallow pool, conduction is an effective heat transfer mechanism and the slab can cool quickly with little or no cracking. However, for a thicker slab or deeper pool, coolability requires cracking of the slab or overlying crust and ingression of water into the debris. Such cracking would be expected to occur as a result of the volume reduction associated with debris cooling and phase change, as well as sparging of offgases produced by any thermal attack of concrete.

2.1.2 Relationship to Containment Failure Mechanisms and Modes

Extensive erosion of concrete by high-temperature core debris is a potential late containment failure mechanism that would be expected to occur many hours after reactor vessel failure and debris release into the containment. Two actual failure mechanisms are considered possible as a result of concrete erosion: penetration of the containment basemat; and sufficient deterioration of the load-carrying capability of the cavity walls that the reactor vessel moves and causes gross mechanical failures of penetrations for piping connected to the reactor vessel. Both of these containment failure mechanisms would be expected to result in large containment failure areas (on the order of several square feet).

2.1.3 Relationship to Source Term

Long-term molten core-concrete attack leading to containment failure influences the expected fission product release for a sequence by providing a large gas and/or corium flow path out of the containment long after vessel failure. The effect on the source term, however, depends on the presence of water in the cavity during a sequence prior to containment failure. For a dry sequence, since the airborne fission product concentration in a closed containment tends to decay with time due to naturally-occurring fission product retention mechanisms, a late containment failure due to MCCI

generally results in modest source terms, relative to early failures. For gross mechanical failures of penetrations for piping, however, the relatively large expected failure size assures a rapid blowdown of the initially available airborne fission products to the environment. Fission products entering the containment atmosphere after the blowdown would experience little driving force from the containment. Thus, fission products evolved by long-term revaporization within the reactor vessel would be subject to the naturally-occurring deposition mechanisms in the containment. Fission products released ex-vessel during MCCI would also be subject to the same deposition mechanisms.

Basemat penetration by MCCI is a late containment failure mode that leads to a large failure area. A rapid blowdown is not assured because the soil underneath the basemat provides an obstructed release path. This also results in very different offsite consequences, relative to other containment failure modes, because the release is to underlying soil rather than the atmosphere. Soil provides a very effective fission product scrubbing mechanism, but a basemat failure can potentially contaminate the local water table.

For a wet sequence, the expected fission product source term would be reduced relative to a dry sequence due to the capture of fission product aerosols by the overlying pool and/or containment spray droplets.

2.2 Experimental Results

A wide variety of molten debris-concrete interaction experiments have been performed at Sandia National Laboratory (SNL) and Kernforschungszentrum Karlsruhe (KfK). In general, these experiments were undertaken to validate models and understanding of MCCI phenomenon. The SNL experiments considered either initially metallic or oxidic melts. Metallic experiments at SNL were usually performed with a stainless steel melt charge, while oxidic experiments were performed with a uranium dioxide and zirconium dioxide melt charge. Two SNL tests have employed both oxides and zirconium metal. The KfK BETA series of experiments featured stainless steel and concrete oxide melt charges.

2.2.1 SWISS: Sustained Heated Metallic Melt/Concrete Interaction with Overlying Pool

A schematic representation of the SWISS experimental apparatus is shown in Figure 2-1. The SWISS experiments performed at SNL consisted of two test runs designed to observe the effect of an overlying pool on MCCI. The SWISS-1 test involved 99.2 lb (45 kg) of stainless steel initially at 3005.6 F (1925 K) inductively heated over a period of about 40 minutes with one power interruption [Blose, 1987]. An average of about 0.205 x 10^6 Btu/h (60 kW) net power was input to the melt charge by the induction source. About 32 minutes after the melt was teemed into the crucible, water was poured over the melt. Erosion was essentially one-dimensional, downward into a 8.5 in (21.6 cm) diameter limestone-common sand concrete plug, because a non-ablating MgO sidewall was used. A value of 95099 Btu/h-ft^2 (300,000 W/m^2) was suggested as an average sideward heat flux lost to the MgO crucible walls. The concrete was a limestone-common sand variety essentially identical to a default type used in the CORCON code [Muir, 1981] and typical of many U.S. plants.

Test SWISS-2 was similar to test SWISS-1 except that water was continuously poured onto the debris immediately after the melt teem, and two power interruptions occurred. A value of 63400 Btu/h-ft^2 (200,000 W/m^2) heat flux to the MgO sidewall was suggested on the sideward heat losses.

2.2.2 BETA: Large Scale Metal/Oxide Interaction Experiments

The BETA test series consisted of a series of large-scale metallic melt experiments conducted at KfK research center [Alsmeyer, 1986]. These experiments were originally conceived and designed to provide reliable experimental data for verification of severe accident programs, such as the WECHSL code [Reimann, 1981].

The BETA tests typically consisted of large, high-temperature metallic melts, initially at 3632°F (2000°C) or higher, produced by thermite reaction. These melts were usually poured into an instrumented siliceous concrete crucible of 15 in (0.38-m) inside diameter (see Figure 2-2). The

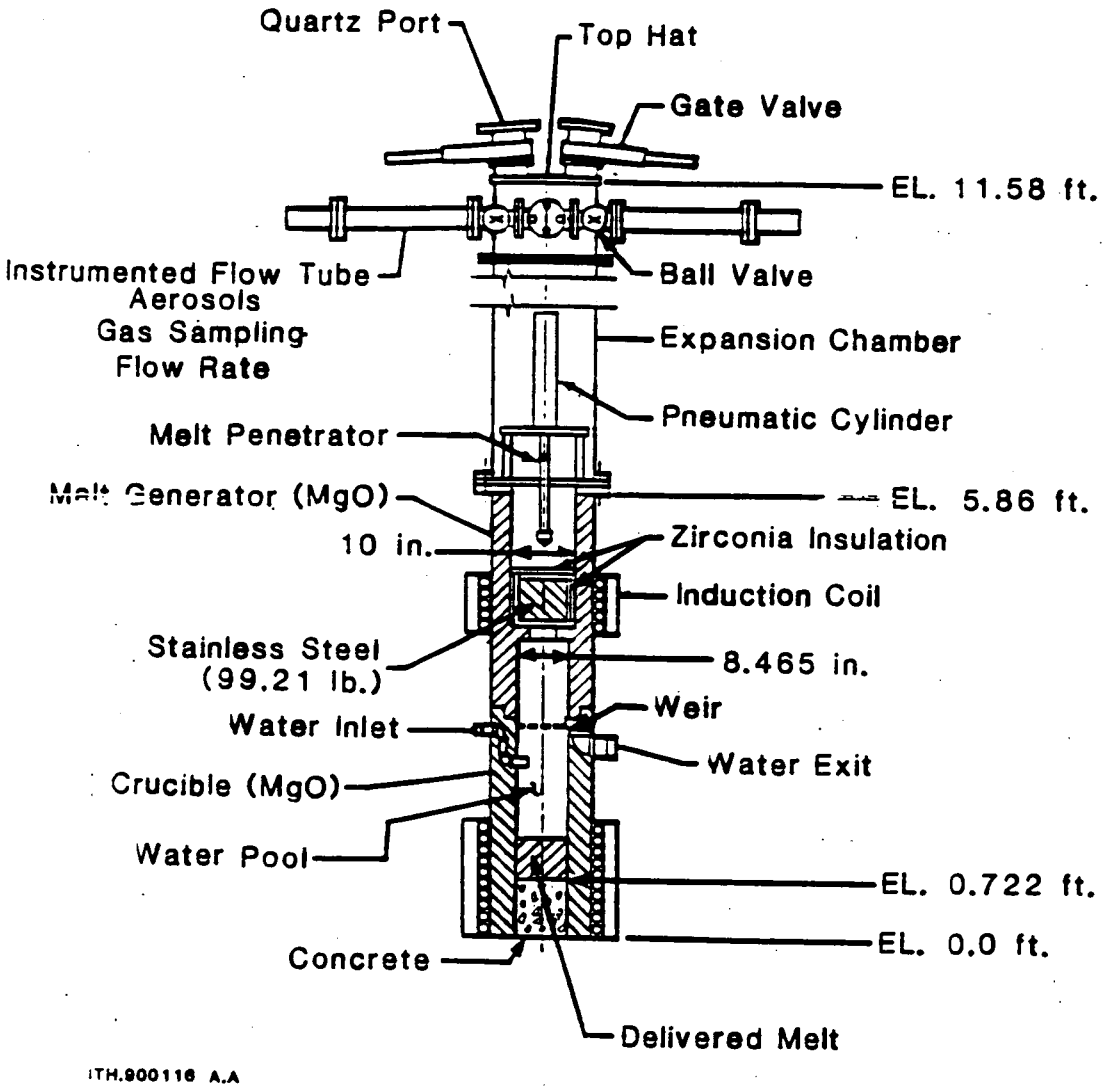

Figure 2-1 The SWISS experimental apparatus.

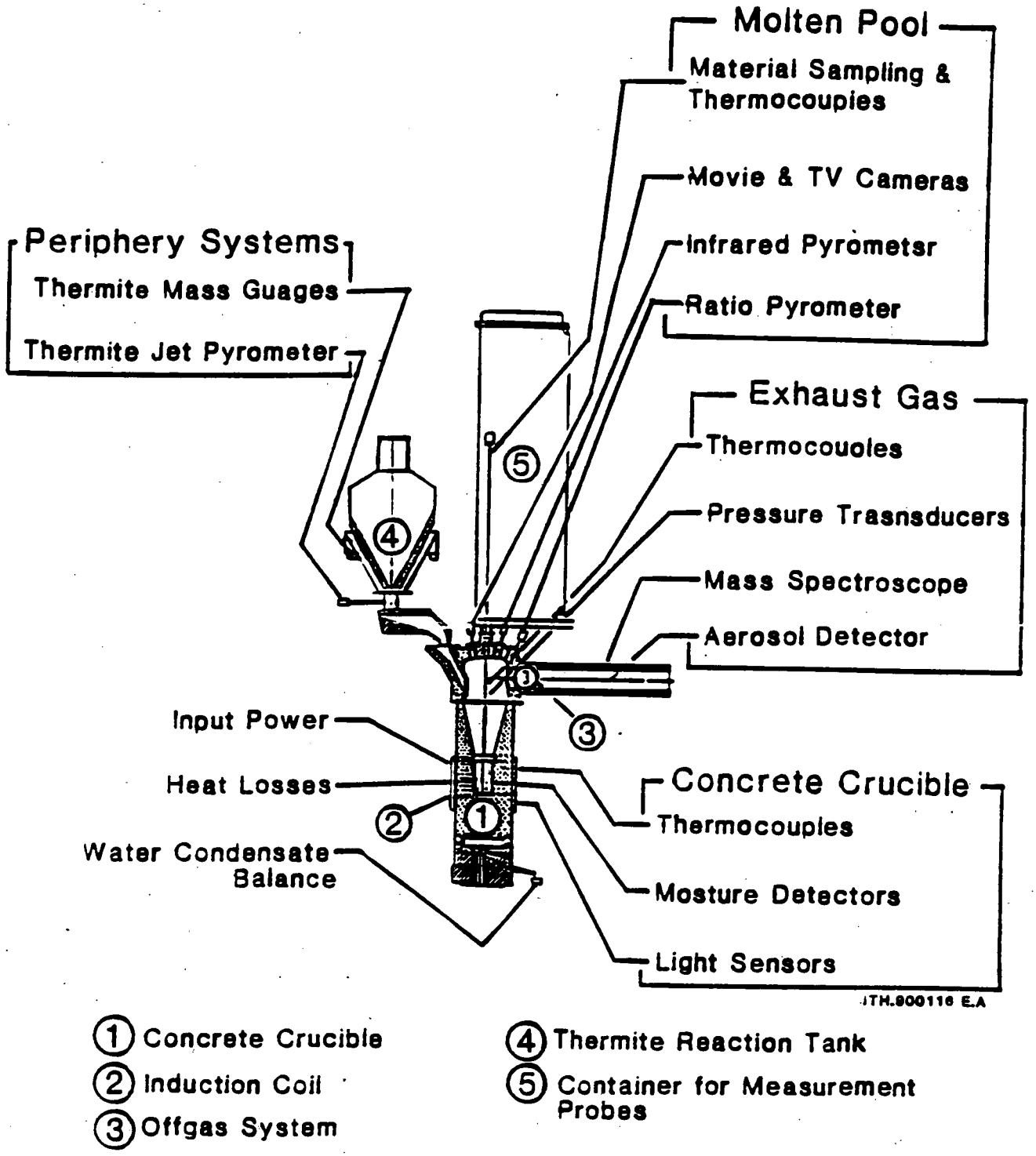

Figure 2-2 BETA experimental apparatus.

interactions were sustained by inductive heating. The BETA experimental facility has the capability to supply up to 6.48 x 10^6 Btu/h (1.9 MW) of inductive heating power, which allowed observations of the various physical and chemical processes occurring during molten melt-concrete interactions for an extended period of time under quasi-steady state conditions. Typical melt charges in the BETA tests were composed of 661.4 lbm (300 kg) of steel and 330.7 lbm (150 kg) of oxides. The steel components typically included Fe, Cr, and Ni. The oxides used were aluminum oxide (Al_2O_3), silicon oxide (SiO_2), and in some cases calcium oxide (CaO). Table 2-1 summarizes the BETA experiments conducted over the span of two years, from 1984 to 1986. The composition of the silicate concrete utilized in the experiments is somewhat similar to the basaltic concrete variety used in the United States. BETA V3 series was an exception as it employed limestone-common sand concrete. No fission product simulants were employed in any BETA tests.

Major results of BETA tests are [Alsmeyer, 1987]):

1. The temperature of the melt pool dropped rapidly from an initial temperature close to 3320.6 F (2100 K) to a temperature slightly above the mixture melting temperature, even when the inductive heating power was very high.

2. The experiments are characterized by the dominance of downward erosion in high power tests, and to a lesser extent in low power tests.

3. Dispersion or entrainment of the metal layer into an overlying oxide layer was observed in the high power tests. It appears that the process of dispersion is driven by the high gas fluxes evolving from the concrete.

4. When CaO was added to the melt pool, no entrainment of metal into the oxide layer was observed. Apparently, CaO serves to lower the viscosity of the oxide layer, and thus, the metal-oxide layers remained stratified. It is noted that all low power experiments resulted in separated metal and oxide layers.

Table 2-1

BETA EXPERIMENTAL MATRIX

Text	Melt	Power/(Btu/hr)	Power/kW	Remarks
V0.1	Iron	0	0	Test of Facility
V0.2	Iron	1.36	400	
V0.3	Iron + Oxide	5.80	~1700	
V1.1	Iron	Pulsed	Pulsed	Pour failed
V1.2	Iron + Oxide	Pulsed	Pulsed	Lorentz-force excluded
V1.3	Steel + Oxide	3.41	1000	
V1.4	Steel	0	0	Transient
V1.5	Steel	1.54	450	
V1.6	Steel + Oxide	3.41	1000	
V1.7	Steel + Oxide	5.80	1700	
V1.8	Steel + Oxide	6.48	1900	No dispersion (CaO)
V1.9	Steel + Oxide	1.36-0.68	400-200	CaO added
V2.1	Steel + Oxide	0.41-0.51	120-150	
V2.2	Steel + Oxide	0.17-0.31	50-90	CaO added
V2.3	Steel + Oxide	0.82	240	CaO added
V3.1	Steel + Oxide	5.80-8.53	1700-2500	US Lime/Comm Sand, Heating from 0-66 s only
V3.2	Steel + Oxide	1.36->3.41	400->1000	US Limestone, 30 min heating
V3.3	Steel + Oxide	2.05-0.68	600-200	US Lime/Comm Sand, 60 min heating
V4.1	Steel + Oxide	3.41-1.02	1000-300	19.685 ft dia crucible

In the BETA V1.8 experiment, 6.48 x 10^6 Btu/h (1900 kW), the highest net inductive heating power of the series was used, corresponding to an internal power density more than a factor of ten higher than that of decay power. A melt charge composed of 771.6 lbm (350 kg) of steel (82% Fe, 10% Cr, 8% Ni) and 286.6 lbm (130 kg) of oxides (70% Al_2O_3, 30% CaO), produced by a thermite reaction, was poured into the interaction cavity at an initial temperature of 3266.6 F (2070 K). The observed downward erosion rate was approximately 0.04 in/s (1 mm/s), resulting in a total eroded depth of about 15.75 in (40 cm) in 7 minutes. Sideward erosion was stated as only a few centimeters (see Figure 2-3).

Experimental results showed that the chromium metal had oxidized completely in about one minute, and hand calculations indicate that gas evolving only from the concrete floor was insufficient for complete oxidation of the chromium. Thus, gases released from decomposition of the sidewall must have entered the debris pool and contributed to chromium oxidation.

The oxide layer was observed to be clearly separated from the metal layer and well mixed with concrete slag, thus entrainment of metal into the oxide layer was not observed. In a similar high-powered (~ 5.8 x 10^6 Btu/h) test V1.7 in which no CaO was added, complete entrainment of metal into the oxide resulted.

The BETA V2 series are low power experiments designed to investigate crust formation and its influence on the melt-concrete interaction. The V2.1 test consisted of the melt charge composed of 661.4 lb (300 kg) steel (90% Fe, 10% Ni) and 330.7 lb (130 kg) oxides (70% Al_2O_3 30% SiO_2) initially at 3632°F (2000°C). The melt pool was sustained at an induced power of approximately 4.09 x 10^5 to 5.12 x 10^5 Btu/h (120 to 150 kW) for more than 100 minutes. This power level is representative of long-term decay power. A total of about 13.78 in (0.35 m) downward and 3.94 in (0.10 m) sideward erosion was observed, with an average 0.0024 in/s (0.06 mm/s) downward erosion rate (see Figure 2-4). In the experiment, sideward erosion stopped at about 1000 seconds after a depth of 3.94 in (10 cm) was attained.

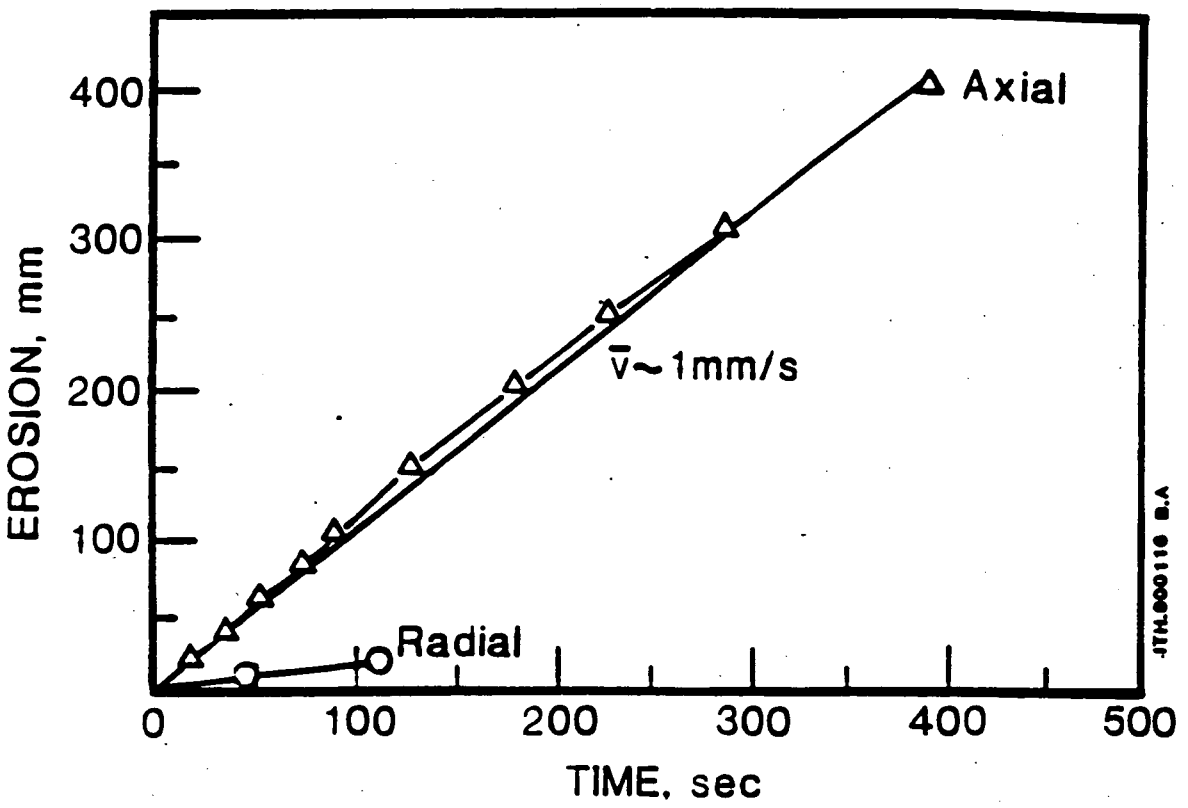

Figure 2-3 Results of the BETA V1.8 experiment.

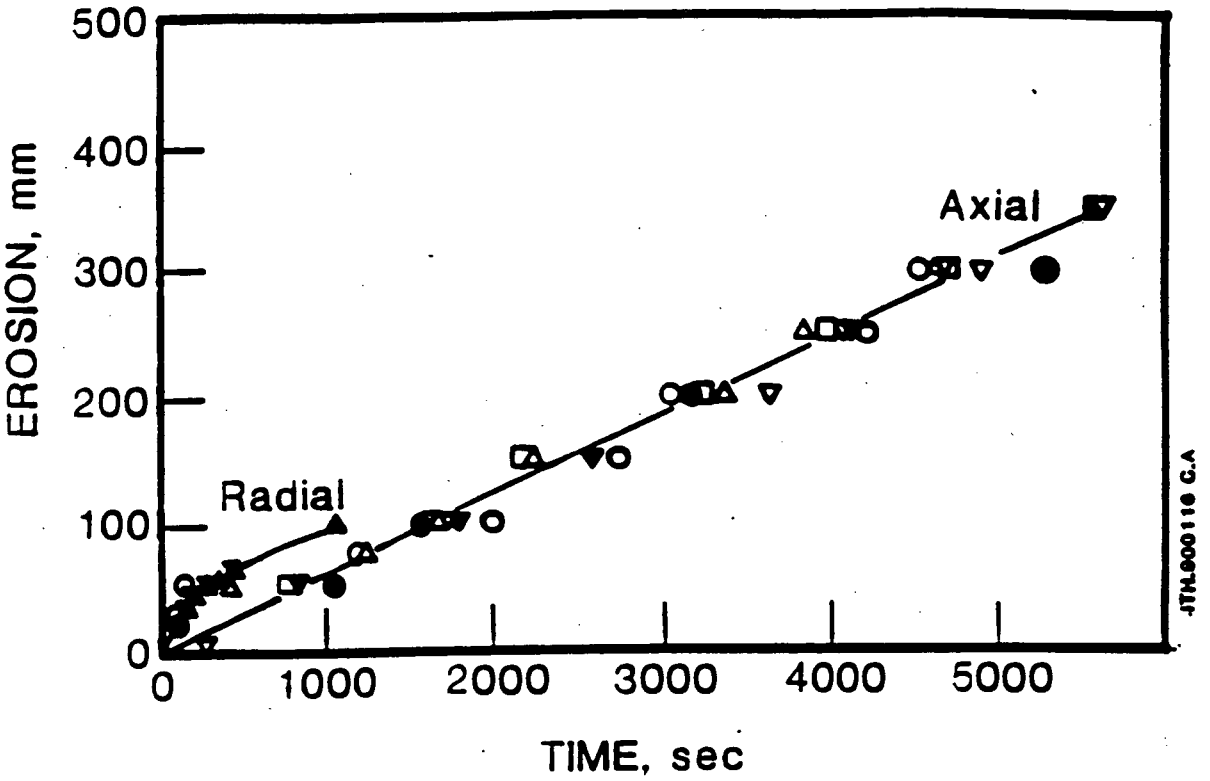

Figure 2-4 Results from the BETA V2 experiments series.

2.2.3 SURC: Sustained-Urania Concrete Interaction Experiments

Sandia National Laboratories is conducting an ongoing series of Sustained Urania-Concrete (SURC) tests. Table 2-2 identifies the SURC experiment matrix, and at the time of this writing, experiments SURC-3, SURC-3A, and SURC-4 are complete.

The interaction crucible for the SURC-4 experiment [CSNI, 1989] consisted of an MgO annulus of 15.75 in (40-cm) inside diameter with a basaltic concrete plug at its base. A schematic of the SURC-4 experimental apparatus is illustrated in Figure 2-5. The test charge for SURC-4 consisted of 440.9 lb (200 kg) SS-304 (approximately 73% Fe, 19% Cr, 8% Ni) inductively heated in the interaction crucible to approximately 2690.6 F (1750 K) prior to the onset of erosion. Fission product simulants were employed to simulate fission product release, consisting of 1.1 lb (0.5 kg) Te, 2.58 lb (1.17 kg) of La_2O_3, 2.71 lb (1.23 kg) CeO_2, and 2.43 lb (1.1 kg) BaO.

A net 2.05×10^5 Btu/h (60 kW) inductive heating power was applied to the test charge for the duration of the test and a value of 31700 Btu/h-ft^3 (100,000 W/m^2) was suggested as representative of the heat loss through the MgO wall. Because of the relatively inert nature of the MgO annulus sidewall to the molten debris, only one-dimensional downward erosion was possible. After quasi-steady concrete erosion was initiated, 44.1 lb (20 kg) of zirconium were instantaneously added to the molten debris to observe the effect of oxidation. Observed erosion was between 9.65 in to 10.83 in (24.5 to 27.5 cm) of concrete.

The melt charge for SURC-3 [Bradley, 1987], composed of 110.2 lb (50 kg) of SS-304 (73% Fe, 19% Cr, 8% Ni), was inductively heated to approximately 3050.6 F (1950 K) prior to being teemed into the interaction crucible. The interaction crucible consisted of an MgO annulus of 7.87 in (20-cm) inside diameter and a limestone-common sand concrete plug base. A schematic of the SURC-3 experiment apparatus is shown in Figure 2-6. A net 1.024×10^5 Btu/h (30 kW) inductive heating power was applied to the melt charge for the duration of the experiment. A value of 31700 Btu/h-ft^2 (100,000 W/m^2) was suggested as representative of heat loss through the MgO

Table 2-2

SURC TEST MATRIX

Test	Melt Charge	Mass (lb)	Mass (kg)	Concrete	Water
1	UO_2-ZRO_2-ZR	551	250	LIMESTONE	NO
2	UO_2-ZRO_2-ZR	551	250	BASALTIC	NO
		COMPLETED			
3	STEEL-ZR	110.2	50	LIMESTONE	NO
3A	STEEL-ZR	110.2	50	LIMESTONE	NO
4	STEEL-ZR	441	200	BASALTIC	NO
5	UO_2-ZRO_2-ZR	551	250	LIMESTONE	YES
6	UO_2-ZRO_2-ZR	551	250	BASALTIC	YES
7	STEEL-B_4C	441	200	LIMESTONE	NO
8	STEEL-B_4C	441	200	BASALTIC	NO

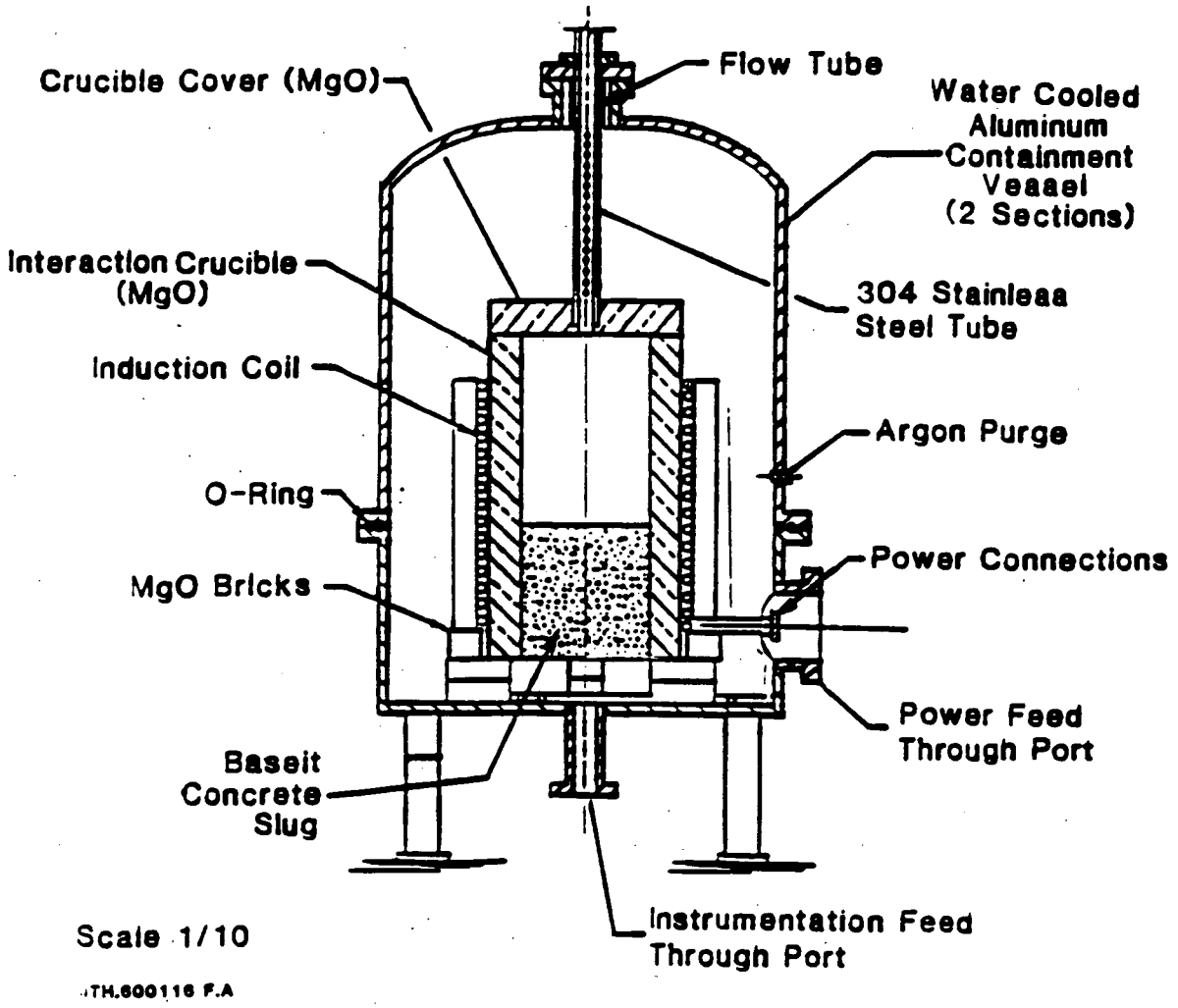

Figure 2-5 SURC-4 experimental apparatus.

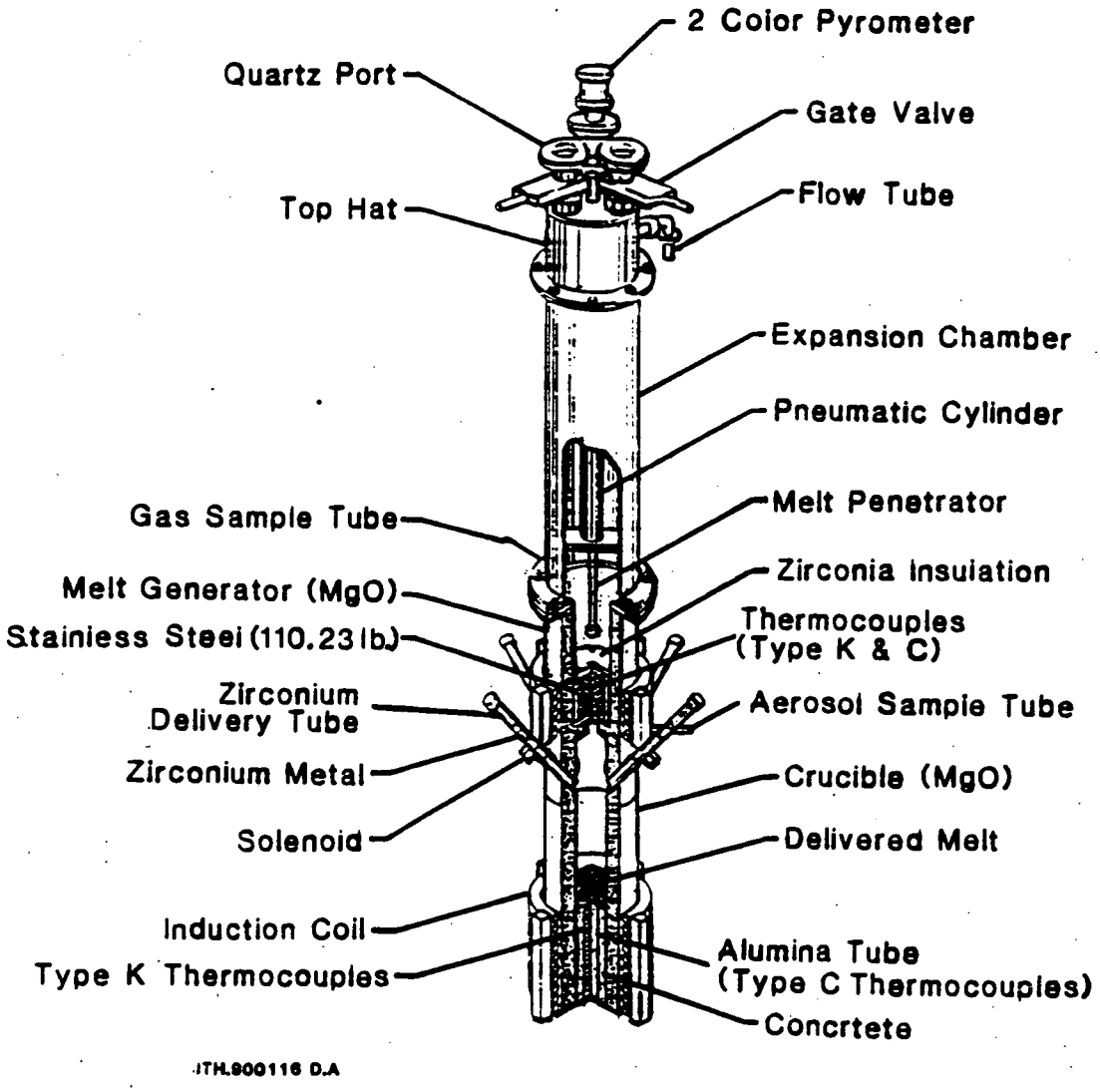

Figure 2-6 SURC-3 experimental apparatus.

wall. Because of the relatively inert nature of the MgO annulus sidewall to the molten debris, only one-dimensional erosion was possible. After quasi-steady concrete erosion was initiated, 3.09 lb (1.4 kg) of zirconium were instantaneously added to the molten debris. Observed erosion was about 13.8 in (35 cm) of concrete.

2.2.4 Summary of Experimental Results

In summary, we can compile the results from several experiments with different scales, different debris material masses and composition, and different power levels to develop a basis on which to provide a method for assessing MCCI and potential failure times (see Tables 2-3 and 2-4). These data have been used to benchmark the core-concrete interactions models used here and in the MAAP code (DECOMP) [EPRI, 1990; Fauske & Associates, Inc., 1990]. These data also provide a basis for estimating the fraction of the debris' downward heat flux to be 0.5 and for estimating the ratio of sideward to downward erosion to be 0.2.

2.3 Analytical Approaches

Results of numerous predictions for the experiments described above have been reported in the literature. However, rather than discuss the results of all of these calculations, the principal computer codes used to obtain the results will be discussed. The principal computer codes used for thermal-hydraulic calculations related to core-concrete interactions are CORCON, WECHSL, and DECOMP; the principal computer codes used for aerosol release calculations related to core-concrete interactions are VANESA and METOXA.

2.3.1 CORCON

Sandia National Laboratory's CORCON [Muir, 1981] is incorporated in the NRC's MELCOR code [Summers, 1990] and the Source Term Code Package (STCP) [Gieseke, 1986]. CORCON models the two-dimensional attack of concrete by core debris during severe accidents in light water reactors. It assumes an immediate separation of the molten core into immiscible layers; namely, a

Table 2-3

SUMMARY OF SELECTED CORE-CONCRETE
INTERACTION EXPERIMENT INITIAL CONDITIONS

Test	Diameter (m/in)	Debris Height[a] (m/in)	Metal Mas (Kg/lb)	Oxide Mass (Kg/lb)	Temperature[b] (K/F)	Input Power (kW/Btu-h)
SWISS-1	0.216/8.5	0.16/6.3	45/99.2	-/-	1925/3005.6	55/187660
SWISS-2	0.216/8.5	0.16/6.3	44/97	-/-	1925/3005.6	60/204720
SURC-1	0.216/8.5	0.18/7.09	50/110.2	-/-	1970/3086.6	30/102360
SURC-4	0.40/15.75	0.20/7.87	200/440.9	-/-	1746/2683.4	60/204720
BETA V1.8	0.38/15.0	0.78/30.7	350/771.6	130/286.6	1970/3086.6	1900/6482800
BETA V2.1	0.38/15.0	0.72/28.3	300/661.4	130/286.6	2173/3452	120/409440

[a]Approximate initial collapsed height.

[b]Either at melt time or at start of erosion.

Table 2-4

OBSERVED ERODED CONCRETE DEPTH AND MASS

Experiment	Eroded Concrete Depth in (cm)	Eroded Concrete Mass lbm (kg)
SWISS-1	6.7 (17)	31.5 (14.3)
SWISS-2	6.7 (17)	31.5 (14.3)
BETA V1.8		
side	0.78 (2)	229.5 (104.3)[b]
down	16 (40)	942.9 (428.6)[c]
BETA V2.1		
side	3.9 (10)	200.9 (92.3)
down	14 (35)	2223 (1010.4)
SURC-4	10 (26)	165 (75.1)
SURC-3	14 (35)	55.7 (25.3)

[a]Mass derived from concrete density (ρ = 2260 kg/m^3) multiplied by estimated volume of concrete eroded.

[b]Low estimate based on 1-D eroded depth only.

[c]High estimated based on 2-D eroded depth and with assuming cylindrical shape of molten corium.

metallic and an oxidic layer. As the MCCI proceeds, the decomposed concrete forms a second oxide layer. The orientation of layers depends on their relative density. During the early stage of concrete attack, a configuration of heavy oxide-metal-light oxide is possible. As the MCCI proceeds, the heavy oxide layer is diluted by the molten concrete (slag) and eventually reaches a point where the density of the heavy oxide layer is less than that of the metallic. At this time, the heavy oxidic and metallic layers are assumed to flip instantaneously, and the heavy oxidic layer combines with the light oxidic layer. CORCON also assumes a gas film exists at the molten core/concrete interface. Heat transfer from the molten core pool to concrete is governed by the convective and radiative processes across the film. In CORCON, the concrete ablation is calculated based on steady-state one-dimensional energy balance at the molten core/concrete interface. The decomposition heat of concrete is calculated based on the user specified concrete decomposition temperature. Transient heat conduction into the concrete is not modeled.

CORCON also assumes that, upon solidification, crusts will form at one or more interfaces with the interior of the layer remaining liquid. If part or all of a layer becomes frozen, energy can only be transferred by heat conduction through crusts, which is ordinarily far less effective than convection. Because of internal heating of debris and the fact that cooling cannot continue unless heat losses exceed sources, freezing is largely self-limiting. A simple quasi-steady-state crust formation model was included in the CORCON code to calculate the thickness of the crust and the rate of heat transfer from the partially solidified core debris to concrete. In order to model the crust formation process, some assumptions were made in CORCON to calculate the liquidus and solidus temperatures of the metallic and oxidic mixtures. For the metallic mixture, a simple fit to the iron-chromium-nickel ternary phase diagram was used. The presence of metals other than Fe, Cr and Ni was ignored. CORCON treats the oxidic mixture as a pseudo-binary system in which the fuel oxides (UO_2 + ZrO_2) form one "component" and concrete and steel oxides form the other; the two components are assumed to form an ideal solution in both the liquid and solid phases.

In CORCON, the oxidation reactions between the metallic constituents and the concrete decomposition gases are assumed to proceed to equilibrium concentrations defined by minimization of the Gibbs free energy for 38 chemical species composed of 11 elements. Carbon is among the 38 species considered in the chemical reactions calculation of CORCON and therefore, the coking reactions are modeled by CORCON.

2.3.2 WECHSL

WECHSL, KfK's stand-alone code [Riemann, 1981], models the two-dimensional concrete attack of the core debris during severe accidents in light water reactors. It assumes the existence of an underlying metallic layer covered by an oxidic layer of fuel, metal oxides, and/or the concrete decomposition products. Heat transfer from melt to concrete is modeled in analogy to boiling phenomena. A film model, discrete bubble model, or transition boiling model for heat transfer are used according to the existing gas flow and inclination of the interface.

When freezing processes become important due to cool-down of the melt, crust formation is modeled starting from the melt/concrete interface and possibly resulting in a fully frozen layer. Crusts are assumed to be permeable to the gases. Transient heat conduction into the concrete is not considered in the WECHSL code. The solidus and liquidus temperatures of the metallic mixture in the WECHSL code are calculated by a simple fit to a chromium-nickel-iron ternary phase diagram. The same set of equations is used in the CORCON and WECHSL codes to predict solidus and liquidus temperatures of the metallic mixture. In WECHSL, the liquidus and solidus temperatures of the oxidic mixture are determined either by a "binary" phase diagram or by a user input table.

In WECHSL, the gases released from the decomposing concrete may oxidize the constituents of the metal layer. The metal oxidation reactions take place in the order Zr, Cr, and then Fe. This means that no Cr-oxidation is considered as long as Zr is present in the melt, etc. The rate of oxidation

for Cr and Zr is limited by the gas supplied from the concrete. A temperature dependent equilibrium constant is used to determine the oxidation rate of Fe.

2.3.3 DECOMP

DECOMP is a subroutine from the MAAP code [EPRI, 1990]. It considers the debris to be either a solid cylinder or a molten pool surrounded by a crust, depending upon its energy. Crust growth/shrinkage based on energy balance describes the solidification process occurring within the molten debris, and temperatures are determined from phase diagrams based on the composition of the debris. Transient conduction calculations are carried out in the concrete floor, sidewall in contact with debris, and upper wall (surroundings), and concrete ablation is allowed in all heat slabs. For the case that the debris is partially molten, the heat transfer coefficient at the molten pool/crust interface is a user-defined constant.

The liquidus and solidus temperatures of the metallic phase of the mixture are determined as follows:

(i) The CORCON fit to the iron-chromium-nickel ternary phase diagram is used to determine the liquidus and solidus of the steel mixture containing Fe, Cr and Ni.

(ii) The Fe-Zr binary phase diagram with Fe replaced by stainless steel is used to obtain the liquid and solidus temperatures of Zr-steel mixture.

In DECOMP the treatment of liquidus and solidus temperatures of the oxidic phase is similar to the CORCON treatment of oxides.

The chemical reaction model of DECOMP considers chemical equilibrium by a Gibbs free energy minimization technique. Chemical equilibrium is calculated in METOXA, another subroutine from the MAAP code, by solving the algebraic relations for mass action and element balances. An ideal solution model is used with three phases: liquid metal, liquid oxides and gases.

Non-ideality is allowed for some compounds through user-input activity coefficients. A Newton-Raphson technique is employed with a reduced set of algebraic relations, known as basis equations. The equations are solved to yield the molar abundances of particular species important to a stable, efficient solution. Reactions and element balances for the basis set are given in [EPRI, 1990].

2.3.4 VANESA

The VANESA code calculates the release of fission products and structural material during MCCI. VANESA models the vaporization of melt species into gases which are produced from concrete decomposition. The thermochemistry and kinetics of this process are modeled mechanistically. As the gases exit the melt, aerosol formation from bubbles breaking the melt surface and from the condensation/nucleation of vapors is modeled empirically.

The corium is modeled as a layered two-phase system: an oxidic layer above a dense metallic layer which is in contact with the concrete basemat. The reaction of CO_2 and H_2O with the major metallic constituents are evaluated to determine the equilibrium oxygen potential. This oxygen potential is assumed to hold for the oxide phase and is used to calculate the equilibrium vapor pressures of species in the M-O-H ternary phase diagram where M is the element of interest. The chemical species considered in the VANESA code are given in [Lee, 1985]. A kinetic analysis, which considers condensed phase transport, transport across the gas/melt interface and gas phase transport, is then performed to estimate the amount of material transferred from the melt to gas bubbles.

2.3.5 METOXA

The fission product chemistry of METOXA, a MAAP subroutine, is described above in Section 2.3.3. In METOXA, aerosol generation occurs only through chemical reactions. Mechanical aerosol generation is not modeled.

These codes are all capable of producing MCCI simulations that agree with experiments given they are used by people experienced in the respective code. In particular, the heat balance on the debris that apportions the distribution upward, sideward, and downward is a key modeling consideration and must be properly described via the code model inputs and boundary conditions. This was demonstrated in an international standard problem that employed the SURC-4 data [CSNI, 1989]. The predicted erosion depths for the various codes were shown to be in good agreement with the experimental results.

3.0 METHOD

The aggressive attack on concrete by molten core debris may lead to a late containment failure if actions are not taken to cover the debris with water and thereby arrest the attack. Even with the appropriate response, deep core debris beds may not be coolable. In [NRC, 1988], the NRC states that experimental evidence exists that suggests core debris beds with depths greater than 9.84 in (25 cm) may not be coolable.

A simple, stand-alone calculation procedure is included in the method to estimate containment failure time due to MCCI. Although MAAP, or a comparable integral code, should be used to address all aspects of MCCI for a sequence (including non-condensable gas generation, ex-vessel fission product release, etc.), the method provided here can be used to estimate containment failure time due to concrete erosion for basic sequence. The procedure outlined here has three advantages: (1) it obviates lengthy MAAP runs, (2) it provides a convenient means of investigating ablation phenomena, and (3) it is scrutable to independent reviewers.

In the event the debris is not coolable, the calculation method to be used to determine the possibility of containment failures caused by molten core-concrete interaction is based on the following simplifying assumptions:

- Erosion of the upper portion of the cavity wall by radiative heat transfer is negligible compared to the direct attack of the core debris.
- Erosion proceeds equally at all locations covered by debris.
- Zirconium is the only important source of chemical energy in the core debris.
- The ratio of the rates of advance of sideward and downward concrete attack is constant.

The evaluation method consists of the following steps:

Step 1: Define failure criteria for basemat and reactor cavity walls.

Step 2: Determine the time required for the concrete attack by core debris released from reactor vessel to exceed the most limiting failure criterion identified in Step 1.

Step 3: Based on extent of concrete attack, select the appropriate treatment of containment failure caused by molten core concrete interaction.

3.1 Step 1: Define Failure Criteria

Core debris-concrete interaction is hypothesized to be able to cause containment failure either by penetrating the cavity floor, liner, and basemat or, by weakening the reactor vessel supports sufficiently such that the reactor vessel and attached piping move and tear out associated penetrations through the containment. For the latter failure type, the failure criterion must account for the weakening of the cavity wall as this wall's thickness decreases due to erosion, as well as the associated weakening of the wall due to the dehydration of the concrete that occurs ahead of the erosion front. The criterion for failure of the cavity wall may be stated functionally as follows:

$$x_{e,s} \geq \left(1 - f_1\right) x_p \qquad (3\text{-}1)$$

where:

$x_{e,s}$ = total concrete erosion in the sideward direction, ft,

x_p = width of the cavity wall, ft,

f_1 = minimum fraction of cavity wall required for reactor vessel support.

Note that for a large, dry PWR such as Kewaunee, the width of the cavity wall is large. Values for f_1 must be in the range $0 < f_1 \leq 1$; a value of 0.5 for f_1 would increase stresses in the containment wall by about a factor of two and would represent removal of design margin corresponding to a safety factor less than two in the original design (since the dehydration front slightly decreases the load-bearing fraction of the wall cross-sectional area).

For basemat penetration, the failure criterion is simply:

$$x_{e,d} \geq x_f + x_b \tag{3-2}$$

where:

$x_{e,d}$ = total concrete erosion in the downward direction, ft,

x_f = thickness of the cavity floor, ft,

x_b = thickness of the basemat, ft.

3.2 Step 2: Determine Overall Time Interval to Exceed Most Limiting Failure Criterion

The calculation method presented below is based on [Plys, 1987]. Typical values for data required by the calculation are provided in Table 3-1. The calculation proceeds in a piecewise continuous fashion to account for changes in the governing phenomena as time passes. The first phase of the erosion process is considered to be an interval during which unoxidized zirconium in the core debris is assumed to react with steam and carbon dioxide liberated by the concrete erosion. During the second phase of the erosion process, the chemical reaction energy is considered negligible and the concrete decomposition enthalpy reduced to reflect the assumed lack of chemical reactions. The calculation method proceeds by determining whether containment failure would be predicted to occur before the zirconium in the core debris bed is depleted. If containment failure occurs first, then the time at which containment failure would occur is obtained by a straightforward calculation. If zirconium depletion would occur first, then the calculation procedure becomes more complicated. First, the time interval to

Table 3-1

MOLTEN CORE-CONCRETE INTERACTION CALCULATION DATA

Molar Weights: A_{zr} = 91.22 lb/lb-mole

A_{CO_2} = 44 lb/lb-mole

A_{H_2O} = 18 lb/lb-mole

Heats of Reaction: Q_{H_2O} = 1.2898×10^5 Btu/lbm (3×10^8 J/Kg) [Plys, 1987]

Q_{CO_2} = 1.1608×10^5 Btu/lbm (2.7×10^8 J/Kg) (no coking assumed) [Plys, 1987]

Concrete Properties	Limestone/ Common Sand	Basaltic	Limestone
ρ_{cn} (lbm/ft^3)	143.59	143.59	143.59
λ'_{cn} (Btu/lbm) [Lee and Kazimi, 1985]	1539	1242.5	1780
f_{H_2O} [Lee and Kazimi, 1985]	.047	.049	.041
f_{CO_2} [Lee and Kazimi, 1985]	.22	.015	.357

Miscellaneous [Plys, 1987]

$\lambda_{cn} = \lambda'_{cn} + c_{p,slag}\ \Delta T$

$c_{p,slag}$ = 0.23885 Btu/lbm-F

ΔT = 932°F during zirconium reaction

= 392°F during iron reaction

reach zirconium depletion is determined. Then, an iterative calculation is required to determine the predicted depth of concrete erosion corresponding to zirconium depletion. Finally, the additional concrete mass that must be eroded to cause containment failure and its corresponding time interval must be determined.

To determine whether containment failure would be predicted to occur before zirconium depletion occurs, the masses of concrete that would be eroded at these times are calculated and compared. To estimate the mass of concrete that has been eroded when the zirconium is completely oxidized, the number of moles of zirconium available for reaction (N_{zr}) must be determined:

$$N_{zr} = m_{zr}/A_{zr} \tag{3-3}$$

where

m_{zr} = mass of unoxidized zirconium in the core debris contained in the cavity, lbm,

A_{zr} = molecular weight of zirconium, lb/lb-mole.

The governing chemical reactions are taken to be:

$$Zr + 2H_2O \rightarrow ZrO_2 + 2H_2 + Q_{H_2O} \tag{3-4}$$

$$\left.\begin{aligned} Zr + CO_2 &\rightarrow ZrO_2 + C \qquad (3\text{-}5a) \\ C + CO_2 &\rightarrow 2CO \qquad (3\text{-}5b) \end{aligned}\right\} + Q_{CO_2}$$

where:

Q_{H_2O}, Q_{CO_2} = heat of reaction per mole of gas produced, Btu/lb-mole (J/Kg-mole).

Thus, by Equation (3-4) two moles of gas are produced for each mole of zirconium reacted:

$$N_g = 2N_{zr} \tag{3-6}$$

The number of gas moles produced per unit mass of concrete eroded (n_g) is given by:

$$n_g = \frac{f_{H_2O}}{A_{H_2O}} + \frac{f_{CO_2}}{A_{CO_2}} \tag{3-7}$$

where:

f_{H_2O}, f_{CO_2} = concrete gas mass fractions for steam and carbon dioxide,

A_{H_2O}, A_{CO_2} = molecular weights of steam and carbon dioxide, lb/lb-mole.

The total concrete mass that would be eroded during phase 1 ($m_{cn,zr}$) may then be estimated as:

$$m_{cn,zr} = N_g/n_g \tag{3-8}$$

The mass of concrete that would be eroded at the time either of the failure criteria are satisfied (see Equations (3-1) and (3-2)), may be estimated using Equation (A-6b) from Appendix A:

$$m_{cn,s} = \rho_{cn} f_s \bar{A}_d x_{e,s}/r_s \quad \text{(lbm)} \tag{3-9a}$$

$$m_{cn,d} = \rho_{cn} f_s \bar{A}_d x_{e,d} \quad \text{(lbm)} \tag{3-9b}$$

where:

ρ_{cn} = concrete density, lbm/ft^3,

$f_s = 1 + r_s \frac{A_s}{A_d}$ rate of total to downward volumetric erosion rate.

$\bar{A}_d$ = average area subjected to downward erosion over the erosion time interval of interest, ft^2,

r_s = ratio of sideward rate of erosion to downward rate of erosion.

If either $m_{cn,s}$ or $m_{cn,d}$ are less than $m_{cn,zr}$, then containment failure would be predicted to occur before the zirconium in the core debris mass was fully oxidized. The time interval of interest may be estimated using Equation (A-8) and the following expression for the integrated core decay power [El-Wakil, 1978]:

$$\int_{t_1}^{t_2} Q_{DK}\, dt = 0.128\, Q_o \left[t_2^{0.74} - t_1^{0.74}\right] \qquad (3\text{-}10)$$

where:

Q_{DK} = core decay power, Btu/h (or MW),

Q_o = core full power, Btu/h (or MW),

t_1 = start of time interval of interest after core shutdown, second,

t_2 = end of time interval of interest after core shutdown, second.

For this case, the time at which the uncoolable core debris bed was formed corresponds to the start of the time interval, while the time that the containment fails is the end of the time interval. Substituting Equation (3-10) into Equation (A-8) and rearranging yields the desired end time:

$$t_2 = \left[t_1^{0.74} + 7.8\, m_{cn} \left(1 - f_q\, Q_r/\left(f_s\, \lambda_{cn}\right)\right) / \left[Q_o\, f_q/\lambda_{cn}\right]\right]^{1.35} \qquad (3\text{-}11)$$

where

m_{cn} = $m_{cn,s}$ or $m_{cn,d}$, whichever corresponds to the containment failure condition,

f_q = fraction of core debris bed power assumed to enter concrete,

λ_{cn} = total erosion enthalpy, Btu/lbm, including sensible heat to concrete melting, sensible heat to corium temperature, slag heat of fusion, and chemical reaction energy addition,

Q_r = total heat of reaction to oxidize zirconium, Btu/lbm, see Equation (A-4).

If containment failure will be predicted to occur after zirconium depletion, then the length of time required to fully oxidize the zirconium in the core debris must be determined, before the containment failure time can be estimated. This requires that the depth of erosion corresponding to $m_{cn,zr}$ be determined. This is done using the following equations in an iterative fashion:

$$x_{d,zr} = m_{cn,zr} / \left(\rho_{cn} \, f_s \, \bar{A}_d \right) \tag{3-12a}$$

$$x_{s,zr} = r_s \, x_{d,zr} \tag{3-12b}$$

where:

$x_{d,zr}$ = depth of eroded concrete when zirconium is depleted, ft,

$x_{s,zr}$ = sideward erosion distance when zirconium is depleted, ft.

The factor f_s is determined by:

$$f_s = 1 + r_s \left(\overline{A_s/A_d} \right) \tag{3-13}$$

where:

A_s = area subjected to sideward erosion, ft^2.

$\overline{A_s/A_d}$ = average value of A_s/A_d over time interval of interest.

The averaged values used in Equations (3-12a) and (3-13) are defined as follows for this time interval of interest:

$$\overline{A_s/A_d} = \frac{1}{2} \left(\frac{A_{so}}{A_{do}} + \frac{A_{s,zr}}{A_{d,zr}} \right) \tag{3-14}$$

$$\bar{A}_d = \frac{1}{2} \left(A_{do} + A_{d,zr} \right) \tag{3-15}$$

If a rectangular geometry is used to approximate a cavity, for example, the initial values for sideward and downward erosion areas, A_{so} and A_{do}, respectively, are:

$$A_{so} = \left(2L_o + 2W_o\right) h_o \qquad (3\text{-}16a)$$

where

L_o, W_o = original cross-sectional dimensions of the cavity, ft,

h_o = original depth of the debris on the cavity floor, ft.

$$A_{do} = L_o W_o \qquad (3\text{-}16b)$$

The values of the sideward and downward erosion areas to be used in the second iteration cycle and all subsequent cycles may be expressed as:

$$A_{s,zr} = \left(2L_o + 2W_o + 8x_{s,zr}\right)\left(h_o + x_{d,zr}\right) \qquad (3\text{-}17a)$$

and

$$A_{d,zr} = \left(L_o + 2x_{s,zr}\right)\left(W_o + 2x_{s,zr}\right) \qquad (3\text{-}17b)$$

Similar expressions would be determined for other uncoolable debris bed configurations.

The steps in the iteration procedure involve estimating and updating $\bar{A}_d$ and $\overline{A_s/A_d}$ as the estimated values for $x_{d,zr}$ and $x_{s,zr}$ change. To start the iteration, use A_{do} for $\bar{A}_d$, and A_{so} and A_{do} in $\overline{A_s/A_d}$. Next, calculate a value for f_s using Equation (3-13), and then obtain first estimates of $x_{d,zr}$ and $x_{s,zr}$ from Equations (3-12a) and (3-12b), respectively. The revised values for erosion distances then should be used to start the next iteration cycle. Update values for $\overline{A_s/A_d}$, f_s, and $\bar{A}_d$ using (in order) Equations (3-17a), (3-17b), (3-14), (3-15), and (3-13). Then, calculate new values for $x_{d,zr}$ and $x_{s,zr}$ using Equations (3-12a) and (3-12b). Satisfactory convergence is obtained when the value of $x_{d,zr}$ changes less than 0.1% from the previous iteration.

Once convergence is reached for the erosion distances, the end time of the interval required to deplete unreacted zirconium in the core debris bed

should be estimated using Equation (3-11), with $m_{cn,zr}$ identified as the appropriate value for the factor m_{cn}.

To then determine the containment failure time, the additional mass of concrete that must be eroded after zirconium is fully oxidized to reach the containment failure condition $\left(\Delta m_{cn}\right)$ must be found. This value may be determined as follows:

$$\Delta m_{cn} = \Delta x \, \rho_{cn} \, f_s \, \tilde{A}_d \tag{3-18}$$

where:

Δx = distance erosion front must advance to cause containment failure, m.

The value for Δx in Equation (3-18) should be selected as the minimum of $\Delta x_{e,s}$ and $\Delta x_{e,d}$:

$$\Delta x_{e,d} = x_{e,d} - x_{d,zr} \tag{3-19a}$$

$$\Delta x_{e,s} = \left(x_{e,s} - x_{s,zr}\right)/r_s \tag{3-19b}$$

where

$\Delta x_{e,d}$ = distance erosion front must advance in downward direction to reach containment failure criterion for downward direction, ft,

$\Delta x_{e,s}$ = distance erosion front must advance in downward direction to reach containment failure criterion for sideward direction, ft.

The values of $\overline{A_s/A_d}$ and $\tilde{A}_d$ to be used in Equations (3-13) and (3-18) should be as follows:

$$\tilde{A}_d = \frac{1}{2}\left(A_{d,zr} + A_{d,cf}\right) \tag{3-20}$$

$$\overline{A_s/A_d} = \frac{1}{2}\left(\frac{A_{s,zr}}{A_{d,zr}} + \frac{A_{s,cf}}{A_{d,cf}}\right) \tag{3-21}$$

where:

$A_{d,cf}$ = cross-sectional area of uncoolable core debris bed at time of containment failure, ft^2,

$A_{s,cf}$ = sideward erosion area of uncoolable core debris bed at time of containment failure, ft^2.

As an example, the values for $A_{s,cf}$ and $A_{d,cf}$ for containment sump geometry would be given by:

$$A_{s,cf} = \left[2L_o + 2W_o + 8\left(x_{s,zr} + r_s\Delta x\right)\right]\left(h_o + x_{d,zr} + \Delta x\right) \quad (3\text{-}22a)$$

$$A_{d,cf} = \left[L_o + 2\left(x_{s,zr} + r_s\Delta x\right)\right]\left[W_o + 2\left(x_{s,zr} + r_s\Delta x\right)\right] \quad (3\text{-}22b)$$

Once Δm_{cn} has been determined, the predicted time of containment failure may be found from Equation (3-11), using the time at which zirconium was depleted as t_1, Δm_{cn} as m_{cn}, Q_r set equal to zero, and the appropriate value of λ_{cn} from Table 3-1.

The result of the preceding calculation is an estimate of the least time required for molten core-concrete interaction to exceed a containment failure criterion. If the criterion stated by Equation (3-1) is the most limiting condition, then containment failure is assumed to be at a penetration as a result of vessel movement; fission products then would be released from the containment building to the environment. If the criterion stated by Equation (3-2) is the most limiting condition, then containment failure is assumed to be caused by basemat penetration; fission products and/or core debris would be released from the containment building to the soil underneath the containment basemat.

4.0 APPLICATION OF THE METHOD TO THE KEWAUNEE NUCLEAR POWER PLANT

4.1 MCCI Failure Criterion (Step 1)

Examination of the Kewaunee Plant shows that containment failure at reactor containment vessel and shield building penetrations caused by erosion of the cavity walls and the embedded structural steel columns (Figure 4-1) that support the reactor vessel will not occur as early as the meltthrough of the basemat. Assuming that the entire core participation in the melt (i.e., 100% of the fuel and lower core plate), a core debris depth of slightly less than 1 ft (see Equation (4-1) for this estimation) would accumulate on the cavity floor at the 580'-3" elevation. This debris depth is based on the premise that none of the debris is swept out of the cavity. With a debris height of roughly 1 ft, the debris will begin to erode in the sideward and downward directions. The erosion will occur at a much faster rate in the downwards direction versus the sideward direction. As the concrete erodes in the sideward direction, it can travel a far distance without compromising the ability of the cavity walls to support the vessel and its associated piping. This is due to the massive amount of concrete in the tall cavity walls in comparison to the expected sideward erosion area. To fail the vessel restraints at the 617' elevation, which is approximately 36 ft higher than the debris pool, would require a sideward erosion distance equivalent to half of the cavity wall thickness. The cavity floor consists of approximately 9.86 ft of concrete which would need to be ablated in order for the containment to fail. This distance is approximately twice the sideward erosion distance required for the containment failure. It is not possible for the corium to travel such a distance sidewards without first penetrating through the entire basemat because the sideways rate of erosion will be much less than the downward rate of erosion, as demonstrated by the experimental evidence discussed above. Basemat penetration is, therefore the MCCI failure criterion for the Kewaunee cavity configuration.

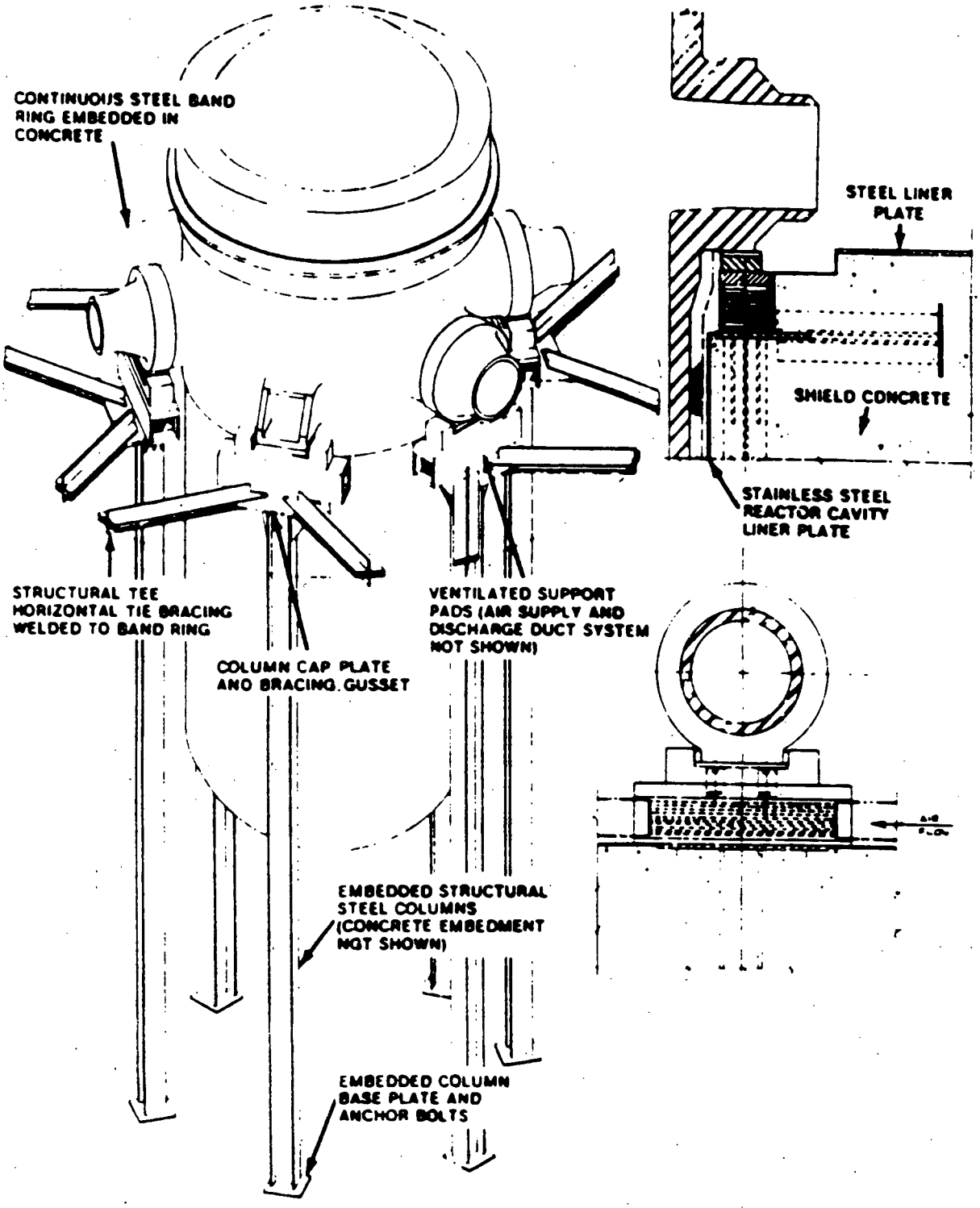

Figure 4-1 Reactor vessel supports in Kewaunee plant (taken from Kewaunee FSAR Figure 5.9-7).

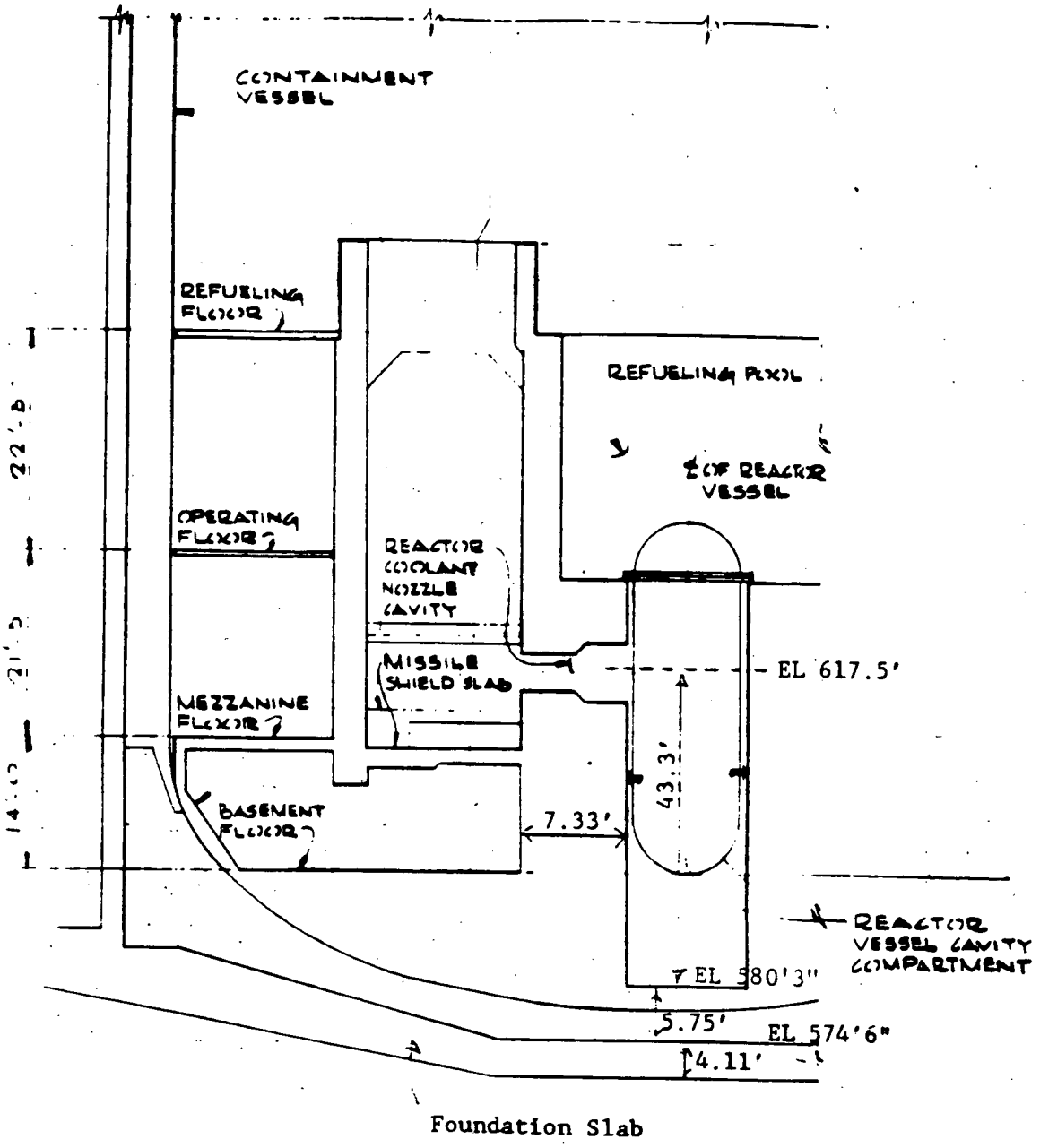

Figure 4-2 Kewaunee reactor cavity compartment (adapted from Kewaunee FSAR Figure 5.9-5 and general arrangement drawing no. 237127A-A210).

4.2 Time Interval to Exceed the Failure Criterion (Step 2)

The time to exceed the failure criterion is determined by the procedure outlined above, subject to a key assumption - the entire core, with its full initial inventory of zirconium and fission products, is expelled instantaneously at the start of the time interval. Vessel failure and core-concrete attack can be delayed for many hours after reactor shutdown if the operator can remove decay heat via the secondary side heat sinks or injection with either high head or low head safety injection pumps. By neglecting potential mitigating operator actions, the decay heat of the debris and the heat transfer to the concrete are overstated. The expulsion of molten debris from the failed vessel would take some finite time period depending on the vessel pressure at the time of failure. However, for a PWR, this time period is very small when compared to the duration for core-concrete attack (many hours, or even days), so it can be thought of as instantaneous.

Although some fraction of the core could remain cooled in-vessel while the bulk of the core is expelled, it is much easier to make the conservative assumption that the entire core is expelled with its full initial inventory of fission products and zirconium. In many accident sequences, a substantial fraction, as much as, say, 50%, of the zirconium can be oxidized in-vessel, as opposed to being oxidized during corium-concrete attack. This potentially decreases the duration of the zirconium oxidation phase and slows corium-concrete attack overall, since the chemical energy of the corium is decreased. This possibility is not considered. Moreover, a substantial fraction of the the core's initial fission product inventory will not reside in the corium attacking the basemat. Fission products are distributed throughout the primary system and containment compartments in a manner that depends upon the accident progression. Volatile fission products initially present in the corium can be vaporized or entrained to form aerosols which are transported throughout the containment. The net effect of these mechanisms reduces the mass of fission products and decay heat in the corium as it attacks the cavity floor.

A small computer code was developed to expedite the repetitive calculations of the procedure and allow for further sensitivity calculations. The data required were taken from Table 3-1, and the Kewaunee MAAP parameter file [Fauske & Associates, Inc., 1992]. (Note: Code input data and results are presented in Appendix B, and the MCCI source code listing is included in Appendix C.) For a large, dry PWR, the condensed debris depth in the cavity is given by:

$$h_o = \frac{\left(\frac{M_u}{\rho_u} + \frac{M_{ZR}}{\rho_{ZR}} + \frac{M_{CSP}}{\rho_{SS}}\right) + 0.10\,\frac{M_{LH}}{\rho_{SS}}}{A_c} \qquad (4\text{-}1)$$

where,

M_u is the mass of UO_2 in the debris bed (119,178 lbm or 54059.5 kg),
M_{ZR} is the mass of zirconium in the debris bed (24,493 lbm or 11110 kg),
M_{CSP} is the mass of the core support plate (2205 lbm or 1000 kg),
M_{LH} is the mass of the lower head (39691 lbm or 18041 kg),
ρ_u is the density of UO_2 (10,100 kg/m_3),
ρ_{ZR} is the density of zirconium (6570 kg/m^3),
ρ_{SS} is the density of stainless steel (8238 kg/m^3), and,
A_c is the cavity floor area (291.7 ft^2 or 27.1 m^2).

Only 10% of the lower head mass is used because the size of the vessel failure will be small in relation to the radius of the lower head. In addition, this calculation uses the assumption that none of the debris has been swept out of the cavity and dispersed into the lower compartment. This overstates MCCI in the cavity and it is clearly conservative for the case where the cavity is initially dry.

The cavity floor is modeled as a rectangle without the necessity of dealing with the complexities of the actual geometry. This is achieved by maintaining the perimeter and the area of the modeled rectangle the same as the perimeter and the area of the cavity floor, respectively. Given the cavity floor area (A_c) and the cavity floor perimeter (P_c), the dimensions

of the equivalent rectangle can be found from the following two requirements:

$$L_o W_o = A_c \tag{4-2}$$

and

$$L_o + W_o = \frac{P_c}{2} \tag{4-3}$$

Solving the above two equations gives

$$L_o = \frac{P_c + \left[P_c^2 - 16\,A_c\right]^{0.5}}{4} \tag{4-4}$$

and

$$W_o = \frac{P_c - \left[P_c^2 - 16\,A_c\right]^{0.5}}{4} \tag{4-5}$$

For the Kewaunee plant, applying $A_c = 291.7$ ft^2 (27.1 m^2) and $P_c = 92.5$ ft (28.2 m) yields $L_o = 38.7$ ft (11.8 m) and $W_o = 7.55$ ft (2.3 m).

Other parameters required for the procedure, such as the ratio of sideward rate of erosion to downward rate of erosion (r_s) and the fraction of core debris power to concrete (f_q), are derived from the experimental evidence cited earlier. The choice of values for these parameters is discussed below.

A ratio of the sideward rate of erosion to the downward rate of erosion must be specified based on the BETA experiments and engineering judgment. Clearly, the lower bound for r_s of zero will result in the maximum downward erosion rate. Also, the downward erosion area will remain constant during the attack for an r_s of zero, resulting in very simple expressions for Δm_{cn}. If r_s is assumed to be zero, an extremely conservative containment failure time can be quickly estimated by hand.

However, even small values of r_s greatly increase containment failure time relative to the $r_s = 0$ assumption because f_s is made larger than 1. The assumption that $r_s = 0$ is quite convenient, but it results in unrealistically conservative answers. Experimental evidence suggests that the ratio of erosion rates is non-zero, but much less than one. From Table 2-4, the BETA experiments indicate an r_s of 0.05 for the V1.8 test and 0.29 for the V2.1 test. The V2.1 test was scaled to reflect long-term decay heat, in contrast to the V1.8 test which reflect a heat generation rate an order of magnitude larger than decay heat. As a result, 0.2 will be used as a value for r_s.

A fraction of core debris bed power assumed to enter the concrete (f_q) must also be specified. A value of 1 is overly conservative because it neglects radiation and/or convection heat transfer from the the top surface of the debris, while a value of 0, on the other extreme, denotes no concrete attack. It is assumed f_q is zero, i.e., MCCI is not a relevant containment failure mechanism, if a deep overlying pool of water can be maintained on the debris. This assumption is based on experimental results demonstrating the ability of water to rapidly quench molten debris and ingress into debris beds to maintain them coolable indefinitely. If the pool cannot be maintained, MCCI will begin after the pool has dried out.

Note that this assumption reduces the complexities of innumerable severe accident sequences to just one consideration - is the debris covered by a deep overlying pool for an indefinite duration? If not, $f_q = 0.5$, based on the methodology of [Fauske & Associates, 1985]. The following section considers which accident sequences will not have an overlying pool. The value of f_q would actually vary from sequence to sequence as a function of accident progression and operator actions. Similarly, for a given severe accident sequence, f_q would be a function of time due to operator actions, accident progression, fission product transport, etc. For now, we focus on the simple "dry" case where f_q is a constant value of 0.5 after debris bed dry-out.

Finally, an initial time for MCCI (t_1) must be specified to calculate the time to exceed the failure criterion. Even in those cases where a pool

cannot be maintained (due to equipment failure, operator error, etc.), MCCI will not begin until the debris bed has dried out. Because the Kewaunee plant has a 34 ft high curb separating the lower compartment from the cavity, water will not spill into the cavity and dry-out will occur after the remaining water in the lower head expelled at the reactor failure has boiled away. For the Kewaunee plant, the dry-out time has been calculated for a large LOCA sequence at 4.0 hrs after scram [Fauske & Associates, Inc., 1992a]. Therefore, t_1 = 4.0 hours.

Substituting these values into the code developed specifically to evaluate the expressions presented in the method, and using a nominal full power for the Kewaunee Nuclear Plant of 0.563 x 10^{10} Btu/h (1650 MW), results in a containment failure time of 97 hours after scram. Code input data and results are presented in Appendix B.

4.3 Uncertainty Considerations

The results presented above are subject to uncertainties. In particular, the fraction of core decay heat power (f_q) is subject to large uncertainty as a result of two considerations: (1) the heat transfer mechanisms from the debris by radiation and convection to overlying water or gas, and, (2) the transport of volatile fission products from the debris by vaporization and/or entrainment to other parts of the containment. The decay heat power fraction to the concrete was taken from [Fauske & Associates, 1985], but no effort was made to account for fission product release from the debris. Fission product release is now accounted for in a simple manner to scope out its potential impact and demonstrate the conservatisms of the aforementioned results. This phenomenon essentially decreases the fraction of decay heat power to the concrete, so fission product release in the cavity can be addressed by varying the parameter f_q.

Fission product release and transport is dependent upon severe accident progression, timing, operation actions, etc. A few MAAP runs can be examined to find a range for the fraction of decay heat energy removed from the debris by transport of volatile fission products. This will improve the accuracy of f_q. MAAP runs performed in support of the Level II portion of

the Kewaunee IPE [Fauske & Associates, Inc., 1992a] can be used to analyze the decay heat distribution between containment compartments for various dominant sequences. This information is located in the tabular output file. For brevity, a station blackout with no operator actions, a small LOCA without the recirculation mode, and a large LOCA without the recirculation mode will be analyzed. Tabular output for each of these runs gives the fraction of core decay heat in the cavity at various times. For the blackout case, 12% of the decay heat is deposited in the primary system, 20% is in the form of released fission products, 63% is deposited in the cavity, and 5% is deposited in the lower compartment. For the large LOCA, 62% of the decay heat is in the cavity at 30 hours into the accident and 38% is in the form of released fission products. And finally, for the small LOCA, 76% of the decay heat is in the cavity at 44 hours and 24% is in the form of released fission products. Based upon these examples, it seems reasonable to assume that in the long term, 70%, rather than 100%, of the decay heat is in the cavity.

Calculations have been made assuming that the cavity floor could be modeled as a rectangle, as opposed to the actual geometry which closely resembles a rectangle placed next to a circle. The actual geometry is not far removed from a rectangle, and, perhaps, the initial cavity floor geometry may be "forgotten" as the melt attacks the concrete. As the debris attacks the concrete and spreads sideways at a uniform rate, the debris geometry resembles the initial geometry less and less. This leads to the supposition that as long as the initial floor area and the perimeter are accurate, the actual geometry of the cavity floor may not be significant.

Additional uncertainty considered here is the impact of the assumed constant erosion rate ratio (r_s). To simplify the calculation, r_s was assumed constant. Furthermore, the average value of r_s which was taken from experimental data ranges from 0.05 (in V1.8 test) to 0.29 (in V2.1 test) depending on the heat supply rate in the experiments. This differs by a factor of 6. It is, therefore, important to take into account the sensitivity of r_s on the containment failure time. In general, the smaller value of r_s means more heat rate will be available to erode downward; therefore, reducing the failure time in the downward direction.

Finally, the the model itself needs to be addressed. As mentioned above, the overall accuracy of the MCCI prediction method presented in this paper depends largely on the values of f_q and r_s. It is always possible to assign the physically meaningful values to f_q and r_s and achieve results similar to the predictions by MAAP. For example, the MAAP calculations as reported by [Fauske & Associates, 1992a] predict that at 24 hours after a large LOCA with no containment safeguards, the cavity floor concrete ablation depth would be 3.2 ft (0.98 m). When using the present model to predict the time to obtain the same cavity floor ablation depth, the results are in descending order: (1) 24.8 hr for $r_s = 0.2$, $f_q = 0.4$, (2) 19.9 hr for $r_s = 0.2$, $f_q = 0.5$. Note that results (1) is comparable to MAAP while results (2) are more conservative with respect to MAAP prediction. The representative failure time of 97 hours calculated for Kewaunee in this paper is also conservative with respect to MAAP.

5.0 CONCLUSIONS

As shown by the following discussion, MCCI can be excluded from consideration as a significant late containment failure mechanism. This is not meant to downplay the significance of MCCI in the Kewaunee Level II PRA, or suggest that containment failure due to concrete melt-through cannot occur under any circumstances. Rather, it is clear that relative to other containment failure mechanisms, MCCI will occur so late in time that: (1) the containment will have failed due to other, more rapidly developing mechanisms, or (2) mitigating actions will almost surely have taken place to arrest MCCI before reaching the containment failure criterion of basemat melt-through. Also, relative to other failure mechanisms, the source term for a basemat melt-through would be small because of the failure time (very late) and location (below ground).

For the dry cavity case, a large LOCA with no injection or containment heat removal was considered. For this sequence, MCCI will begin shortly after reactor vessel failure, but the containment will also pressurize as the containment atmosphere directly is heated by the debris. A linear extrapolation of this slow containment heating as calculated by MAAP [Fauske & Associates, 1992], indicates containment failure about 85 hours after the initiating event. This estimate is well before the time to reach the MCCI containment failure criterion of about 97 hours. Even if containment overpressurization is hypothetically ruled out, the ablation would have to go several days without the operators attempting to cool the debris in order to fail containment due to MCCI. Otherwise, recovery actions could be taken to halt the ablation by covering the debris with subcooled water.

The wet cavity case is any sequence where ECCS injection and containment heat removal are available to keep the debris bed covered. Low pressure recirculation with RHR heat exchangers operating could be used to cover the debris via the vessel hole, and remove decay heat from the containment. However, if low pressure recirculation were available, core damage would not have occurred in the first place. This means of arresting MCCI is considered only as a possible recovery action. These insights recognize that

in the Kewaunee containment, water cannot find its way from the lower compartment to the cavity.

Failure due to MCCI is precluded for the wet case because of the ability of water to quench molten debris and ingress into debris beds to render them coolable. If a pessimistic view of ingression is taken for the wet case (that is, ingression cannot occur) calculations could be performed, just as they were performed for the dry case, by selecting an appropriate power fraction into the concrete (f_q). However, these calculations would show failure times of hundreds of hours, and we would therefore revert back to the same conclusions as the dry case.

This discussion has focused on two simple accident scenarios, i.e., dry and wet, to simplify consideration of the innumerable accident sequences that might actually involve MCCI. If the debris cannot remain continuously covered, the sequence is thought to be dry. Other accident sequences involving a more complex set of operator interventions that do not fall into either of the two simple classes defined here, require individual analysis, such as MAAP runs, to determine exact containment failure mode and timing. Such analysis, conducted as part of an IPE sensitivity study, would not contradict the basic conclusion that MCCI can be neglected relative to other containment failure mechanisms for the Kewaunee IPE.

6.0 REFERENCES

Alsmeyer, H., 1986, Beta Experiments for Verifying the WESCHL-Codes; Experimental Results for Melt-Concrete Interaction, English Translation.

Alsmeyer, H., et al., 1987, "Beta Experimental Results on Melt/Concrete Interactions: Silicate Concrete Behavior", Proceedings of the Committee on the Safety of Nuclear Installations (CSNI) Specialists' Meeting on Core Debris-Concrete Interactions, EPRI NP-5054-SR.

Blose, R. E., et al., 1987, SWISS: Sustained Heated Metallic Melt/Concrete Interactions with Overlying Water Pools, NUREG/CR-4727, SAND85-1546.

Bradley, D. R., and Copus, E. R., 1987, "Significant Results from SURC-3 and SURC-3A Experiments", Presented at 15th Water Reactor Safety Meeting, National Bureau of Standards, Gaithersburg.

CSNI, 1989, "SURC-4 Experiment on Core-Concrete Interactions," Committee on the Safety of Nuclear Installations, CSNI Report No. 155, Volume 2.

El-Wakil, M. M., 1978, Nuclear Heat Transport, The American Nuclear Society, LaGrange Park, Illinois.

Farahani, A., and Corradini, M. L., 1990, "MAAP Modeling of the Kewaunee Nuclear Power Plant", University of Wisconsin Report to Wisconsin Public Service Corp.

Fauske & Associates, Inc., 1985, "Approximate Source Term Methodology for Pressurized Water Reactors," FAI/85-58.

Fauske & Associates, Inc., 1990, MAAP 3.0B User's Manual, also an EPRI report to be published.

Fauske & Associates, Inc., 1992, "Containment Data Collection Notebook", Kewaunee IPE.

Fauske & Associates, Inc., 1992a, "Kewaunee Nuclear Plant Source Term Notebook", FAI/92-88.

Gieseke, J. A., et al., 1986, "Source Term Code Package, A User's Guide (Mod. 1)", Battelle Columbus Division, NUREG/CR-4587, BMI-2138.

IDCOR, 1985, Grand Gulf Nuclear Station - Integrated Containment Analysis", IDCOR Technical Report 23.1GG, Mississippi Power and Light Co.

Lee, M., and Kazimi, M. S., 1985, Modeling of Corium/Concrete Interaction, MITNE-267.

Muir, J. G., et al., 1981, "CORCON/Mod1: An Improved Model for Molten Core/Concrete Interaction", NUREG/CR-2142, SAND80-2415.

NRC, 1975, WASH-1400, Reactor Safety Study, NUREG/75-0114.

NRC, 1988, letter to All Licensees Holding Operating Licenses and Construction Permits for Nuclear Power Facilities, "Individual Plant Examination for Severe Accident Vulnerabilities - 10 CFR 50.54(f)", Generic Letter No. 88-20.

Plys, M. G., 1987, "Hand Calculations for Core-Concrete Attack and containment Failure Timing With Applications to Lasalle and Grand Gulf", Presentation to NUREG-1150 Molten Core-Containment Expert Review Group, Albuquerque, NM.

Reimann, M., and Murfin, W. B., 1981, "The WECHSL Code: A Computer Program for the Interaction of Core Melt with Concrete", KfK-2890.

Summers, R. M., et al., 1991, "MELCOR 1.8.0: A Computer Code for Nuclear Reactor Severe Accident Source Term and Risk Assessment Analyses", Sandia National Laboratories, Albuquerque, NM.

APPENDIX A

Derivation of Concrete Erosion Calculation

The calculation presented below is based on the method presented by [Plys, 1987]. This calculation is based on the following assumptions:

- The mass erosion rate is linearly proportional to the decay heat rate plus heat of chemical reactions.
- Only reaction heats from the downward attack are accounted.
- Sideward erosion speed is assumed a constant fraction of downward erosion speed (i.e., $r_s = U_s/U_d$ = constant).

The energy balance for the eroded concrete according to the first assumption may be written as:

$$\rho_{cn}\,\lambda_{cn}\left(U_d A_d + U_s A_s\right) = Q \qquad \text{(A-1)}$$

where

ρ_{cn} = concrete density, lbm/ft^3,

λ_{cn} = total erosion enthalpy, Btu/lbm, including sensible heat to concrete melting, sensible heat to corium temperature, slag heat of fusion, and decomposition reactions.

U = erosion speed, ft/s,

A = area, ft^2,

Q = input power, w, including decay power and chemical reactions,

d = downward,

s = sideward.

The mass balance for the eroded concrete yields:

$$m_{cn} = \int_o^t \rho_{cn} \left[U_d A_d + U_s A_s\right] dt \qquad \text{(A-2a)}$$

$$= \int_o^t \left[Q/\lambda_{cn}\right] dt \qquad \text{(A-2b)}$$

where

m_{cn} = total eroded concrete mass, lbm.

The input power in Equation (A-1) may be written as:

$$Q = f_q \left\{Q_{dk} + \rho_{cn}\, U_d A_d \left[\frac{f_{H_2O}}{18} Q_{H_2O} + \frac{f_{CO_2}}{44} Q_{CO2}\right]\right\} \qquad \text{(A-3)}$$

where

f_q = power fraction into concrete,

Q_{dk} = decay power, Btu/h,

f_{H_2O}, f_{CO_2} = gas mass fraction in concrete,

Q_{H_2O}, Q_{CO_2} = heat of reaction per mole gas to liberate H_2 and CO, Btu/lb-mole.

Typical values for the latter quantities are:

$$Q_{H_2O} \simeq 1.2898 \times 10^5 \text{ Btu/lb-mole } H_2O$$

$$Q_{CO_2} \simeq 1.1608 \times 10^5 \text{ Btu/lb-mole } CO_2$$

for overall reactions to H_2 and CO.

If we define:

$$Q_r = \left[\frac{f_{H_2O}}{18} Q_{H_2O} + \frac{f_{CO_2}}{44} Q_{CO_2}\right] \quad \text{(A-4)}$$

and

$$f_s = 1 + \frac{U_s A_s}{U_d A_d} = 1 + r_s \frac{A_s}{A_d} \quad \text{(A-5)}$$

Then, Equation (A-2a) may be rewritten as:

$$m_{cn} = \rho_{cn} f_s \int_o^t U_d A_d \, dt \quad \text{(A-6a)}$$

$$= \rho_{cn} f_s \bar{A}_d x_d \quad \text{(A-6b)}$$

where:

x_d = depth of eroded concrete, ft,

$\bar{A}_d$ = average surface area of downward concrete erosion, ft^2.

Equation (A-2b) may be rewritten as:

$$\lambda_{cn} m_{cn} = f_q \int_o^t Q_{dk} \, dt + f_q \rho_{cn} Q_r \bar{A}_d x_d \quad \text{(A-7)}$$

Manipulating Equations (A-6b) and (A-7) then yields:

$$m_{cn} = \frac{\left(f_q/\lambda_{cn}\right) \int_o^t Q_{dk} \, dt}{1 - f_q Q_r / \left(f_s \lambda_{cn}\right)} \quad \text{(A-8)}$$

$$x_d = m_{cn} / \left(\rho_{cn} f_s \bar{A}_d\right) \quad \text{(A-9)}$$

$$x_s = r_s x_d \quad \text{(A-10)}$$

APPENDIX B

Code Input and Calculations

```
KEWAUNEE DRY CASE - 100% ZIRCONIUM REACTION
 0.5      !F1 MINIMUM FRACTION OF CAVITY WALL REQUIRED FOR VESSEL SUPPORT
 2.23     !XP WIDTH OF CAVITY WALL (M)
 0.0      !XSP DIST. BETWEEN UNCOOLABLE DEBRIS BED & CAVITY WALL (M)
 3.006    !XF THICKNESS OF CAVITY FLOOR (M)
 0.0      !XB   "       "  BASEMAT (M)
11110.    !MZR MASS OF UNOXIDIZED ZIRCONIUM (KG)
 0.0736   !FH2O CONCRETE GAS MASS FRACTION FOR STEAM
0.2729    !FCO2    "      "    "     "      "  CO2
11.8      !LO    DEBRIS LENGTH (M)
 2.3      !WO    DEBRIS WIDTH (M)
0.272     !HO    DEBRIS HEIGHT (M)
 0.2      !RS    RATIO OF EROSION RATES
14400.    !TINIT INITIAL TIME (SEC)
0.5       !FQ    DECAY HEAT FRACTION INTO CONCRETE
1.65E9    !QO    FULL POWER (WATTS)
4.09E6    !LCN   LATENT HEAT DURING OXIDATION (J/KG)
3.80E6    !LCNP    "     "   AFTER     "        "
```

KEWAUNEE DRY CASE - 100% ZIRCONIUM REACTION
KEWAUNEE MCCI CALCULATIONS
DECAY HEAT FRACTION IS 0.50000 EROSION RATIO IS 0.20000

SIDEWARD FAILURE CRITERION IS 1.1150 METERS
DOWNWARD FAILURE CRITERION IS 3.0060 METERS
OVERALL FAILURE CRITERION IS 1.1150 METERS

NO. OF INITIAL MOLES OF ZIRCONIUM - 121.79
MOLES OF GAS PRODUCED - 243.59
NO. OF GAS MOLES PER MASS OF CONCRETE - 0.10291E-01
MASS OF CONCRETE ERODED DURING OXIDATION - 23670.
INITIAL SIDEWARD EROSION AREA - 7.6704
INITIAL DOWNWARD EROSION AREA - 27.140
FINAL SIDEWARD EROSION AREA - AT FAILURE - 100.97
FINAL DOWNWARD EROSION AREA - AT FAILURE - 63.556
AVERAGE DOWNWARD EROSION AREA - 45.348
RATIO OF EROSION AREAS AT FAILURE - 0.93568
FACTOR FOR EROSION AREA AT FAILURE - 1.1871

CONTAINMENT FAILS AFTER CONCRETE FULLY OXIDIZED

MASS OF CONCRETE ERODED AT FAILURE CRITERIA - .37220E+06 KG
MASS OF CONCRETE ERODED BY ZIRGONIUM OXIDATION - 23670. KG

ITERATIVE SCHEME CONVERGES ON XDZR TO - 0.95880E-01 %
FACTOR FOR EROSION AREA BY ZIRC. OXID. - 1.0884
DOWNWARD EROSION AREA FOR ZIRC. OXID. - 29.054
SIDEWARD EROSION AREA FOR ZIRC. OXID. - 17.478
THICKNESS ERODED BY ZIRC. OXID. - 0.33619
TIME FOR ZIRCONIUM OXIDATION - 8.5392 HOURS AFTER SCRAM

CONTAINMENT FAILS AT 97.084 HOURS AFTER SCRAM

APPENDIX C

MCCI Calculation Source Code

```
C MCCI POSTION PAPER CALCULATIONS
      IMPLICIT REAL (A-H,K-Z)
      CHARACTER*80 TITL
C
C     XES      - SIDEWARD FAILURE CRITERIA
C     F1       - FRAGTION OF WALL REQUIRED FOR VESSEL SUPPORT
C     XP       - SHORTEST DISTANCE BETWEEN DEBRIS AND VESSEL SUPPORT WALL
C     XSP      - VESSEL SUPPORT WALL THICKNESS
C     XED      - DOWNWARD FAILURE CRITERIA
C     XF       - DRYWELL FLOOR THICKNESS
C     XB       - THICKNESS OF THE BASEMAT
G     NZR      - NUMBER OF MOLES OF ZIRCONIUM
C     MZR      - MASS OF UNOXIDIZED ZIRCONIUM IN THE CORE DEBRIS
C     AZR      - MOLECULAR WEIGHT OF ZIRCONIUM
C     NG       - NUMBER OF MOLES OF GAS PRODUCED FOR EACH MOLE OF ZIRCONIUM
C     NGC      - NUMBER OF GAS MOLES PRODUCED PER UNIT MASS OF CONCRETE ERODED
C     FH2O     - CONCRETE GAS MASS FRACTION FOR STEAM
C     FCO2     - CONCRETE GAS MASS FRACTION FOR CARBON DIOXIDE
C     AH2O,ACO2 - MOL. WEIGHTS FOR STEAM AND CARBON DIOXIDE
C     MCNS     - MASS OF CONCRETE ERODED SIDEWAYS FOR FAILURE CRITERIA
C     MCND     - MASS OF CONCRETE ERODED DOWNDARD FOR FAILURE CRITERIA
C     MCNZR    - TOTAL CONCRETE ERODED DURING PHASE 1 - ZIRC. OXIDATION
C     RHOCN    - DENSITY OF CONCRETE
C     FS       - FACTOR FOR SIDEWARD EROSION RELATIVE TO DOWNWARD EROSION
C     AD       - AVERAGE AREA SUBJECTED DOWNWARD EROSION
C     RS       - RATIO OF SIDEWARD RATE OF EROSION TO DOWNWARD RATE OF EROSION
C     TFINAL   - END OF TIME INTERVAL OF INTEREST
C     TINIT    - BEGINING OF TIME INTERVAL OF INTEREST
C     FQ       - FRACTION OF CORE DEBRIS BED POWER ASSUMED TO ENTER CONCRETE
G     QR       - TOTAL HEAT OF REACTION TO OXIDIZE ZIRCONIUM
C     LCN      - TOTAL EROSION ENTHALPY
C     Q0       - INITIAL CORE POWER
C     L0,W0,H0 - INITIAL BED LENGTH, WIDTH, HEIGHT
C     XDZR     - DEPTH OF ERODED CONCRETE WHEN ZIRCONIUM IS DEPLETED
C     XSZR     - SIDEWARD EROSION DISTANCE WHEN ZIRCONIUM IS DEPLETED
C     ADZR     - DOWNWARD EROSION AREA     "       "       "     "
C     ASZR     - SIDEWARD EROSION AREA     "       "       "     "
C     AD0      - ORIGINAL DOWNWARD BED AREA
C     AS0      - ORIGINAL SIDEWARD BED AREA
C     AD       - AVERAGE DOWNWARD EROSION AREA
C     ASAD     - AVERAGE AS/AD DURING THIS TIME INTERVAL
      READ (21,1000) TITL
1000  FORMAT(A80)
      READ (21,*) F1
      READ (21,*) XP
      READ (21,*) XSP
      READ (21,*) XF
      READ (21,*) XB
      READ (21,*) MZR
      READ (21,*) FH2O
```

```
      READ (21,*) FCO2
      READ (21,*) LO
      READ (21,*) WO
      READ (21,*) HO
      READ (21,*) RS
      READ (21,*) TINIT
      READ (21,*) FQ
      READ (21,*) QO
      READ (21,*) LCN
      READ (21,*) LCNP
      DATA AZR,AH2O,ACO2,RHOCN,QH2O,QCO2,XMAX,IMAX
     #  /91.22,18.0,44.0,2300.0,
     #  3.0E8,2.7E8,10.0,100000/
C WRITE OUT EROSION RATE AND DECAY HEAT FRACTION INTO CONCRETE TO KEEP TRACK
C OF VARIOUS RUNS
      WRITE(22,49) TITL
 49   FORMAT(' ',A80)
      WRITE(22,50) FQ,RS
 50   FORMAT (' KEWAUNEE MCCI CALCULATIONS ',/,
     #  ' DECAY HEAT FRACTION IS ',G13.5,' EROSION RATIO IS ',G13.5,/)
C SIDEWARD FAILURE CRITERIA
      XES=(1.0-F1)*XP+XSP
      WRITE(22,51) XES
 51   FORMAT (' SIDEWARD FAILURE CRITERION IS ',G13.5,' METERS')
C BASEMAT PENETRATION FAILURE CRITERIA
      XED=XF+XB
      WRITE(22,52) XED
 52   FORMAT (' DOWNWARD FAILURE CRITERION IS ',G13.5,' METERS')
C FAILURE CRITERIA
      XFAIL=MIN(XES,XED)
      WRITE(22,53) XFAIL
 53   FORMAT (' OVERALL  FAILURE CRITERION IS ',G13.5,' METERS',//)
C ZIRCONIUM DEPLETION OR CONTAINMENT FAILURE?
C FIND NUMBER OF MOLES OF ZIRCONIUM
      NZR=MZR/AZR
      WRITE(22,61) NZR
 61   FORMAT (' NO. OF INITIAL MOLES OF ZIRCONIUM        - ',G13.5)
G MASS OF CONCRETE ERODED DURING ZIRCONIUM DEPLETION PHASE (MCNZR)
      NG=2.0*NZR
      WRITE(22,62) NG
 62   FORMAT (' MOLES OF GAS PRODUCED                    - ',G13.5)
C NUMBER OF GAS MOLES PRODUCED PER UNIT MASS OF CONCRETE ERODED
      NGC=FH2O/AH2O+FCO2/ACO2
      WRITE(22,63) NGC
 63   FORMAT (' NO. OF GAS MOLES PER MASS OF CONCRETE    - ',G13.5)
      MCNZR=NG/NGC
      WRITE(22,64) MCNZR
 64   FORMAT (' MASS OF GONGRETE ERODED DURING OXIDATION - ',G13.5)
C FIND FS AND AD
      AS0=(2.0*L0+2.0*W0)*H0
```

```
      WRITE(22,65) AS0
 65   FORMAT (' INITIAL SIDEWARD EROSION AREA           = ',G13.5)
      AD0=L0*W0
      WRITE(22,66) AD0
 66   FORMAT (' INITIAL DOWNWARD EROSION AREA           = ',G13.5)
      IF (XED.LT.XES) ASF=(2.0*L0+2.0*W0+8.0*(RS*XFAIL))*(H0+XFAIL)
      IF (XES.LT.XED) ASF=(2.0*L0+2.0*W0+8.0*(XFAIL/RS))*(H0+XFAIL)
      WRITE(22,67) ASF
 67   FORMAT (' FINAL SIDEWARD EROSION AREA - AT FAILURE = ',G13.5)
      IF (XED.LT.XES) ADF=(L0+2.0*(RS*XFAIL))*(W0+2.0*(RS*XFAIL))
      IF (XES.LT.XED) ADF=(L0+2.0*XFAIL)*(W0+2.0*XFAIL)
      WRITE(22,68) ADF
 68   FORMAT (' FINAL DOWNWARD EROSION AREA - AT FAILURE = ',G13.5)
      AD=0.5*(AD0+ADF)
      WRITE(22,69) AD
 69   FORMAT (' AVERAGE DOWNWARD EROSION AREA           = ',G13.5)
      ASAD=0.5*(AS0/AD0+ASF/ADF)
      WRITE(22,70) ASAD
 70   FORMAT (' RATIO OF EROSION AREAS AT FAILURE       = ',G13.5)
      FS=1.0+RS*ASAD
      WRITE(22,71) FS
 71   FORMAT (' FACTOR FOR EROSION AREA AT FAILURE      = ',G13.5,/)
C FIND MASS OF CONCRETE THAT WOULD BE ERODED AT THE TIME EITHER FAILURE
C CRITERIA ARE SATISFIED
      IF (RS.GT.0.0) MCNS=RHOCN*FS*AD*XES/RS
      MCND=RHOCN*FS*AD*XED
C CONTAINMENT FAILURE BEFORE ZIRCONIUM FULLY OXIDIZED?
      MCNMIN=MIN(MCNS,MCND)
      IF (MCNMIN.LT.MCNZR) THEN
C CONTAINMENT FAIL OCCURS BEFORE THE ZIRCONIUM FULLY OXIDIZED
      QR=FH2O*QH2O/AH2O+FCO2*QCO2/ACO2
C SEE EQUATIONS 10 AND 11 OF POSITION PAPER
      TFINAL=(TINIT**0.74+7.8*MCNMIN*(1-FQ*QR/(FS*LCN))
     #  /(Q0*FQ/LCN))**1.35
      WRITE (22,13) TFINAL/3600.0
 13   FORMAT (' CONTAINMENT FAILS BEFORE CONCRETE FULLY OXIDIZED',/,
     #  'AT TIME = ',G10.5,' HOURS',/)
      WRITE (22,14) MCNMIN,MCNZR
 14   FORMAT (' MASS OF CONCRETE ERODED AT FAILURE CRITERIA    = '
     #  ,G10.5,' KG',/,
     #           ' MASS OF CONCRETE ERODED BY ZIRCONIUM OXIDATION = '
     #  ,G10.5,' KG',/)
      GO TO 99
      ELSE
      WRITE (22,15)
 15   FORMAT (' CONTAINMENT FAILS AFTER CONCRETE FULLY OXIDIZED',/)
      WRITE (22,14) MCNMIN,MCNZR
      CONTINUE
      ENDIF
C CONTAINMENT WILL FAIL AFTER ZIRCONIUM DEPLETION. FIND DEPTH OF
```

```
C EROSION CORRESPONDING TO MCNZR INITIALIZATION
      MCNZR=2.0*MZR/AZR/(FH2O/AH2O+FCO2/ACO2)
C
G DO LOOP OVER XSZR,XDZR
      DO 10 I=1,IMAX
      XDZR=XDZR+(XMAX/IMAX)
      XSZR=RS*XDZR
      ADZR=(LO+2.0*XSZR)*(WO+2.0*XSZR)
      ASZR=(2.0*LO+2.0*WO+8.0*XSZR)*(HO+XDZR)
      AD=0.5*(ADO+ADZR)
      ASAD=0.5*(ASO/ADO+ASZR/ADZR)
      FS=1.0+RS*ASAD
      ERROR=ABS(XDZR-MCNZR/RHOCN/FS/AD)/XDZR
      IF (ERROR.LT.0.001) GO TO 20
 10   CONTINUE
 20   CONTINUE
      WRITE(22,75) ERROR*100.0
 75   FORMAT (' ITERATIVE SCHEME CONVERGES ON XDZR TO  = ',G13.5,
     #  ' %')
      WRITE(22,72) FS
 72   FORMAT (' FACTOR FOR EROSION AREA BY ZIRC. OXID. = ',G13.5)
      WRITE(22,73) ADZR
 73   FORMAT (' DOWNWARD EROSION AREA FOR ZIRC. OXID.  = ',G13.5)
      WRITE(22,74) ASZR
 74   FORMAT (' SIDEWARD EROSION AREA FOR ZIRC. OXID.  = ',G13.5)
      WRITE (22,54) XDZR
 54   FORMAT (' THICKNESS ERODED BY ZIRC. OXID.        = ',G13.5)

      TOXID=(TINIT**0.74+7.8*MCNZR*(1-FQ*QR/(FS*LCN))
     #  /(QO*FQ/LCN))**1.35
      WRITE (22,56) TOXID/3600.
 56   FORMAT (' TIME FOR ZIRCONIUM OXIDATION           = ',G13.5,
     #  ' HOURS AFTER SCRAM',/)
C DETERMINE CONTAINMENT FAILURE TIME
      XFAIL=MIN(XED-XDZR,(XES-XSZR)/RS)
      ASCF=(2.0*LO+2.0*WO+8.0*(XSZR+RS*XFAIL))*(HO+XDZR+XFAIL)
      ADCF=(LO+2.0*(XSZR+RS*XFAIL))*(WO+2.0*(XSZR+RS*XFAIL))
      AD=0.5*(ADZR+ADCF)
      ASAD=0.5*(ASZR/ADZR+ASCF/ADCF)
      FS=1.0+RS*ASAD
      MCN=XFAIL*RHOCN*FS*AD
      QR=0.0
C BE SURE TO USE CORRECT VALUE OF LAMBDA - EROSION ENERGY
      TFINAL=(TOXID**0.74+7.8*MCN*(1-FQ*QR/(FS*LCNP))
     #  /(QO*FQ/LCNP))**1.35
      WRITE (22,16) TFINAL/3600.
 16   FORMAT (' CONTAINMENT FAILS AT ',G10.5,' HOURS AFTER SCRAM',/)
 99   CONTINUE
      STOP
      END
```

FAI/91-53

A PHENOMENOLOGICAL EVALUATION SUMMARY ON THRUST FORCES AT REACTOR VESSEL FAILURE IN SUPPORT OF THE KEWAUNEE INDIVIDUAL PLANT EXAMINATION

Submitted To:

Wisconsin Public Service Corporation
Green Bay, Wisconsin

Prepared By:

Fauske & Associates, Inc.
16W070 West 83rd Street
Burr Ridge, Illinois 60521
(708) 323-8750

Final Issue

February 1993

ABSTRACT

Vessel thrust forces, created when molten core debris is ejected from a failed reactor vessel during a severe accident, has been identified as a potential containment failure mechanism. The concern is that such forces could cause the reactor to shift position and tear containment penetrations for piping connected to the primary system.

Based on the assessment contained herein, this postulated mechanism is dismissed from further consideration in the Kewaunee IPE. A basic analysis for the magnitude of the thrust force at vessel failure indicates that this force is comparable to the dead weight of the vessel itself. In addition, the vessel is constrained by the supports for the hot and cold leg nozzles, making it extremely difficult to move the vessel. Even if the vessel could move, the Kewaunee containment is configured so that reaction forces cannot be transmitted to the containment wall. Therefore, this postulated containment failure mechanism is constrained by the plant design basis and no further consideration is merited.

TABLE OF CONTENTS

	Page
ABSTRACT	i
TABLE OF CONTENTS	ii
LIST OF FIGURES	iii
LIST OF TABLES	iii
1.0 PURPOSE	1
2.0 PHENOMENA	2
2.1 Description	2
2.2 Experience	2
2.3 Analysis	5
3.0 METHODOLOGY	7
3.1 Vessel Breach Radius	7
3.2 Vessel Blowdown Jet Thrust Estimate	11
4.0 PLANT-SPECIFIC APPLICATION	15
4.1 Issues	15
4.1.1 Weight of Vessel Structure and Internals	15
4.1.2 RPV Supporting Structure	16
4.1.3 Propagation of Initial Jet Thrust to Containment Walls	18
4.2 Conclusion	20
5.0 SUMMARY	22
6.0 REFERENCES	23

LIST OF FIGURES

Figure No.		Page
1	Kewaunee reactor vessel and supporting structure	3
2	TMI-2 core end state	5
3	PWR calculated mass discharged and breach radius versus time for a LOCA.	9
4	Reactor vessel failure	12

LIST OF TABLES

Table No.		Page
1	Kewaunee Reactor Vessel Internals.	10

1.0 PURPOSE

The potential failure of the containment building due to vessel thrust forces when molten core debris is ejected from the reactor vessel during a severe accident has been a subject of concern for the Nuclear Regulatory Commission (NRG) Staff since the Reactor Safety Study [NRC, 1975] identified it as a possible containment failure mode. The concern is that the thrust force caused by molten core debris being ejected from a failed reactor vessel would be large enough to cause the reactor vessel to shift its position, and pull the steam generator or primary loop piping sufficiently to tear containment penetrations. The timing of the postulated containment failure resulting from this mechanism (i.e., shortly after vessel failure), has potentially important ramifications regarding the radiological source term. Containment functions would be compromised and natural fission product deposition mechanisms would not have sufficient time to significantly affect (reduce) the masses of fission products that could be released through the failure location. In Generic Letter 88-20 [NRC, 1988], the NRC recommends that the magnitude of the vessel thrust force be assessed to determine its potential to cause containment failure. The objective of this paper is to assess the possibility for containment failure due to excessive vessel thrust force for the Kewaunee Nuclear Plant.

2.0 PHENOMENA

2.1 Description

Figure 1 depicts the Kewaunee reactor vessel and its supporting structures. The reactor vessel is supported on six vertical steel H-Columns embedded in the biological shield concrete. Reactor pressure vessel support is designed in such a way as to prevent the vessel from lateral and torsional movement during a design basis accident (DBA) LOCA. The tops of these columns are furnished with ventilated support structures to provide for a suitable temperature gradient between the heated sections of the reactor vessel coming in contact with the support structures. Fitted key slot blocks that are furnished with the reactor and bolted to the support pads provide for free radial thermal expansion of the RPV. Machined keys that are integral with the reactor vessel nozzles and support lugs are shimmied for sliding fits in the key slots and restrain the vessel from movement in any horizontal direction. To shift the reactor vessel and tear containment penetrations, the thrust force generated by corium ejection must be large enough to lift the dead weight of the vessel and its internals, fail the supporting structure, and transmit a sufficient force to the containment walls. This concern is partially addressed by estimating the maximum thrust force which could be generated and comparing it to the vessel weight and the loads necessary to fail the vessel support structure. After considering the maximum thrust force, the plant design should be evaluated to determine if any force that would threaten containment penetration integrity would be transmitted to the containment wall.

2.2 Experience

The quantification of vessel blowdown forces is strongly dependent on assumptions regarding the mode of reactor vessel failure. The only pertinent industry experience which lends insight into the location and size of a reactor vessel failure is the TMI-2 accident. During the TMI-2 accident, ~20 tonnes of molten corium were released to the lower plenum of the vessel, about 224 minutes after reactor scram. Although the accident

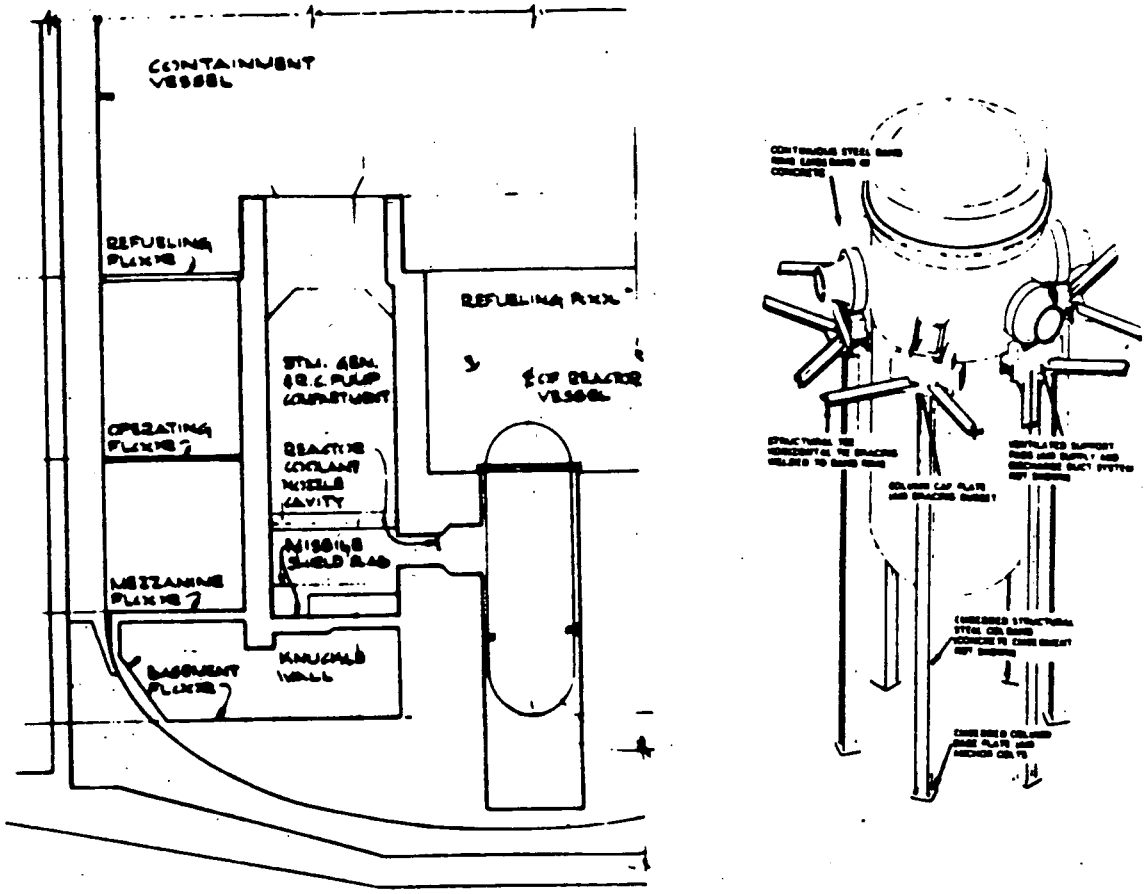

Figure 1. Kewaunee reactor vessel and supporting structure (adapted from [Kewaunee FSAR]).

was terminated by continued cold leg injection, the accident resulted in the end-state condition shown in Figure 2. Video inspection of the lower plenum revealed melt ablation of a lower instrument guide tube, in spite of the fact that the lower plenum was filled with water throughout the accident. The instrument tube did not fail external to the vessel and the debris did not exit the guide tube to the containment atmosphere. This experience, combined with fundamental analyses, strongly suggest that gross failure of the reactor head would occur long after instrument guide tube failure. Cronenberg and Tolsman have made estimates of ablation of both the lower head itself and lower head instrument penetrations for the TM1-2 conditions [Cronenberg and Tolsman, 1989]. To estimate lower head ablation, they considered two cases: conduction limited heat transfer from the debris to the lower head, and a strong jet of molten debris impinging on the lower head, causing an enhanced convective heat transfer process. For the TMI-2 conditions, limited melt ablation of the 5.5" thick head was predicted. Calculations for the ablation of the instrument penetrations, however, indicate potential failure.

2.3 Analysis

Reactor vessel blowdown concerns can be addressed adequately using first principles and readily available plant data. In principle, the jet thrust during vessel blowdown can be found and compared to the vessel and internals weight, as well as to the allowable load on the vessel and supporting structure. To perform this analysis it is necessary to characterize the vessel and containment geometries as well as the actual blowdown itself. While sufficient data is available to determine the problem geometry with a high degree of certainty, the blowdown of molten core debris from the failed vessel is more difficult to quantify. For instance, determining the thrust developed during the blowdown depends on the vessel pressure, core debris mass and density, and vessel failure mode. In the following sections, these uncertainties are addressed to bound the thrust which would result from reactor vessel failure. Furthermore, the vessel dead weight and support structures as well as the containment geometry are evaluated to determine their capability to withstand the blowdown forces.

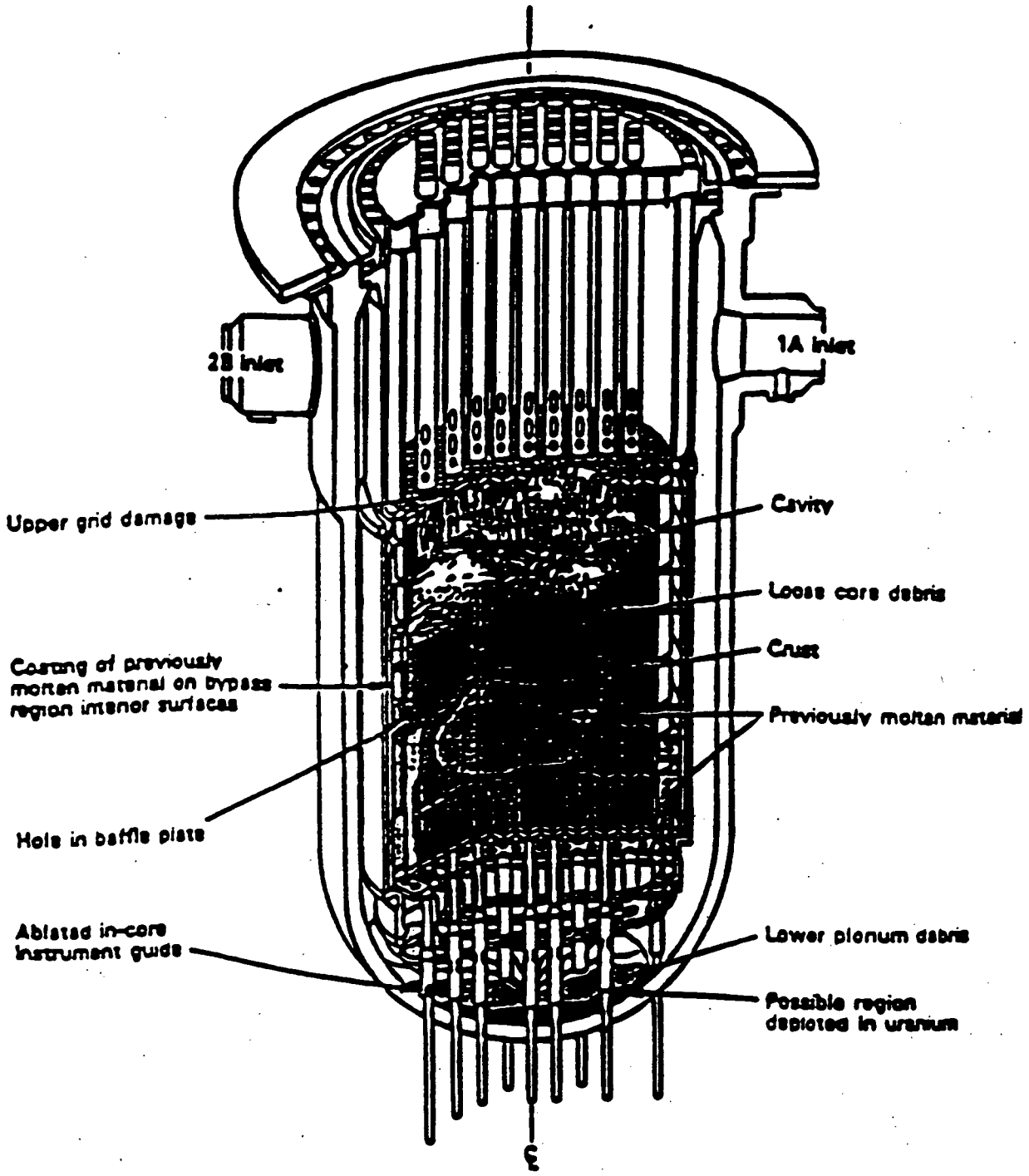

Figure 2 TMI-2 core end state. (From Nuclear Technology, Vol. 87, August, 1989.)

The best estimate assessment of the vessel failure mode is that vessel failure would occur at a lower head penetration. However, if the penetrations were to retain their integrity, the likely failure location would be at or near the surface of the debris pool and would be due to creep rupture. Given the strong temperature dependence of the creep rupture phenomenon, the anticipated failure mode would be a localized failure of the vessel wall, followed by RCS depressurization due to gas blowdown. In this case most of the core debris would remain in the RPV. The close proximity of the cavity wall (Figure 1) to the RPV would restrict any significant sideward movement of the vessel due to blowdown thrust forces.

3.0 METHODOLOGY

3.1 Vessel Breach Radius

Several parameters which characterize the reactor vessel blowdown must be defined to estimate the resulting jet thrust force. Reactor vessel pressure and corium density, two such parameters, can be specified with reasonable certainty, or can be assigned conservative values to ascertain the upper bound for the problem and will not be considered in any detail here. Another key parameter, the vessel failure area, however, is subject to more uncertainty and selecting an appropriate value is less obvious. If the failure area is assumed to be large, say 10 ft^2, the jet force could reach 9 x 10^6 lb_f, albeit only briefly, since the lower plenum debris would be expelled in a matter of seconds through such a large opening. However, it is much more likely that the vessel breach will be the size of a lower head penetration than the size of the vessel diameter. This conclusion is supported by actual plant experience, in the form of the TMI-2 accident, as discussed in Section 2.2.

The consensus in the severe accident community is that the vessel boundary failure will occur at a lower head penetration/vessel clad weld and not in the 6 to 12 in (15-30 cm) thick vessel wall. The MAAP code assumes that failure occurs at the penetration/vessel clad weld rather than by failure of the lower head itself. MAAP requires the number of failed vessel penetrations and the radius of a failed penetration as input parameters to calculate the corium flowrate. The corium flowrate is used to determine the radial heat transfer coefficient to the vessel lower head by the Colburn-Reynolds analogy. The breach radius rate of change is then determined by:

$$\frac{dr}{dt} = \frac{h\left[T_c - T_{s,m}\right]}{\rho_s\left[C_s\left[T_{s,m} - T_s\right] + \gamma_s\right]} \qquad (1)$$

where

h is the radial heat transfer coefficient,
T_c is the corium temperature,
$T_{s,m}$ is the steel melting point,
ρ_s is the density of steel,
T_s is the temperature of intact steel,
γ_s is the heat of fusion of steel, and,
C_s is the heat capacity of steel.

Figure 3 shows that the initial vessel failure size would be the size of a vessel penetration, and the vessel failure radius would continue increasing as melt is expelled until there is no molten material left in the lower plenum. After the molten material has been expelled, the vessel would continue depressurizing as water and/or gases are subsequently expelled through the final hole. At a radius of 8" over 175,000 lbm (80,000 kg), which is about all the possible molten material (see Table 1), have been expelled from the core. This means that to obtain an 8" radius, all the possible molten material in the vessel (fuel, cladding, lower core plate) would have to be molten in the lower plenum at the time of vessel failure. This is physically unreasonable because all the possible molten material cannot accumulate in the lower plenum prior to vessel failure. An IDCOR report on debris coolability [Fauske & Associates, Inc., 1983] shows that upon contact with molten debris, vessel penetrations will be ablated within 60 seconds and vessel failure will begin. It is not reasonable that all the material would melt and accumulate in the lower plenum within this 60 second timeframe.

A second, less probable, mode of vessel failure which has been given some consideration is the direct failure, due to plastic and creep strain, of the reactor vessel lower head shell. This is in contrast to the thermal attack and subsequent failure of a single lower head penetration. Although this vessel failure mode is less physically realistic than the thermal attack of a single lower head penetration, it will result in a larger vessel breach. Thus, this second vessel failure mode will serve as an upper bound on the vessel failure size. Estimates for this larger vessel failure size

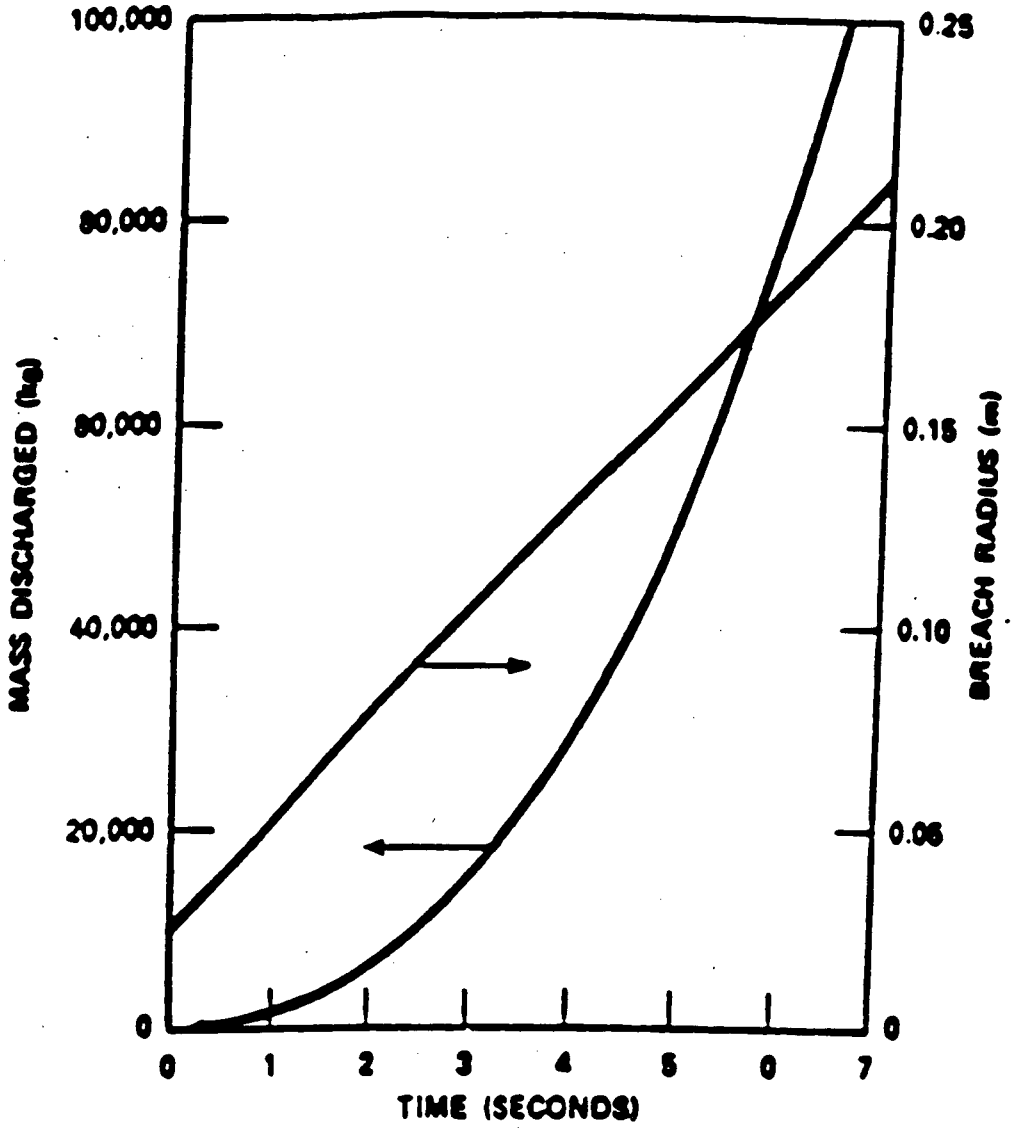

Figure 3 PWR calculated mass discharged and breach radius versus time for a LOCA.

Table 1

KEWAUNEE REACTOR VESSEL INTERNALS

	Initial Masses	
	kg	lbs
Zircaloy Cladding	11,110	24,442
Control Rods & Others	5,410	11,902
UO_2 Fuel	54,060	118,931
Lower Core & Support Plates	1,136	2,500
Upper Core Plates	8,636	18,999
Upper Plenum Internals	50,000	110,000
Core Barrel	70,125	154,600
TOTAL	200,477	441,374

are available from IDCOR [Anderson, 1983] as well as NRC analyses [NRC, 1989]. The IDCOR analysis reports that thermal attack on the vessel lower head would result in a plastic and creep strain induced failure on the order of 2.5 feet in radius. The NRC study, based on expert opinions, considered vessel failure areas up to 2.0 m^2, or vessel failure radii up to 2.6 ft.

To add further conservatism to this analysis, a failure area twice that considered in the studies mentioned above is used here to quantify the upper bound of the vessel breach. Thus, a vessel failure of 4.0 m^2 (i.e., radius of 3.7 feet), is considered. Due to the short duration of the blowdown which would occur as the result of a 4.0 m^2 vessel breach, additional ablation of this initial breach would be negligible and therefore will not be considered here.

In summary, the vessel breach size for this analysis is bounded by a best estimate value based on the failure of a single lower head penetration and a conservative estimate assuming a strain induced failure of the reactor vessel lower head. The best estimate breach radius is specified as 0.67 feet (8 inches) while the conservative upper bound breach radius is 3.7 feet.

3.2 Vessel Blowdown Jet Thrust Estimate

A basic analysis is presented to estimate the jet thrust which could be expected during the expulsion of molten debris through a failed reactor vessel. Figure 4 characterizes the analytical model which will be presented here. Molten corium is ejected through a failure with diameter d into an atmosphere at pressure P_∞. P_v is the reactor vessel pressure and P_e is the pressure at the vessel exit. By conservation of momentum, the jet thrust is given by:

$$F_j = \rho A V^2 + \left(P_e - P_\infty\right) A \qquad (2)$$

where V is the flow velocity, ρ is the corium density, and A is the failure area. For an incompressible fluid, such as molten corium, flow will be subsonic for the conditions of interest here, and P_e can be set equal to P_∞

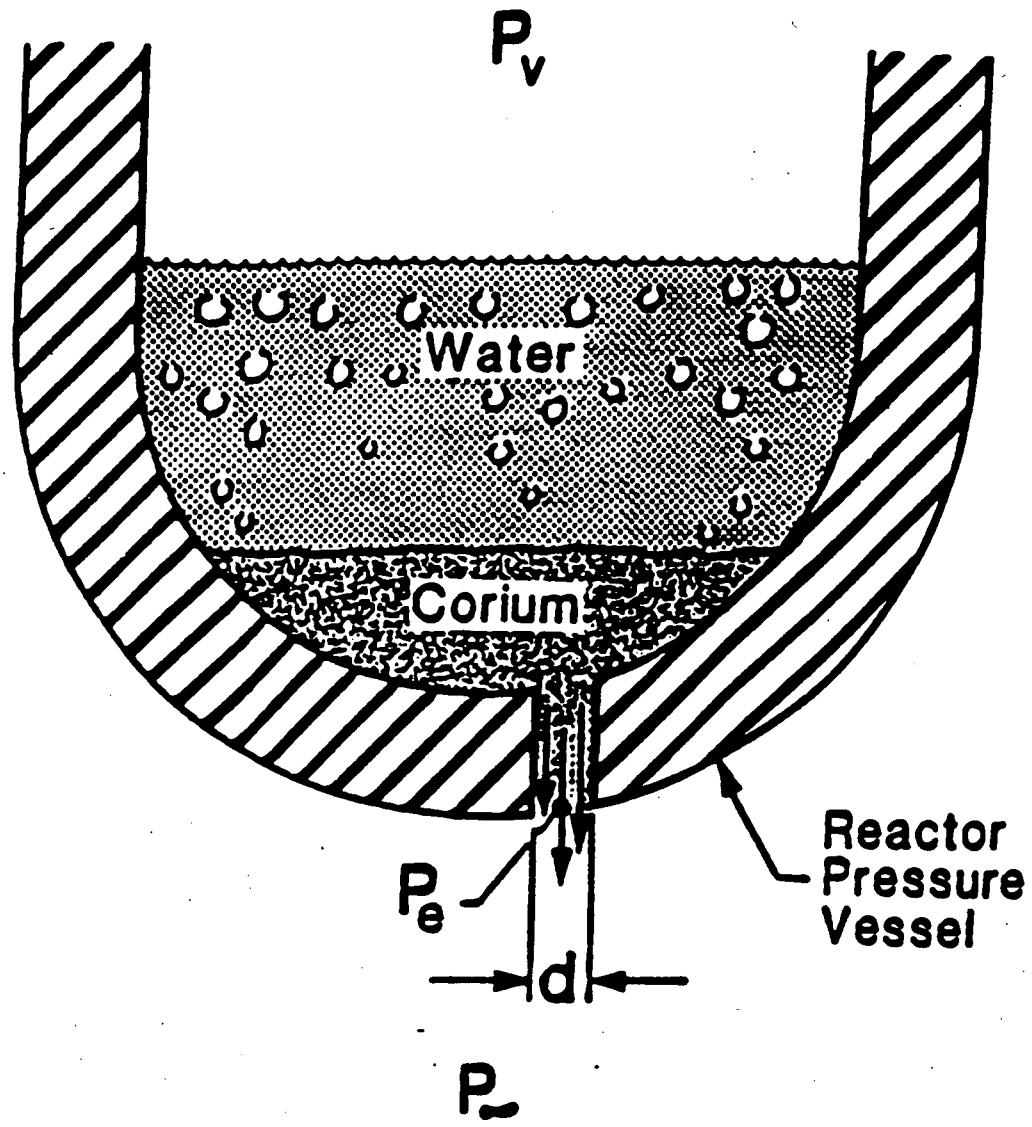

Figure 4 Reactor vessel failure.

to further simplify the jet thrust calculation. The flow will be subsonic because the speed of sound in the fluid melt will be much higher than the flow velocity. Although a value for the speed of sound in molten core material is not available, the speed of sound in other liquids such as water (4885 ft/s) or mercury (4757 ft/s) [White, 1979] is much greater than the expected flow velocity, which might be on the order of hundreds of feet/second. Therefore, to estimate the jet thrust only the flow velocity and failure area must be determined. The density of corium is usually assumed to be ~ 500 lbm/ft^3 (8000 kg/m^3).

Bernoulli's equation is used to estimate the flow velocity:

$$V = \sqrt{\frac{2\left(P_v - P_\infty\right)}{\rho}} \qquad (3)$$

A value of 2500 psia (17.2 MPa) is assumed for P_v to provide a conservative estimate for the velocity. This assumed value, the Kewaunee vessel design pressure [FSAR], provides an upper bound for the pressure driving molten corium out the vessel during severe accident conditions. Flow velocity is relatively insensitive to the atmosphere pressure P_∞, since $P_v \gg P_\infty$. A value of 14.7 psia is assigned to P_∞. These assumptions result in a velocity of 213 ft/s (65 m/s), which is far below the speed of sound in most liquids, thereby verifying the assumption of subsonic flow.

The vessel failure area is evaluated based on the bounding breach radii as discussed in Section 3.1. If the best estimate breach radius of 0.67 ft is used, then the thrust force is

$$F_j = 500\ \text{lb}_m/\text{ft}^3\ (213\ \text{ft/s})^2\ \pi\ (0.67\ \text{ft})^2\ \frac{1\ \text{lb}_f}{1\ \text{lb}_m\ 32.2\ \text{ft/s}^2}$$
$$= 994{,}000\ \text{lb}_f$$

The upper bound on the jet thrust can be conservatively estimated using a failure radius of 3.7 ft as discussed in Section 3.1. Substituting into the expression for jet thrust, this yields

$$F_{j,max} = 500\ lb_m/ft^2\ (213\ ft/s)^2\ \pi\ (3.7\ ft)^2\ \frac{1\ lb_f}{1\ lb_m\ 32.2\ ft/s^2}$$

$$= 30.3 \times 10^6\ lb_f$$

4.0 PLANT-SPECIFIC APPLICATION

4.1 Issues

4.1.1 Weight of Vessel Structure and Internals

The thrust force calculated in Section 3.2 is compared to the combined weights of the reactor vessel and its internals. The mass of the reactor vessel alone, as calculated for the Kewaunee MAAP parameter file [Fauske & Associates, Inc., 1990], is 438,585 lbm. The mass of the vessel internals to be added to this number accounts for all the mass that the jet force must act upon, including those portions of the damaged core (i.e., fuel and cladding) that do melt, as well as the masses of other structures that do not melt, such as the upper plenum internals and the core barrel. Table 1 lists the masses of these components as calculated for the Kewaunee MAAP parameter file [Fauske & Associates, Inc., 1990]. Adding the masses of the internal components to the mass of the vessel results in a total mass of 8.8×10^5 lb_m. This results in an upper-bound estimate of the vessel dead weight of about 8.8×10^5 lb_f, assuming that the entire mass of core debris is in the lower plenum. However, the core debris mass would continually decrease as the debris is expelled. Excluding the combined mass of the fuel, clad, control rods, and the lower core support plate from the total mass calculation yields a lower bound dead-weight estimate of 7.22×10^5 lb_f.

The estimated range for the force necessary to move the vessel and its internals upward, 7.22×10^5 to 8.8×10^5 lb_f, is slightly lower than the best estimate jet thrust value of 9.94×10^5 lb_f. This simple, conservative analysis is done without considering the ability of the vessel support structures to withstand thrust loads. The load bearing capability of the vessel support structure is analyzed below to further demonstrate that the vessel blowdown force is far less than the force needed to move the vessel and thereby tear containment penetrations.

4.1.2 RPV Supporting Structures

Reactor vessel blowdown concerns can be addressed adequately using first principles and readily available plant data. In principle, the jet thrust during vessel blowdown can be found and compared to the vessel and internals weight, as well as the allowable load on the vessel and supporting structure. Plant design should also be considered. Although the basic calculation presented here indicates that these thrust forces are comparable to the vessel weight, the supporting structure for the vessel and the primary system will prevent the vessel from moving. The reactor vessel is supported on six vertical steel H-columns embedded in the biological shield concrete wall (Figure 1). Hot and cold legs penetrate the 7.33' thick reactor shield wall [Pioneer Service & Engineering, 1968]. Restraints are provided for the hot and cold leg pipes in the penetrations of the shield wall. The lateral movement of pipe at the restraint is limited to 1.5" excluding the deformation of the pipe but including the gap [Kewaunee FSAR)].

The shield wall is essentially a rigid structure that will not deform under the loads presented here. To see this, consider the condition necessary to fail the shield wall in compression. This would occur if the imposed stress due to the vessel blowdown jet thrust is greater than the allowable compressive stress of the shield wall concrete, i.e.,

$$\sigma = \frac{F_j}{n\, t_s\, (D_c + D_h)} > S_{ac} \qquad (4)$$

where

σ = imposed stress,

F_j = jet thrust (Equation (1)),

S_{ac} = allowable compressive stress in bearing,

t_s = shield wall thickness,

D - pipe diameter, and

n - number of steam generator loops.

Subscripts c and h are for the cold and hot legs, respectively. The following values are used:

F_j - 999,000 lbs

S_{ac} - 4000 psi [Kewaunee FSAR]

D_c - 27.5 in [Kewaunee FSAR]

D_h - 29 in [Kewaunee FSAR]

t_s - 7.33 ft [Pioneer Service & Engineering, 1968]

n - 2 [Kewaunee FSAR]

which results in σ - 100.5 psi.

This is far below the allowable compressive stress of 4000 psi. Therefore, the integrity of the shield wall will not be threatened by jet thrust forces under the postulated conditions.

Jet thrust forces at vessel failure will not damage the hot and cold leg piping. The upward thrust force will tend to place the hot and cold leg piping in shear because the piping is constrained by the reactor shield wall; the thrust will tend to cause a guillotine rupture in the legs. The thrust force necessary to cause this is estimated from:

$$F = \tau n \pi (D_c t_c + D_h t_h) \qquad (5)$$

where,

τ - allowable shear stress,

D = pipe diameter (D_c = 27.5", D_h = 29"),

t = pipe thickness (t_c = 2.6875", t_h = 2.8125"),

c = subscript for cold leg,

h = subscript for hot leg,

n = 2.

Hot and cold leg pipe diameters are chosen for conservatism. Actually the reactor vessel nozzles, which are much thicker than the piping itself, would bear most of the thrust force. Dimensions for the piping are obtained from Table 4.1-2 of the FSAR. The allowable shear stress is assumed to be the ultimate shear strength of stainless steel. This is 50,000 psi [Machinerys' Handbook, 1989].

Substituting these values into equation (5) gives a force of 48.8 x 10^6 lb_f. For this force, a failure radius of 4.7 ft is required, based on equation (1). This is 85% of the inner radius of of the cylindrical part of the RPV, thereby making a force of 48.8 x 10^6 lb_f impossible. Moreover, the failure radius is likely to be much less than the vessel radius, so the integrity of the hot and cold legs will remain intact.

The only question that remains is whether or not the displacement of the hot and cold legs, the maximum displacement the shield wall would allow, would also cause a shift in the rest of the primary system. This is not credible, due to the system of restraints for the hot and cold legs, as well as the steam generators. In addition, as discussed in the following section, this dislocation cannot be transmitted to containment walls where the penetrations are located.

4.1.3 Propagation of Initial Jet Thrust to Containment Walls

It is also useful to consider other analyses of jet thrust loads that are part of the design basis for the Kewaunee plant. On page 5.9.7 of the

Kewaunee FSAR, the jet thrust loads from rupture of various pipes used in compartment structure design are listed:

Break Location	Jet Force
Primary loop hot leg	1800 kips
Primary loop cold leg	1600 kips
Crossover (pump suction leg)	2250 kips
Steam line	813 kips
Feedwater line	277 kips

With the exception of the feedwater line break location, the listed jet forces are comparable to or greater than the jet force calculated for vessel failure. This is further demonstration that jet thrust at vessel failure will not affect containment integrity. Since Kewaunee compartment structures were built to withstand a jet force of 1800 kips and 1600 kips in the hot and cold legs, there is no reason to believe that a force of 999 kips at the reactor vessel bottom would affect the hot or cold legs; the same goes for the pump suction leg.

Plant design precludes transmission of jet forces to the containment at penetrations. To addreess this point, consider Section 5.9 of the Kewaunee FSAR:

> "The reactions of jet forces in primary loop piping caused by pipe rupture, are restrained by means of heavy structural steel weldment brackets rigidly anchored at various points throughout the internal concrete structures. In order to limit the asymmetric LOCA loads for the postulated reactor coolant pipe break in the nozzle region, restraints have been provided for the hot and cold leg pipes in the penetrations of the reactor shield wall."

and Section 5.2.1:

> "The main steam piping between the anchor inside containment and the first isolation valve outside of the containment has a wall thickness selected by using 1.5 times the system pressure and normal code allowable stress values. The main steam piping anchor inside containment is designed to sustain the full force resulting from a 360° circumferential break of the main steam piping."

This passage indicates any reactor coolant loop piping which penetrates the containment will shear off at the internal concrete structure anchor located inside and close to the containment vessel wall, assuming that it is subjected to a large enough jet force, rather than tearing the containment penetration. The containment penetration will be unaffected by the jet force and containment isolation will be maintained. This conclusion is further supported by the following item from Section 5.3.1 of the Kewaunee FSAR:

> "Leakage through all fluid line penetrations not serving accident-consequence-limiting systems is minimized by a double-barrier. The double-barriers take the form of closed pipe systems, both inside and outside the Reactor Containment Vessel, and various types of isolation valves. The double-barrier arrangement provides two reliable low-leakage barriers between the Reactor Coolant System or containment atmosphere and the environment. The failure of any one barrier will not prevent suitable isolation."

Based on these statements, it is concluded that the Kewaunee Nuclear Power Plant can withstand the jet thrust force applied to the reactor coolant system at vessel failure without failing containment penetrations. Therefore, because a sufficient jet thrust force to displace reactor system piping cannot be developed, and because such a force would not fail the containment anyway, this containment failure mode is not a concern for the Kewaunee IPE.

4.2 Conclusion

The preceding calculations show that the expected jet thrust force at vessel failure would be about 9.94×10^5 lb_f. If the coolant loop piping and shield wall are considered then a force of at least 48.8×10^6 lb_f would be required to dislodge the reactor vessel. This far exceeds the expected 9.94×10^5 lb_f jet thrust as well as the 30×10^6 lb_f upper bound on the blowdown force. Thus, displacement of the reactor vessel under any plausible reactor vessel failure conditions will not occur. Based on the containment design described in the Kewaunee Safety Analysis Report it is concluded that the Kewaunee Nuclear Plant can withstand the jet thrust force applied to the reactor coolant system at vessel failure without failing

containment penetrations. Containment failure due to blowdown forces acting on the reactor vessel and reactor system piping is not a concern for the Kewaunee Nuclear Plant.

5.0 SUMMARY

Calculations have been performed to determine the jet thrust which would result from failure of the Kewaunee reactor vessel lower head induced by thermal attack of molten core debris. Additional calculations have been presented to investigate the force required to fail the reactor vessel structural supports (i.e., failure of the primary loop piping or the reactor shield wall) and overcome the reactor vessel dead weight. Based on the results of these calculations, it is apparent that the expected jet thrust at vessel failure is not sufficient to prematurely fail the containment by tearing containment penetrations. Furthermore, it is not conceivable that, in any case, sufficient thrust forces could be generated to displace the reactor coolant system piping. Therefore, because sufficient jet thrust force to displace the reactor coolant system cannot be developed, and because such a force would not fail the containment anyway, this containment failure mode is not a concern for the Kewaunee Nuclear Plant.

6.0 REFERENCES

Anderson, L. E., et al., 1983, "Effects of Hypothetical Core Melt Accidents on a PWR Vessel with Top-Entry Instruments", IDCOR.

Cronenberg, A. E., and Tolsman, E. L, 1989, "Thermal Interaction of Core Melt Debris with Three Mile Island Unit 2 Vessel Components", Nuclear Technology, Vol. 87.

Fauske & Associates, Inc., 1983, Final Report on Debris Coolability Vessel Penetration and Debris Dispersal, IDCOR Technical Report 15.2B.

Fauske & Associates, Inc., 1990, "Kewaunee Nuclear Plant MAAP Parameter File."

IDCOR, 1983, IDCOR Technical Report 10.1, "Containment Capability of Light Water Nuclear Power Plants".

IDCOR, 1983b, "MAAP Users Manual," IDCOR Technical Report 16.3, Fauske & Associates, Inc.

Kewaunee FSAR, "Kewaunee Nuclear Power Plant Final Safety Analysis Report," Wisconsin Public Service Corporation.

Machinery's Handbook, 1984, 22nd Edition, Industrial Press Inc., New York.

NRC, 1975, "Reactor Safety Study - An Assessment of Accident Risks in U.S. Commercial Nuclear Power Plants", U.S. NRC Report WASH-1400 (NUREG-75/014), 1975.

NRC, 1988, NRC letter to all Licensees holding Operating Licenses and Construction Permits for Nuclear Power Facilities, "Individual Plant Examination for Severe Accident Vulnerabilities - 10 CFR 50.54(f)", Generic Letter No. 88-20.

NRC, 1989, "Severe Accident Risks: As Assessment for Five U.S. Nuclear Power Plants", U.S. NRC Report, NUREG-1150.

Pioneer Service & Engineering, 1968, "Kewaunee Nuclear Power Plant General Arrangement Cross Section Drawing No. 237127A-A210."

White, F. M., 1979, "Fluid Mechanics", McGraw-Hill Book Company, New York.

FAI/91-119

A PHENOMENOLOGICAL EVALUATION SUMMARY ON THERMAL LOADING OF CONTAINMENT PENETRATIONS IN SUPPORT OF THE KEWAUNEE NUCLEAR PLANT INDIVIDUAL PLANT EVALUATION

Submitted To:

Wisconsin Public Service Corporation
Green Bay, Wisconsin

Prepared By:

Fauske & Associates, Inc.
16W070 West 83rd Street
Burr Ridge, Illinois 60521
(708) 323-8750

Final Issue

September 1992

ABSTRACT

This phenomenological evaluation summarizes an assessment of the susceptibility to failure of the containment penetrations due to thermal loadings that may occur during postulated severe accidents. The failure of the leak tightness of containment penetrations could provide a pathway through the containment structure for the release of fission products. This paper addresses the mechanical and electrical penetrations, the personnel airlocks, and the equipment hatch in the Kewaunee containment.

The assessment concludes that the postulated thermal loadings due to severe accidents in the Kewaunee containment will not cause failure of the various containment penetrations. Thus, failure of the containment boundary due to penetration failure will not be included as a separate node for long term containment failure in the event tree for the Kewaunee containment.

TABLE OF CONTENTS

	Page
ABSTRACT	i
1.0 PURPOSE	1
2.0 PHENOMENA	2
2.1 Description	2
2.1.1 Controlling Physical Processes	3
2.1.2 Relationship to Containment Failure Mechanisms and Modes	5
2.1.3 Relationship to Source Term	6
2.2 Experimental Results	8
2.2.1 Sandia/INEL Severe Accident Seals and Gaskets Test Program	8
2.2.2 Sandia/CBI Personnel Airlock Testing	10
2.2.3 Sandia Electrical Penetration Assemblies Program	12
2.3 Analyses	15
3.0 METHODOLOGY	19
4.0 PLANT SPECIFIC APPLICATIONS	22
4.1 Issues	22
4.1.1 Penetration Designs	22
4.1.2 Penetration Locations	28
4.1.3 Potential Severe Accident Conditions	28
4.2 Assessment of Impact of Severe Accident Conditions	30
4.2.1 Assessment of D. G. O'Brien EPAs	32
4.2.2 Assessment of Conax Penetrations	34

TABLE OF CONTENTS

	Page
4.3 Uncertainties	38
4.4 Conclusions	38
5.0 SUMMARY	40
6.0 REFERENCES	41

LIST OF FIGURES

Figure No.		Page
4-1	Typical cold piping penetration	23
4-2	Typical hot piping penetration	24
4-3	Electrical penetration assembly (D. G. O'Brien)	25
4-4	Single electrical penetration (D. G. O'Brien)	26
4-5	Electrical penetration assembly (Conax Design)	27
4-6	Containment gas temperatures in annular compartment	35
4-7	Volatilization rate of polysulfone and Kapton	37

LIST OF TABLES

Table No.		Page
2-1	Summary of Compression Seal Test Results	10
2-2	Electrical Penetration Design Parameter Summary	15
4-1	Summary of Elevations of Large Penetrations	29
4-2	Summary of Typical Containment Region Temperatures	31

1.0 PURPOSE

Potential containment penetration failures attributable to thermal loading conditions following reactor vessel breach in severe accidents is a containment performance concern identified by the Nuclear Regulatory Commission (NRC) Staff, NRC contractors, and the nuclear industry. Long term exposure of non-metallic materials to elevated temperatures (thermal loading) accelerates degradation of such materials such that their functionality is reduced or lost. Containment atmosphere heating by molten core debris and the resulting high containment temperatures could adversely affect the integrity of penetration non-metallic seal materials, and could subsequently produce a containment failure flow path to the auxiliary building. The timing and location of containment failures associated with this mechanism (i.e., long after vessel failure) could have potential ramifications with respect to radiological source terms.

In Generic Letter No. 88-20, the NRC recommends that the capability of containment penetrations to withstand high temperature conditions be assessed to determine the potential for containment breach. This paper's objective is to develop a strategy to account for thermally induced containment penetration failures in the source term portion of the Kewaunee IPE.

2.0 PHENOMENA

2.1 Description

Compression seals and gaskets form an important part of the containment pressure boundary in many operable mechanical penetrations, such as equipment hatches and personnel air locks. If metal-to-metal contact does not exist between the sealing surfaces of these penetrations, the gaskets represent the only barrier to prevent leakage through the containment boundary at these locations. There are also electrical penetration assemblies (EPAs) which are used to provide a leak-tight pass-through for electrical cables. Typical penetration seal materials include ethylene propylene (EPDM), silicone, and neoprene.

Potential loading conditions for containment penetrations are produced by the dynamic and static pressure and temperature variations that may occur during severe accidents within the containment. Several mechanisms for producing localized loading conditions during severe accidents could be postulated. These mechanisms could include the global heating and pressurization of the containment atmosphere by postulated severe accident phenomena such as direct containment heating, hydrogen burns, or core-concrete interactions. Additionally, these postulated mechanisms could include direct impingement by or submergence of penetrations in dispersed core debris, localized hydrogen burns or detonations, or heating by deposited fission products. The potential loadings due to pressurization are considered in the Containment Overpressurization position paper and potential loadings due to localized hydrogen burns or detonations are considered in the Hydrogen Combustion position paper. Direct impingement or submergence in debris of the penetrations is precluded in Kewaunee by the physical layout of the containment and the location and segregation of the mechanical and electrical containment penetrations. Very long term degradation of non-metallic components during accident management and recovery actions should be addressed in the Kewaunee equipment survivability study. The potential for containment penetration failure by thermal loading is the subject of this evaluation.

Containment penetration thermal loading is a postulated event in which penetration non-metallic seal materials are exposed to elevated containment temperatures for prolonged time periods during a severe accident. It has been hypothesized that following vessel failure, containment gas temperatures may reach sufficient levels to reduce penetration seal leakage control performance to the extent that a containment breach effectively occurs at an earlier point than the failure times associated with other potential long term containment failure mechanisms (i.e., overpressurization or concrete ablation induced failures). The impact on containment failure timing thus depends on the gas temperatures achieved, the exposure time at elevated temperatures, and the characteristics of the materials involved.

2.1.1 Controlling Physical Processes

The basic issues related to penetration thermal loading are the differences, if any, between the anticipated design basis and severe accident thermal loadings for non-metallic penetration seal materials, and the potential for accelerated adverse thermal effects on material properties that influence sealing performance. In regards to thermal loadings, previous studies [IDCOR, 1983] indicate that at elevated containment gas temperatures and pressure, containment failures attributable to mechanical responses are likely to supersede concerns about non-metallic materials performance. Consequently, the thermal loading interval that should be addressed for an IPE severe accident assessment is the period preceding containment failure. Particular attention should be given to the portion of this period following vessel failure, when temperatures beyond the anticipated design basis temperature profile are most likely to be encountered. Section 4.2 of this document assesses the amount of degradation for Kewaunee penetrations during this interval.

The physical processes which impose thermal loads on non-metallic penetration materials in severe accidents are considered to be fundamentally the same as those processes addressed for design basis environmental qualification work. Penetrations employing non-metallic components and/or compounds, are equipped with at least a two-stage seal boundary. The first seal is internal to the containment (inboard), and the second, mechanically

and thermally in series with the first is the external containment boundary (outboard). This arrangement indicates that at the outset of any given accident sequence, heat will be transferred directly to the inboard seals by convection as gases move across exposed seal surfaces or as steam condenses on them. The gas flow rate required to support a significant degree of convection is not precisely calculated in this evaluation but it is conservatively assumed so that the exposed seal surface temperature will not lag behind the containment gas temperature. Apart from any existing leakage paths however, the portions of inboard seal surfaces that perform the sealing function are at least partially protected from convection by the structures in contact with them. As the event progresses, these structures will begin to conduct heat to the functional seal surfaces, especially after the saturation point is attained. Later yet, the inboard penetrations may also experience radiation heat transfer from core debris.

Heat transfer to outboard seals is expected to be principally by conduction. As was the case for the inboard seals, heat absorption by the penetration components preceding thermal saturation and heat losses via conduction to the containment liner and wall would delay outboard seal thermal loading. A small amount of convection may occur due to direct contact with containment gases from any inboard seal leakage should it occur. Nevertheless, the overall convective contribution to outboard seal thermal loading is expected to remain small, in absolute terms and compared to conduction, at all times preceding significant loss of inboard seal performance. From that point forward, outboard seal thermal loading is expected to occur through essentially the same, albeit delayed, process progression as inboard seal thermal loading. In total, it appears reasonable that between the intrinsic lag time associated with conduction and heat losses and the minor convection influence, outboard seals will be no more vulnerable to thermal degradstion than the inboard seals in either design basis or severe accident events.

It is also reasonably clear that for both seals, there are no inherent severe accident characteristics, including vessel failure and containment atmosphere heating by core debris, that distinguish them from design basis events in terms of noticeably altering the penetration seal thermal loading

processes. Beyond that, the driving physics associated with heat flux application to penetration seals is consistent between design basis and severe accidents. Following vessel failure in a severe accident, containment gas temperatures beyond those addressed for design basis events could be expected to accelerate aging effects for non-metallic parts, including dry-out, shrinkage, embrittlement, cracking or fragmentation, and possibly melting.

The general issue is the extent and timing of all such responses. Whether severe accidents or design basis events, temperature effects on the seals are not expected to differ in physical form. Therefore, the goal of Section 4 is to evaluate the potential for severe accident temperature profiles to degrade penetration seal performance to the point of significantly increasing the fission product release source term. The specific question is whether or not total thermal loads applied to the seals at the time and temperature preceding the 700°F limit will produce the same containment leakage and fission product release rates that may be attributable to other mechanisms upon reaching this limit. Further explanation of the basis of the 700°F limit is mentioned, in detail, in Section 2.2.1.

2.1.2 Relationship to Containment Failure Mechanisms and Modes

Loss of penetration integrity (pressure boundary) due to thermal attack represents a potential containment failure mode that would be distinguishable at a point several hours after reactor vessel failure in most severe accident sequence progressions. The largest potential for penetration failure due to thermal loading is expected to coincide with core melt accidents where ex-vessel debris coolability and subsequent containment heat removal capabilities are unavailable. Station blackout (SBO) events, pipe break in containment, loss of coolant accidents (LOCA), and transients with all vessel injection and containment heat removal facilities disabled, fall within this category. Amongst these, events that lack primary system depressurization in advance of vessel failure would be expected to have the minimum amount of time available preceding containment failure due to penetration thermal attack. This would result from dispersal of water in the cavity and early debris dryout.

The anticipated containment failure mechanism related to penetration thermal loading is excessive leakage flow from the containment to the auxiliary building, or directly to the environment after vessel failure that results from penetration seal interface thermal degradation. The leakage area that may be observed depends on the containment gas temperature levels achieved, the accident sequence time duration at elevated temperatures, the coinciding containment pressures, and the specific thermal response characteristics of the non-metallic seal materials involved. Individual penetration seal failures would each yield a very small leakage flow area, but efforts to precisely quantify the overall leakage area for any given severe accident sequence are made difficult by the potential for concurrent pressure, nuclear radiation, or chemical interaction impacts on seal condition. On the other hand, it is considered reasonable that even in rapidly occurring accident scenarios, significant increases in the total containment leakage area via this mechanism would be noted at least several hours after vessel failure, and would then develop at a relatively gradual pace (although possibly accelerating).

In the brief period directly after vessel failure, a gas temperature spike may be detected in the reactor cavity that reaches a peak of approximately 450-550°F. However, this temperature spike in the cavity does not generate a perceptible temperature impulse in the annular and upper compartments where the penetrations are located. This means that the integrated heat energy that could potentially be delivered to the inboard penetration seals at vessel failure would be essentially negligible, and from a practical standpoint, extremely unlikely to produce any noticeable impact on seal thermal degradation progress. The largest leakage area increase rates are expected to be encountered only in the final stages preceding containment failure. It is also quite possible that seal material displacement aside, the total leakage area developed would be insufficient to support containment depressurization. The containment leakage is likely to be self limiting instead of catastrophic.

2.1.3 Relationship to Source Term

Penetration thermal attack leading to containment failure influences the anticipated fission product source term by creating gas flow paths out of containment following vessel failure. Initially disregarding the individually small (and likely narrow) flow paths potential to promote substantial aerosol plugging, such paths could limit the effectiveness of fission product retention mechanisms. Given the large likelihood that flow path development will occur over a span of several hours following vessel failure, fission product retention mechanisms that occur within this period can be expected to diminish the airborne source term inventory prior to the development of an enhanced leakage area.

To begin with, corium-concrete interactions may be initiated during this time frame in cases where an adequate water supply is not available for debris coolability. The possibility that at least some quantities of non-volatile fission product aerosols as well as noble gases and volatile fission products will eventually move through penetration seal leakage flow paths cannot be dismissed as out of hand. Another occurrence of a physical nature that may bear some mention is the potential for revaporization of fission products previously deposited on heat sink surfaces (largely within the primary system). Airborne fission product masses attributable to revaporization, and that could presumably exit the containment before it reaches failure, would almost certainly be minor if distinguishable at all. Nevertheless, in conjunction with seal degradation, such an event could be loosely construed as an adverse source term effect potentially facilitated by penetration thermal attack.

Events generated through operator actions can also influence the relationship between penetration thermal loading and the source term. Activating containment heat removal processes and/or initiating (or recovering) vessel injection systems after vessel failure would fall into this category. As another example, if containment sprays are available they would remove significant fission product aerosol masses. Spray usage will also reduce and stabilize containment pressure. Consequently, this will

reduce the differential pressure that would drive fission products through penetration seals once they were degraded.

The time available following vessel failure and prior to potential penetration seal leakage would also allow for substantial fission product retention through naturally occurring deposition mechanisms. Aerosol inertial impaction, gravitational sedimentation, and hygroscopic removal will all occur.

There are two definitive points that best describe the relationship between penetration thermal degradation and associated severe accident source terms. First and foremost, no significant increases in seal leakage, and therefore no serious fission product release contributions, will be detected in the time period directly after core damage (melt). The largest and most intense fission product masses enter containment during this period, and in light of the delayed, slowly developing nature of the containment failure area, it is reasonably clear that apart from inert gases, large proportions of these masses will be permanently deposited in the containment or failure path (penetration). The release of inert gases may begin somewhat earlier (although at a reduced release rate) in various sequences due to thermally accelerated seal leakage, however the total release mass is not expected to be noticeably affected. Secondly, the most noteworthy releases related to penetration thermal degradation would likely be recognized in conjunction with corium-concrete interaction.

2.2 Experimental Results

Several experimental studies have been performed and documented that provide valuable insights regarding penetration thermal degradation under elevated temperature conditions. This work was primarily performed by Sandia National Laboratories and Idaho National Engineering Laboratory (INEL), and focuses on physical responses of commonly utilized penetration non-metallic materials to thermal and thermal/radiation aging. Descriptions and results summaries for some of these efforts follow.

2.2.1 Sandia/INEL Severe Accident Seals and Gaskets Test Program

In this recent test series (reported in [Brinson and Graves, 1988; Bridges, 1987]), samples of typical penetration seal materials and cross-sectional shapes were placed in a pressurized (143 - 160 psig) test fixture, and exposed to slowly increasing temperatures. The tests were conducted in two sets; one without any gap between the fixture mating surfaces (i.e. metal-to-metal) and the other with a fixed gap. Sample materials included ethylene-propylene (EPDM), silicon, and neoprene synthetic rubbers, and some sample sets were radiation aged in advance. For the EPDM and silicone materials, the atmosphere compositions used were nitrogen, steam, and air, while only nitrogen was used for neoprene. In each test, a record was made of the temperature at which significant seal leakage was detected.

Although not unexpected, one of the more interesting results was that irrespective of material, shape, or atmosphere composition, none of the metal-to-metal tests yielded leakage considered significant up to the 700°F maximum temperature. In the fixed gap tests (Table 2-1), the lowest notable leakage (failure) temperature was 460°F for neoprene, and the highest was somewhere beyond 700°F for silicon rubber in dry nitrogen. Within this range, it was intriguing to note that EPDM was affected by atmosphere composition differences far less than the silicon rubber. Although EPDM had a much lower maximum failure temperature, 669°F (in steam), it also had a far higher minimum failure temperature than silicon. In fact, EPDM leakage occurred within a relatively narrow band of 557 - 669°F regardless of atmosphere makeup, while the silicon rubber failures varied widely from a low of 486°F (steam) to the high of > 700 °F (nitrogen) already mentioned. Only one test was performed in air for each of these materials, and these were apparently restricted to a circular cross-section. However, temporarily setting aside obvious database limitations, there was again some indication that silicon rubber is more sensitive to atmosphere composition than EPDM in terms of failure temperature reduction. The results summary [Clauss and Parks, 1989] suggests that oxygen present in steam and/or air facilitates what is likely to be an oxidation process. This line of thought was further supported by commentary provided in the results summary to the

Table 2-1

SUMMARY OF COMPRESSION SEAL TEST RESULTS

Material	Number of Tests	Test Environment	Range of Failure Temperature (°F)	Mean Failure Temperatures (°F)
EPDM	5	Steam	626-669	647
	8	Nitrogen	577-667	613
	1	Air	651	651
Silicone	8	Steam	486-592	512
	2	Nitrogen	> 700	> 700
	1	Air	681	681
Neoprene	3	Nitrogen	460-500	487

effect that post-test examinations revealed charring and a powdery consistency in some samples. Though not stated explicitly, it can be inferred from the data that although these observations likely applied to both the silicon and EPDM samples, the silicon rubber was probably affected to a larger extent. Whether oxidation or another chemical reaction took place, the data seemed to imply that EPDM failure temperatures were more consistent and slightly higher on average in oxygenated environments than they were in nitrogen. The physical basis for such indications is not clear at the moment (they could eventually be considered anomalous), but at the minimum they slightly enhance the belief that degrading chemical reaction influences on the EPDM were minimal within the test environments and temperature range.

Other evidence provided by these tests included what was generally described as an overall loss of springback (i.e., resiliency) properties. The importance of this particular effect relative to the penetration thermal degradation issue per se is considered minimal, as it does not dimensionally distort or displace seal material (so as to create leakage paths). However, it may be a consideration with respect to containment failure mechanisms expected to follow penetration seal thermal degradation, including thermally induced dimensionsl responses of structures in contact with the seals. For any response that tends to draw a structure away from a seal component, a loss of seal material springback would then increase the leakage path flow area because of the seal's reduced ability to expand into the developing gap. In contrast, the observed effect that does have a more direct bearing on the matter at hand is that in all of the fixed gap tests other than the silicon rubber - nitrogen set, it was apparent that seal shrinkage and/or other dimensionsl reduction processes must have indeed occurred to produce leakage rates sufficient to represent failures. The powdery consistency previously mentioned for some of the samples could be indicative of such a process, taking the form of superficial surface disintegration (or fragmentation). Any shrinkage evident might have been produced through melting and subsequent evaporization, or sublimation of certain constituents within the seal material matrix.

Certain results absent from this test program may be as meaningful from a practical standpoint as results that were attained. As an example, there were apparently no extensive mass losses for any samples in any test atmosphere, despite the degradation effects observed. Seal performance was definitely diminished, but not to an extent effectively equaling complete seal removal, which was the potential maximum discussed earlier (Section 2.1.2). The point is that as far as the materials and shapes addressed in the tests are concerned, it could be feasible to better define (and hopefully reduce) leakage flow area upper limits, and consequently the extent of impacts on severe accident source terms.

2.2.2 Sandia/CBI Personnel Airlock Testing

In this test program, an actual full-scale airlock assembly (surplus from a cancelled PWR; Callaway Unit 2) was subjected to environmental conditions considered applicable to certain design basis (LOCA) and severe accident events. The gasket material used in this airlock assembly was EPDM. In general terms, the overall objective of the program was to study potential adverse impacts on the pressure integrity of such devices attributable to these conditions. The conduct and results of these efforts are detailed in [Julien and Peters, 1989].

For most if not all of the individusl tests performed, it appears that the primary focus of attention was on mechanical pressurization responses of assembly structures that could tend to facilitate leakage. In one case however, the test conditions involved, and results achieved, were particularly relevant to the penetration thermal degradation issue. The airlock inner door (inside containment) temperature was held at 650°F while the atmosphere (air) temperature inside this airlock was raised to > 800°F. Pressure inside the containment (i.e., corresponding to the containment side) was then increased from ambient to ~ 150 psig, and at this point significant leakage through the inner door (inside containment) seals was detected. Leakage presumably initiated to some lesser extent at a lower pressure, distinctions between seal material and structure response effects promoting leakage were not entirely clear, and the test pressure upper limit almost certainly far exceeded containment pressures expected during the

penetration thermal loading time period of concern for virtually all foreseeable severe accident sequences. Regardless of these factors, it was important to note that under test conditions pertinent to penetration thermal attack, the EPDM seal material apparently responded in a manner that was highly consistent with findings from the experiments discussed in the preceding section (2.2.1).

Perhaps even more importantly, no leakage developed through the airlock assembly outer door seals, primarily due to the simple fact that the outer door temperature was significantly lower than the 650°F inner door temperature. The implication is that for any typical inboard/outboard penetration seal arrangement, the benefit of potential heat loss to passive heat sinks via inner and outer seal connecting structures should not be arbitrarily reduced to that of a simple conservatism in the overall source term evaluation process. It appears reasonable that the total thermal energy inputs to outer (containment boundary) seals could be noticeably less than the total imposed on inner seals. Therefore analytical measures used to specify or bound seal failure times, as well as fission product release leakage flow areas, should at least attempt to take advantage of this point within the limits of sound engineering judgement.

2.2.3 Sandia Electrical Penetration Assemblies Program

This comprehensive program included testing directly aimed at both PWR and BWR electrical penetration assembly (EPA) containment leakage control performance and electrical functionality under severe accident conditions. Three electrical penetration assembly designs - one each by Conax, D. G. O'Brien and Westinghouse - were tested as part of the Electrical Penetration Assemblies Program at Sandia, as described in [Clauss, 1989]. These tests were aimed at containment leakage control performance and electrical functionality under severe accident conditions, and they provide a good representation of the different seal materials used in containment applications. Generally speaking, the tests were patterned after typical plant design basis environmental qualification (EQ) programs conducted in the past, with the exception that the test pressure and temperature were far above the limits used for design basis work.

Sample preparation included radiation and thermal aging adequate to emulate the anticipated end of service life physical state of the device. The PWR EPAs tested were various models in the D. G. O'Brien design (see Table 2-2 for various model numbers tested). A majority of the EPAs installed at Kewaunee are D. G. O'Brien designs, with the remainder of EPAs designed by Conax. According to some of the literature available about this test [USNRC, 1980], preparatory aging met and to some degree exceeded harsh environmental aging levels of past EQ programs. Following this initial phase, the test itself was performed by exposing the PWR EPAs to pressures of 155 psig and temperatures of 361 °F for a period of ten days, and monitoring to detect leakage development and/or electrical dysfunction. The correspondence to pressure and temperature conditions that apply to the overall penetration thermal degradation concern and preceding experimental program discussions should again be emphasized. Though electrical performance fell below acceptable levels after four hours, the pertinent result concerning penetration seal thermal degradation was that over the test duration and post-test cooldown, no measurable leakage was observed.

This outcome was naturally considered quite favorable, but on the whole it may not have been as illuminating as results obtained from programs already discussed. The primary reason was that testing was limited to a single sample of a device that might not conservatively represent the range of EPA designs and non-metallic EPA materials. Other materials or designs that may not protect non-metallic components or compounds quite as effectively (from atmospheric chemical reactions or heat transfer) as this example could produce less favorable leakage control performance under similar conditions. Tests with other atmospheric compositions would have also been desirable to determine if packings, epoxy potting compounds, or other non-metallic components unique to EPAs were either more vulnerable or more resistant to effects observed in the synthetic rubber gasket tests.

Table 2-2

Electrical Penetration Design Parameter Summary

Design Parameter	M45	M02	M13	M19	M06	M16
Number of Modules per Flange	1	2	2	1	2	2
Number of Conductors per Module	1 1000 mcm	3#2/0	12#10	3 Coax 33#16	1 75 Triax	14#16 Iron Constan. T/C
Provision for Connection	Test Lead	Mating Plug	Mating Plug	Mating Plug	Mating Plug	Mating Plug
Conductor Size	#12 AWG	3#2/0	12#12	2 RG-59 20#16	RG-11 AU	14#16
Cooductor Insulation	XLPE	XLPE	XLPE	XLPE	XLPE	EPR
Connector Conductor Material						
Receptacle	OHFC	TeCu	TeCu	Steel Alloy	Steel Alloy	Iron Constan.
Plug	TeCu	TeCu	TeCu	TeCu	TeCu	TeCu
Calculated Module Weight (lbs)	100	15	8	13	5	5
Total Penetration Weight (lbs)	100	30	16	13	10	10
Minimum Insulation Resistance @ 500 VDC (MΩ)	1000	100	100	100	$1x10^6$	100
Design Continuous Current Rating (amps)	1000	155	35	N/A	N/A	N/A
Short Time Overload Current Rating (amps)	4000	1085	245	N/A	N/A	N/A
Fault Current Overload Rating (amps)	50000	17325	2500	N/A	N/A	N/A
High Potential Test in Production Assemblies (VRMS, 60 Hz)	36000	2200	2200	1500	3000 VDC	1500
Module Volume (in^3)	129	59	24	59	13	16
Penetretion Volume (in^3)	129	118	49	59	25	33

Despite such limitations, potential benefits were realized for EPA work related to penetration thermal attack through this test. It was conservative with respect to aging, test pressure and temperature upper limits. In other respects, the data obtained from this test provides a basis for comparison between the thermal and chemical properties of the materials and design of the tested EPA with others currently in use.

As mentioned above, the electrical performance of the tested EPAs did degrade during testing for extended intervals. A ten day test at severe conditions (361 °F and 155 psig steam environment) [Bustard, 1989] revealed a degradation in electrical performance (faults to ground) over the first two days of the test. It was concluded that the EPAs would have functioned as designed for the first 24 hours of the severe accident conditions. This would satisfy the mission time selected for the Kewaunee IPE. However, for extended periods as would be required for AM and recovery actions, the performance of the electrical system would be dependent on the specific, voltage, current, and impedence requirements for a given cable (power, control or instrument).

2.3 Analyses

Analytical methods development in this area have thus far been largely limited to work in support of design basis environmental qualification programs pursuant to [USNRC, 1980; Szukiewicz, 1981]. This situation may in part be attributable to three factors. First, in spite of experiments already conducted, research has not yet provided enough comprehensive data that is specifically applicable to the wide range of non-metallic materials and penetration designs in use now and for the foreseeable future. Secondly, examinations of experimental data that has become available are ongoing processes. Although there are distinct and encouraging prospects for analytical model developments, predicting the completion points for the examinations and precisely what they may yield remains highly impractical. Finally, real or perceived uncertainties regarding severe accident boundary conditions that may be input to prospective analytical methods, environment temperature profiles in particular, could inhibit the development process to some degree at least.

Though not ideal, such a status is not necessarily a dilemma in terms of plant-specific penetration thermal attack analytical efforts for severe accidents. The methods referred to for past environmental qualification (EQ) work could be as suitable for severe accidents as they were for design basis analyses they applied to originally. Additionally, existing EQ techniques may be appropriate for non-metallic materials utilized in mechanical as well as electrical penetrations, given that the concern about penetration thermal attack in this paper is basically restricted to containment sealing performance (as opposed to including electrical functionality). A classic example of the specific calculation techniques used in previous EQ programs is detailed in [Sargent & Lundy, 1990].

A number of considerations provide support for applying EQ methods to severe accident transients. The first is that in both design basis and severe accident events, any penetration non-metallic components/compounds involved have the same starting point in terms of initial physical condition. Regardless of later scenario developments, these materials would still be assumed to have experienced thermal and radiation exposure levels under normal operating conditions equivalent to the anticipated end of service life. Secondly, from event initiation to the point of vessel failure, temperature profiles for severe accident types most associated with penetration thermal attack (see Section 2.1.2) are at worst considered to be no more intense than profiles typical of design basis events. Common design basis large LOCA or steam line break cases (inside containment) often involve rapid gas temperature increases in this initial period, peaking within a few minutes at approximately 300-400°F, and rarely falling below 250°F before the 10 - 12 hour point.

Questiona about the adequacy of existing EQ calculations for severe accident work, if any, are likely to be centered on gas temperature levels, characteristics, and timing after vessel failure. A fundamental point in this area is that for severe accidents, the period between vessel failure and containment failure or recovery is expected to predominantly fall within a reasonably narrow range of ~ 5 - 15 hours in duration, with corresponding total event times (i.e., from event initiation) rarely exceeding 24 hours. Exposure of penetration non-metallic seal materials to temperatures beyond

the design basis 340°F peak would of course represent only a portion of the period following vessel failure. It thus seems reasonable that methods designed and considered acceptable for time frames typically as long as six months would be equally capable of handling significantly smaller durations.

The same is true for differences between the temperature profile characteristic curves for design basis and severe accidents. Specific curve shape differences are certainly not unusual, but from a practical standpoint the curves can be loosely described as similar in shape. As the nature of the Arrhenius equation is to generate the integrated area under any given curve, no sensitivities are inherent to what are essentially sign differences only in comparable curve slopes.

Distinctions between design basis and severe accident temperature levels are not expected to be represent sufficient cause for concern about existing EQ calculation suitability for severe accident applications. The basic principle is that thermal degradation effects for the materials addressed exponentially accelerate as a function of exposure time at temperature values applicable to the analysis period. The anticipated peak (global) temperatures for postulated severe accidents differ by a factor of less than two. Uncertainties remaining in this area are also likely to be offset by the fact that in past EQ program applications of these methods, qualified life results exceeding the 40 year plant design life by factors of three or more were not unusual for the materials analyzed. In these circumstances, potential accuracy limitations for current EQ analysis methods are mitigated by the fact that while the answers given by qualified life calculations are on the order of years, any results exceeding severe accident overall durations by factors of as little as one order of magnitude should be considered acceptable for purposes of penetration thermal attack analyses.

3.0 METHODOLOGY

Thermal loadings of the containment penetrations may possibly lead to containment failure during postulated severe accident conditions. Thus, it is necessary to assess the containment success criteria and plant response for severe accident sequences.

The design configuration of the various mechanical and electrical penetrations as well as the personnel airlock, the equipment hatch and the auxiliary access airlock have an impact on their susceptibility to thermal attack and should, therefore, be assessed. If the penetrations are made only of metallic material, the issue of penetration degradation due to high temperature is not relevant.

Non-metallic penetration and sealant material can function up to and probably beyond a steam temperature of 486°F. However, non-metallic sealants need to be assessed for their ability to withstand conditions anticipated during postulated severe accident sequences. The Arrhenius methodology typically used for environmental qualification provides a technique for performing this analysis. Typical MAAP run results for the gas temperatures of the various containment compartments can be used to address this issue by determining the maximum temperatures which the penetrations will experience. Environmental qualification documents provide information on the sealant materials.

Non-metallic seals usually degrade with age, but at elevated temperatures the degradation reaction proceeds at an accelerated rate. Thermal degradation is generally determined by a single temperature-dependent reaction that follows the Arrhenius law. The rate at which such an elementary reaction proceeds is described by the Arrhenius equation

$$\frac{dq}{dt} = Ce^{-\phi/kT} \qquad (3\text{-}1)$$

where

$\frac{dq}{dt}$ = reaction rate,

ϕ = activation energy for the reaction in eV,

C = constant determined by experiment,

k = the Boltzman constant, 8.617×10^{-5} eV/K,

T = the absolute temperature at which the reaction is occurring, K.

If ϕ is independent of temperature, Equation (3-1) can be integrated with respect to time to give

$$q = Cte^{-\phi/kT} \tag{3-2}$$

where t is the time over which the reaction occurs and q is the quantity of material reacted.

If the quantity of material reacted at seal failure is denoted q_f, then the integrated equations for two identical penetration seals, one at temperature T_1 which fails at time t_1 in the chemical reaction, the other at temperature T_2 which takes time T_2 to fail, are written

$$q_f = Ct_1e^{-\phi/kT_1} \tag{3-3}$$

$$q_f = Ct_2e^{-\phi/kT_2} \tag{3-4}$$

These two equations can be combined to give

$$\ln \frac{t_1}{t_2} = \frac{\phi}{k}\left(\frac{1}{T_1} - \frac{1}{T_2}\right) \tag{3-5}$$

where t_2 is the time at temperature T_2 required to produce the same amount of thermal degradation that takes place in a longer time t_1 at a lower temperature T_1.

Equation (3-5) can be used to determine the activation energy of a sealant material (or a whole penetration) given a "lifetime plot" (time to failure vs. temperature). Lifetime plots are usually given in the experimental qualification data for the penetrations themselves and for the

sealant materials. Selecting a time and temperature from the lifetime curve allows one to find a value of q that corresponds to the point at which thermal attack has proceeded to penetration failure (q_f).

Once ϕ and q_f are known, the ability of the penetrations to survive a severe accident can be determined:

1) Calculate the extent to which thermal attack occurs during a 40 year service life at 120 F (321.9 K). Call this value q_s.

2) Calculate the extent of thermal attack that occurs during the accident. Call this value q_a.

3) Compare $q_s + q_a$ to q_f. If q_f is greater, thermal attack has not occurred to an extent sufficient to fail the penetrations during the accident time.

Finally, the location and segregation of the various containment penetrations needs to be reviewed regarding the possibility of direct contact by core debris during debris dispersion or submergence. In general the containment penetrations are located in the annular compartment, so the non-metallic seals on these penetrations must withstand the temperatures in the annular compartment during a severe accident. The possibility of direct contact between debris and penetrations is more likely in containments where the cavity opens directly into a section of the annular compartment with nearby penetrations.

4.0 PLANT SPECIFIC APPLICATIONS

4.1 Issues

4.1.1 Penetration Designs

The several types of containment penetrations used in the Kewaunee containment are displayed in Figures 4-1 to 4-5. The design configuration and means of sealing these penetrations are important in assessing their susceptibility to thermal degradation. If non-metallic gasket or sealing material is employed, it should be evaluated for its thermal stability and ability to prevent leakage at elevated temperatures. The mechanical systems penetrations are categorized into two general types of piping penetrations: i.e., those that are not required to accommodate thermal movement (cold penetrations, Figure 4-1) and those designed to accommodate thermal expansion (hot penetrations, Figure 4-2).

Both hot and cold piping penetration assemblies consist of a containment penetration nozzle, a process pipe, penetration sleeve, and a flexible seal. These provide a leak tight barrier that does not employ non-metallic sealing. Likewise, the electrical penetrations are constructed to provide the same integrity. The electrical penetrations at Kewaunee are constructed so that they do utilize non-metallic seals as a leakage barrier. The EPAs installed in Kewaunee's original design were provided by D. G. O'Brien, but several Conax penetrations have been added since then. The equipment hatch, personnel airlock, and emergency personnel hatch all employ gaskets made of silicone rubber and their vulnerability to thermal degradation should also be considered.

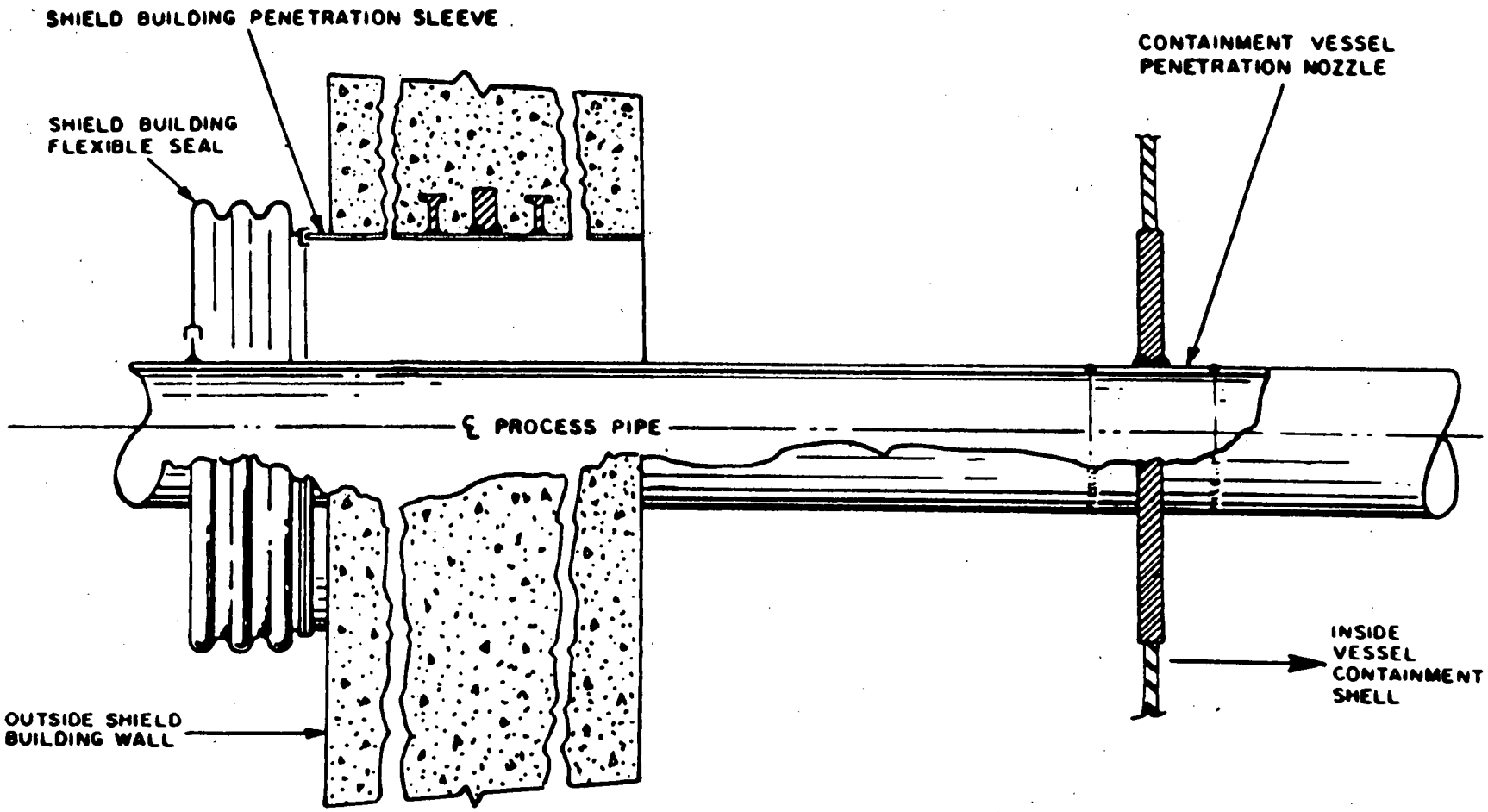

Figure 4-1. Typical cold piping penetration.

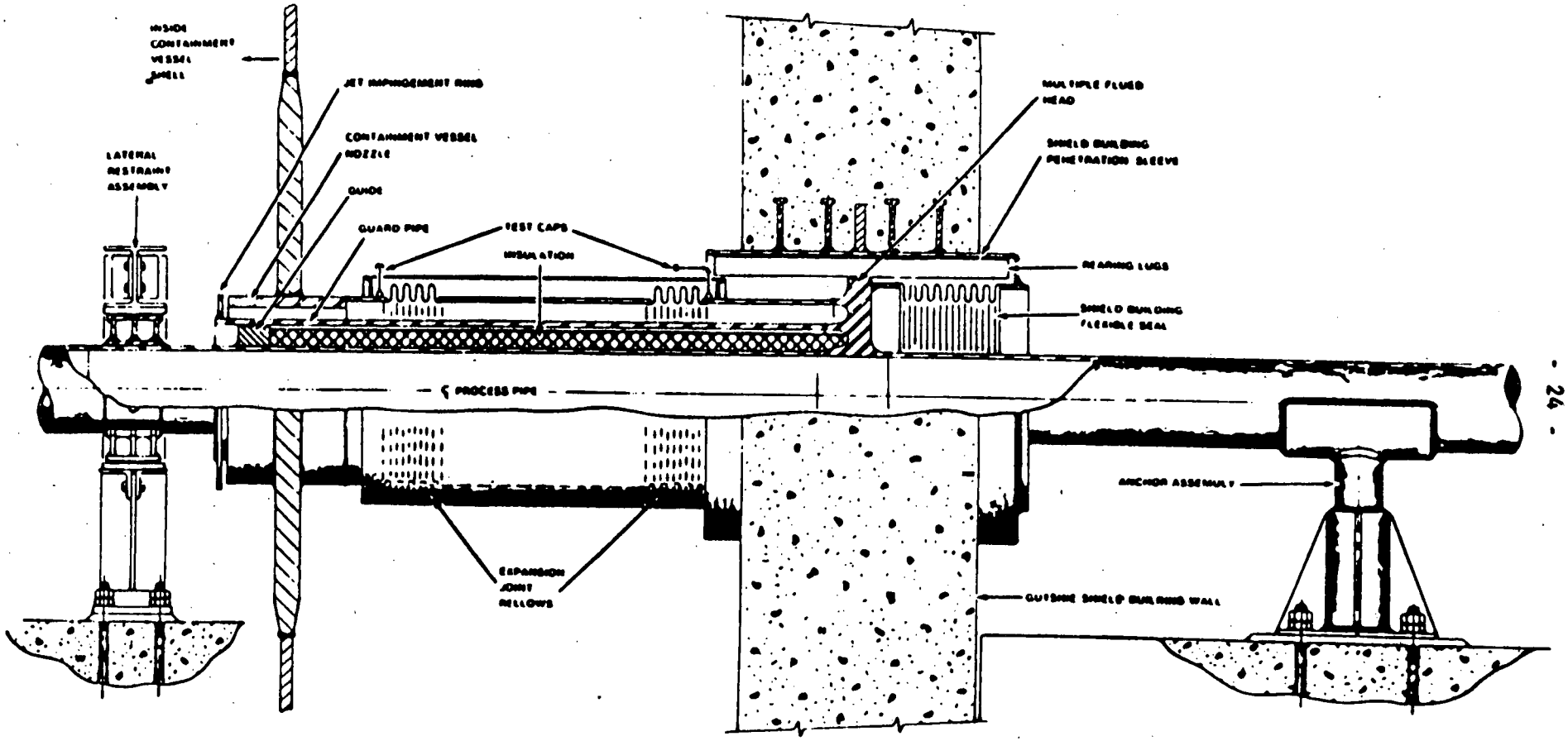

Figure 4-2 Typical hot piping penetration.

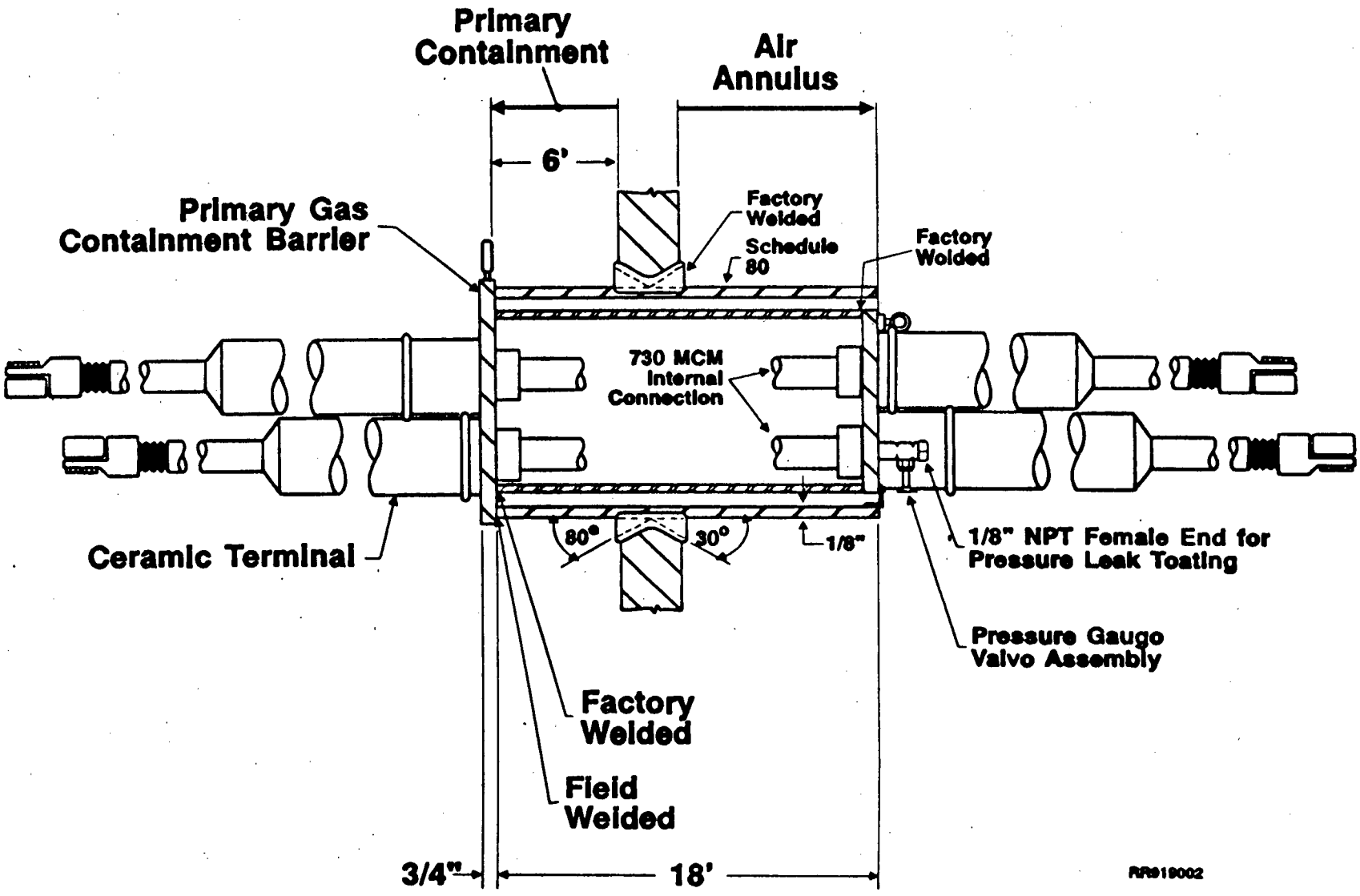

Figure 4-3 Electrical penetration assembly (D. G. O'Brien).

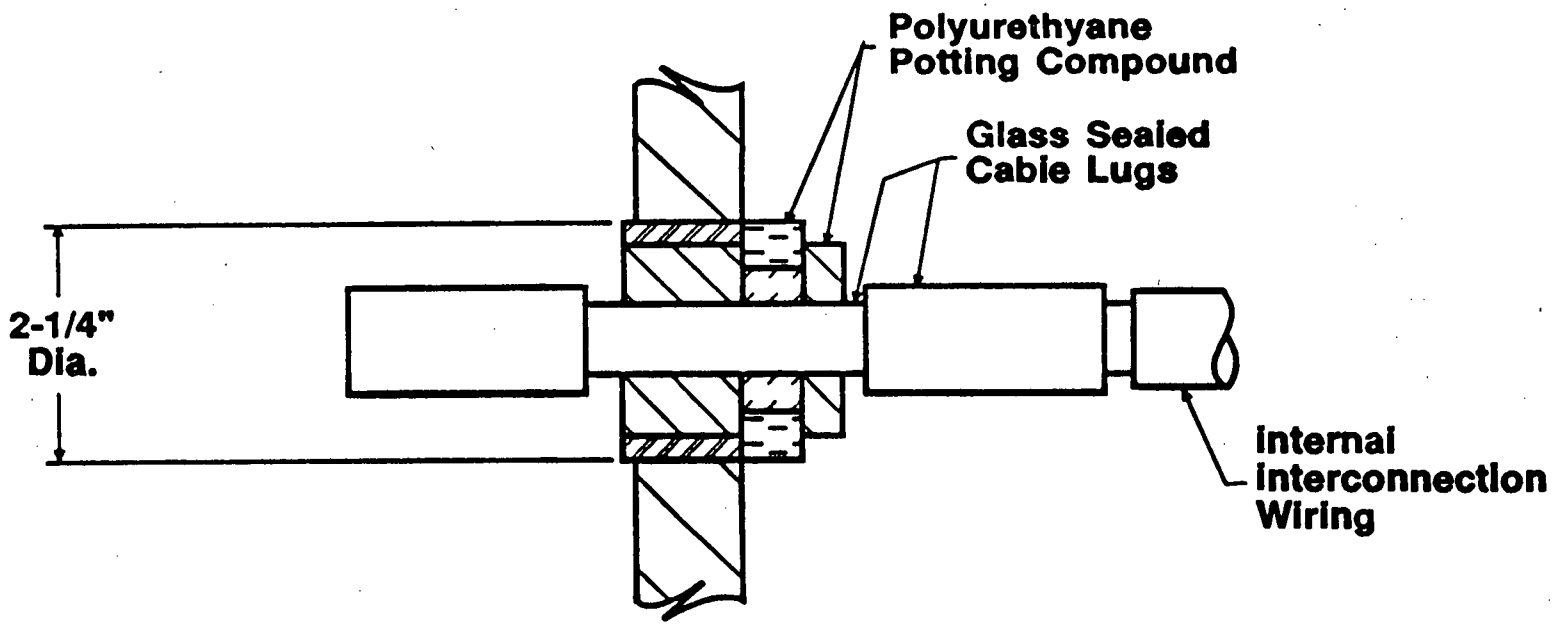

Figure 4-4 Single electrical penetration (D. G. O'Brien).

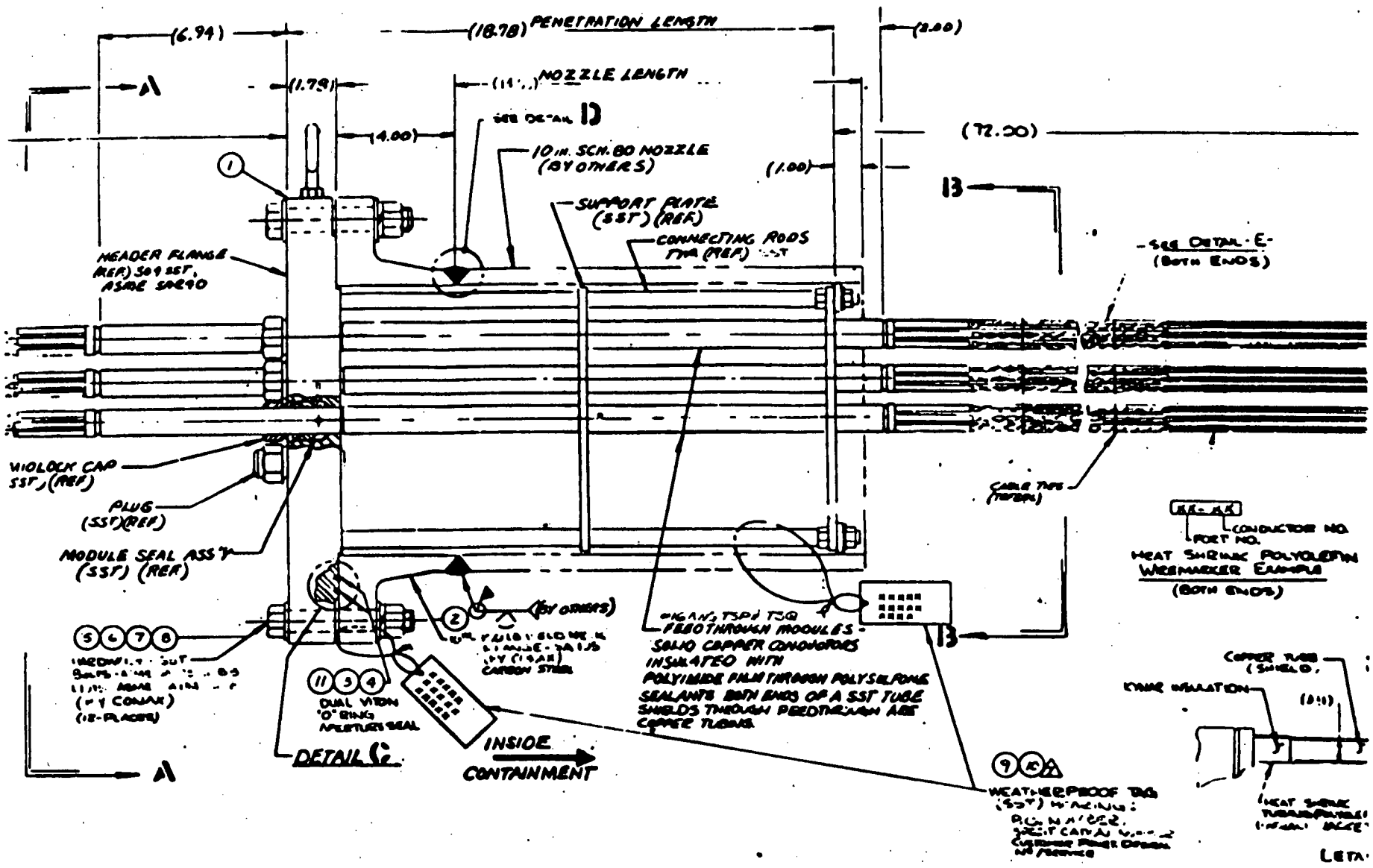

Figure 4-5 Electrical penetration assembly (Conax design).

4.1.2 Penetration Locations

The relative location of the various penetrations and the local internal containment configuration also impact their susceptibility to thermal attack. These geometrical considerations provide additional assurance that severe accident events which postulate debris dispersal will not cause direct contact of debris and penetrations. Direct debris contact could challenge the integrity of even the metallic penetration components or welds. DCH events in Kewaunee are not expected to disperse a large amount of debris into the annular compartment. The location of the mechanical and electrical penetrations was explicitly reviewed regarding the potential for direct contact by core debris during the Kewaunee containment walkdown. Direct impingement or submergence of penetrations in debris is precluded by the physical layout of containment. The dispersed material will not be a large unified mass, rather it will be a mist of small particles incapable of generating the heat required to melt through the penetrations. Additionally, since the EPAs are located in the annular compartment, the concern of penetration submergence is further mitigated. The cavity floor is at the 580'3" elevation which is far below the elevation of the lowest mechanical and electrical penetrations, which is at the 608' 0 elevation. Table 4-1 provides the elevations of the bottom of each of the large penetrations in the containment. The lowest of these elevations is 606'0" for the equipment hatch which is also well above the containment floor elevation.

4.1.3 Potential Severe Accident Conditions

The temperature in containment during severe accidents can vary over a range of approximately 120°F to 390°F for the upper and annular compartments (see Table 4-2). For loss of coolant sequences and other sequences with significant masses of water delivered to containment, the containment temperature corresponds to saturated conditions. For sequences with more limited masses of water delivered to containment such as station blackout (which also includes the loss of active containment heat removal systems)

Table 4-1

SUMMARY OF ELEVATIONS OF LARGE PENETRATIONS

	Bottom Elevation
Equipment Hatch	606'0"
Personnel Airlock	649'6"
Emergency Airlock	626'0"

the containment temperature is of the order of 390°F or less for the first 48 hours of the severe accident. The lowest mechanical/electrical penetrations are located at the 606'0" containment level, approximately 26 feet above the reactor cavity where molten corium debris would be located after vessel failure. The reactor cavity is subjected to the highest temperatures during severe accidents due to debris dispersal and potential core-concrete interactions or hydrogen burns being generally confined to this containment region (see the Direct Containment Heating [Fauske & Associates, 1990] and Molten Core-Concrete Interaction [Fauske & Associates, 1991] position papers). However, the containment penetrations are not located in this containment region. In particular, they are located in a completely separate compartment and are not directly exposed to this elevated temperature.

The temperatures provided in Table 4-2 are typical values for the Kewaunee plant. It should also be noted that the duration of the penetrations exposure to high temperatures is also important. Thus, transient temperature conditions due to perhaps intermittent hydrogen burns for example should not be used to set the peak sustained temperature.

4.2 Assessment of Impact of Severe Accident Conditions

It is concluded that the failure of containment mechanical penetrations due to thermal attack during severe accident conditions does not represent a unique or potential failure mechanism for the containment boundary. This conclusion is based on the fact that the mechanical penetrations do not contain non-metallic gaskets or seal that could be susceptible to the potentially elevated containment gas temperatures.

The large penetrations (personnel airlocks and equipment hatch) do have non-metallic gaskets which are made of silicone rubber. However, based on the research summarized in Section 2.2.2 of this paper, the non-metallic penetration and sealant material will function up to and probably beyond temperatures of 486 °F (steam). The maximum gas temperatures that are anticipated for postulated severe accident sequences in the Kewaunee containment that the several large penetrations will be exposed to are less

Table 4-2

SUMMARY OF TYPICAL CONTAINMENT REGION TEMPERATURES

Accident Sequence	Average Gas Temperature (°F)		
	Lower Compartment	Upper Compartment	Annular Compartment
Station Blackout	410	380	390
Small LOCA	310	310	310
Large LOCA	330	330	330

than 450 °F. Even if it is assumed that the gasket material could be heated to a temperature > 470 °F within the configuration of the several locks and hatches, the gasket material would not be expected to deteriorate or leak. These locks employ a double barrier design. This design configuration was demonstrated by testing (see Section 2.2.2) to be able to withstand conditions that bound those expected in the Kewaunee containment during severe accidents without leakage from the containment.

The electrical penetration assemblies in the Kewaunee containment utilize a silicone potting compound as part of their leak tight pressure retaining barrier. The electrical penetrations incorporated in the Kewaunee containment design are D. G. O'Brien and Conax designs. Detailed description of the manufacturer's test data is contained in the D. G. O'Brien Test Procedure Manual. It is concluded that based on the tests (see Section 2.2.3) performed on numerous D. G. O'Brien designs, that Kewaunee's EPA's have been relatively modeled in the Sandia experiments thus allowing interpretation of those results to apply to Kewaunee's EPAs. Since the maximum gas temperatures that are anticipated for postulated severe accident sequences in the Kewaunee relevant containment regions are less than 500 °F, the non-metallic materials are expected to function during such severe accident events.

4.2.1 Assessment of D. G. O'Brien EPAs

To further support this conclusion, a degradation equivalency calculation provided from the Environmental Qualification for electrical components [USNRC, 1980] can be implemented by substituting typical severe accident temperatures for Kewaunee into the Arrhenious equation developed in Section 3. The representative temperature envelopes were selected after reviewing MAAP results for Kewaunee for several types of sequences. These sequences and corresponding temperatures and locations are recorded in Table 4-2. Station blackout sequences were selected to describe the most conservative severe accident temperature profiles. These temperatures along with the necessary information provided by the Kewaunee EQ documentation will be implemented into the methodology discussed in Section 3 to determine how well the EPA will function during severe accidents.

Experiments used to calculate the ultimate lifetime of the penetrations are presented in the Environmental Qualification (EQ) data for the D. G. O'Brien penetrations [Kewaunee EQERs, Section 14.1-6]. These experiments simulate 40 years of service life and a design basis LOCA. The failure criterion selected was a penetration leak rate of 1×10^{-6} cc/sec. For the purposes of severe accident analysis this leak rate is insignificant. The normal containment leakage is 100 cc/sec, so penetration leakage during an accident will not be relevant until it approaches 1 cc/sec. There are no thermal attack experiments available that test the penetrations with a 1 cc/sec leak rate as a failure criterion. For this analysis the degree of thermal degradation of a physical property of the sealant material is used as a failure criterion.

The degradation of the sealant material during these severe accident sequences is calculated by using the Arrhenious equation discussed in Section 3. The first step is to calculate a value of q that corresponds to the point at which thermal attack has proceeded to penetration failure (q_f). Using (Eq. 3-2) and testing material data provided by [Kewaunee EQERs, Section 14.1-6], q_f is calculated as:

$$q_f = Cte^{-\phi/KT} = 1.057 \times 10^{-8}\ C$$

where:

t = time over which reaction occurred = 1000 hr
C = constant determined by experiment
ϕ = activation energy for reaction = .98 eV
K = Boltzmann constant = 8.617×10^{-5} eV/K
T = absolute temperature at which reaction is occurring = 450 K.

The next step was to calculate the extent to which thermal attack during a 40 year service life at 120°F (321.9°K) and the extent to which thermal attack occurs during a severe accident. These values will be referred to as $q_s + q_a$ respectively. Using equation (3-2) and the temperatures above, the value for q_s is calculated to be 1.605×10^{-10}C.

Now the calculation for amount of thermal attack due to severe accident conditions is considered. The first step is to establish the temperature the seal would be exposed to. Figure 4-6 is the gas temperature in the annular compartment for a station blackout sequence. Selecting an average temperature of 390°F (470 K) and a 48 hour mission time, solve (Eq. 3-2) for q_a. The calculation yields 1.487×10^{-9} C as the amount of thermal attack on the penetrations during a severe accident.

Clearly $q_s + q_a$ (1.64×10^{-9} C) is less than q_f (1.057×10^{-8} C), so the D. G. O'Brien penetration seals are not expected to fail during a severe accident. The length of time for which the penetration seals will survive severe accident conditions may be estimated by setting $q_{a/max} = q_f - q_s$ and then solving for the time term. Solution of of this equation states that the containment penetration will last 335 hours at 390°F, well beyond the 48 hour mission time.

In summary, the silicone potting compound in the D. G. O'Brien penetrations can last 2500 years before it experiences substantial thermal degradation. At 390°F, the epoxy material can last 14 days. A station blackout at Kewaunee will typically last approximately 65 hours before containment failure on overpressure, thus the non-metallic material in Kewaunee penetrations will not experience thermal attack sufficient to prematurely fail the containment.

4.2.2 Assessment of the Conax Penetrations

The electrical penetration assemblies manufactured by Conax also utilize non-metallic materials as part of their leak-tight pressure retaining barriers. The Conax penetrations at Kewaunee use polysulfone as the sealant material. The Conax penetrations generally use polysulfone as the sealant material, except for the medium-voltage penetrations, which use Viton "O" ring seals.

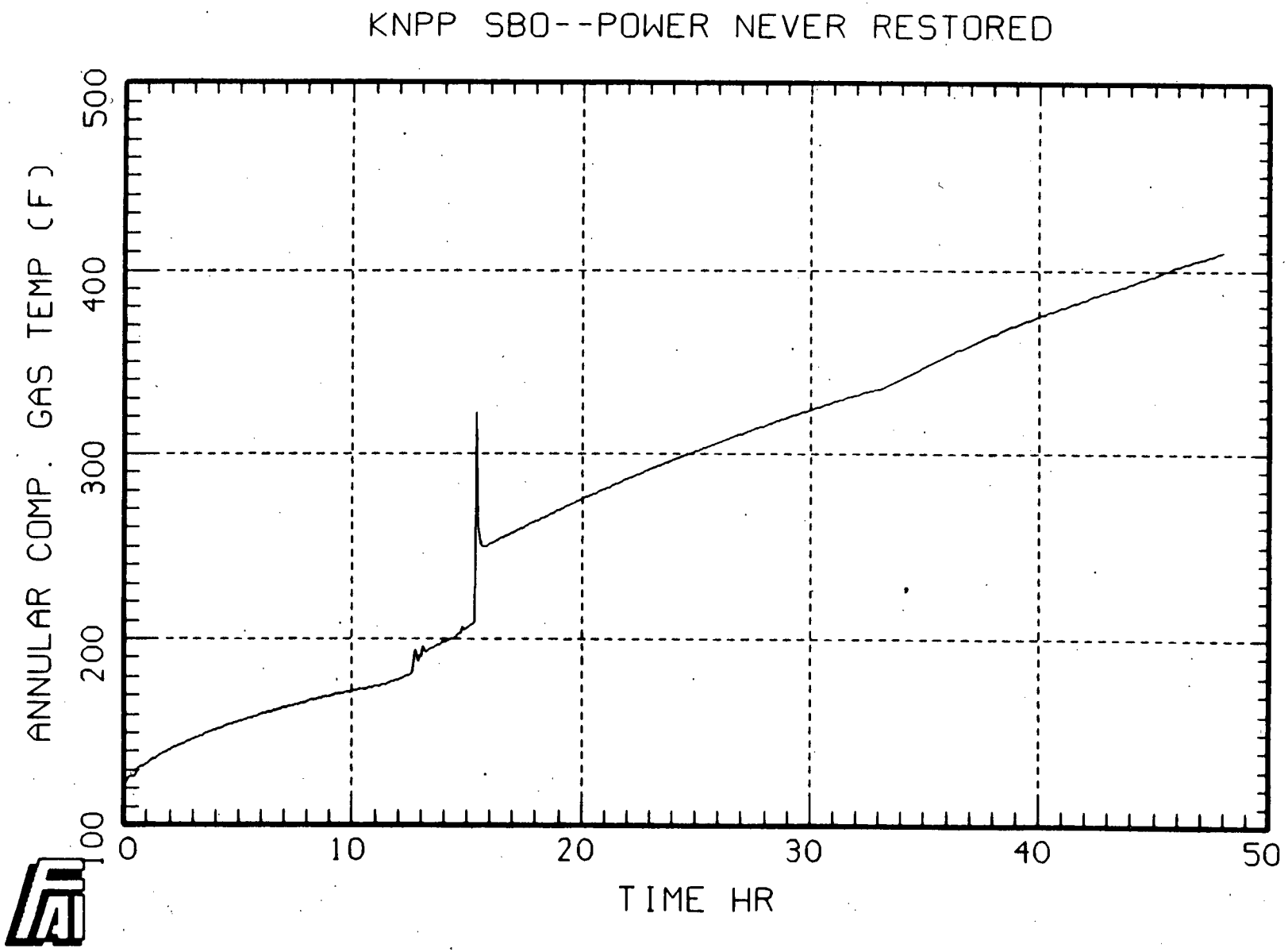

Figure 4-6 Containment gas temperatures in annular compartment. (SBO sequence.)

The recommended maximum long-term service temperature for Viton (a fluoroelastomer) is 400°F. If used at or below this temperature it will seal almost indefinitely, and at 550°F (288°C) the service limit is 10 days (Ref. Conax report IPS-325). Also, the "O" rings are completely enclosed within a metal groove and plate. Thermal attack of the Viton "O" rings is not a concern during a severe accident.

Experiments used to calculate the ultimate lifetime of the penetrations are presented in the Environmental Qualification (EQ) data. These experiments simulate 40 years of service life and a design basis LOCA. The failure criterion selected was a penetration leak rate of 10^{-6} cc/sec at 60 psig. For the purposes of severe accident analysis this leak rate is insignificant. The normal containment leakage is 100 cc/sec, so penetration leakage during an accident will not be relevant until it approaches 1 cc/sec. There are no thermal attack experiments available that test the penetrations with a 1 cc/sec leak rate as a failure criterion.

The limiting sealant material in the Conax EPAs at Kewaunee is the polysulfone thermoplastic. This material could be analyzed using the Arrhenius methodology of Section 3.0 and the lifetime plot for electric conductor feedthroughs (Figure 5.7.1 in Conax EQ report IPS-473). However, the failure criterion used in creating that lifetime plot was a leakage rate of 10^{-6} cc/sec.

For the present analysis the percent volatilization of the sealant material is used as the failure criterion. Data is available on the percentage of volatilization of polysulfone as a function of time and temperature (Ref. Conax report IPS-325). This data is presented in Figure 4-7 in terms of the volatilization rate. (Also shown is the volatilization rate for Kapton, the conductor insulation film.) Clearly the polysulfone sealant (and the Kapton) experiences little or no volatilization at temperatures below 300°C (570°F).

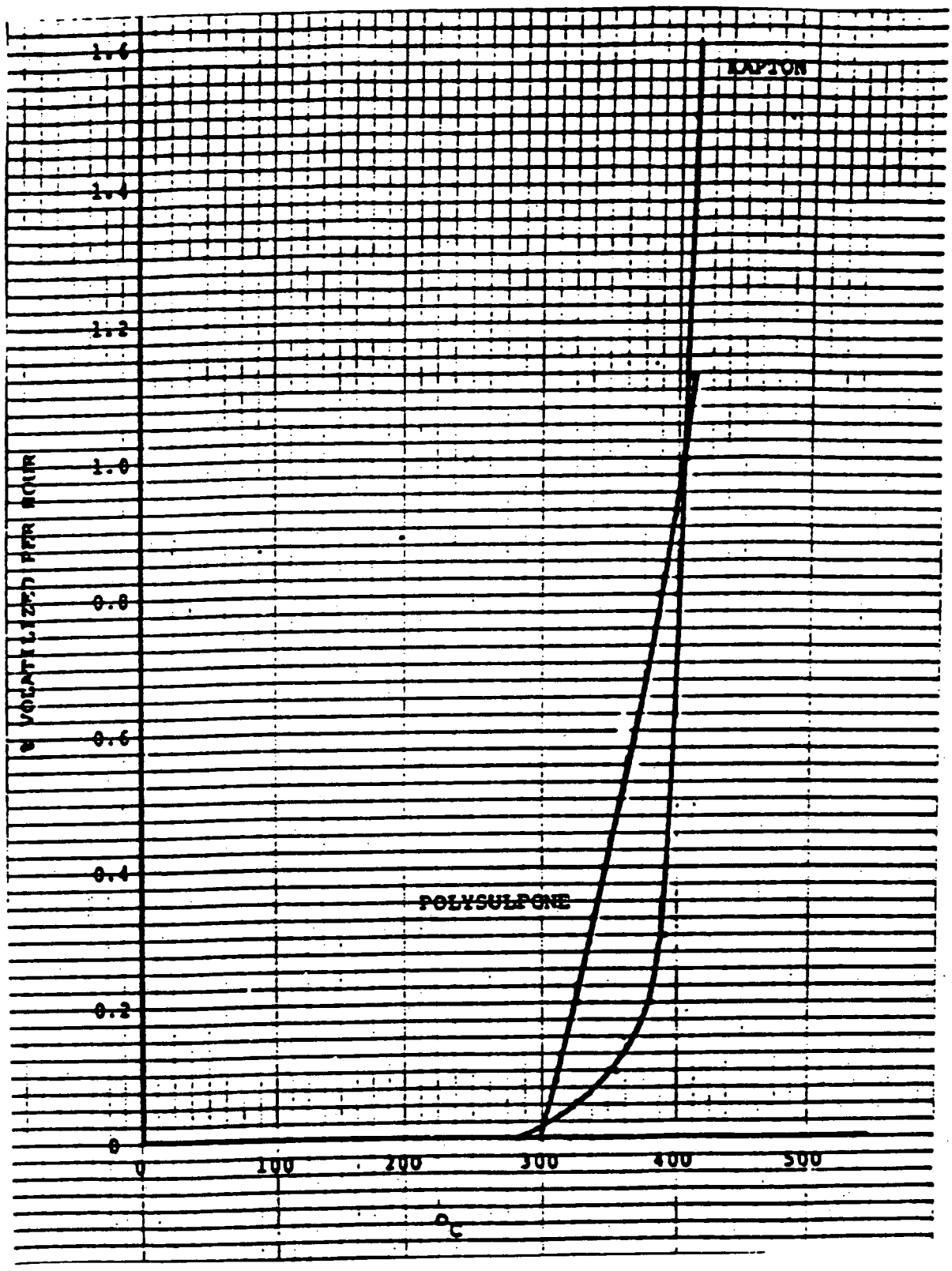

Figure 4-7 Volatilization rate of polysulfone and Kapton.

In summary, the polysulfone used in the Conax penetrations experiences no volatilization under typical PWR severe accident conditions. A station blackout at Kewaunee will typically last approximately 40 hours before containment failure on overpressure. The non-metallic material in Kewaunee's Conax electrical penetrations will not experience thermal attack sufficient to prematurely fail the containment.

4.3 Uncertainties

The major uncertainties associated with thermal loadings of the containment penetrations involve the magnitude and duration of the containment gas temperature. The NRC sponsored test programs discussed in this evaluation attempted to provide bounding conditions for postulated severe accidents. Thus, to the extent that the testing of full scale penetration samples and material samples did bound the severe accident condition the key uncertainties have been addressed. The range of predicted Kewaunee containment conditions falls within the envelope of tested conditions so the major uncertainties have been included.

4.4 Conclusions

The failure of containment mechanical and electrical penetrations due to thermal loading during severe accidents does not represent a unique or potential failure mode for the Kewaunee containment boundary. The piping penetrations do not contain any non-metallic gaskets or seals, and the design configuration of the operable penetrations (hatches and air locks) was demonstrated by testing to be able to withstand the containment conditions expected during a severe accident at the Kewaunee Nuclear Plant. An EQ-type analysis of the electrical penetrations indicates that severe accident conditiona will not threaten the integrity of the EPAs within the 48 hour mission period.

This conclusion is also based upon the location and segregation of the containment penetrations. The possibility of direct contact by core debris or submergence in a debris bed or pool is precluded by the location of the penetrations. Specifically, the penetrations are located in the upper or

annular compartments. In the event of vessel failure, core debris would be contained largely within the reactor cavity and possibly the lower compartment. There are no direct paths whereby corium could contact any containment penetrations. Thus, the containment geometry will provide a passive means of isolating the penetrations from the core debris.

5.0 SUMMARY

The major uncertainties associated with thermal loadings of the containment penetrations involve the magnitude and duration of elevated containment gas temperature. The NRC sponsored test programs discussed in this evaluation attempted to provide bounding conditions for postulated severe accidents. Thus, to the extent that the testing of full scale penetration samples and material samples did bound the severe accident conditions, the key uncertainties have been addressed. The range of predicted Kewaunee containment conditions falls within the envelope of tested conditions so the major uncertainties have been included.

The mechanical penetrations do not employ non-metallic gaskets or seals and, therefore, are not susceptible to the containment gas temperatures. The large penetrations do have non-metallic gaskets that can withstand temperatures up to and beyond 486°F. Typical severe accident containment gas temperatures for the Kewaunee nuclear plant are in the range of 390°F at the penetration locations. Under these conditions, tbe seal materials are not expected to deteriorate and leak. Finally, the penetrations are located in the annular and upper compartments; this configuration precludes both direct contact by core debris during debris dispersion and submergence in a debris pool.

Thus, failure of the containment penetrations due to thermal loading will not be included as a separate node for long term containment failure in the Kewaunee containment event trees (CETs).

6.0 REFERENCES

Bridges, T. L., 1987, "Containment Penetration Elastomer Seal Leak Rate Tests", USNRC Report NUREG/CR-4944 (SAND87-7118), Idaho National Engineering Laboratory, Idaho Falls, ID.

Brinson, D. A. and Graves, G. H., 1988, Evaluation of Seals for Mechanical Penetrations of Containment Buildings, USNRC Report NUREG/CR-5096 (SAND88-7016), Sandia National Laboratories, Albuquerque, NM.

Bustard, L. D., 1989, Equipment Qualification (EQ) - Risk Scoping Study, USNRC Report NUREG/CR-5313 (SAND88-3330), Sandia National Laboratories, Albuquerque, NM.

Clauss, D. B., 1989, Severe Accident Testing of Electrical Penetration Assemblies, USNRC Report NUREG/CR-5344 (SAND89-0327), Sandia National Laboratories, Albuquerque, NM.

Clauss, D. B. and Parks, M. B., 1989, "Performance of Containment Penetrations Under Severe Accident Loadings", Proceedings of the 17th Water Rector Safety Information Meeting, Rockville, MD.

Conax Corporation, 1985, Report IPS-325, Rev. D., "Design Qualification Material Test Report for Materials Used in Conax Electric Penetration Assemblies and Electric Conductor Seal Assemblies."

IDCOR, 1983, IDCOR Technical Report 10.1, "Containment Structural Capability of Light Water Nuclear Power Plants" (Section 2.4.1), Technology for Energy Corp., Knoxville, Tennessee.

IDCOR, 1986, IDCOR Technical Report 17.5, "An Investigation of High-Temperature Accident Conditions for Mark 1 Containment Vessels" (Tasks 2 and 3), CBI NA-CON, Inc., Oak Brook, Illinois.

Julien, J. T. and Peters, S. W., 1989, "Leak and Structural Test of Personnel Airlock for LWR Containments Subjected to Pressures and Temperatures Beyond Design Limits", NUREG/CR-5118 (SAND88-7115), Sandia Nationsl Laboratories, Albuquerque, NM.

Kewaunee Environmental Qualification Evaluation and Review Sections 12.3 and 4, and 14.1-6.

NRC, 1988, NRC letter to all Holders of Operating Licenses and Construction Permits for Nuclear Power Facilities, "Individual Plant Examination for Severe Accident Vulnerabilities - 10 CFR 50.54(f)", Generic Letter No. 88-20.

Szukiewicz, A. J., 1981, Interim Staff Position on Environmental Qualification of Safety-Related Electrical Equipment, USNRC NUREG-0588 (Rev. 1), U.S. Nuclear Regulatory Commission, Office of Nuclear Reactor Regulation, Division of Safety Technology, Washington, D.C.

USNRC, 1980, Environmental Qualification of Class 1E Equipment, USNRC Office of Inspection and Enforcement Bulletin No. 79-01B.

FAI/91-157

A PHENOMENOLOGICAL EVALUATION SUMMARY ON CONTAINMENT OVERPRESSURIZATION IN SUPPORT OF THE KEWAUNEE INDIVIDUAL PLANT EXAMINATION

Submitted To:

Wisconsin Public Service Corporation
Green Bay, Wisconsin

Prepared By:

Fauske & Associates, Inc.
16W070 West 83rd Street
Burr Ridge, Illinois 60521
(708) 323-8750

Final Issue

March 1993

ABSTRACT

The potential failure of a large dry containment due to overpressurization has been identified as a concern by the Nuclear Regulatory Commission (NRC) Staff, NRC contractors, and the nuclear industry. A variety of pressurization mechanisms could jeopardize containment integrity at one or more locations, and at times that depend on the nature and circumstances of the accident sequences involved. In a large, dry containment, primary contributors to increasing containment pressure include steam created by boiling of the primary system inventory if pressure suppression functions are not available, non-condensible gases from either concrete erosion or metal-water reactions, or combustible gas deflagrations/detonations if they occur. Uncertainties about the timing (after vessel failure) and the location of postulated containment failures resulting from overpressurization have potentially important ramifications regarding the radiological source term. Depending upon the timing and location of postulated failures, natural fission product deposition mechanisms may not have sufficient time to significantly reduce the masses of fission products that could be released.

To address this concern, containment failure modes associated with containment overpressurization are assessed in terms of containment failure timing, size, location, and a fragility curve giving a probabilistic representation of failure at critical locations as a function of containment pressure. Containment failure timing due to overpressurization can be early or late relative to vessel failure, depending on the physical process causing the pressurization. Direct containment heating (DCH) and steam explosions are postulated to cause early containment failure because they occur just after vessel failure and lead to rapid pressurization. Hydrogen combustion is postulated to be an early or late containment failure mechanism, depending upon the details of the accident sequence. (These physical processes are described in the appropriate Phenomenological Evaluation Summaries.) Overpressurization due to steaming and/or noncondensible gas generation by molten core-concrete interaction (MCCI) can be an early or late failure mechanism, although for the risk dominant sequences,

it is a late containment failure mode. For example, a station blackout at Kewaunee results in vessel failure in a few hours and containment failure, on overpressurization, at several tens of hours.

Regarding failure sizes, the ultimate strength limit of involved structures can be achieved rapidly in some instances where the total energy delivered (to the containment) is sufficient to result in large rupture areas. Conversely, this limit may be approached gradually, and the energy delivered may only be enough to induce relatively small rupture areas unlikely to become any larger than that necessary to stabilize the containment pressure (i.e., create a choked flow condition). Phenomena like DCH, ex-vessel steam explosions, hydrogen detonation, and certain containment steam mass addition events could presumably engender large failures, although the likelihood of these phenomena is extremely small for the Kewaunee Nuclear Plant. In contrast, some volume heating and/or mass addition phenomena would represent a gradual shell mechanical loading and limited energy delivery situation, thus leading to no more than small to medium size failures. Examples include concrete attack events or steam added to the containment.

Analyses and experimental data, both Kewaunee-specific and generic in nature, have been used to characterize the ultimate containment failure pressure in terms of a fragility curve. This fragility curve expresses the probability of containment failure as a function of pressure. Using a Monte Carlo technique and ultimate failure pressures for critical locations at Kewaunee, a best estimate curve is developed and presented here. Results show a mean failure pressure of 150 psig (165 psia), a lower bound (5%) of 121 psig (136 psia), and an upper bound (95%) of 176 psig (191 psia). The fragility curve shows that failure is most likely to occur due to stresses in the shell wall. Based on experimental evidence, the best estimate failure mode for the Kewaunee containment is a large, catastrophic failure.

TABLE OF CONTENTS

	Page
ABSTRACT	i
TABLE OF CONTENTS	iii
LIST OF FIGURES	v
LIST OF TABLES	v
1.0 PURPOSE	1-1
2.0 PHENOMENA	2-1
2.1 Description	2-1
2.1.1 Controlling Physical Processes	2-1
2.1.2 Relationship to Containment Failure Mechanisms and Modes	2-2
2.1.3 Relationship to Source Term	2-5
2.2 Experimental Results	2-7
2.2.1 Sandia 1:8 Scale Steel Model Containment Tests	2-7
2.2.2 Sandia 1:6 Scale Model Containment Pressure Test Program	2-10
2.2.3 Sandia/CBI Personnel Airlock Testing	2-12
2.2.4 EG&G Containment Penetration System Testing	2-14
2.2.5 Sandia Electrical Penetration Assemblies (EPA) Program	2-14
2.3 Analyses	2-15
2.3.1 IDCOR Technical Report 10.1	2-15
3.0 METHODOLOGY	3-1
3.1 Structural Analyses	3-1
3.2 Containment Overpressure Failure Probabilities	3-2
3.2.1 Monte Carlo Method	3-7

TABLE OF CONTENTS (Continued)

		Page
4.0	PLANT SPECIFIC APPLICATION	4-1
4.1	Kewaunee Containment Structure	4-1
4.2	Ultimate Failure Pressures	4-3
4.2.1	Cylindrical Shell Wall: Hoop Direction	4-3
4.2.2	Stress Intensity at Vessel Dome	4-5
4.2.3	Containment Bottom Head Failure	4-6
4.2.4	Major Penetrations	4-7
4.2.5	Uncertainty in Ultimate Pressure Capacity	4-10
4.3	Containment Failure Probabilities	4-11
4.4	Conclusions	4-14
5.0	SUMMARY	5-1
6.0	REFERENCES	6-1

LIST OF FIGURES

Figure		Page
2-1	Sandia 1:8 scale steel model containment. From [Koenig, 1986]	2-8
2-2	Sandia 1:6 scale reinforced concrete containment model. From [Clauss, 1989a]	2-11
2-3	1:6 scale model liner stretchout showing leakage From [EPRI, 1989]	2-13
2-4	Arrangement of circumferential stiffeners in Sequoyah containment	2-17
4-1	Sketch of Kewaunee containment design	4-2
4-2	Sketch of Kewaunee basemat	4-8
4-3	Kewaunee basemat details	4-9
4-4	Kewaunee containment fragility curve	4-13

LIST OF TABLES

Table		Page
3-1	Possible Containment Failure Modes for Four Potential Failure Locations	3-5
4-1	Ultimate Stress Capacity for Kewaunee Containment	4-12

1.0 PURPOSE

In Generic Letter 88-20 [NRC, 1988], the NRC recommends that the containment failure modes associated with overpressurization be assessed to determine the potential radionuclide source terms. The objective of this paper is to describe the containment overpressurization failure modes that must be considered in the source term assessment portion of the Kewaunee Nuclear Plant IPE. This analysis involves the containment failure location, failure size, and a treatment of containment fragility which shows the probability of failure at each critical location as a function of containment pressure.

2.0 PHENOMENA

2.1 Description

Containment overpressurization is a postulated event in which the pressure loads applied to the containment boundary during a severe accident eventually exceed the boundary's ultimate strength at its most vulnerable point(s). This event has been hypothesized as a means of containment failure through one or more of several potential physical mechanisms. Common to most, if not all, of these mechanisms is the transfer of large quantities of heat to the containment atmosphere from sources such as the primary system or dispersed core debris. The extent of pressurization, its timing, and the pressurization rate all depend on a number of factors, including the accident sequence characteristics involved, the containment geometric configuration, etc. At the heart of the matter however, is the need to define the containment pressure limit and to determine how much pressurization the containment will undergo during a severe accident.

2.1.1 Controlling Physical Processes

Several controlling physical processes have been postulated that can be considered relevant to containment overpressurization in severe accidents. Such processes result in either heating the gas and/or vapor mass in the containment's finite volume, or increasing the gas/vapor mass existing in the finite volume. These processes, or pressure sources, include potential ex-vessel vapor (steam) explosions, combustion, core-concrete interaction, and direct containment heating (DCH).

Processes that exclusively involve beating of the existing containment volume include gas combustion and direct heating of the containment atmosphere by finely fragmented core debris. Steam generation, due to either rupture of the primary system or flashing of water accumulated in the containment by core debris ejected from the vessel, initially adds mass to the containment atmosphere but eventually becomes a containment volumetric heating mechanism. Concrete attack by molten core debris represents a situation where heat and mass are more or less simultaneously added to the

containment volume. Chemical reactions that may occur in such cases directly release heat as well as contribute significant masses of aerosols and non-condensible gases, which in their turn also become containment volume heating mechanisms. These pressurization mechanisms have been considered individually in other phenomenological evaluation summaries performed in support of the IPE.

2.1.2 Relationship to Containment Failure Mechanisms and Modes

Containment overpressurization can be a potential early or late failure mode. Depending on the specific accident sequence characteristics, overpressurization failures may be observed across a wide range of event times, either substantially before or substantially after vessel failure. Apart from direct bypass or failure to isolate events (where containment pressure retention capability is assumed to fail by definition), the potential for containment overpressure failures exists in most severe accident scenarios where pressure suppression facilities, namely the containment fan coolers and/or containment sprays, are disabled.

The failure mechanism associated with overpressure of the containment is due to exceeding the ultimate strength of certain structural components or attachments. Efforts to precisely and confidently characterize this mechanism can be (and have been) extraordinarily complicated for severe accident purposes. There are four fundamental considerations; 1) failure flow size (area), 2) failure location, 3) failure timing, and 4) the pressure at which failure may occur. As discussed below, some aspects of the containment failure modes do not depend on the physical process (or combination of processes) that causes overpressurization. Failure location and the pressure levels at which failure may occur depend upon the containment design, construction and materials, but not on the process causing the pressurization. However, containment failure timing, i.e., early or late, and failure size do depend on the physical process and the rapidity of the pressurization.

Regarding failure sizes, the ultimate strength of involved structures may be achieved rapidly in some postulated sequences, and the total energy

delivered (to the containment) may be sufficient to result in large rupture areas. Conversely, this limit may be approached gradually, and the energy delivered may only be sufficient to induce relatively small rupture areas that are unlikely to become any larger than what is necessary to stabilize the containment pressure (i.e., to create a choked flow condition). Based on the analytical results for DCH, steam explosions and hydrogen combustion, cases in this "gradual loading" category (for example, concrete attack or steaming to the containment) are significantly more likely to occur than rapid loading, high energy cases.

Although there are innumerable containment details that could fail under over-pressurization conditions, there are only a few possible over-pressure failure locations that need consideration with respect to source term estimates. By and large, for a large, dry containment, a failure location creates a flowpath to either the auxiliary building, the atmosphere, or into the soil in some instances. Each of these flowpaths has different fission product retention mechanisms, which results in different source terms for each. For a direct release to the atmosphere, fission product retention is negligible, of course. Some amount of fission product retention can be credited to the auxiliary building, depending upon its configuration, and a considerable amount of fission product retention can be credited to a release through soil, although the exact amount would depend upon soil composition, temperature, porosity, etc. Therefore, a failure in either the dome, cylinder, equipment hatch, or any containment detail above grade that does not fail into the auxiliary building, results in essentially the same fission product release path, and only the "weakest" of these details requires further consideration. Similarly, the weakest detail can be selected for failure to the auxiliary building or to the soil.

Factors that control overpressure failure timing are somewhat better defined than factors associated with size and location variables. Pressurization rates occurring in the containment regions during a severe accident exert the greatest influence on the time when a failure can be expected. Pressurization rates are themselves controlled by the pressure source phenomena characteristics, the containment boundary conditions when the phenomena originate, and containment physical characteristics (region

geometry in particular). Extensive effort has been made to analytically model the physical basis for how the various phenomena actually generate pressure. For the most part, these models are sensitive to crucial boundary conditions and plant characteristics. In short, means are available to predict containment region pressures as a function of accident elapsed time. Furthermore, the pressurization rates revealed in development of these models appear to fall within a relatively low range regardless of pressure source phenomena distinctions. This strongly suggests that loading of the containment shell and other pressure boundary components can be considered essentially static rather than dynamic. On this basis, overpressure failure timing is reduced to a matter of the rapidity at which actual pressures reach the pressure retention capacities (i.e., the pressure point corresponding to ultimate strength stress levels) of containment boundary components.

Because engineered safeguards and pressure suppression functions (containment sprays and fan coolers) would be unavailable, a station blackout sequence exemplifies late overpressure failure due to steaming and noncondensible gas generation. In this sequence, the water on the cavity and lower compartment floors is steamed away following vessel failure. The containment continues to pressurize due to the direct heating of the atmosphere by the debris and the generation of noncondensable gases by molten core-concrete interaction (MCCI) until eventually the containment fails.

Although early containment failure due to steaming and non-condensible gas generation is not a likely scenario [U.S. Nuclear Regulatory Commission, 1989], there are some accident sequences, particularly certain LOCA sequences, where containment failure occurs <u>prior</u> to vessel failure. In these instances, fan coolers are not available, but the core is cooled by low pressure recirculation without RHR heat exchangers. If the containment spray system does not include a heat exchanger, then it cannot be used to continually remove decay heat and suppress containment pressure. Therefore, steaming from the core removes decay heat, but pressurizes the containment until it ultimately fails. Vessel failure occurs sometime thereafter.

Containment pressure levels at which failures may occur are another reasonably well defined consideration. Geometry and material properties are clearly the primary influences in determining containment boundary component responses to mechanical (pressure) loads. Hand calculations and finite-element analyses have been used to determine containment response (strain) as a function of pressure for plant-specific geometries. Containment failure is usually defined at some strain, say 1%, where containment integrity can no longer be maintained.

The containment may also experience concurrent thermal loads which affect the overall stress levels exerted on any given component. Thermal loads associated with the high containment region temperatures in severe accidents could conceivably reach levels which negatively impact structural material properties. The integrity of carbon steel, for example, is severely impacted at temperatures above 1200 °F due to creep-rupture mechanisms. For a large, dry containment, however, local temperatures in the containment will not reach this high value for very long even during severe accident conditions, as shown by the MAAP results presented in [EPRI, 1990] for representative severe accident sequences in a large, dry containment. For typical LOCA sequences the gas temperatures in containment generally do not exceed 450 °F. For typical station blackout sequences gas temperatures in the cavity can become very high (~1800 °F) for only a brief period, while temperatures in the rest of the containment stay below 600 °F. Such a high cavity temperature is not of concern here for two reasons: (1) there are no steel containment details (penetrations) in the cavity, and, (2) the melting point of concrete is about 2240 °F.

2.1.3 Relationship to Source Term

Containment failure attributable to overpressurization influences the expected fission product source term of a severe accident by way of the gas flow path created between the containment and the environment, be it directly into the atmosphere, through the soil, or into the auxiliary building. However, the severity of the source term depends on the failure location and failure timing.

The effect of different failure locations has been discussed in the previous section. Previous generic and plant-specific structural analyses have indicated that for large dry concrete containments, locations in the containment cylinder (i.e., the hoop tendons in most cases) and the junction of the cylinder and the basemat have the largest degree of vulnerability. Some uncertainty persists on this topic in virtually all studies that have been performed. This is partly attributable to the fact that various major construction details were not always rigorously assessed to the extent that plant-specific applicability could be ascertained. Also, some uncertainty is inherent in the containment material properties and fabrication methods, regardless of the extent of plant-specific assessment. For many containments, it is important to note that a failure in the containment cylinder would, in all likelihood, result in a direct release to the environment, while a failure at the cylinder-basemat junction would be well below ground. A cylinder-basemat junction failure leads to a greatly reduced source term (to the atmosphere) because soil, especially cool, damp soil, is a very effective scrubbing mechanism. It also worth noting that a failure at the cylinder-basemat junction could possibly be covered by an overlying water pool, which would create another effective fission product scrubbing mechanism.

Whenever release flow is not expected to pass through a water pool or spray mechanism, overpressure failure timing is a key source term factor. Failure in the immediate time period of vessel failure is clearly the most serious, since the overall airborne fission product mass produced by a severe accident is never greater than it is in the time frame directly after vessel failure. A containment overpressure failure that occurs far in advance of vessel failure can actually result in a significantly smaller source term than a failure at or near vessel failure. The proviso in this respect is that the failure flow area created must be large enough to markedly depressurize the containment before vessel failure takes place, thus minimizing the pressure differential driving release flow to the environment. Whenever containment pressurization lags considerably behind vessel failure, substantial fission product retention through naturally occurring deposition mechanisms is facilitated. This would also apply to fission products evolved by long-term revaporization within the vessel.

2.2 Experimental Results

A few experimental results relevant to containment overpressurization in large, dry PWR containments are highlighted here. In addition to experimental programs that tested the overall response of a 1:6 reinforced concrete containment model and a 1:8 scale steel shell model, experimental programs that considered the response of individual containment details (personnel airlocks, mechanical penetrations, etc.) are also considered.

2.2.1 Sandia 1:8 Scale Steel Model Containment Tests

The following excerpt from [Koenig, 1986] along with Figure 2-1, provides a brief description of the experimental apparatus:

> The 1:8-scale model (similar to a free-standing steel ice condenser or BWR Mk-III) was designed and built by Chicago Bridge and Iron Company to the ASME code. It had a design pressure of 40 psig, stood over 30 ft high (including the support columns), and was 14 ft in diameter. The majority of the model was constructed of A516 steel 3/16 inch thick except for the support fixture, which was 1-1/8 inch thick, and the reinforced areas around penetrationa, which were 3/8 inch thick. Included were a number of penetrations and features present in an actual containment building. These included five piping penetrations ranging in size from 1-9/16 inch to 6-7/8 inch outside diameter, a constrained pipe penetration 8-5/8 inch outside diameter, two personnel lock representations, and two operable equipment hatches. The exterior shell was reinforced with circumferential stiffening rings.
>
> One of the two personnel locks was located between the second and third stiffening rings from the bottom, and the other, at the elevation of the seventh formed stiffener from the bottom (about mid-height). The stiffener was routed around the airlock. The equipment hatches were 30 inches in diameter, equipped with hinged doors, and located just above mid-height of the cylinder approximately 120° apart. Due to the closing mechanism used, the model hatch doors were stiffer than those in some containments and, therefore, had a higher buckling pressure. The intent of

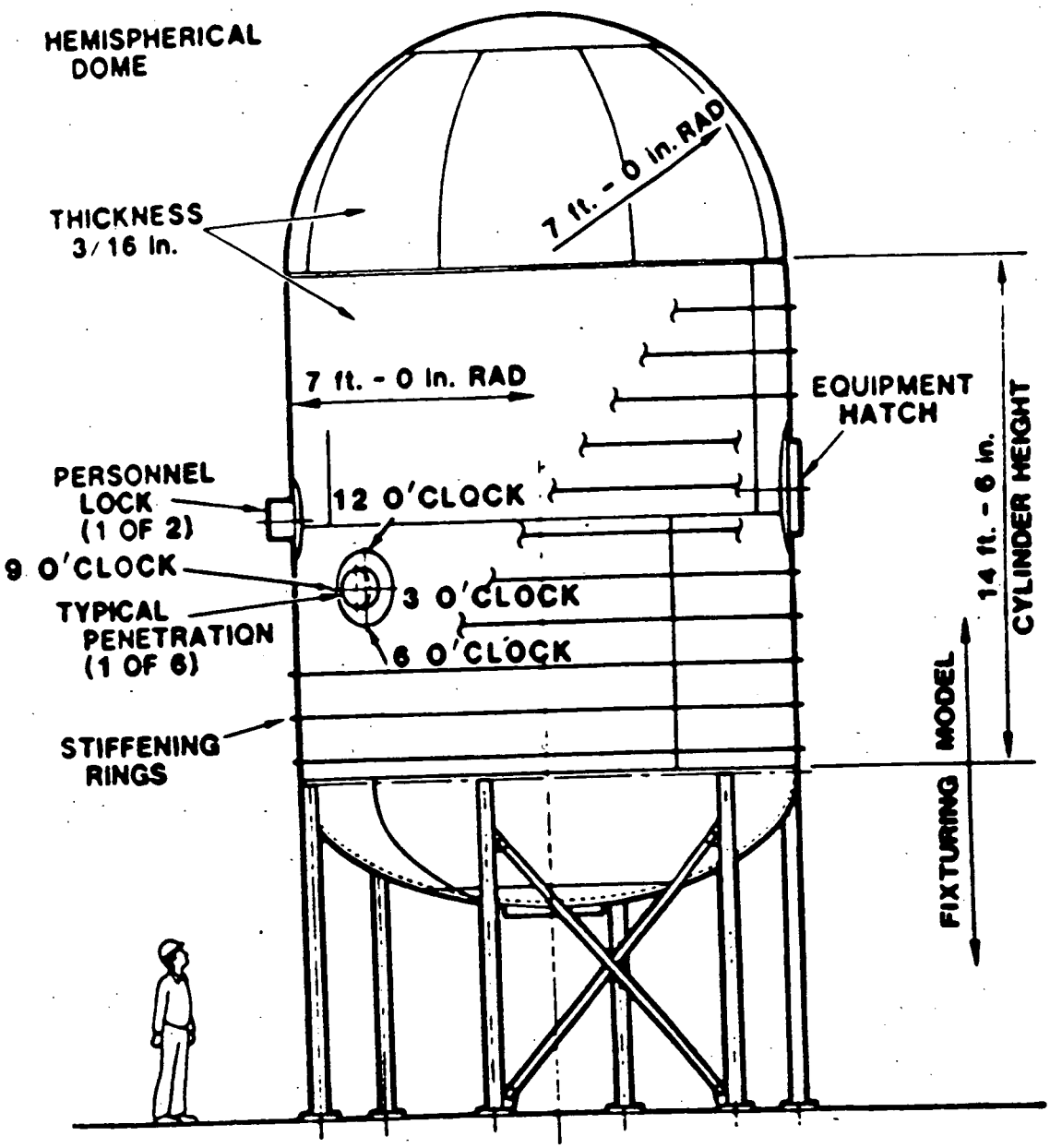

Figure 2-1 Sandia 1:8 scale steel model containment. From [Koenig, 1986].

this experiment, however, was not to test for hatch buckling pressures. Two diametrically opposed piping penetrations were constrained by welding an internal pipe between them. This was done to simulate the rigidity of feedwater lines. The shell material around all penetrations was reinforced with thickened plate sections to follow the area replacement rule.

Experimental procedure and test results, as presented in [Koenig, 1986], are summarized here as well. The test was conducted over a three day long period in which the containment was ultimately pressurized to 195 psig. On the first day, the model was pressurized to 140 psig, in increments of 20 psig, and no leakage was detected during the day. Overnight, leakage stabilized at 0.2% mass per day. On the second day, the model was pressurized, in increments of a few psi, from 140 psig to 170 psig. A leak rate test showed that leakage overnight was limited to 0.2% mass per day. On the third day, the model was successively pressurized to 172.5, 175, 180, 185, 190 and 195 psig. A catastrophic rupture occurred five minutes after the pressure was raised to 195 psig.

To use these experimental results for the Kewaunee ultimate containment analysis a failure size and mode must also be determined in addition to the failure pressure. The catastrophic rupture at 195 psig fragmented the model into 12 major pieces. Some of these pieces were hurled hundreds of feet from the original model location, in spite of an overhead structure built to restrain any fragments generated. Catastrophic failure occurred only after circumferential and longitudinal strains far exceeded 0.2%, which is the value usually associated with yield stress. In fact, strain gages showed that yielding occurred above 165 psig. At the failure pressure of 195 psig, strain histories for gages in the cylindrical section of the model showed values of at least 2.0%. In some locations maximum strains were as high as 3 or 4%, or even higher. Results of [Koenig, 1986] shows that actual failure seems to have occurred after strain reached about 4%; after a strain of 3.66%, large increases in strain were noted.

The conclusions drawn from this test are that failures in free standing steel shell containments can be catastrophic (large rupture rather than leakage), and, the use of yield stress as a failure criterion is unduly conservative. Therefore, containment failure should not occur until material strains reach values in excess of 4%, or so. This assumption leads to higher failure pressures relative to the use of yield as a failure criterion. However, the failure area in a steel shell containment can be very large, where, as source term analysis is concerned, large is anything more than a few square feet. A catastrophic rupture can be averted if some limiting component, perhaps an equipment hatch or personnel airlock, will fail by leakage before the shell itself is ruptured. This was clearly not the case for the Sandia 1:8 scale model test.

2.2.2 Sandia 1:6 Scale Model Containment Pressure Test Program

This 1987 test (reported in [Clauss, 1989a]) involved destructive testing of a 1:6 scale reinforced concrete model considered representative of large, dry PWR containment designs (see Figure 2-2). Conventional materials were used for the concrete aggregate and the #4 (1/2" dia.) primary rebar. Containment details such as a liner, equipment hatches, personnel airlocks and penetrations were represented in the model, which was built to ASME/ACI code. An integral basemat was included but the dead load internal to the containment was not. Tests were conducted at ambient, as opposed to elevated, temperatures, but this does not present a limitation for a large, reinforced concrete containment, because severe accident temperatures will not be high enough to affect material properties for this containment type. In brief, the test objectives were to determine the failure pressure and location for the device, and produce a wida spectrum of structural failure data for further analysis. The test was conducted by pressurizing the facility in 10 psi steps early on and 2 to 3 psi pressure steps at the end. Final test pressure was 145 psig. A small leakage was noted near equipment hatch "A" at 125 psig and in equipment hatch "B" at 138 psig. Equipment hatch "A" began to ovalize at 128 psig, as the horizontal diameter increased nearly 1/2". Leakage could not be quantified at this point. At 140 psig, however, leakage was measured to be 13% mass/day.

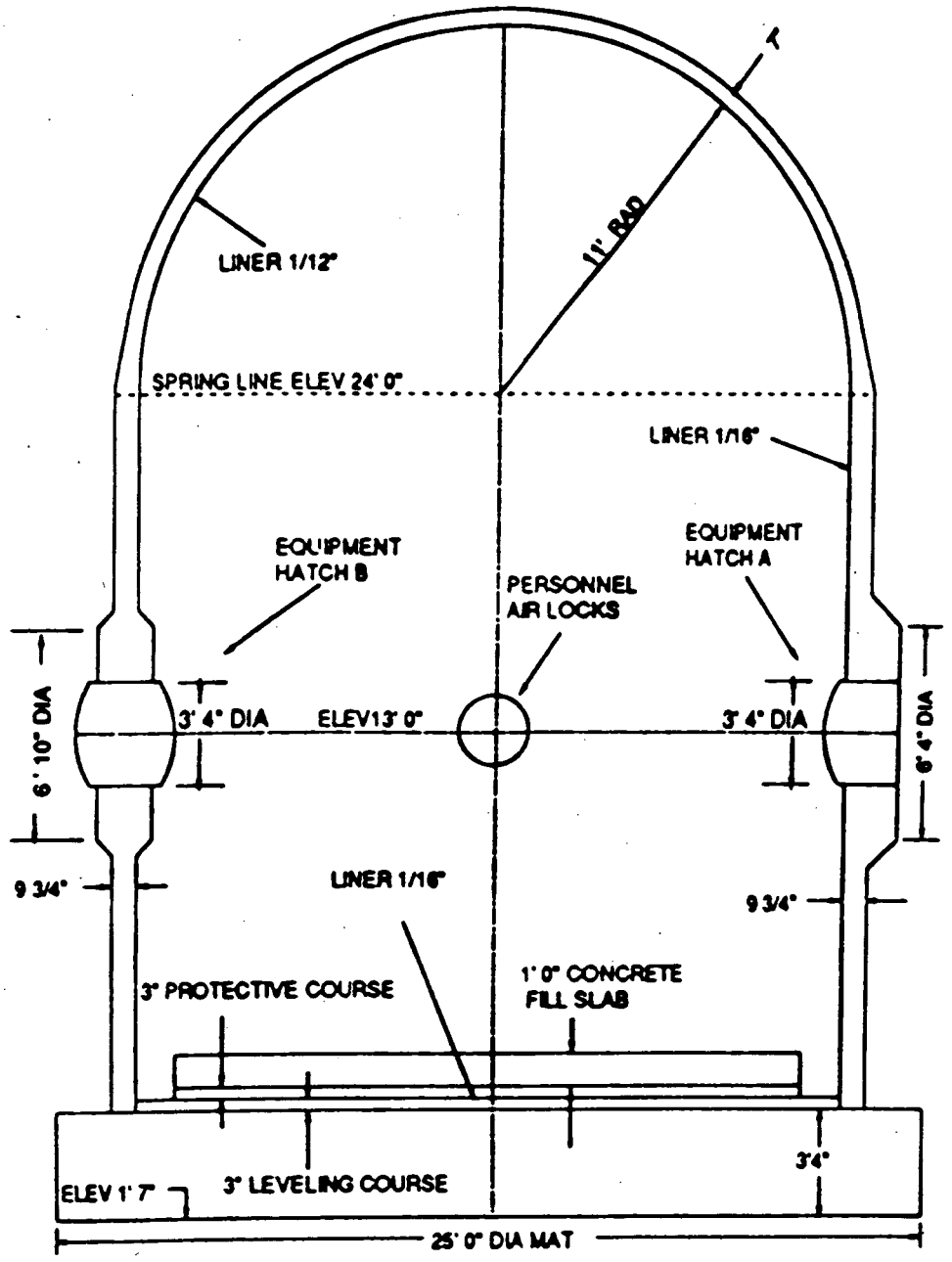

Figure 2-2 Sandia 1:6 scale reinforced concrete containment model. From [Clauss, 1989a].

Leakage became very large (over 200% mass/day) between 140 and 145 psig, suggesting that liner tears occur at these pressure levels. Leakage occurred due to strain concentrations in the vicinity of containment penetrations as shown by Figure 2-3.

Two important conclusions of the work are: (1) pre-test analyses gave good results for cylinder displacements, rebar strains, liner strains, etc., and, (2) pre-test analyses of the bending areas of the containment, namely the cylinder-basemat junction, were not in good agreement with test results. Post-test analysis was performed on the cylinder basemat junction to make use of test results and improve on the original predictions. Revised predictions for liner tearing at basemat-cylinder junction show failure at 152 to 154 psig.

2.2.3 Sandia/CBI Personnel Airlock Testing

In this test program, an actual full-scale airlock assembly (surplus from a cancelled PWR; Callaway Unit 2) was subjected to environmental conditions considered applicable to certain design basis (LOCA) and severe accident events. In general terms, the overall objective of the program was to study potential adverse impacts on the pressure integrity of such devices attributable to these conditions. The conduct and results of these efforts are detailed in [Clauss, 1989a]. Test pressures as high as 300 psig were applied during this program.

In most of the individual tests performed, no pressure boundary integrity losses whatsoever were detected, structural responses notwithstanding. For one case however, the test conditions did yield a significant degree of inner door seal leakage. In this specific case, the airlock inner door temperature was held at 650 °F while the atmosphere (air) temperature inside this door was raised to 800 °F. Pressure inside the door (i.e., corresponding to the containment side) was then increased from ambient to 150 psig, and at this point the leakage referred to was detected.

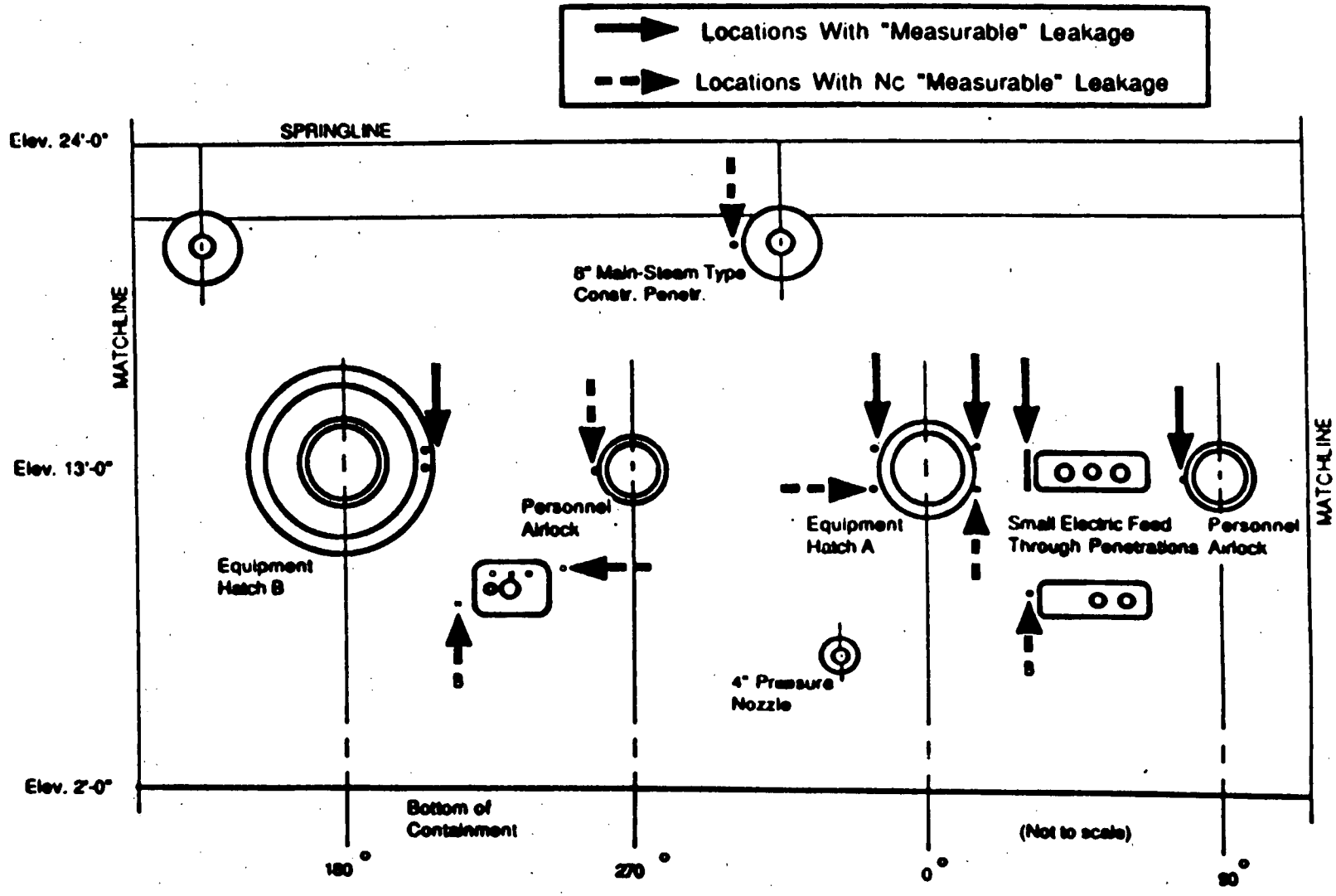

Figure 2-3 1:6 scale model liner stretchout showing leakage.
From [EPRI, 1989].

Note that even at these elevated temperatures, which will be expected in a large, dry containment, the airlock would not begin to leak on overpressure until after other containment details, namely the equipment hatch and hoop rebars, (as demonstrated by the 1:6 scale test) had already failed.

2.2.4 EG&G Containment Penetration System Testing

Idaho National Engineering Laboratory performed a series of full-scale tests to determine the performance of mechanical, or piping, penetrations systems under design basis and severe accident conditions [MacDonald, et al.]. In particular, three separate piping systems complete with valves, penetrations, supports and piping were subjected to design basis conditions of 280 °F and 120 psig without any signs of failure for the duration of the test. These piping systems modeled the containment spray system (an 8" gate valve), the containment purge and vent system (an 8" butterfly valve), and a nominal small diameter (2") globe valve piping system. These three systems were configured so that results "would be applicable to a high percentage of plants".

Results indicate that there was significant plastic strain in the piping sections and many of the piping supports were badly deformed, but there was no buckling of the piping sections and the penetration assemblies showed no damage. The tested systems performed well and the program conclusion was that leak integrity and valve operability will most likely be maintained during severe accidents which challenge light water containments.

2.2.5 Sandia Electrical Penetration Assemblies (EPA) Program

The EPA program [Clauss, 1989b] tested electrical penetrations from three manufacturers - Conax, D.G. O'Brien, and Westinghouse. For a large, dry PWR containment, D. G. O'Brien assemblies were tested under a severe accident profile. This profile consisted of: (1) ramping the temperature and pressure from ambient to 293 °F and 60 psia, (2) then to 361 °F and 155 psia in 12 hours using saturated steam, and, (3) holding these conditions for the remainder of a 10 day test. There were no detectable leaks through the EPA during the severe accident test.

2.3 Analyses

2.3.1 IDCOR Technical Report 10.1

Determination of the ultimate containment structural capability of these nuclear power plants selected for detailed study in the Industry Degraded Core Rulemaking (IDCOR) Program is the main objective of Task 10. The results presented in the report are based upon studies which were completed as part of a specific probabilistic risk assessment (PRA) or a similar study. The results of the ultimate containment capability studies for Zion, Indian Point, Sequoyah, Yankee Power, Browns Ferry, Limerick, etc, are contained within this report. In general, the results have shown that the internal containment pressure may be increased between two to four times the design basis pressure for most designs. Since it is assumed that there will be no dynamic-type loads placed upon containment, a relatively simple analysis may be used to estimate the containment's ultimate capability. The larger structural capability margins available are due mainly to inherent conservatisms in the design methodologies as well as actual material properties which are significantly better than the design values. It was also found that the most likely failure mode for the right circular cylinder portions of a containment is excessive hoop stress, or strain, which could result in the formation of a meridional gap. Although leak rates, prior to catastrophic failure, through cracked, reinforced concrete containment structures have been determined for unlined containments, no similar data exists for the steel lined concrete containments or for the free standing steel shell containments common in the United States. Adequate analysis and experimental data to support "leak-before-break" arguments for steel shell containments also do not exist.

Within [IDCOR, 1983], a study was done on Sequoyah, a low leakage free standing steel shell consisting of a cylindrical wall, a hemispherical dome, and a bottom liner plate encased in concrete. The steel containment vessel is provided with both circumferential and vertical stiffening on the exterior of the shell. Those stiffeners are required to satisfy design requirements for transient pressure loads combined with seismic, thermal, and operating loads. The circumferential stiffeners were installed on

approximately 10-feet centers to ensure stability and alignment of the shell. Vertical stiffeners are spaced at 4° intervals, and other locally stiffened areas are provided around major openings and penetrations as required. Figure 2-4 shows the arrangement of the circumferential stiffeners.

Four analyses were performed in this study: (1) an axisymetric analysis to determine the critical section, (2) an elasto-plastic analysis of a panel at the critical section, (3) an analysis to determine the capacity under ASME Section III service Level A, and (4) an analysis for service level C requirements.

The axisymmetric shell of revolution analysis was performed in order to locate the critical area in the shell under internal pressure. When this area was established, it was analyzed in detail using an elastic-plastic finite element panel analysis. If the containment vessel has no stiffeners, such is the case at Kewaunee, internal pressure, P, would result in a hoop stress of

$$\sigma_t = PR/t \qquad (2\text{-}1)$$

where R is the vessel radius and t is shell thickness [IDCOR, 1983].

The results of this investigation, plus a finite element shell anslysis indicate that, for an axial space greater than 10 ft., the hoop stress at the midspan is equivalent to an unstiffened shell. From this it was determined that the hoop stress in the gap between the 778 feet 6 inches and the 788 feet elevation governs maximum static pressure.

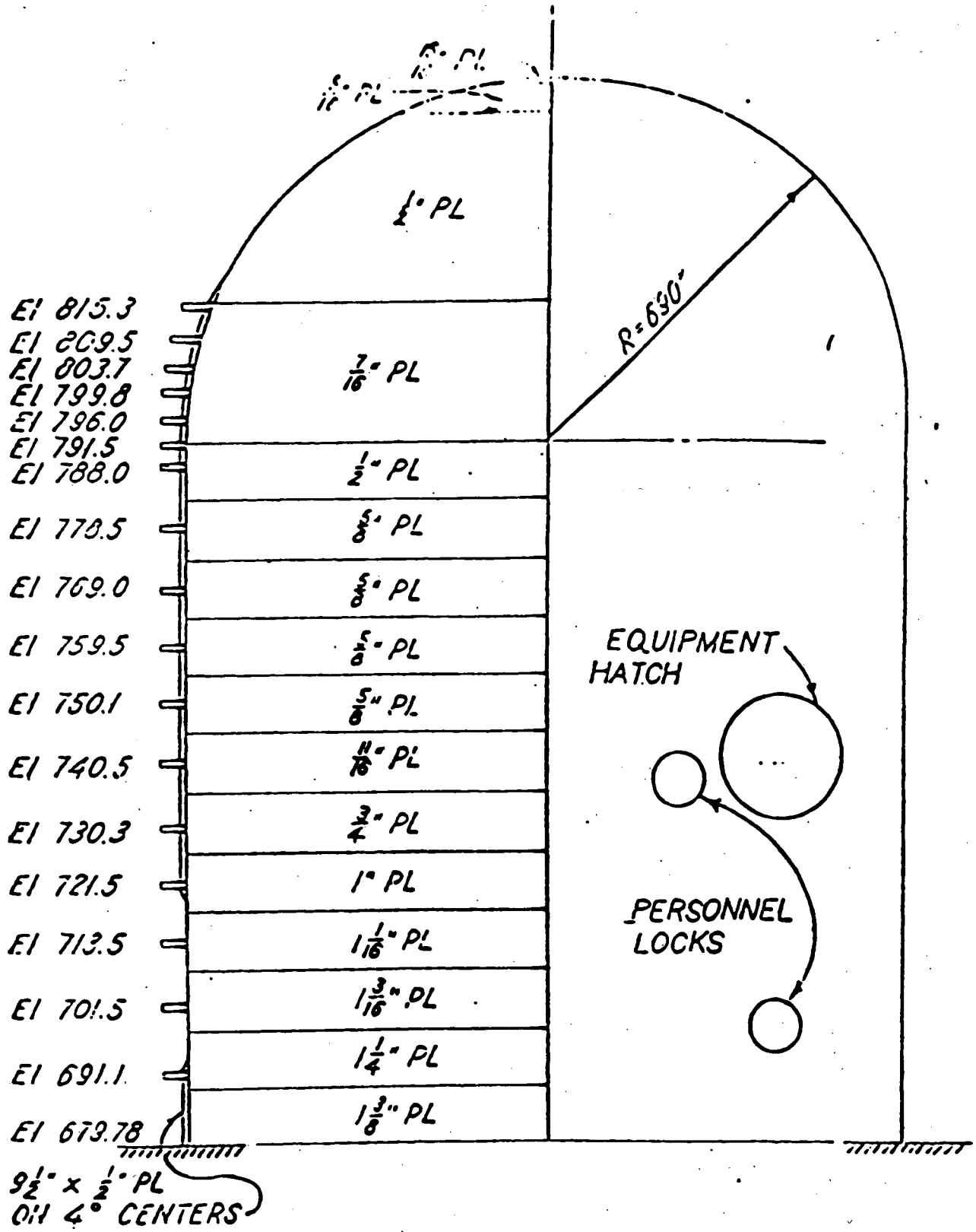

Figure 2-4 Circumferential stiffeners in Sequoyah.

3.0 METHODOLOGY

The method used to evaluate containment failure modes due to overpressurization has two aspects. First, the pressure capability of the containment must be determined from a structural analysis in terms of limiting failure locations, mean failure pressures and associated standard deviations. Then a probabilistic representation of this capability is calculated. The end result is a fragility curve which shows the probability of containment failure as a function of containment pressure.

3.1 Structural Analysis

Normally, only a certain number of limiting failure locations need to be considered for a large, dry containment. Nearly all of the above-grade failure locations would create a direct flowpath to the environment (atmosphere). The auxiliary shield is neglected in this analysis and it is simply assumed that any failure location above grade leads to a direct pathway to the atmosphere. This conservative assumption ignores the potential for fission product retention in the auxiliary building (which is difficult to quantify) and avoids the complication of determining which failure locations lead to the auxiliary building. Failure locations below grade result in very different source terms because of scrubbing by soil.

Limiting failure locations, mean failure pressures and standard deviations associated with mean failure pressures must be obtained from a plant-specific structural analysis. Typical containment locations that should normally be considered for a free standing steel shell containment are listed below:

1. Cylindrical steel shell wall (hoop and vertical directions)
2. Dome
3. Basemat
4. Equipment hatch

5. Personnel airlock

6. Emergency airlock

7. Other containment penetrations that may fail at pressure lower or close to those listed above, if any.

Due to complexities in containment structural analyses, this paper assumes that the plant-specific ultimate strength analysis results are available from a separate study. If these results are not available, an estimate can be achieved using the original design calculations.

3.2 Containment Overpressure Failure Probabilities

Failure of containment structure is probabilistic in nature. Containment failure pressure can be considered as a random variable due to uncertainties in analysis and inherent randomness of material properties and fabrication methods. If the expected (mean) values of failure pressure and their associated standard deviations at all potential failure locations are known, failure probabilities for given containment pressures can be calculated. Here, a Monte Carlo method for calculating these probabilities is employed.

The method used to calculate the failure probability of the Kewaunee containment assumes that the failure probability distributions follow log normal distributions. The probability density function (pdf) for failure with a log-normal distribution at one location is written as

$$f(P_f;\ \mu',\sigma') = \frac{1}{\sigma'\ P_f\sqrt{2\pi}} \exp\left[-\frac{(\ln P_f - \mu')^2}{2\ \sigma'^2}\right] \qquad (3\text{-}1)$$

where P_f is the containment failure pressure (independent variable). Variables μ' and σ' are parameters related to the mean value (μ) and standard deviation (σ) by the following relations:

$$\mu = e^{\mu' + \frac{1}{2}\sigma'^2} \tag{3-2}$$

and

$$\sigma^2 = \mu^2(e^{\sigma'^2} - 1) \tag{3-3}$$

Values of μ' and σ' must be known in order to generate a pdf of the form of Equation (3-1). Given a mean (μ) and a standerd deviation (σ), one can determine the parameters μ' and σ' by solving Equations (3-3) and (3-2) as

$$\sigma' = \sqrt{\ln\left[\left(\frac{\sigma}{\mu}\right)^2 + 1\right]} \tag{3-4}$$

and

$$\mu' = \ln\left[\frac{\mu}{\sqrt{1 + \sigma^2/\mu^2}}\right] \tag{3-5}$$

Therefore, a pdf can be constructed from the knowledge of μ and σ using Equations (3-4) and (3-5).

If there is only one failure location, the probability (Pr) that the containment has failed at a given pressure $\leq P_c$ is simply given by the cumulative normal distribution function

$$\Pr(P_c; \mu, \sigma) = \int_0^{P_c} \frac{1}{\sigma' x\sqrt{2\pi}} \exp\left[-\frac{(\ln x - \mu')^2}{2\sigma'^2}\right] dx \tag{3-6}$$

For failure subject to several potential failure locations, the probability density functions for each location could overlap. The degree of overlap depends on the proximity of the mean failure pressures and the deviation of these pressures from the means. It is necessary to know mean failure pressures and standard deviations associated with all potential failure locations in order to evaluate overall failure probabilities. For a case of 4 potential failure locations, there are 32 modes of failure in

total. These failure modes are listed in Table 3-1. Four of these represent failure modes with containment pressures higher than one of the four failure pressures (type A); 12 modes with containment pressures higher than two of the four failure pressures (type B), 12 modes with containment pressures higher than three of the four failure pressures (type C), and 4 modes with containment pressures higher than all four failure pressures (type D). The left most numbers in Table 3-1 represent failure locations since containment pressures are higher than failure pressures at those locations. For failure mode types B, C and D, it is assumed that locations with the smallest failure pressure fail first even though containment pressure (P_c) is greater than failure pressures at other locations. Due to subsequent depressurization, it can be assumed further that only the location with the smallest failure pressure fails. With this assumption, the failure modes are simplified to those shown in Table 3-1. It is noted that each failure location has equal number of failure modes (i.e., 8 modes each).

Each failure mode in Table 3-1 has a probability associated with it. For example, a probability for failure mode A-4 is given by:

$$Pr\ (A\text{-}4) = Pr_3 \cdot (1 - Pr_1)\ (1 - Pr_2)\ (1 - Pr_4) \qquad (3\text{-}7)$$

Probabilities for failure mode types B, C, and D will involve complicated evalustions of double or triple integrals of joint probability density functions. However, the overall containment failure probability can be determined without the knowledge of probabilities for each mode. Since the sum of failure probability and non-failure probability is always unity, we can write

$$Pr\left[\begin{matrix}\text{containment failure:} \\ \text{4 potential locations}\end{matrix}\right] = 1 - Pr\ (\text{containment not failed})$$

$$= 1 - (1 - Pr_1)(1 - Pr_2)(1 - Pr_3)(1 - Pr_4) \qquad (3\text{-}8)$$

Table 3-1

POSSIBLE CONTAINMENT FAILURE MODES FOR 4 POTENTIAL FAILURE LOCATIONS (1, 2, 3, 4)

Modes	Characteristics*	Failure Location
0	$P_c < (1, 2, 3, 4)$	none
A-1	$1 \leq P_c < (2, 3, 4)$	1
A-2	$4 \leq P_c < (1, 2, 3)$	4
A-3	$2 \leq P_c < (1, 3, 4)$	2
A-4	$3 \leq P_c < (1, 2, 4)$	3
B-1	$1 < 4 \leq P_c < (2, 3)$	1
B-2	$4 < 1 \leq P_c < (2, 3)$	4
B-3	$1 < 2 \leq P_c < (3, 4)$	1
B-4	$2 < 1 \leq P_c < (3, 4)$	2
B-5	$1 < 3 \leq P_c < (2, 4)$	1
B-6	$3 < 1 \leq P_c < (2, 4)$	3
B-7	$4 < 2 \leq P_c < (1, 3)$	4
B-8	$2 < 4 \leq P_c < (1, 3)$	2
B-9	$4 < 3 \leq P_c < (1, 2)$	4
B-10	$3 < 4 \leq P_c < (1, 2)$	3
B-11	$2 < 3 \leq P_c < (1, 4)$	2
B-12	$3 < 2 \leq P_c < (1, 4)$	3

*Explanation of characteristics:

1) P_c is the containment pressure
2) Each number represents the magnitude of failure pressure at that location.
3) The left most number denotes the failure location. (Only one failure location is assumed at a time.)
4) The relative magnitudes of failure pressures at locations in parentheses does not matter.

FAI/91-138

A PHENOMENOLOGICAL EVALUATION SUMMARY ON LINER MELT-THROUGH IN SUPPORT OF THE KEWAUNEE NUCLEAR PLANT INDIVIDUAL PLANT EVALUATION

Submitted To:

Wisconsin Public Service Corporation
Green Bay, Wisconsin

Prepared By:

Fanske & Associates, Inc.
16W070 West 83rd Street
Burr Ridge, Illinois 60521

Finsl Issue

January 1993

TABLE OF CONTENTS

		Page
1.0	PURPOSE	1
2.0	CONCLUSIONS	2
3.0	REFERENCES	4

LIST OF FIGURES

Number		Page
1	Sketch of Kewaunee containment design	3

1.0 PURPOSE

In [NRC, 1988a], the NRC recommends that molten core debris coolability be assessed to determine the potential for attack and melt-through of the containment steel shell. It is postulated that during a high pressure melt ejection (HPME), molten corium could become entrained in the blowdown jet stream and then deposit directly on the containment walls in the annular compartment. The objective of this paper is to assess the possibility of such a phenomenon occurring and whether or not it could challenge containment integrity at the Kewaunee Nuclear Power Plant.

Liner melt-through influences the expected fission product source term for a sequence by providing a large gas flow path out of containment shortly after vessel failure. Since the airborne fission product concentration in a closed containment tends to decay with time due to naturally-occurring fission product retention mechanisms, such an early containment failure generally increases the source term. Also, the relatively large expected failure size assures a rapid blowdown of the initially available airborne fission products to the environment and auxiliary building, which generally reduces its fission product retention effectiveness.

The major physical process affecting the possibility of liner melt-through is closely related to the direct containment heating phenomenon. The possibility of a localized vessel failure should severe accident conditions result in molten debris draining into the lower plenum was first addressed in the Zion [CECo, 1981] and Indian Point [Con. Ed and PASNY, 1982] Probabilistic Safety Studies. Along with this, the possibility of dispersing high temperature debris from the reactor cavity due to rapid steam generation in the cavity or due to high pressure blowdown of the primary system was considered. Given the geometry of the Kewaunee reactor cavity and the conditions for a high pressure melt ejection, such a dynamic debris transfer could occur.

2.0 CONCLUSION

Due to the design of the Kewaunee containment and cavity, when corium is dispersed from the reactor vessel, it is collected in the cavity, which has no direct path to the steel liner. Therefore, during a low primary system pressure failure of the vessel, the molten corium will exit the vessel onto the cavity floor. As one can see in Figure 1, when molten core debris is deposited in the cavity after a low pressure melt injection, it can not immediately challenge the containment integrity by melting through the containment steel liner. Subsequently, for a vessel failure at a low primary system pressure, the possibility of containment failure by liner melt-through at low pressure melt injections is bounded by the plant design basis and therefore, no further consideration is merited.

As previously mentioned, the only method of achieving a state where molten corium is in direct physical contact with the containment steel shell is a high pressure melt ejection. During a postulated high pressure melt ejection, immediately after the melt is discharged, the primary system will blow down causing particles of molten debris to become entrained in the gas stream. These particles then exit the cavity via the instrument tunnel. Due to the obstructions in the instrument tunnel (i.e., seal table plate), the flowpath of the stream is subjected to a 90° change in direction. Since the particulated debris is much denser than air, a majority of this suspended debris is de-entrained from the flowpath by collisions with the ceiling above the seal table and the seal table itself. According to [FAI,1991] approximately 26,000 Kg is postulated to be entrained in the blowdown stream, with 72% becoming de-entrained at the seal table. This leaves approximately 7000 Kg of particulate debris still entrained in the seal table area. Due to the fact that this material is now almost strictly composed of the smallest particles which were able to make the 90° turn and that there are many other obstructions (i.e., pipes, structures, etc.) that will impede further corium transport, the possibility of acquiring a substantial coherent mass in one area capable of generating enough heat to melt the containment steel liner is practically zero. Consequently, due to the inability of substantial coherent corium masses of coming into contact

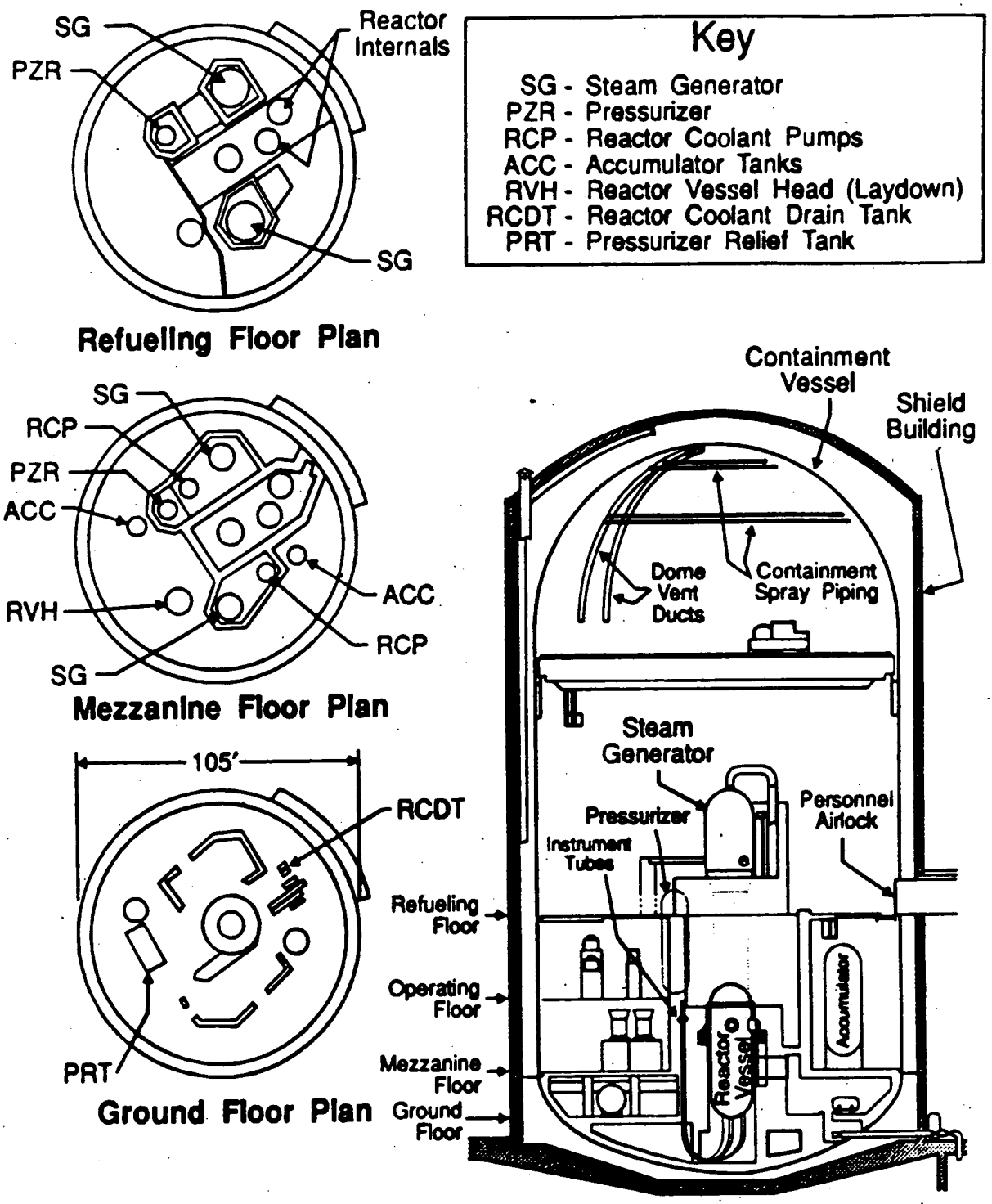

Figure 1. Sketch of Kewaunee containment design (taken from Kewaunee FSAR).

with the containment steel shell, the possibility of containment failure due to liner melt-through during a HPME at the Kewaunee Nuclear Power Plant is also bounded by plant design basis and therefore will not be considered as a potential containment failure mechanism in the Kewaunee IPE.

3.0 REFERENCES

Commonwealth Edison Company (CECo), 1981, Zion Probabilistic Safety Study, Chicago, Illinois.

Consolidated Edison (Con.Ed.) and the Power Authority of the State of New York (PASNY), 1982, Indian Point Probabilistic Safety Study, New York, NY.

Fauske and Associates, 1991, "Phenomenological Evaluation Summary on Direct Containment Heating in Support of the Kewaunee Individual Plant Evaluation," FAI/91-123.

NRC (1988), letter to All Licensees Holding Operating Licenses and Construction Permits for Nuclear Power Facilities, "Individual Plant Examination for Severe Accident Vulnerabilities - 10 CFR 50.54(f)," Generic Letter No. 88-20.

FAI/91-120

A POSITION PAPER REGARDING POTENTIAL CONTAINMENT FAILURE BY DIRECT BYPASS IN SUPPORT OF THE KEWAUNEE NUCLEAR PLANT INDIVIDUAL PLANT EVALUATION

Submitted To:

Wisconsin Public Service Corporation
Green Bay, Wisconsin

Prepared By:

Fauske & Associates, Inc.
16W070 West 83rd Street
Burr Ridge, Illinois 60521

Final Issue

September 1992

ABSTRACT

Direct bypass refers to severe accident sequences that involve releases of fission products from the primary system directly to outside of the primary containment. Such scenarios require the occurrence of an opening in the primary system pressure boundary outside of the primary containment that creates an unisolable (or unisolated) flow path from the primary system. Typical initiating events for such sequences at a large, dry PWR include low pressure system piping failures induced by inadvertent exposure to full primary system pressure (i.e., interfacing system Less-of-Coolant Accidents) and steam generator tube ruptures with a failure to isolate the ruptured steam generator. Subsequent system failures are required that prevent coolant make-up to the reactor vessel. Regardless of the hypothesized sequence of events, however, the common feature of all of these scenarios is that the substantial fission product retention capabilities of the primary containment are rendered ineffective.

TABLE OF CONTENTS

	Page
ABSTRACT	ii
1.0 PURPOSE	1
2.0 REFERENCES	2

1.0 PURPOSE

The Nuclear Regulatory Commission (NRC) has indicated its concern about the possibility of containment bypass in [1] by stating that the first nodal decision in the Containment Event Tree (CET) used in the containment performance evaluation should be to determine the likelihood that the containment is bypassed, failed, or unisolated prior to core damage. However, the NRC also recognizes that the occurrence of a sequence involving direct bypass of the primary containment may be extremely remote. In [1], the NRC sets the sequence screening criteria for direct bypass sequences at 1.0E-7 per year of reactor operation. Bypass sequences with a probability of occurrence less than this cut-off value do not have to be reported in the list of important sequences determined by the Individual Plant Evaluation (IPE). Bypass sequences with a probability of occurrence greater than this cut-off value have to be reported along with an estimate of the probability of a significant fission product release to the environment. Also per [1], the containment performance assessment for direct bypass sequences must include consideration of the phenomenological uncertainties associated with fission product releases to the environment. The major uncertainties in the fission product source term for direct bypass sequences include the masses and types of fission products that are released from the primary system as well as the effectiveness with which these fission products are retained in the auxiliary building.

The treatment of direct bypass sequences in the Kewaunee IPE will be consistent with the NRC guidance indicated above. The systems analysis (front-end) activity in the IPE will evaluate the likelihood of occurrence of direct bypass sequences. Plant damage states corresponding to sequences that result in a likelihood of occurrence above 1.0E-7 per year of reactor operation will be transferred to the containment event trees (CETs) and probabilities for the resulting release categories will be determined. Fission product releases to the environment for these release categories will be estimated using the Modular Accident Analysis Program (MAAP). A set of source term calculations will be performed using MAAP to provide best-estimate values as well as to address the uncertainties and sensitivity cases identified below.

As part of the Level II activities, a steam generator tube rupture with a failure to isolate the ruptured steam generator will be analyzed to determine the source term associated with a direct bypass of the primary containment. Sensitivity studies concerning operator actions associated with a steam generator tube rupture (i.e., flooding the ruptured steam generator versus letting it dry out) will be analyzed as part of the sensitivity studies performed on the Level II representative sequences. Treatment of the issue of direct containment bypass in this manner satisfies the NRC screening criteria for bypass sequences, as well as addresses various sensitivities associated with operator actions.

2.0 REFERENCES

[1] NRC letter to All Licensees Holding Operating Licenses and Construction Permits for Nuclear Power Reactor Facilities, "Individual Plant Examination for Severe Accident Vulnerabilities - 10 CFR 50.54(f)," Generic Letter No. 88-20, dated November 23, 1988.

FAI/91-124

A POSITION PAPER REGARDING CONTAINMENT FAILURE TO ISOLATE IN SUPPORT OF THE KEWAUNEE NUCLEAR PLANT INDIVIDUAL PLANT EVALUATION

Submitted To:

Wisconsin Public Service Corporation
Green Bay, Wisconsin

Prepared By:

Fauske & Associates, Inc.
16W070 West 83rd Street
Burr Ridge, Illinois 60521

Final Issue

September 1992

ABSTRACT

Failure to isolate refers to severe accident sequences that involve a mechanical or operational failure to achieve containment isolation prior to the initiation of core damage. The resulting flow area to the auxiliary building is in addition to that associated with normal containment leakage. For such scenarios, releases of fission products from the primary system flow to the primary containment and then to the auxiliary building. Typical initiating events for such sequences at a large, dry PWR plant include plant transients, loss-of-offsite power, station blackout (SBO), as well as various possible primary system piping failures that lead to Loss-of-Coolant Accidents (LOCAs). Subsequent system failures are required that prevent coolant make-up to the reactor vessel. Regardless of the hypothesized sequence of events, however, the common feature of all of these scenarios is that the substantial fission product retention capabilities of the primary containment are impaired.

TABLE OF CONTENTS

	Page
ABSTRACT	i
1.0 PURPOSE	1
2.0 REFERENCES	2

1.0 PURPOSE

The Nuclear Regulatory Commission (NRC) has indicated its concern about the possibility of containment isolation failure in [1] by stating that the first nodal decision in the Containment Event Tree (CET) used in the containment performance evaluation should be to determine the likelihood that the containment is bypassed, failed, or unisolated prior to core damage. The issue concerning direct containment bypass is discussed in a separate position paper [2]. Also per [1], the containment performance assessment for failure-to-isolate sequences must include consideration of the phenomenological uncertainties associated with fission product releases to the environment. The major uncertainties in the fission product source term for failure-to-isolate sequences include the masses and types of fission products that are released to the primary containment, the timing of these releases, the effect of the increased containment leakage flow on its operative fission product removal mechanisms, as well as the effectiveness with which these fission products are retained in the auxiliary building.

The treatment of containment isolation failure sequences in the Kewaunee IPE will be consistent with the NRC guidance indicated above. The first nodal decision in the CETs sequences will be related to the likelihood of containment isolation failure. The systems analysis (front-end) activity in the IPE will evaluate the likelihood of occurrence of failure to isolate for the various sequences determined and provide that information to the containment performance analysis activity. Sensitivity analyses will be performed using the Modular Accident Analysis Program (MAAP) to determine the fission product release rates for relevant piping diameters. A set of source term calculations will be performed using MAAP to provide best-estimate values as well as to address the uncertainties identified above.

2.0 REFERENCES

[1] NRC Letter to All Licensees Holding Operating Licenses and Construction Permits for Nuclear Power Reactor Facilities, "Individual Plant Examination for Severe Accident Vulnerabilities - 10 CFR 50.54(f)," Generic Letter No. 88-20, dated November 23, 1988.

[2] Fauske & Associates, Inc., 1991, Kewaunee Position Paper Regarding Potential for Direct Containment Bypass, FAI/91-120.

[3] "Containment Isolation System Notebook for Kewaunee Nuclear Power Station," Section 4.12, Wisconsin Public Service Co., January 29, 1990.